PHOTOELECTROCHEMISTRY

A thesis submitted for the degree of

Doctor of Philosophy

by

F. S. Fisher

University College

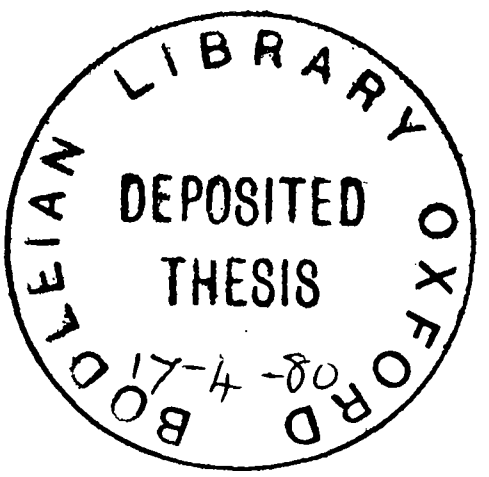

Physical Chemistry Laboratory

South Parks Road

Oxford 1978.

ABSTRACT

The purpose of this work was to assess the potential of the Ru(II)(bipy)$_3$ complexes as photogalvanic systems, using the criteria obtained from the theory for an ideal photogalvanic solar cell developed by Albery and Archer. To this end two techniques were developed to measure the rate of the thermal back reaction between the high energy photoproducts Ru(III) and Fe(II). The thermal back reaction is a serious loss process in such a cell.

The first technique, the Optical Rotating Disc Electrode, was improved by the design and construction of new apparatus. It allowed measurement of most of the important parameters of a photogalvanic cell and confirmed much of the theory for such a cell. The second technique, Flash Electrolysis, first used by Perone, was developed for use with a transparent disc electrode. Further investigations of the thermal back reaction were made using the Stopped Flow technique.

The results of these experiments on Ru(III)(bipy)$_3$ and its derivatives show that the reaction obeys the Marcus theory of electron transfer. However the activation parameters are dominated by "compensation effects" which, at the elevated temperatures of a practical photogalvanic cell ($> 60^{o}C$), reduce the differences between different derivatives. The very similar rates of reaction so produced are much too high for the

development of an efficient photogalvanic cell. $Ru(II)(bipy)_3$ systems thus provide a useful model for other possible photogalvanic systems but cannot be of any practical use themselves.

..... his dectroscophonius photosensition under suprasonic light control may be logged for by our none too distant futur·es as soon astone values can be turned out from Chromophilimos, limited at a millicentime the microamp .....

Finnegans Wake, James Joyce

To Catherine

ACKNOWLEDGMENTS

I wish to thank my supervisor John Albery, the whole research group for their help and encouragement and in particular Andrew Foulds, Philip Bartlett, Robert Hillman and Richard Compton. I am also indebted to Michael Heslop, Andrew Whiting and Ivan March for their technical assistance in constructing apparatus.

My family have been a constant source of strength.

I would like to thank Mrs Elizabeth Price and Mrs Margot Long for their excellent typing.

Finally I wish to thank B.P. for their financial support during this research.

CONTENTS

CHAPTER 1

INTRODUCTION

Photoelectrochemistry is the study of all electronic processes in which a flux of photons can cause a change in the flux of electrons at an electrode. The definition may be subdivided into three main categories according to where the light is absorbed:

1) Absorption by the electrode (e.g. at a semiconductor electrolyte interface).

2) Absorption at the surface of an electrode (e.g. in a dye layer attached to the surface of an electrode).

3) Absorption in the electrolyte.

This thesis is solely concerned with 3), photogalvanic processes, in which light is absorbed in the electrolyte and the photoproduct(s) migrate to, and then react at the electrode.

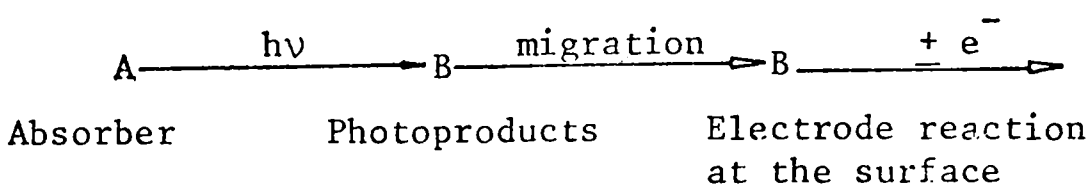

B is usually the electron transfer quenching product of the excited state of A.

$$\left.\begin{array}{l} A \xrightarrow{h\nu} A^* \\ A^* + Z \longrightarrow B + Y \end{array}\right] \quad \text{in solution}$$

$$B \pm e^- \longrightarrow A \quad \text{at electrode}$$

where A/B and Y/Z are redox couples.

This general scheme has the advantage that the starting material, A, is regenerated by reduction/oxidation at the electrode so that the process may be repeated indefinitely. The scheme suggests a photogalvanic cell in which a flux of photons into the solution is converted into a flux of electrons at the electrode. Light is thus converted into electrical energy; a welcome device in view of the present energy shortage, and the main reason for pursuing this line of research.

Figure 1:1 shows the processes occurring in such a cell. Light is absorbed by A to produce A^*. A^* is electron transfer quenched by Z and the electron transfer products, B and Y, migrate to opposited electrodes where they are converted back to A and Z, giving up their charge and passing current through the external circuit.

It is worth noting that, if A^* were to react at the electrode, this too would be a photogalvanic process. However such systems are not considered in this thesis for two reasons.

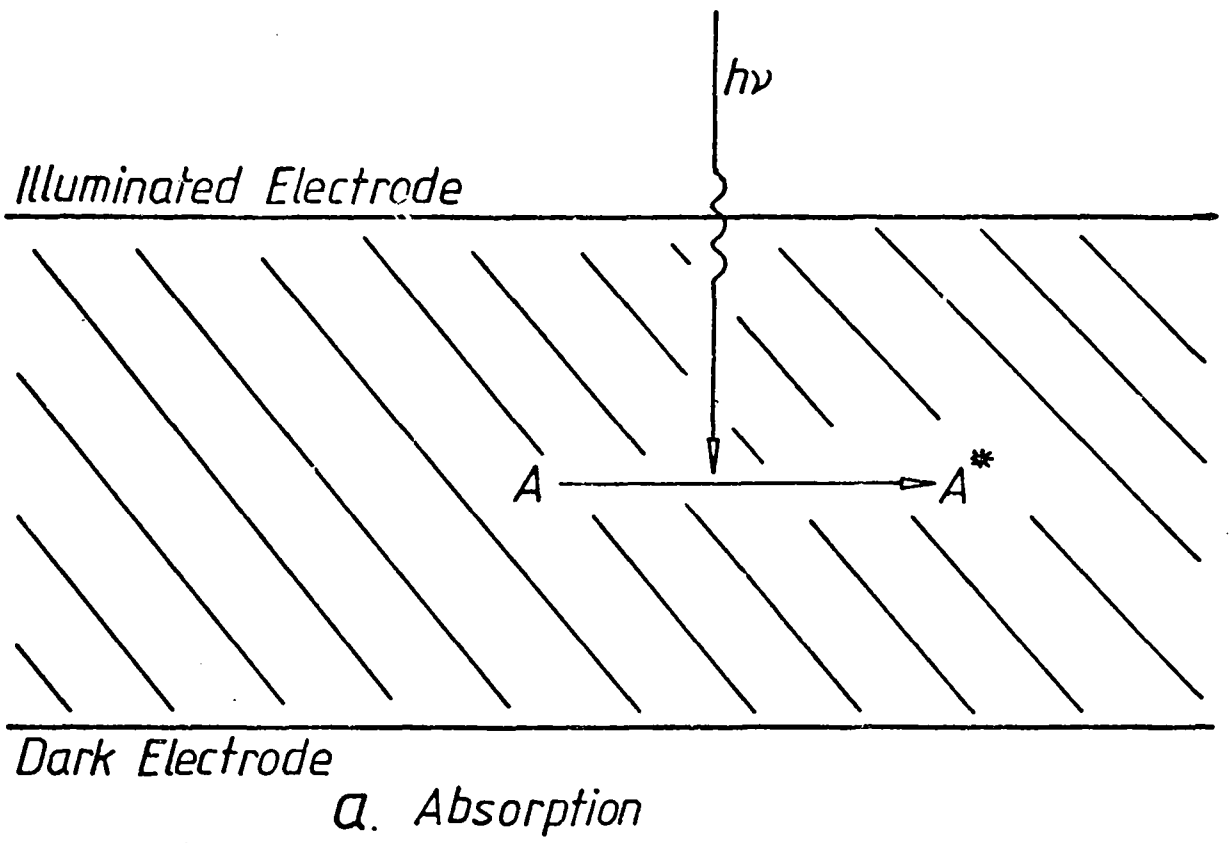

a. Absorption

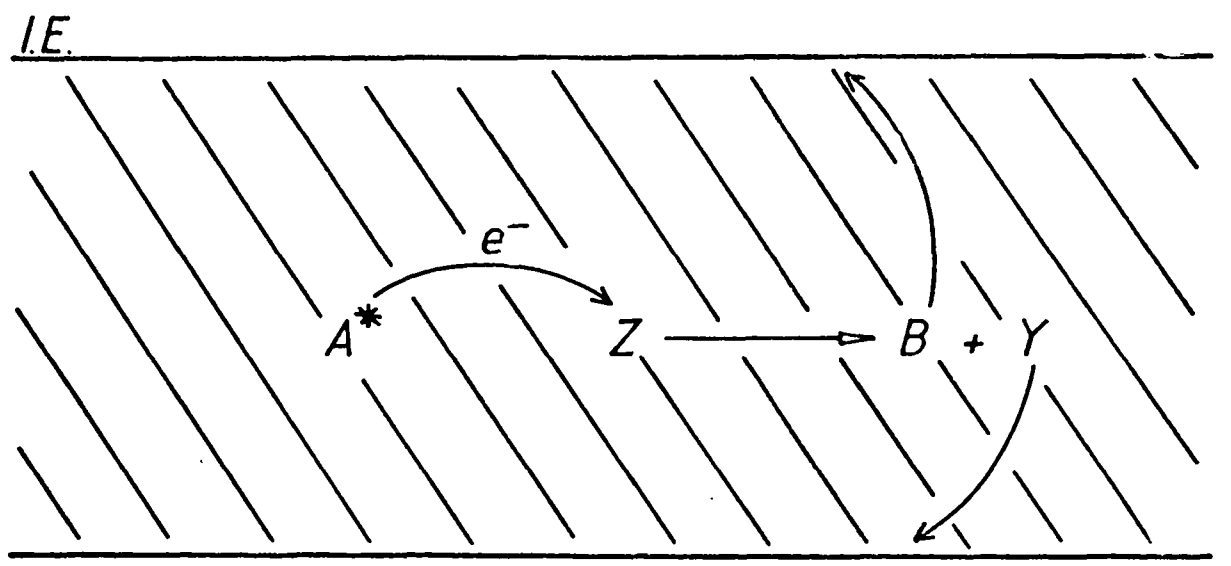

b. Electron Transfer Quenching and Diffusion

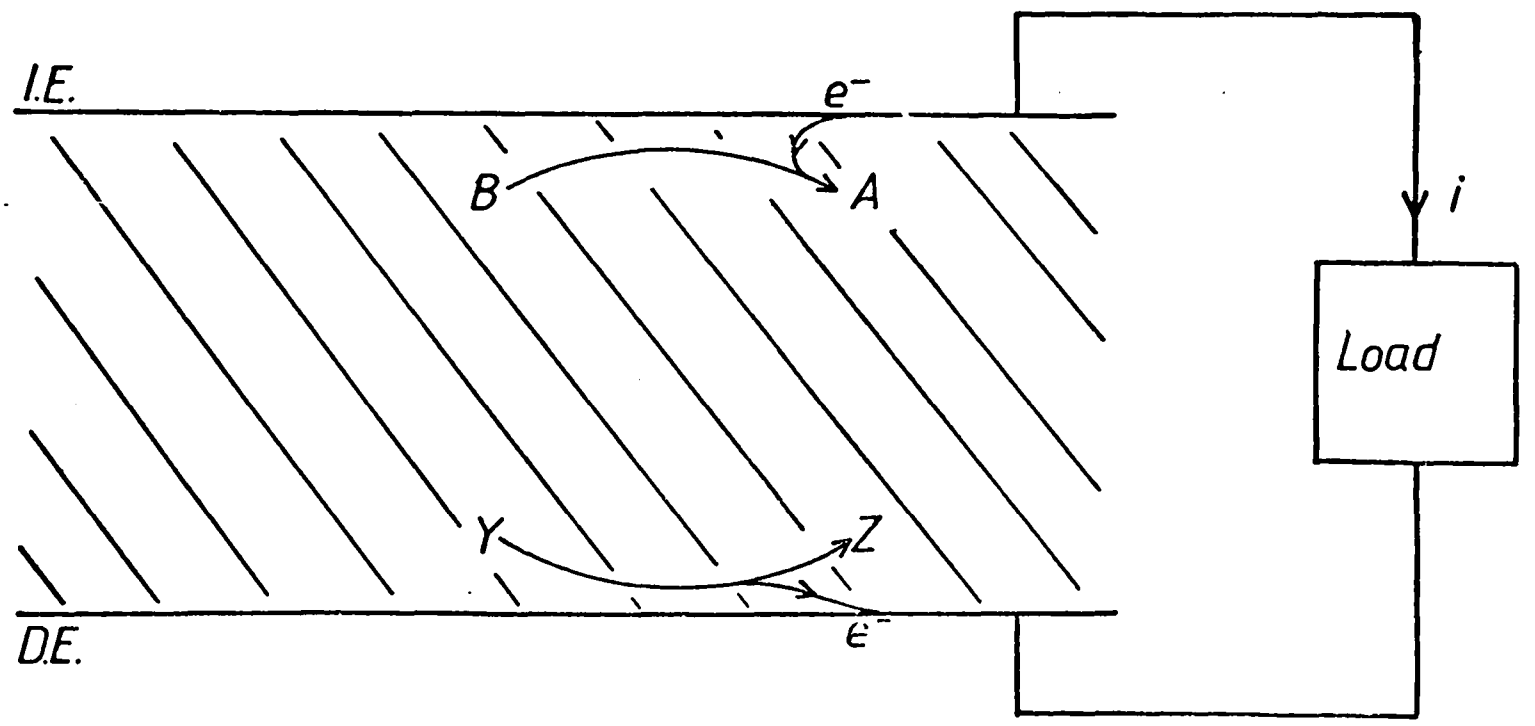

c. Electrode Reaction and Regeneration of Starting Materials

Fig 1 : 1

The Photogalvanic Cell

1) Excited states are very short-lived in solution and do not have time to migrate to the electrode before deactivation.

2) Electrodes act as very good quenchers of excited states.

Figure 1:2 shows this schematically. There is no net electron transfer and the energy is degraded as heat.(An exception to this is the reaction of some excited states at semiconductor electrodes[1]. The electronic structure of the semiconductor both prevents rapid quenching and allows a net electron transfer. However 1) limits the efficiency of these systems and they are not considered here.)

The most important requirement for a photogalvanic cell is therefore electron transfer quenching which traps the photon energy for long enough to collect it at the electrode. Electron transfer quenching was first observed for the Thionine/Ferrous system by Weiss[2] and studied in more detail by Rabinowitch[3] in 1940. However it was not until more recently that work on this and other electron transfer quenching systems has been directed towards the production of an efficient photogalvanic cell.

It is apparent that the efficiency of a photogalvanic cell will depend on the rates of various electron transfer reactions. A brief summary of the Marcus-Levich theory of outer sphere electron transfers is therefore given.

MARCUS-LEVICH THEORY

The theory describes the electron transfer in terms of a number of separate steps.

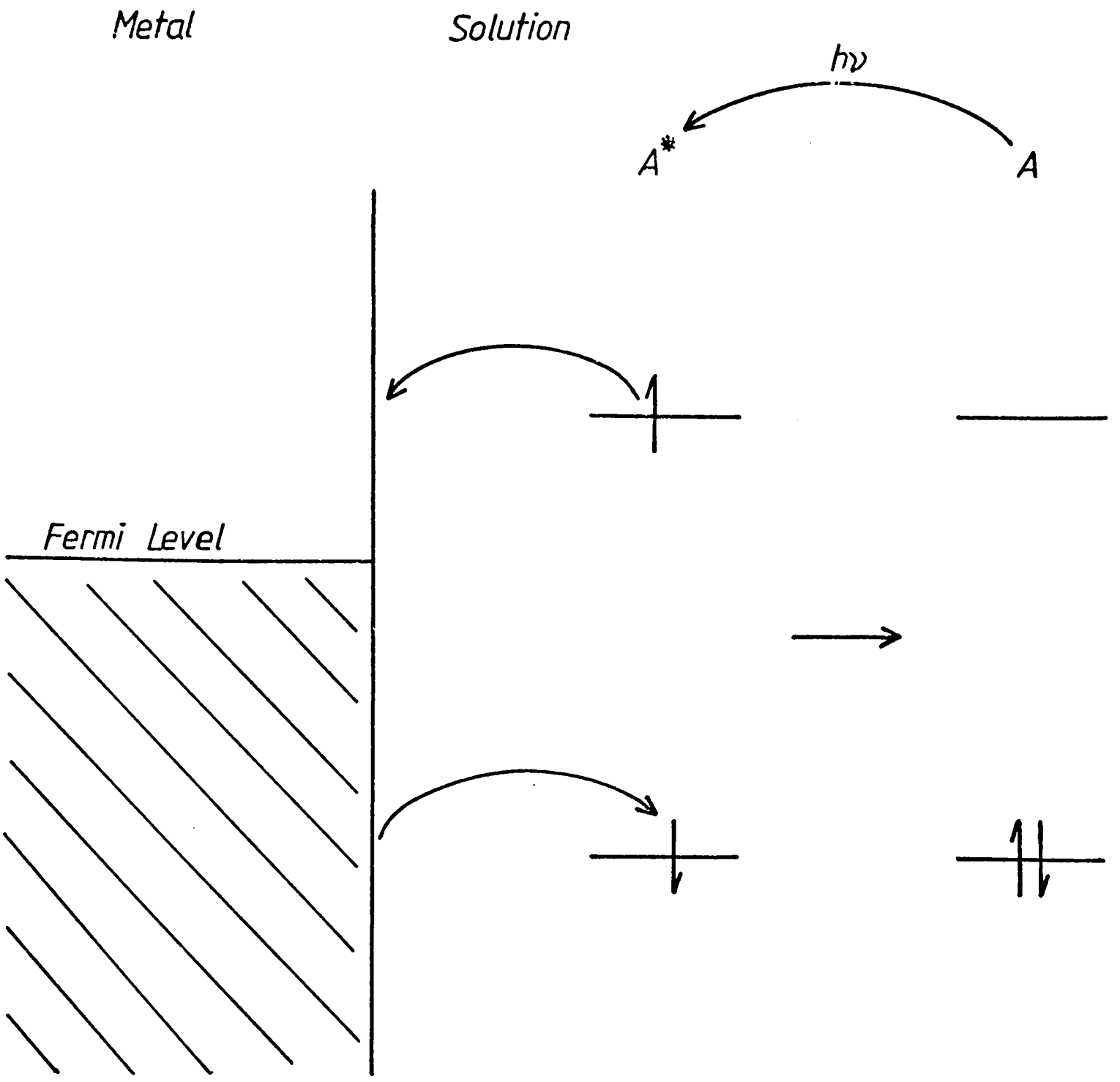

Fig 1 : 2

Excited State Quenching by Metal Surface

		Characteristic Time
(1)	Diffusion together of the reactants	$> 10^{-8}$ s.
(2)	Reorientation of the ion atmosphere	$\sim 10^{-8}$ s.
(3)	Reorientation of the solvent dipoles	$\nu_s \approx 10^{-11}$ s.
(4)	Alteration to ligand-ion bond distances	$\sim 10^{-14}$ s.
(5)	Electron transfer	10^{-16} s.

The very good time separation of the various processes allows them to be treated one at a time. The electron transfer occurs so rapidly that all the nuclei are "frozen" as the electron moves from one centre to the other. As no energy is radiated or absorbed during this process it is isoenergetic. This lead Marcus and Levich to describe a one electron transfer in terms of the following model with P/P^+ and Q/Q^- as the two couples.

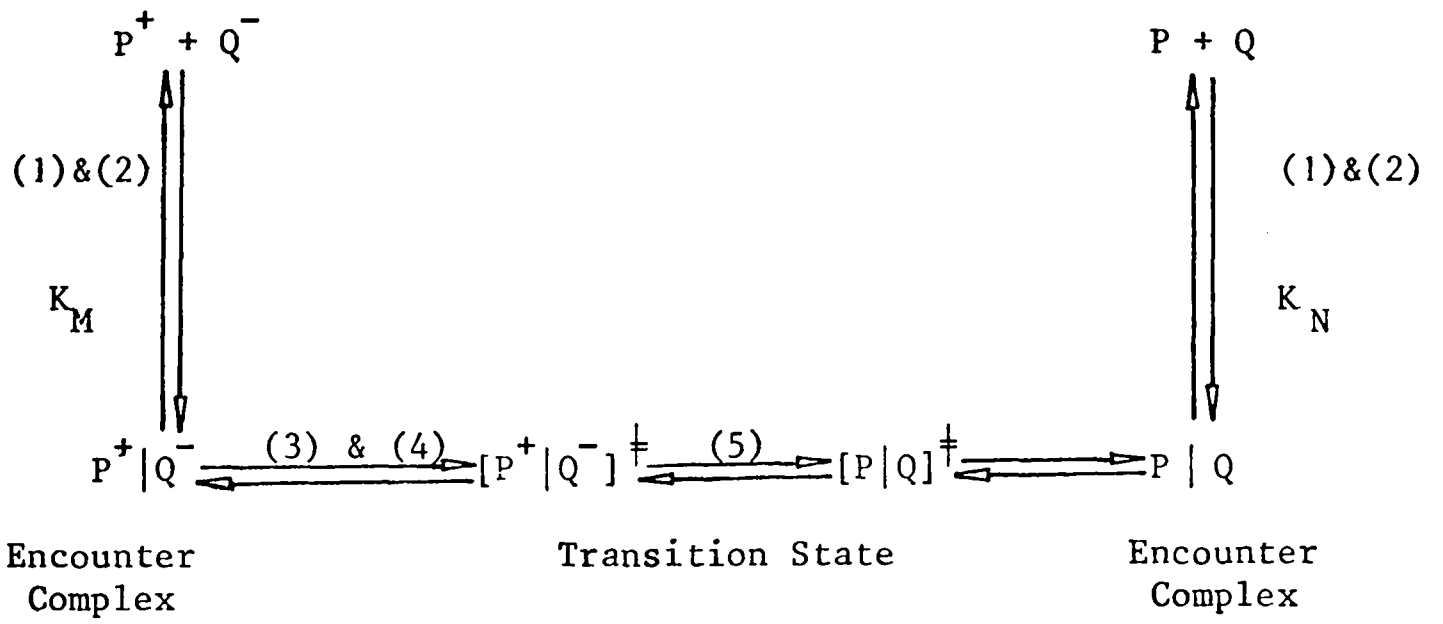

where ‡ refers to the transition state.

They described the solvent reorganisation around the encounter complex, (3) & (4), as due to the chance fluctuations of the solvent dipoles. The variation in energy with displacement

along the reaction coordinate was assumed to be parabolic (i.e. the solvent undergoes simple harmonic motion). Figure 1:3 shows this schematically.

Simple coordinate geometry[4] then gives a relation for the free energy of activation of the reaction

$$P^+|Q^- \longrightarrow P|Q$$

Encounter Complex → Encounter Complex

where $$G_{\ddagger} = \frac{(G_{\Delta} + G_s)^2}{4\,G_s}$$

where $G_{\ddagger}$, G_{Δ} and G_s are as defined in Figure 1:3.

If it now assumed that the free energy changes for formation of the two encounter complexes from the separated reactants are similar

$$\text{e.g.} \quad K_M \approx K_N \sim 1\ M^{-1}$$

then a number of relations can be derived[5-8] for the general system:

$$P^+ + P \underset{}{\overset{k_{11}}{\rightleftharpoons}} P + P^+$$

$$Q^- + Q \underset{}{\overset{k_{22}}{\rightleftharpoons}} Q + Q^-$$

$$P^+ + Q^- \underset{}{\overset{k_{12}}{\rightleftharpoons}} P + Q$$

The subscripts 11 and 22 refer to exchange reactions and 12 refers

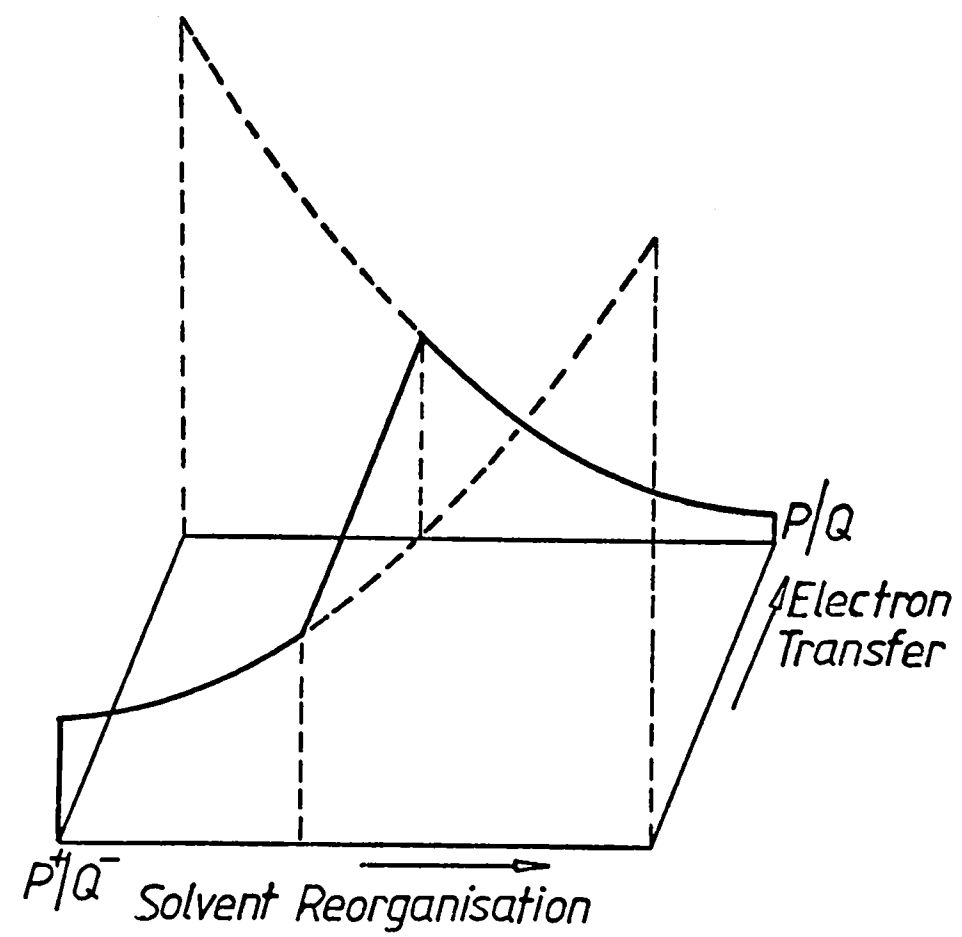

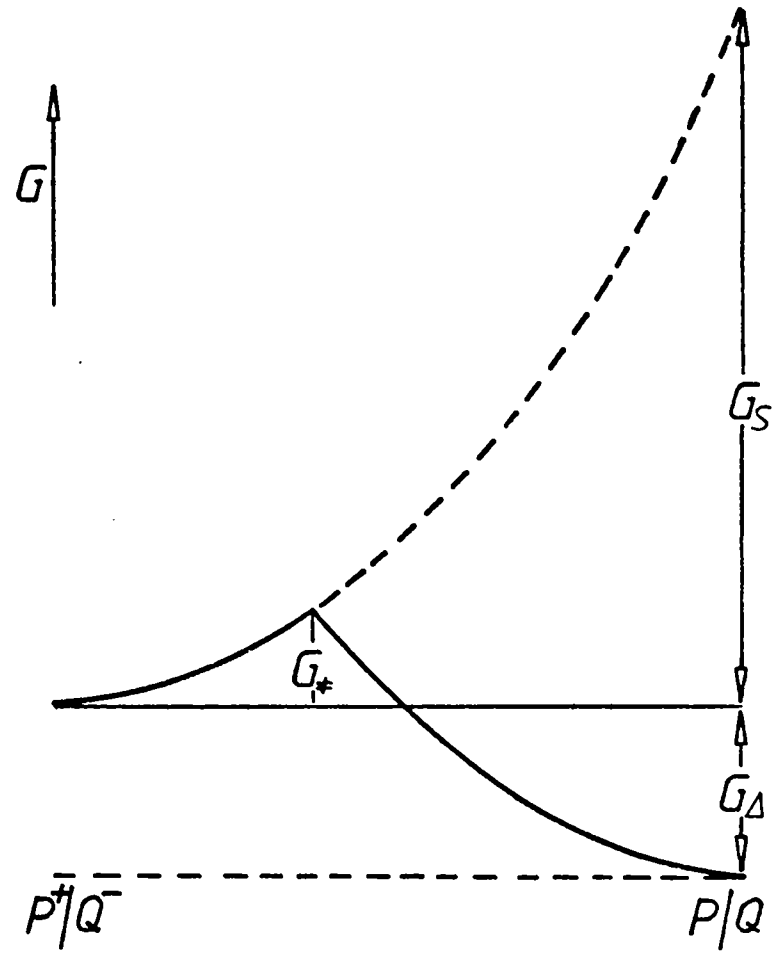

Fig 1 : 3

Solvation Energy Changes — E.T. at Isoenergetic Point

to the cross reaction.

$$\ln k_{12} = \ln(k_{11}k_{22}K_{12})^{\frac{1}{2}} + \frac{\ln k_{12}}{4 \ln \left[\frac{k_{11}k_{12}}{K_N \nu_s}\right]} \qquad (1:1)$$

$$\Delta G^{\ddagger}_{12} = \frac{\Delta G^{\ddagger}_{11}}{2} + \frac{\Delta G^{\ddagger}_{22}}{2} + \frac{\Delta G^{o}_{12}}{2}(1 + \alpha) \qquad (1:2)$$

$$\Delta S^{\ddagger}_{12} = \frac{\Delta S^{\ddagger}_{11} + \Delta S^{\ddagger}_{22}}{2}(1 - 4\alpha^2) + \frac{\Delta S^{o}_{12}}{2}(1 + 2\alpha) \qquad (1:3)$$

$$\Delta H^{\ddagger}_{12} = \frac{\Delta H^{\ddagger}_{11} + \Delta H^{\ddagger}_{22}}{2}(1 - 4\alpha^2) + \frac{\Delta H^{o}_{12}}{2}(1 + 2\alpha) \qquad (1:4)$$

$$\text{where } \alpha = \frac{\Delta G^{o}_{12}}{4(\Delta G^{\ddagger}_{11} + \Delta G^{\ddagger}_{22})} \qquad (1:5)$$

These expressions relate the kinetics and thermodynamics of the symmetrical exchange reactions to the kinetics and thermodynamics of the cross reactions. They provide a useful guide to the rates of reactions which can be expected in an ideal cell, which is now described.

THE IDEAL PHOTOGALVANIC CELL

Albery and Archer in a series of papers[9-11] have developed the theory for an ideal photogalvanic cell. The best geometry for such a cell is shown in Figure 1:1. The electrolyte is in a thin layer between the two electrodes. The top, illuminated,

electrode is transparent so that light passing through it can be absorbed as close to it as possible. This allows B to migrate the shortest possible distance to the electrode. This is important as B must reach the electrode before being destroyed by the thermal back reaction

$$A + Z \underset{k_{-2}}{\overset{h\nu,\phi}{\rightleftharpoons}} B + Y \qquad (1:6)$$

The thermodynamic equilibrium lies heavily in favour of A and Z. The thermal back reaction simply generates heat in the solution and makes no contribution to the electrical power output.

Having generated B and Y, with quantum efficiency ϕ, it is important that they migrate to opposite electrodes and react there. In such a cell the concentration of electrolyte is high so that there is no electric field, as in a photovoltaic cell, to separate B and Y. (Moreover in most of the systems studied so far B and Y have the same sign charge so that an electric field would not direct them to different electrodes.) The only transport mechanism is thus diffusion, and B and Y are equally likely to diffuse to either electrode. The electrodes must therefore discriminate between the two couples. There are sixteen different combinations in which the two couples are either active (reversible) or inactive (irreversible) at the two electrodes. Four of these are represented in Table 1:1. Of the twelve cases not shown eight are when both couples are irreversible at one or both electrodes. These are rejected as no current can pass

TABLE 1:1

Photogalvanic cells with reversible (R) and irreversible (I) electrode kinetics

Couple	Illuminated Electrode A/B	Illuminated Electrode Y/Z	Dark Electrode A/B	Dark Electrode Y/Z	
Case 1	R	R	R	I	Reject
Case 2	R	I	R	I	Concentration Cell
Case 3	R	I	I	R	Differential Electrode Kinetics (A)
Case 4	R	I	R	R	Differential Electrode Kinetics (B)

and thus no power can be produced. The other four, in which the Y/Z couple is reversible at both electrodes are rejected as no voltage is produced. The reason for this is that it transpires that for an efficient cell $[B] \ll [Z] \approx [Y]$ in the light and $[B] = 0$ in the dark. The concentrations of Y and Z are thus little different at light and dark electrodes and, as they determine the potential, no voltage is developed.

Considering now the four remaining cases in Table 1:1

Case 1: This is rejected as both couples are reversible at the illuminated electrode. The electrode will simply catalyse the homogeneous back reaction with the generation of heat and no net electron transfer.

$$A + Z \underset{}{\overset{h\nu}{\rightleftharpoons}} B + Y \quad \phi$$ In solution

$$B \xrightarrow{+ e^-} A$$

$$Y \xrightarrow{- + e^-} Z$$

$$B + Y \qquad A + Z$$ At the electrode.

Case 2: These are the conditions for a photogalvanic concentration cell for the A/B couple. Calculations by Albery and Archer[12] show that, although a respectable potential can be generated at open circuit, on load only $\sim RT/F = 59$ mV can be obtained. This is because, at open circuit, a large concentration difference in B between the two electrodes can be maintained. But as soon as a current is passed B is produced at the back electrode and the difference is greatly reduced. The conversion

efficiency for photons to electrons passing around the external circuit, $N_{h\nu}$, (the photoelectrochemical collection efficiency) is also low $\sim 0.3\phi$. The maximum efficiency of such a cell would be <0.3% which is much too low to be of any practical use.

Case 3: This represents the best system in which the electrode can differentiate between the two couples and thus set up the boundary conditions needed to separate B and Y. A respectable potential can be developed $\sim (E^{o}_{A/B} - E^{o}_{Y/Z}) = \Delta E$ under load, and $N_{h\nu}$ approaches ϕ. This leads to a maximum possible efficiency of 18% for the conversion of sunlight to electrical power, although, as will be discussed in the next section, a more realistic figure might be half that.

Case 4: This also represents a solution as good as Case 3, as the illuminated electrode can differentiate between the two couples, and the dark electrode potential is still determined by the Y/Z couple because no B reaches this electrode as it is destroyed by Y before it can diffuse across the cell.

CALCULATION OF EFFICIENCY OF AN IDEAL PHOTOGALVANIC CELL

Using Fick's second law of diffusion across a unit area

$$\frac{\partial c}{\partial t} = D \frac{\partial^2 c}{\partial x^2} \qquad (1:7)$$

where c is the concentration

t is the time

x is the distance

and D is the diffusion coefficient.

A differential equation describing the mass transport of B in the cell can be formulated.

A steady state is invoked so that $\frac{\partial c}{\partial t} = 0$ and the equation for B is

$$D \frac{\partial^2 [B]}{\partial x^2} + \phi I \varepsilon [A] - k_{-2}[B][Y] = 0 \qquad (1:8)$$

Diffusion — Photochemical Generation — Thermal Back Reaction

where D is the diffusion coefficient of B in $cm^2\ s^{-1}$

x is the distance from the illuminated electrode in cm.

[A],[B] and [Y] are in mol cm^{-3}.

I is the light intensity in moi photons $cm^{-2}\ s^{-1}$

ε is the extinction coefficient of A on the natural logarithmic scale

and k_{-2} is the rate constant for the reaction of B and Y in $M^{-1}\ s^{-1}$

There is no convective mass transport as it is assumed that the electrode spacing is too small to allow natural convection.

This assumption is justified by the conditions found below for maximum efficiency.

The light intensity is given by

$$\frac{\partial I}{\partial x} = - \varepsilon [A] I \qquad (1:9)$$

with $I = I_o$ at $x = 0$.

It is convenient at this stage to introduce several characteristic lengths.

1) The Cell Length, X_L, is the distance between the electrodes.

2) The Optical length, X_ε, is defined as

$$X_\varepsilon = (\varepsilon . [A]_D)^{-1} \qquad (1:10)$$

where $[A]_D$ is the concentration of A in the dark. Most of the light is absorbed in this length as the cell is not bleached. i.e. the concentration of A is little changed in the light.

3) The Generating length, X_G, is defined as

$$X_G = (D/\phi \varepsilon I_o)^{\frac{1}{2}} \qquad (1:11)$$

and is the average distance which A diffuses in a light intensity, I_o, before conversion to B.

4) The reaction length, X_k, is defined as

$$X_k = (D/k_{-2}[Y])^{\frac{1}{2}} \qquad (1:12)$$

and is the average distance which B diffuses before conversion to A.

The solution of equations (1:8) and (1:9) for the maximum power per unit area of cell, W_{max}, is not simple because of the number of independent variables. However it can and has[11] been done and the result is

$$W_{max} = 0.8F\phi I_o[|\Delta E| + \frac{RT}{F}(\ln \frac{\phi I_o \varepsilon}{k[Z]} - 1.6)] \qquad (1:13)$$

$$\simeq 0.8F\phi I_o \Delta E \qquad (1:14)$$

where k is the pseudo first order rate constant for the reaction of B and Y

$$k = k_{-2}[Y] \qquad (1:15)$$

The conditions for this maximum are that

$$20X_\varepsilon \approx X_k \approx 2X_G < X_L \qquad (1:16)$$

These conditions for the characteristic lengths have sensible physical explanations. The most important is that $X_\varepsilon << X_k$.

This is to ensure that the thermal back reaction does not destroy the photogenerated B before it can diffuse back to the illuminated electrode. The condition for X_G ensures that the solution does not bleach. If this happens there is no longer any A present to absorb the light and the cell produces no power. X_L is the longest length and this means that the dark electrode does not interfere with the trapping of the photons and the reaction of B on the illuminated electrode.

If a typical value for the God-given parameter, I_o, is inserted

$$I_o = 1.6 \times 10^{-3} \text{ mol photons } m^{-2} \quad [13]$$

and optimistic values for ΔE and ϕ are used

$$\Delta E = 1.1V \quad \text{and} \quad \phi = 1$$

then $$W_{max} = 140 \text{ W } m^{-2}$$

which corresponds to a conversion efficiency of 18%. In order to achieve this very good conversion efficiency quite severe constraints are imposed by equation (1:16). For the best possible values of $D = 10^{-5} \text{ cm}^2 \text{ s}^{-1}$ and $\varepsilon = 10^8 \text{ cm}^2 \text{ mol}^{-1}$

$$X_G \sim 10^{-3} \text{ cm} \qquad (1:17)$$

and thus $$X_\varepsilon \sim 10^{-4} \text{ cm} \qquad (1:18)$$

giving $$[A] \sim 0.1 \text{ M}.$$

A must therefore be quite soluble although this is by no means a prohibitive figure.

A much more difficult condition is found for the electrochemical rate constant, k', for the conversion of B to A on the illuminated electrode, which must satisfy the condition

$$k' > D/X_\epsilon \sim 10^{-1} \text{ cm s}^{-1} \qquad (1:19)$$

This is unlikely to be fulfilled as most electrochemical rate constants are $<10^{-2}$ cm s^{-1}.

Another constraint is imposed by the value of X_G of 10^{-3} cm which means that the kinetics of the reaction of B and Y must satisfy the condition

$$k_{-2}[Y] < 40 \text{ s}^{-1} \qquad (1:20)$$

and the concentration of Y must be at least twice the photogenerated concentration of B to ensure that there is no concentration polarisation at the dark electrode so that the concentration relationships are:

$$[Y] > 2[B] \sim 10^{-2}[A] \sim 10^{-3}\text{M} \qquad (1:21)$$

(1:20) and (1:21) lead to

$$k_{-2} < 4 \times 10^{3} \text{ M}^{-1} \text{ s}^{-1}$$

This is a comparatively slow second order rate constant for electron transfer given the very high driving force (ΔE = 1.1V) for the reaction.

Figure 1:4 shows the concentration profiles for the ideal cell (note the change in scale between [B] and the other components). The light is absorbed in a very thin layer close to the top electrode and most of the B generated diffuses to and reacts at the electrode. The Y/Z couple must be inactive at the front electrode and both diffuse across the cell. Because Y and Z must carry the current across a much greater distance

$$20\ X_{\varepsilon} \sim X_{L}$$

the concentration difference, caused by the constant concentration gradient, is much greater than for B.

The concentration of A is affected little by the light and remains at its high value of 10^{-1} M.

Thus summarising:

1) $[A] \sim 10^{-1}$ M

2) The electrochemical rate constant for A/B on the illuminated electrode must be very rapid, $k > 10^{-1}\ s^{-1}$.

3) Despite its large driving force of 1.1 V the electron transfer between B and Y must be very slow ($k_{-2} < 4 \times 10^{3}\ M^{-1}\ s^{-1}$).

4) The electron transfer for the quenching of A^{*} and Z must be rapid so that all the photons are trapped.

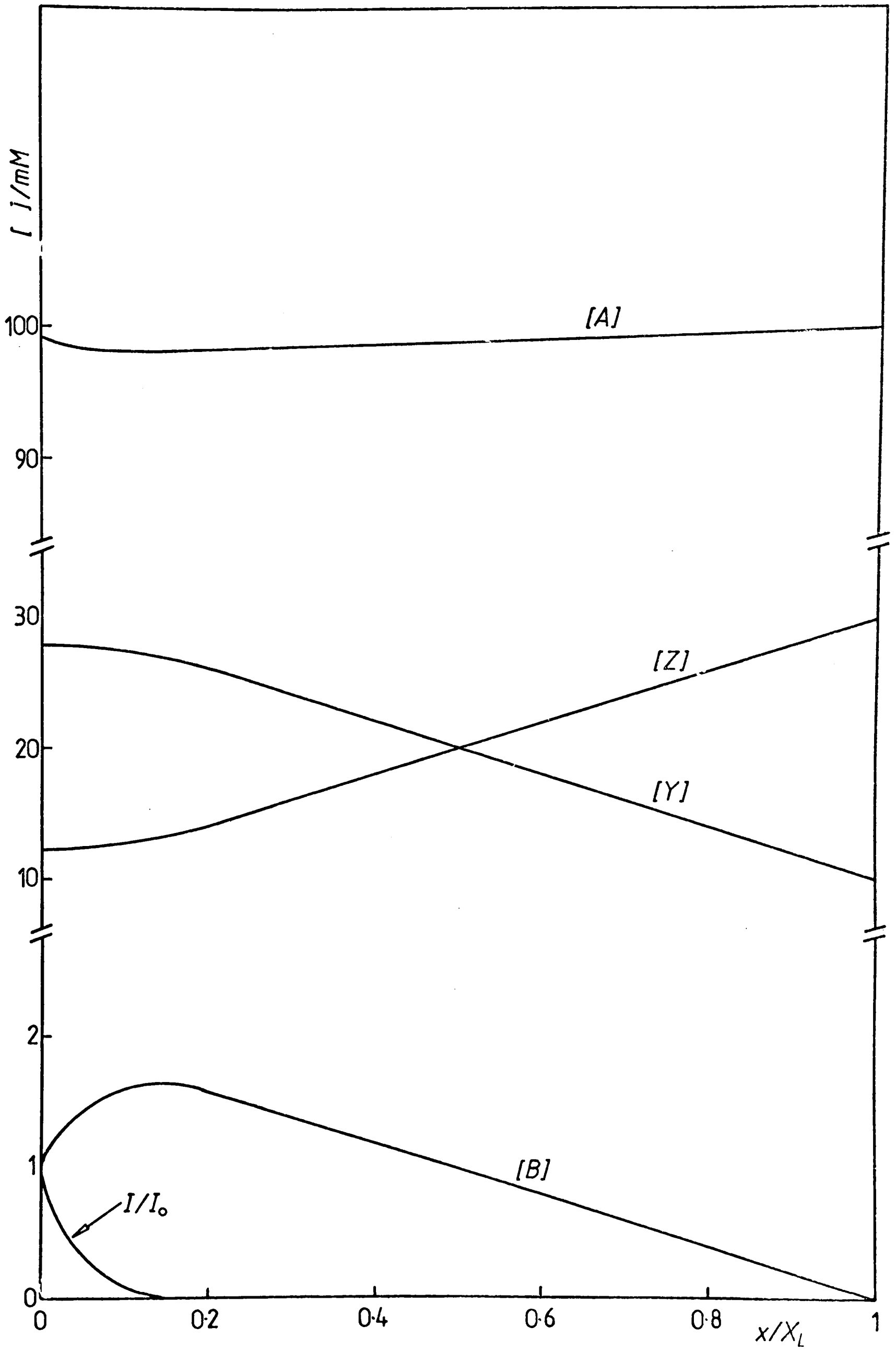

Fig 1 : 4

Concentration Profiles in a Photogalvanic Cell

Unfortunately electron transfer reactions which obey the Marcus theory are very unlikely to satisfy 3) because of the relation between the driving force of the reaction and the rate constant.

It is clear that the ideal photogalvanic cell is very difficult, if not impossible to achieve. However a relaxation of (1:16) to

$$X_\varepsilon \approx X_G \approx X_k$$

gives $[A] \sim 10^{-2}$ M

$$k' \sim 10^{-2} \text{ cm s}^{-1}$$

and $$k_{-2} < 4 \times 10^4 \text{ M}^{-1} \text{ s}^{-1}$$

which greatly reduces the difficulty of meeting the conditions and leads to a drop in efficiency of only a factor of $\frac{1}{2}$ to 9%.

PHOTOGALVANIC SYSTEMS

There are many systems for which there is evidence of electron transfer quenching. The two which have attracted the most attention, because their properties are closest to ideal photogalvanic systems are

1) The complexes $Ru(II)L_3$ where L is a 2,2'bipyridyl or a 1:10 phenanthroline derivative (Fig 1:5) and

2) the thiazine dyes and in particular thionine (Figure 1:5).

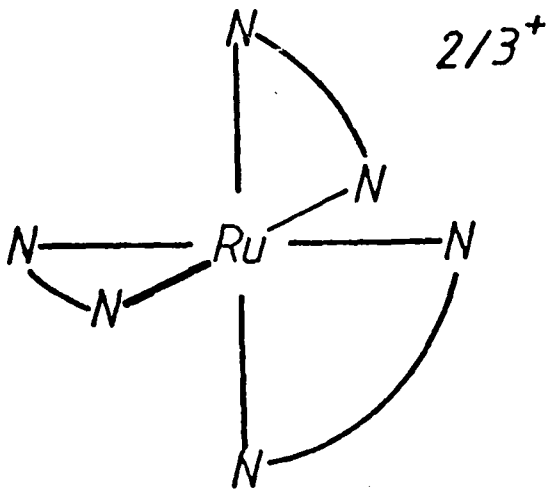

bipy

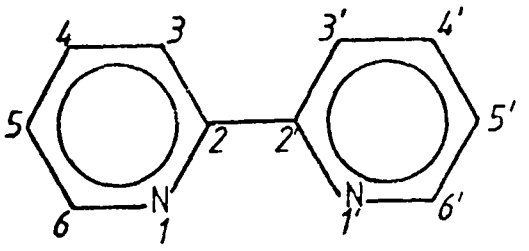

phen

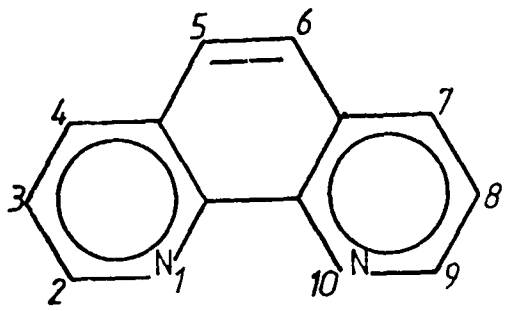

biquinoline

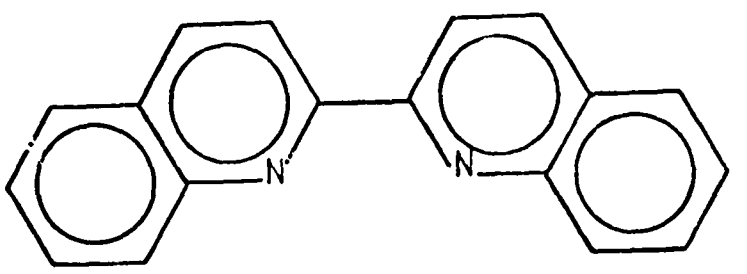

Thionine

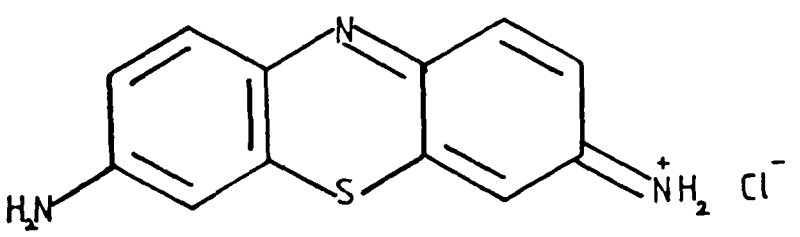

Fig 1 : 5

Photogalvanic Systems

Their properties with reference to a photogalvanic cell are now reviewed.

Ruthenium Systems

a) Absorption and the excited state

$Ru(bipy)_3Cl_2$ was first synthesised in 1936 by Burstall[14]. Figure 1:6 shows the visible absorption and emission[15] spectra for the compound. After some debate[16-19] the band at 452 nm has been assigned as a $d \rightarrow \pi^*$ charge transfer transition. After rapid thermal equilibration and intersystem crossing of high efficiency this gives rise to an excited state of emission lifetime 0.6 μs[20] (at room temperature). This excited state is described[21] as a group of closely spaced levels with no well defined spin label[22] due to strong spin orbit coupling. This explains the anomalous lifetime of the state which is intermediate between that of spin allowed fluorescence ($<10^{-8}$s) and spin forbidden phosphorescence ($>10^{-3}$s).

The absorption characteristics of the $Ru(II)L_3$ are not ideal. The decadic extinction coefficients lie in the range $1 - 3 \times 10^4$ M^{-1} cm^{-1} which is a factor of 5 short of the theoretical ideal of $\sim 10^5$ M^{-1} cm^{-1}. The wavelength of the absorption is also not perfect as the band covers only a small proportion of the solar spectrum. However some modificiation of the absorption band has proved possible. Klassen[23] and Daul[24] have synthesised the biquinoline complex (Figure 1:5)

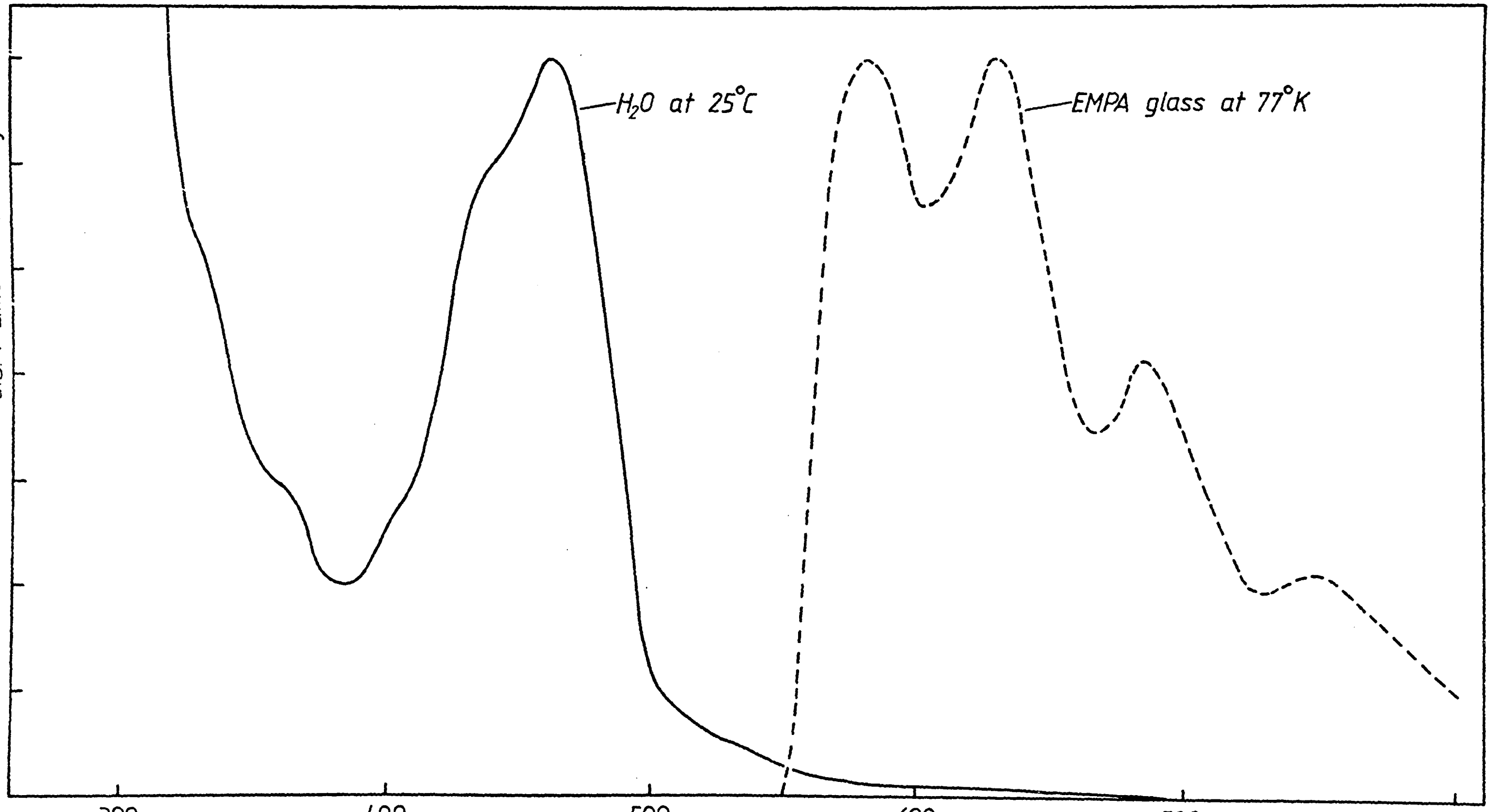

Fig 1 : 6

Absorption and Emission Spectra of $Ru(bipy)_3^{2+}$

$Ru(II)L_3$. In this complex the d orbitals on the central metal atom are unaffected in energy but there is a large drop in the π^* energy of the ligand due to the greater delocalisation. Thus the absorption maximum for $Ru(II)bipy)_3$ is at 523 nm[23].

One potentially useful feature of all the $Ru(II)L_3$ compounds is that higher energy transitions (e.g. $\pi \rightarrow \pi^*$ in the ligands) all lead to the same $d\pi^*$ excited state with high efficiency[15]. This is similar to the behaviour in semiconductor solar cells where the whole absorption band leads to the same energy $e^- - p^+$ pairs.

b) Quenching

Electron transfer quenching of $Ru(II)(bipy)_3^*$ was first observed by Gafney and Adamson[25] and since then a great many electron transfer quenchers for this excited state have been found. The excited state has properties of both the strongly reducing $Ru(I)(bipy)_3$, due to the electron in its π^* orbital, and of the strongly oxidising $Ru(III)(bipy)_3$, due to the hole in its d orbitals. Thus the electrode potentials are (v N.H.E.)

$Ru(III)L_3/Ru(II)L_3$ + 1.26 V [26]

$Ru(II)L_3^*/Ru(I)L_3$ + 0.84 V [27,28]

$$Ru(III)L_3/Ru(II)L_3^* \qquad -0.84\ V^{26}$$

$$Ru(II)L_3/Ru(I)L_3 \qquad -1.26\ V^{24}$$

(where L = bipy)

$Ru(II)L_3$ therefore shows both reductive quenching with, for example, Eu^{2+} aq.[30] and $Fe(CN)_6^{4-}$ [28] and oxidative quenching with Fe^{3+} aq.[31], Th^{3+} aq.[32], Eu^{3+} aq.[26], Cu^{2+} aq.[33], paraquat[31], and many nitroaromatics[34].

The reaction with Fe^{3+} aq.

$$Ru(II)L_3^* + Fe(III) \xrightarrow{k_q} Ru(III)L_3 + Fe(II) \quad k_q = 2.7\times10^9\ M^{-1}s^{-1}\ ^{26}$$

where L = bipy

has been most extensively studied and it is this system which is studied in this thesis.

The most important feature for a photogalvanic cell is that the overall quantum yield, ϕ, for the whole process

$$Ru(II)L_3 + Fe(III) \xrightarrow{h\nu} Ru(III)L_3 + Fe(II) \qquad \phi$$

should be as near unity as possible. This depends on the efficiency of all the individual steps.

$$Ru(II)L_3 \xrightarrow{h\nu} Ru(II)L_3^* \qquad (1:17)$$

$$Ru(II)L_3^* \longrightarrow Ru(II)L_3 + h\nu \qquad k_r \qquad (1:18)$$

$$Ru(II)L_3^* \longrightarrow Ru(II)L_3 + \text{heat} \qquad k_\Delta \qquad (1:19)$$

$$Ru(II)L_3^* \xrightarrow{Fe(III)} Ru(III)L_3 \qquad k_q \qquad (1.20)$$

$$Ru(II)L_3^* \xrightarrow{Fe(III)} Ru(II)L_3 + \text{heat} \qquad k'_\Delta \qquad (1:21)$$

k_Δ is small as the efficiency of (1:20) is found to be 0.8 ± 0.2[26]. The combined processes (1:18) and (1:19) give rise to the lifetime τ (~0.6μS) and thus to give a high yield of Ru(III).

$$k_q[Fe(III)] >> 1/\tau.$$

or $[Z] \equiv [Fe(III)] >> 1/\tau k_q = 6 \times 10^{-4}$ M.

This is easily fulfilled as [Z] must be greater than $\sim 10^{-2}$M to carry the current in a photogalvanic cell.

(c) Back reaction kinetics

The electron transfer between $Ru(III)(bipy)_3$ and Fe(II)

$$Ru(III)(bipy)_3 + Fe(II) \underset{}{\overset{k_{-2},K}{\rightleftharpoons}} Ru(II)(bipy)_3 + Fe(III)$$

k_{-2} in 1.0 M $HClO_4$ = 1.0 x 10^6 M^{-1} s^{-1} [31]

has been the subject of a number of studies by both stopped flow[26] and flash photolysis[31]. In general the reactions for various $Ru(III)L_3$ complexes (where L are substituted bipyridyl and 1:10 phenanthroline derivative) are rather faster than required for an ideal cell ($<4 \times 10^3\ M^{-1}\ s^{-1}$). In this thesis the reactions are studied further in order to predict ways in which the systems might be modified to slow down this fast loss process. Further discussion of this reaction is thus left until the end of the thesis.

Thionine Systems:

(a) Absorption and Emission

An absorption spectrum for Thionine is shown in Figure 1:7. The absorption process is a singlet to singlet transition.

$$Th \xrightarrow{h\nu} {}^1Th^*$$

The excited singlet has a lifetime of 0.66 μs[35] and converts with high efficiency to the triplet

$${}^1Th^* \xrightarrow{k_f} Th + h\nu$$

$${}^1Th^* \xrightarrow{k_{ISC}} {}^3Th$$

where $k_{ISC} >> k_f$.

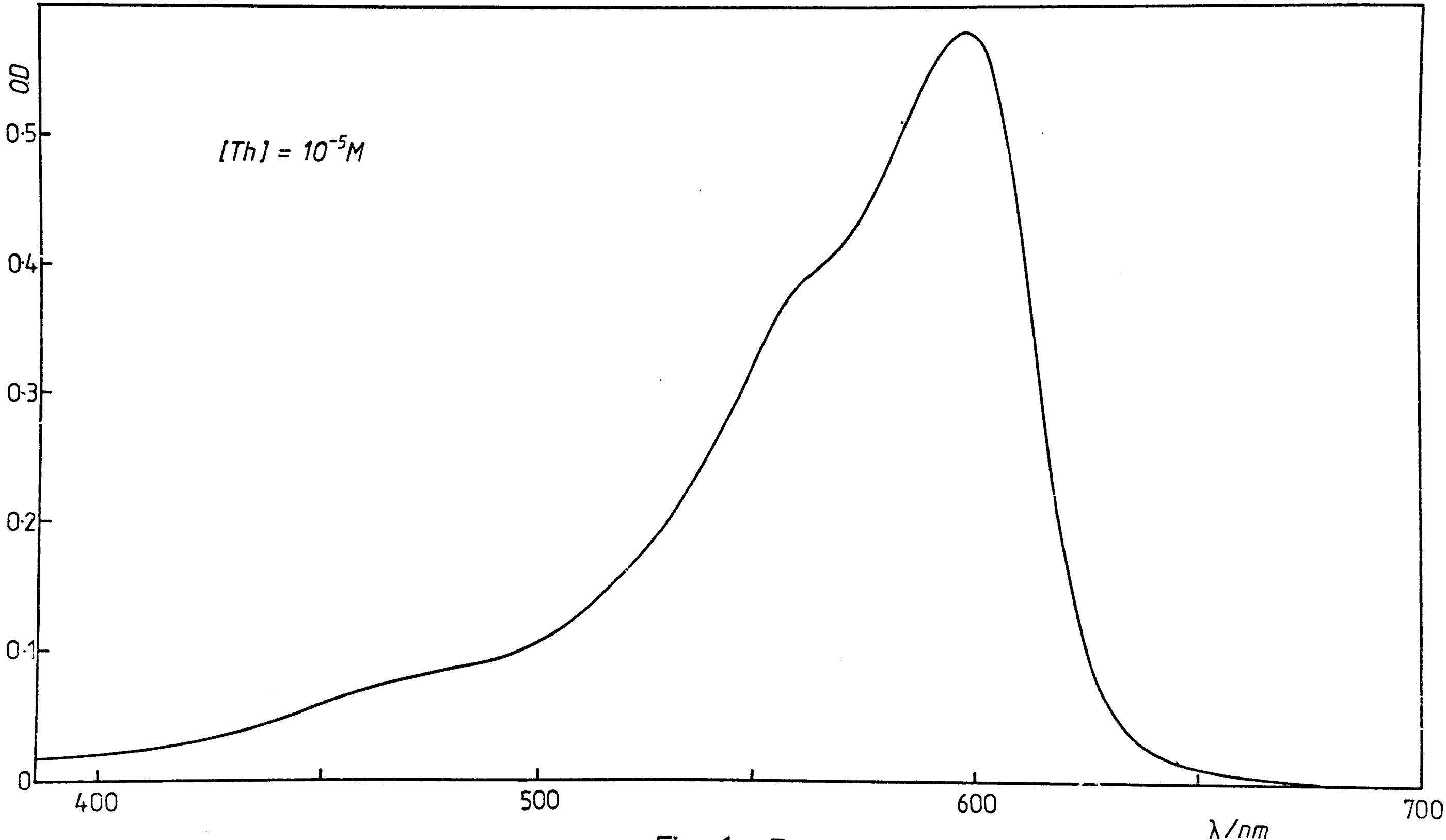

Fig 1 : 7

Absorption Spectrum of Thionine

The triplet has a lifetime of $20\,\mu s$[35] and it is the triplet which is electron transfer quenched.

There are three main problems with the absorption of Th.

1) Thionine is only sparingly soluble (~ 1 mM) so that despite its high extinction coefficient ($\varepsilon_{max} = 5.8 \times 10^4$ at 597 nm) the optical length cannot be reduced enough for a photogalvanic cell.

2) A photogalvanically inactive dimer is formed at relatively low concentrations

$$2\ Th \underset{}{\overset{K}{\rightleftharpoons}} [Th]_2 \qquad K = 750\ M^{-1}$$ [36]

this feature is common to many of the thiazine dyes.

3) The absorption band is typical of an organic dye and covers only a small part of the solar spectrum.

An attempt to solve 1) and 2) by synthesising sulphonated thionines has been made by Suoto Bachiller[37] in this laboratory. Some measurements on the properties of these sulphonated thionines are described in this thesis.

As yet no systematic work has been done to solve 3) by modifying the thionine chromophore although some work has been done by Lichtin[38] on dye sensitisation of the ferrous/thionine system.

(b) Quenching

Both the singlet and the triplet of thionine have been shown to be quenched by Fe(II)

$$^1Th^* + Fe(II) \xrightarrow{^1k_q} \text{Products} \qquad ^1k_q = 4 \times 10^9\ M^{-1}\ s^{-1}\ [35]$$

$$^3Th^* + Fe(II) \xrightarrow{^3k_q} S^{\cdot} + Fe(III) \qquad ^3k_q = 3 \times 10^7\ M^{-1}\ s^{-1}\ [35]$$

where $S^{\cdot}$ is the semithionine radical.

It is not clear yet whether the singlet quenching is by electron transfer or energy transfer, however the very short lifetime of the singlet allows efficient conversion to the triplet and subsequent reductive quenching by Fe(II). The overall quantum efficiency for the production of semithionine has been measured by Harriman[39] and in this laboratory[40] and is 0.55; lower than the ideal of 1.

(c) Back Reaction Kinetics

The thermal back reaction for thionine is complicated by the semithionine intermediate which dismutates rapidly and reacts with Fe(III) and possibly Fe(II).

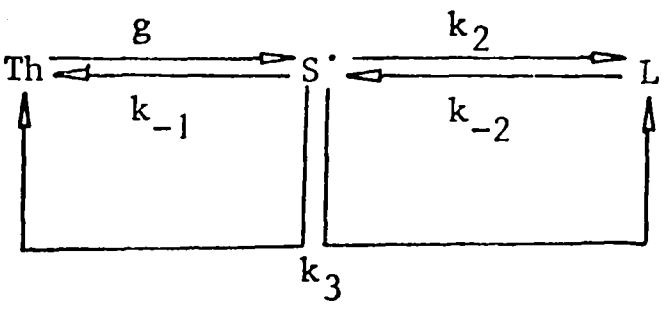

where $k_{-1} = 7.9 \times 10^4\ M^{-1}\ s^{-1}$ [35]

$k_{-2} = 2.6 \times 10^2\ M^{-1}\ s^{-1}$ [35]

$k_3 = 2.4 \times 10^9\ M^{-1}\ s^{-1}$ [35]

and Th is thionine, S$^{\cdot}$ is semithionine and L is leucothionine.

However a simplification is possible because at moderate light intensities when an appreciable quantity of S$^{\cdot}$ is produced the dimutation is so rapid that most of the photoproduct is present as L. k_{-2} thus becomes the important back reaction process. The reaction is slow enough to meet the requirements of a photogalvanic cell and it and the back reactions of some modified thionines are investigated in this thesis.

THE EXPERIMENTS IN THIS THESIS

Previous photogalvanic investigations in this laboratory[40-41] have centred round the use of the optical rotating disc electrode (ORDE). The electrode is a semi-transparent conducting film deposited on the end of a quartz rod. Contact is made to the side of the rod, which may be rotated. Light is shone down the rod and through the electrode and is thus absorbed as close as is possible to the electrode, where the photoproducts may be detected. This configuration allows great sensitivity by reducing the distance which short-lived intermediates must migrate to an electrode. It has the great advantage that the controlled mass transport of the rotating disc allows the flux

of photoproducts to be calculated.

Three types of experiment are described in this thesis.

i) A new ORDE apparatus was designed and built. It was then used to investigate a number of $Ru(II)L_3$ complexes.

ii) A technique first used by Perone[42-49] was developed to measure the rate of the thermal back reaction using a stationary optical disc electrode. The technique is essentially flash photolysis with electrochemical detection. A short flash of light was passed down the electrode and the photoproducts were detected as a function of time by following the current at the electrode. The technique was used to investigate a number of $Ru(II)L_3$ complexes and some of the modified thionines synthesised by Suoto Bachiller.

iii) Further investigations of the thermal back reaction were carried out using the stopped flow technique

CHAPTER 2

THEORY

This chapter begins with a brief description of the theory for the rotating disc electrode, R.D.E. This is followed by more detailed accounts of the optical rotating disc electrode, O.R.D.E., and flash electrolysis at an optical disc electrode.

THE ROTATING DISC ELECTRODE

The mass transport to a rotating disc electrode has been described by many workers[50-52]. When a disc electrode is rotated a steady flow pattern is imposed on the solution as shown in Figure 2:1a. The system is described in cylindrical polar coordinates ϕ, r and x. The solutions to the velocity components v_x, v_r and v_ϕ found by von Karman[50] are

$$v_x = (\omega\nu)^{\frac{1}{2}} X(x/X_{Hy}) \qquad (2:1)$$

$$v_r = r\omega\, R(x/X_{Hy}) \qquad (2:2)$$

$$v_\phi = r\omega\, \Phi(x/X_{Hy}) \qquad (2:3)$$

where v is in cm s^{-1}

ω is the rotation speed in radians s^{-1}

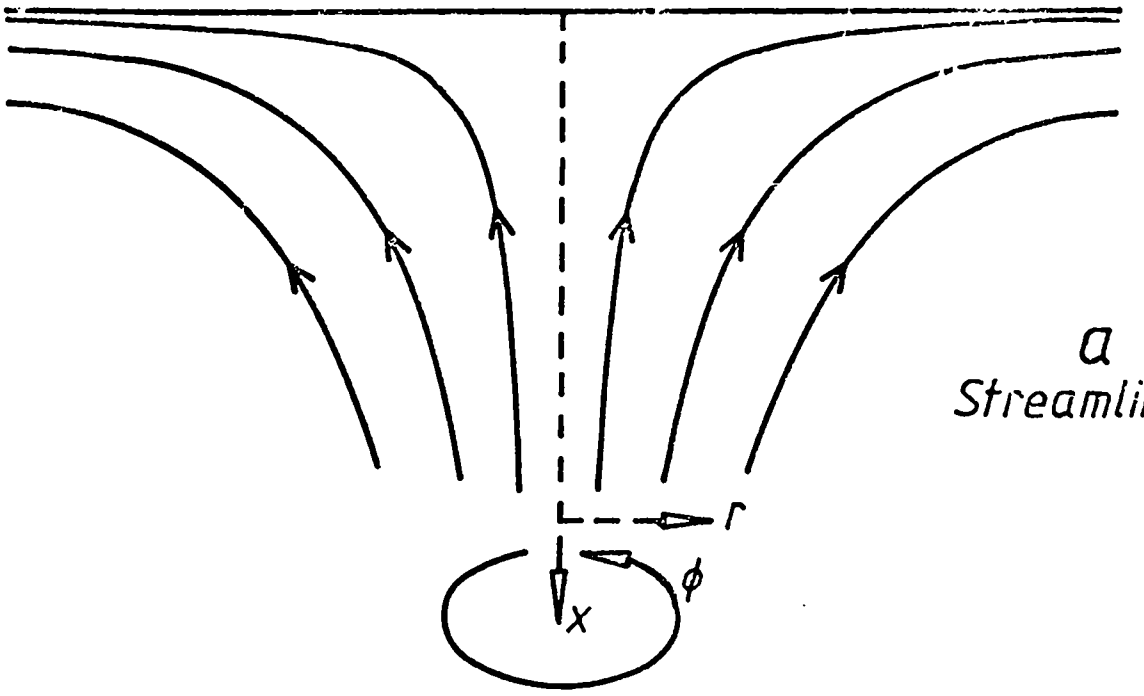

a
Streamlines

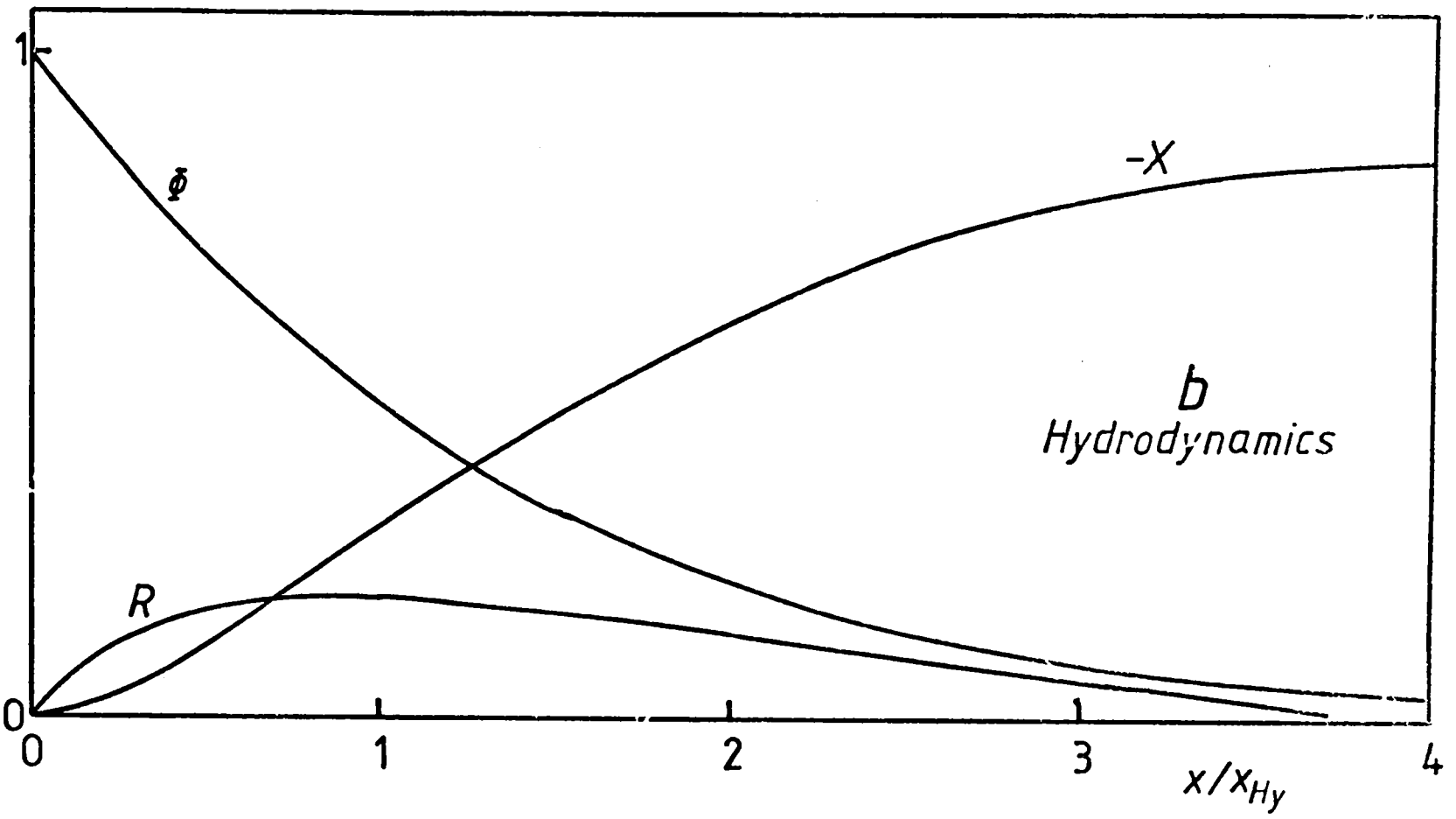

b
Hydrodynamics

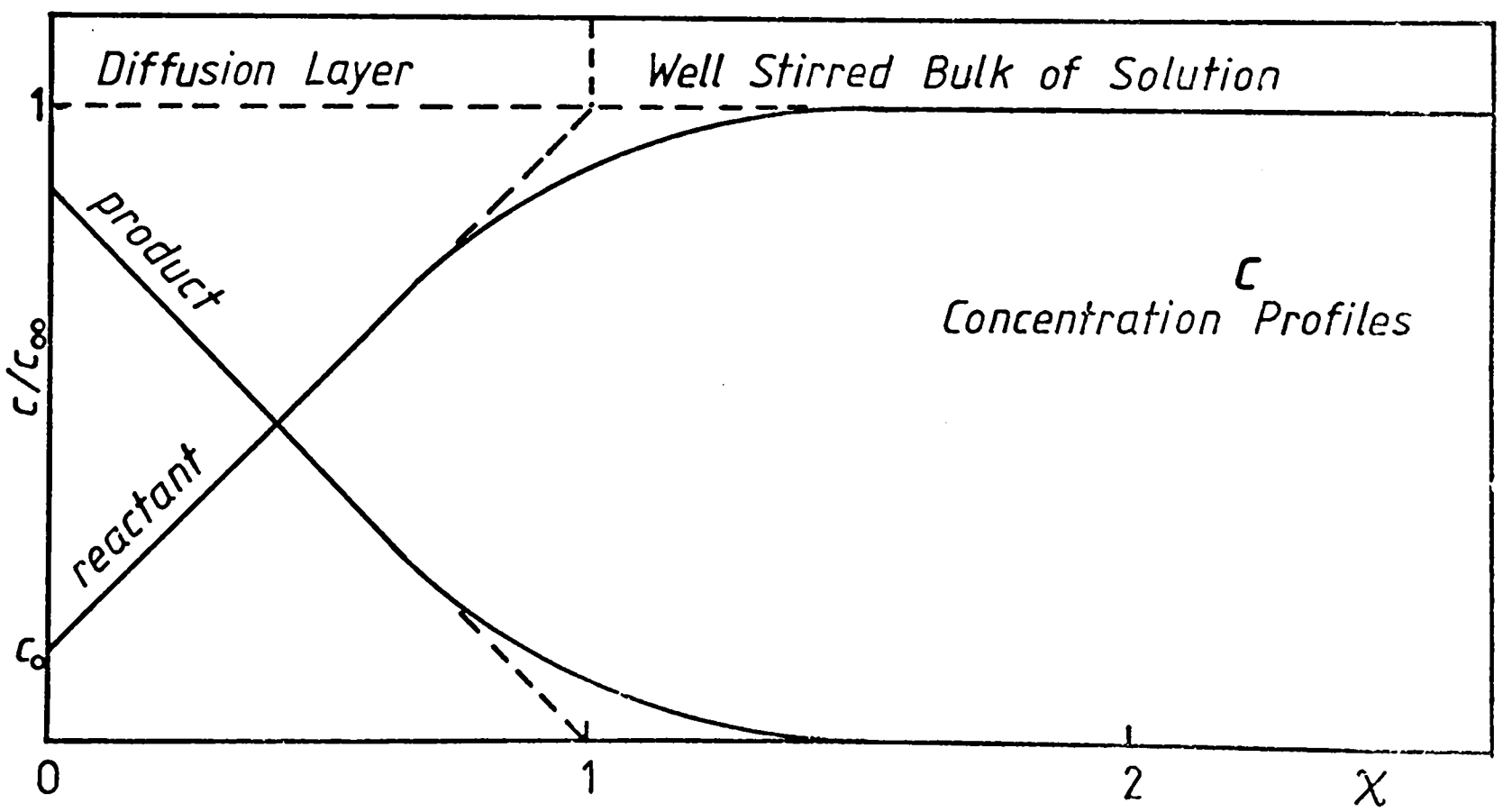

c
Concentration Profiles

Fig 2 : 1

The Rotating Disc Electode

$\nu(= \eta/\rho)$ is the kinematic viscosity in $cm^2\ s^{-1}$

X, R and Φ are functions of x/X_{Hy}

X_{Hy} $(= \sqrt{\nu/\omega})$ is the thickness of the hydrodynamic layer in cm.

X, R and Φ are shown in Figure 2:1b. The most important feature of these solutions is that v_x is independent of r which means that transport of material to the disc is uniform. This is not an essential feature of an electrode; the tube and the ring electrodes both have non uniform accessibility. However it simplifies the theoretical treatment for the RDE and greatly simplifies the treatment for the ORDE.

The solution of the hydrodynamic flow allowed Levich[53] to solve the mass transport to the electrode. The full differential equation is

$$\frac{\partial c}{\partial t} = D\left(\frac{\partial^2 c}{\partial r^2} + \frac{1}{r}\frac{\partial c}{\partial r} + \frac{1}{r^2}\frac{\partial^2 c}{\partial \phi^2} + \frac{\partial^2 c}{\partial x^2}\right) - v_r \frac{\partial c}{\partial r} - \frac{v_\phi}{r}\frac{\partial c}{\partial \phi} - v_x \frac{\partial c}{\partial x} \qquad (2:4)$$

where c is the concentration in mol cm^{-3}

t is in s

D is the diffusion coefficient in $cm^2\ s^{-1}$.

This equation is simplified for the RDE by the following conditions

1) A steady state is achieved so that $\frac{\partial c}{\partial t} = 0$.

2) As the system has an axis of symmetry all the velocity components are independent of ϕ. Thus $\frac{\partial c}{\partial \phi} = 0$.

3) $\frac{\partial c}{\partial r}$ must be zero as $r \to 0$. If not the term $\frac{1}{r}\frac{\partial c}{\partial r} \to \infty$ as $r \to 0$, which is impossible. And, as v_x is independent of r, $\frac{\partial c}{\partial r} = 0$ for all r.

This simplifies equation (2:4) to

$$D \frac{\partial^2 c}{\partial x^2} = v_x \frac{\partial c}{\partial x} \qquad (2:5)$$

There is one important boundary condition for this equation, that $c \to c_\infty$ as $x \to \infty$, where c_∞ is the concentration of species in the bulk of the solution. Solving for the surface flux, j, gives

$$\frac{j}{D} = \left(\frac{\partial c}{\partial x}\right)_{x=0} = \frac{c_\infty - c_o}{x_D} \qquad (2:6)$$

where $$X_D = 0.643\, W^{-\frac{1}{2}}\, \nu^{1/6}\, D^{\frac{1}{2}} \qquad (2:7)$$

W is the rotation speed in Hz

j is in mol cm^{-2} s^{-1}

and c_o is the surface concentration in mol cm^{-3}.

The flux must be equal to the rate of reaction at the surface so that

$$j = k' c_o \qquad (2:8)$$

where k' is the electrochemical rate constant in cm s^{-1}.

Defining the diffusion rate constant k_D as

$$k_D = \frac{D}{X_D} \qquad (2:9)$$

where k_D is in cm s^{-1}.

Substitution in (2:6) gives

$$\frac{1}{j} = \frac{1}{k' c_\infty} + \frac{1}{k_D c_\infty} \qquad (2:10)$$

Several important relations for the current, i, at the RDE may now be derived, as

$$i = n F A j \qquad (2:11)$$

where

i is in Amps

n is the number of electrons transferred

F is the Faraday in C mol^{-1}

and A is the electrode area in cm^2.

1) The limiting current : When $k' >> k_D$ the current is limited by the diffusion to the electrode and $c_o \rightarrow 0$. Equation (2:10) becomes

$$\frac{1}{j} = \frac{1}{k_D c_\infty} \tag{2:12}$$

or

$$i_L = 1.554\ nFA\ c_\infty \nu^{-1/6} D^{2/3} W^{\frac{1}{2}} \tag{2:13}$$

2) The current-voltage curve: For the system

$$O \underset{-e^-,\ k'_{-1}}{\overset{e^-,\ k'_1}{\rightleftharpoons}} R \tag{2:14}$$

The surface rate constants are given by

$$k'_1 = k'_o\, e^{-\alpha(E-E')F/RT} \tag{2:15}$$

$$k'_{-1} = k'_o\, e^{+\beta(E-E')F/RT} \tag{2:16}$$

where E' is the formal electrode potential in V

E is the potential of the electrode in V

k'_o is the surface rate constant when $E = E'$

and α and β are the transfer coefficients. At any potential E for the simple one electron system $\alpha+\beta = 1$, by the principle of

microscopic reversibility.

a) Reversible systems : when $k'_o >> k_D$ the electron transfer at the surface of the electrode is fast enough to maintain thermodynamic equilibrium. The surface concentrations are thus given by the Nernst equation

$$E = E' + \frac{RT}{nF} \ln \frac{[O]_o}{[R]_o} \qquad (2:17)$$

Taking $[O]_\infty = c$ and $[R]_\infty = 0$

then $[O]_o + [R]_o = c$

and $$E = E' + \frac{RT}{nF} \ln \left(\frac{[O]_o}{c - [O]_o} \right) \qquad (2:18)$$

and substituting equations (2:6) and (2:12) in (2:18)

$$E = E' + \frac{RT}{nF} \ln \left(\frac{i_L}{i} - 1 \right) \qquad (2:19)$$

This equation describes the typical shape of a reversible "wave".

b) Irreversible systems : when $k'_o << k_D$ the system is termed irreversible. The exchange currents when $E = E'$ are no longer sufficient to maintain thermodynamic equilibrium at the electrode. They are very much smaller than the diffusion limited

current. In general for the steady state

$$j = k'_1[O]_o - k'_{-1}[R]_o \qquad O \rightleftharpoons R \text{ at electrode} \tag{2:20}$$

$$= k'_D([O]_\infty - [O]_o) \quad \text{Diffusion of O towards electrode} \tag{2:21}$$

$$= k'_D([R]_\infty - [O]_o) \quad \text{Diffusion of R away from electrode} \tag{2:22}$$

From equation (2:12) the limiting fluxes for O and R are

$$j_O = k_D[O]_\infty \text{ and } j_R = k_D[R]_\infty \tag{2:23}$$

Eliminating the concentrations from these five equations

$$j = \frac{j_O k'_1 - j_R k'_{-1}}{k_D + k'_1 + k'_{-1}} \tag{2:24}$$

Figure 2:2 shows a typical current voltage curve for $k'_o \ll k_D$. It is clear that, to pass a current, E must be significantly different from E'. And from equation (2:15) and (2:16) it is clear this will produce a great difference in k'_1 and k'_{-1}. This allows simplification of equation (2:24).

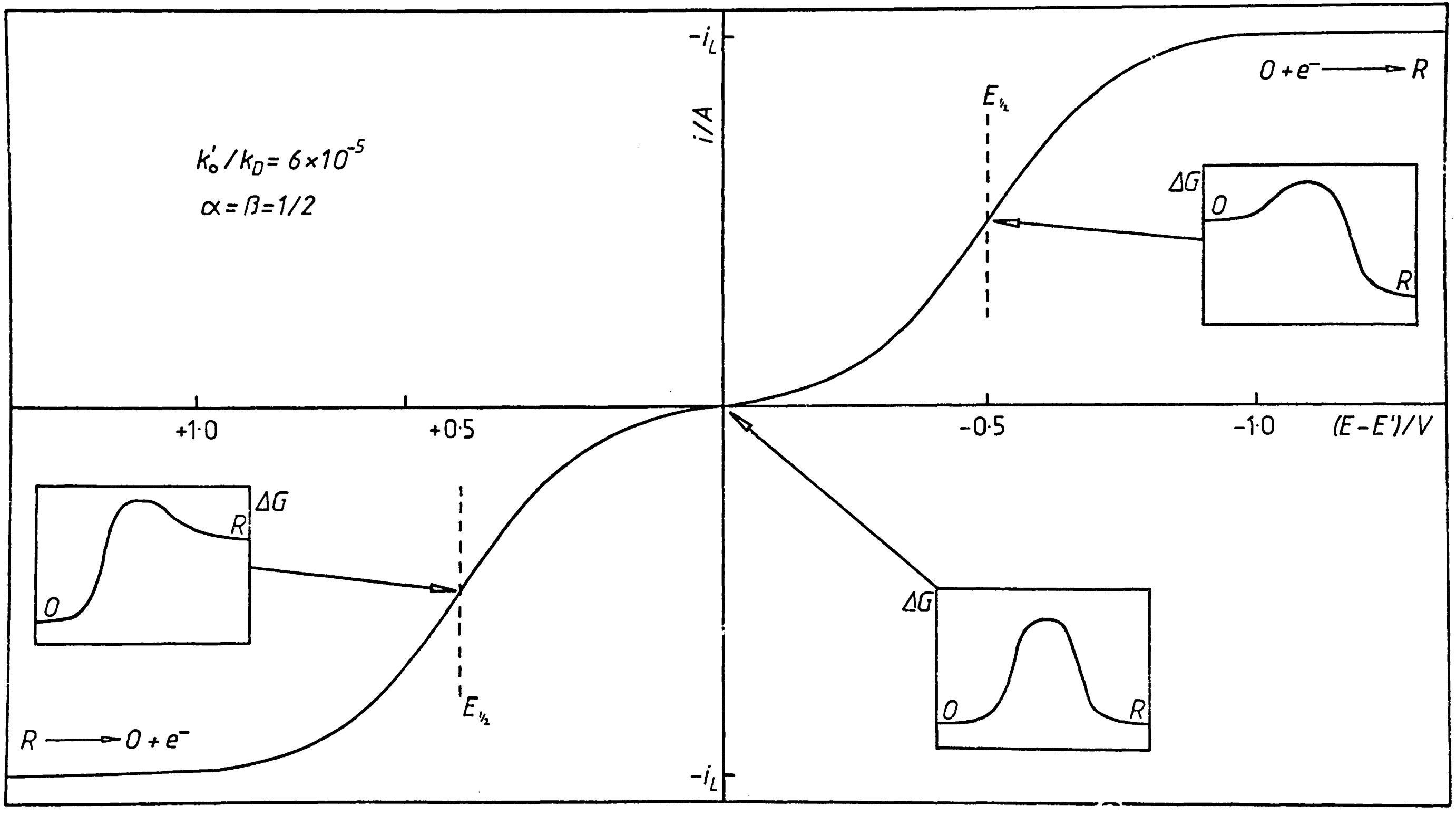

Fig 2 : 2

Irreversible Current-Voltage Curve

Taking $E < E'$

then $$k'_{-1} << k'_1$$

and equation (2:24) simplifies to

$$j = \frac{j_0 k'_1}{k_D + k'_1} \qquad (2:25)$$

or

$$\frac{j_0}{j} - 1 = \frac{k_D}{k'_1} \qquad (2:26)$$

Substituting equation (2:15) in (2:26) and rearranging gives

$$E = E' + \frac{RT}{\alpha F} \ln \frac{k'_o}{k_D} + \frac{RT}{\alpha F} \ln (i_L/i - 1) \qquad (2:27)$$

This is the current-voltage relation for the irreversible "wave".

THE OPTICAL ROTATING DISC ELECTRODE

As described in Chapter 1 uniform parallel light shines through the electrode into the solution generating B with quantum efficiency ϕ

$$A + Z \underset{k_{-2}}{\overset{h\nu,\phi}{\rightleftharpoons}} B + Y$$

In order to set up the differential equation for the convective diffusion of B we make various assumptions:

1) That the light makes only a small perturbation on the concentration of A. This means that the light intensity, I, follows a Beer-Lambert profile.

$$I = I_o e^{-\varepsilon[A]x} \qquad (2:28)$$

where I, I_o, ε, $[A]$ and x are as described in chapter 1.

2) That $[Y] >> [B]$ so that the back reaction is pseudo first order with rate constant, k, where

$$k = k_{-2}[Y] \qquad (2:29)$$

and k is in s^{-1}.

3) That the X/Y couple is irreversible at the electrode and that the potential of the electrode is such that all the B reaching the electrode is converted to A. This is the condition necessary to measure the photogenerated flux of B arriving at the electrode.

All three of these assumptions agree with the conditions necessary for an ideal photogalvanic cell found in chapter 1.

Given these assumptions the convective diffusion equation is

$$D\frac{\partial^2[B]}{\partial x^2} + v_x\frac{\partial[B]}{\partial x} + \phi I_o \varepsilon[A]e^{-\varepsilon[A]x} - k[B] = 0 \qquad (2:30)$$

Diffusion Convection Generation Back reaction

The system has four characteristic lengths.

$X_{Hy} = (\nu/\omega)^{\frac{1}{2}}$ the thickness of the hydrodynamic layer

X_D (eq. 2:17) the thickness of the diffusion layer

and X_k and X_G the reaction length and optical length are as defined in chapter 1.

(X_G, which features in chapter 1, is not used as assumption 1) means that X_G is very much longer than all the other lengths.)

From these lengths three further parameters are defined which describe the ratio of the diffusion layer thickness to that of the other layers.

$$H_o = X_D/X_{Hy} \sim 10^{-1} \qquad (2:31)$$

$$\kappa = X_D/X_k \qquad (2:32)$$

$$\beta = X_D/X_\epsilon \qquad (2:33)$$

The concentration is normalised by defining

$$u = [B]D/\phi\beta X_D I_o$$

and the distance from the electrode is normalised by defining

$$\chi = x/X_D.$$

Then equation (2:30) becomes

$$\frac{\partial^2 u}{\partial \chi^2} + (v_x X_D/D)\frac{\partial u}{\partial \chi} + e^{-\beta\chi} - \kappa^2 u = 0 \qquad (2:34)$$

As the electrode destroys all B reaching it the boundary condition for u is

at $\chi = 0$ $u = 0$

and as the light penetrates a finite distance

as $\chi \to \infty$ $u \to 0$

The equation must now be solved for the flux of B at the electrode which is

$$j = D \left.\frac{\partial [B]}{\partial x}\right|_{x=o} = \phi\beta I_o u'_o \qquad (2:35)$$

where $$u'_o = \left(\frac{\partial u}{\partial \chi}\right)_{\chi=o} \qquad (2:36)$$

In order to solve the differential equation a simple expression for v_x is needed. v_x is however a complex function obtained by Cochran[51] by numerical integration. It is shown again in Figure 2:3 (solid line) with an approximation to it (dotted line). The approximation is used to solve the equation in three separate regions:

1) for $x > X_{Hy}$ or $\chi > \chi_{Hy}$ we define

$$v_x = 0.88(\omega\nu)^{\frac{1}{2}} \qquad (2:37)$$

where $$\chi_{Hy} = 1.3\ H_o^{+1}$$

Equation (2:34) then becomes

$$3.7\ H_o^{-2} \frac{\partial u}{\partial \chi} + e^{-\beta\chi} - \kappa^2 u = 0 \qquad (2:38)$$

There is no diffusion term as convection dominates.

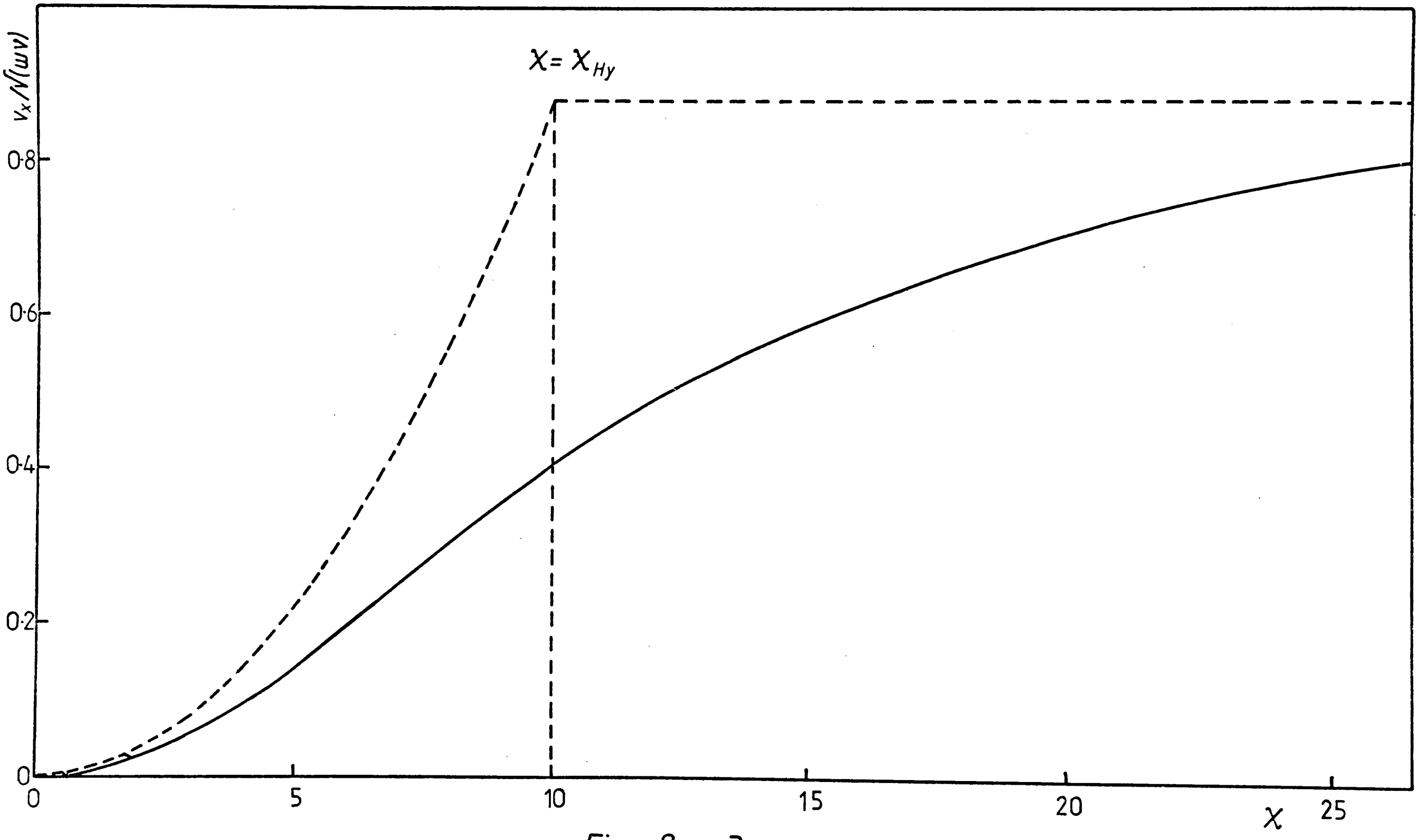

Fig 2 : 3

Flow Velocity and Approximation

This equation is then solved with the boundary condition given above (at $\chi \to \infty$ $u \to 0$) for u at $\chi = \chi_{Hy}$ and gives

$$u_{Hy} = (e^{-\beta\chi_{Hy}})/(\kappa^2 + 3.7H_o^{-2}\beta) \qquad (2:39)$$

and this is the boundary condition to be fed into the next region.

2) For $1 < \chi < \chi_{Hy}$ (the hydrodynamic layer) we approximate v_x by putting

$$v_x = Cx^2 \qquad (2:40)$$

where

$$C = 0.88(\omega\nu)^{\frac{1}{2}}/\chi_{Hy}^2 \qquad (2:41)$$

and equation (2:34) becomes

$$2.1\ \chi^2\ \frac{\partial u}{\partial \chi} + e^{-\beta\chi} - \kappa^2 u = 0 \qquad (2:42)$$

This is in turn solved for u at $\chi = 1$ and gives

$$u_1 = u_{Hy} + e^{-[\frac{\kappa^2}{2.1}(1 - \frac{1}{\chi_{Hy}})]} + \frac{e^{-[\beta+\kappa^2/2.1]}}{2.1}\int_1^{\chi_{Hy}} e^{-[\beta\chi - \frac{\kappa^2}{2.1\chi}]} \cdot \frac{d\chi}{\chi^2} \qquad (2:43)$$

This appalling expression happily simplifies. When $\kappa > 1$ any [B] made outside the diffusion layer decomposes before reaching the

electrode. When $\beta > 1$ very little light penetrates through the diffusion layer. Thus for a significant contribution to the current from material generated outside the diffusion layer both β and κ must be less than 1. Under these conditions equation (2:43) reduces to

$$u_1 = u_H + 0.48 \qquad (2:44)$$

This boundary condition is now fed into the final stage of the calculation.

3) For $\chi < 1$ (the diffusion layer) equation (2:29) becomes

$$\frac{\partial^2 u}{\partial \chi^2} + e^{-\beta\chi} - \kappa^2 u = 0 \qquad (2:45)$$

(directly comparable to equation (1:3) for the photogalvanic cell). It is solved with the boundary conditions at $\chi = 0$ and $\chi = 1$, for the concentration gradient at $\chi = 0$, u'_o, and gives

$$u'_o = \frac{\kappa}{\sinh \kappa} u_1 + \frac{\cosh \kappa - (\beta/\kappa)\sinh \kappa - e^{-\beta}}{\kappa^2 - \beta^2} \qquad (2:46)$$

Figure 2:4 displays the approximate solutions to this equation on the $\beta\kappa$ plane. The solutions are given in terms of the photoelectrochemical collection efficiency, $N_{h\nu}$, defined in chapter 1 as

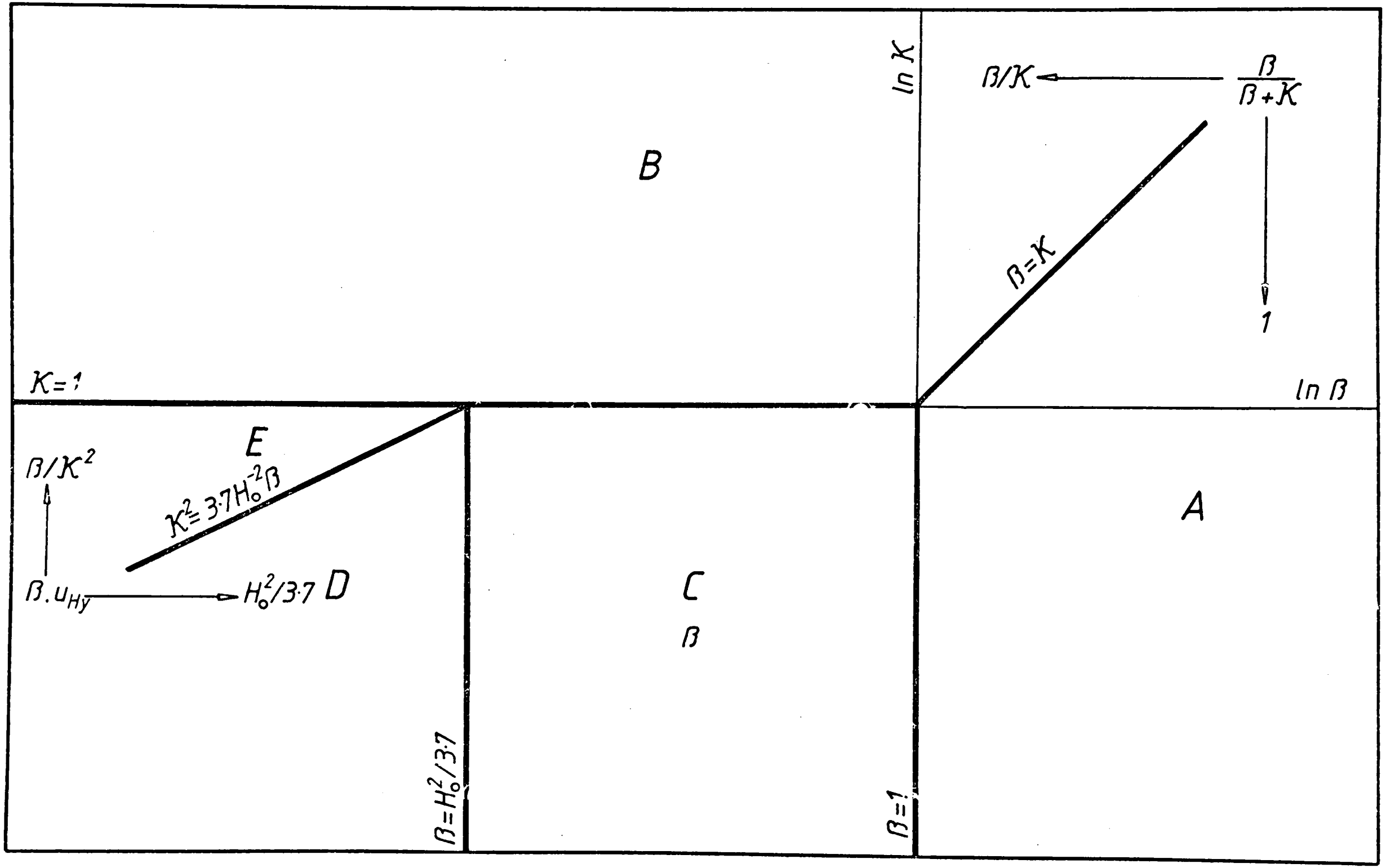

Fig 2 : 4

Photoelectrochemical Collection Efficiency as a Function of β and K

$$N_{h\nu} = j/I_o = \phi\beta u'_o.$$

Bartlett[54] has recently used a much more accurate approximation to v_x using

$$v_x = (\omega\nu)^{\frac{1}{2}} \quad X(\chi) \qquad (2:47)$$

where $$X(\chi) = 0.886 \tanh \frac{a\chi^2}{1+\chi} \qquad (2:48)$$

and $a = 0.57588.$

Then by numerical integration of equation (2:34) he obtained values for $N_{h\nu}$ displayed as a contour diagram in Figure 2:5.

This shows that the initial crude approximation to $X(\chi)$ is very good. Deviations from the true values occur only when both X_k and X_ε are between X_D and X_{Hy} (i.e. where the approximation is worst). The maximum deviation in the values of $N_{h\nu}$ are only 15% in this region. In this thesis all experiments were conducted with $X_k < X_D$ where the deviations from the analytical solutions are < 0.2% so that the analytical solutions are used in the analysis of the experimental data.

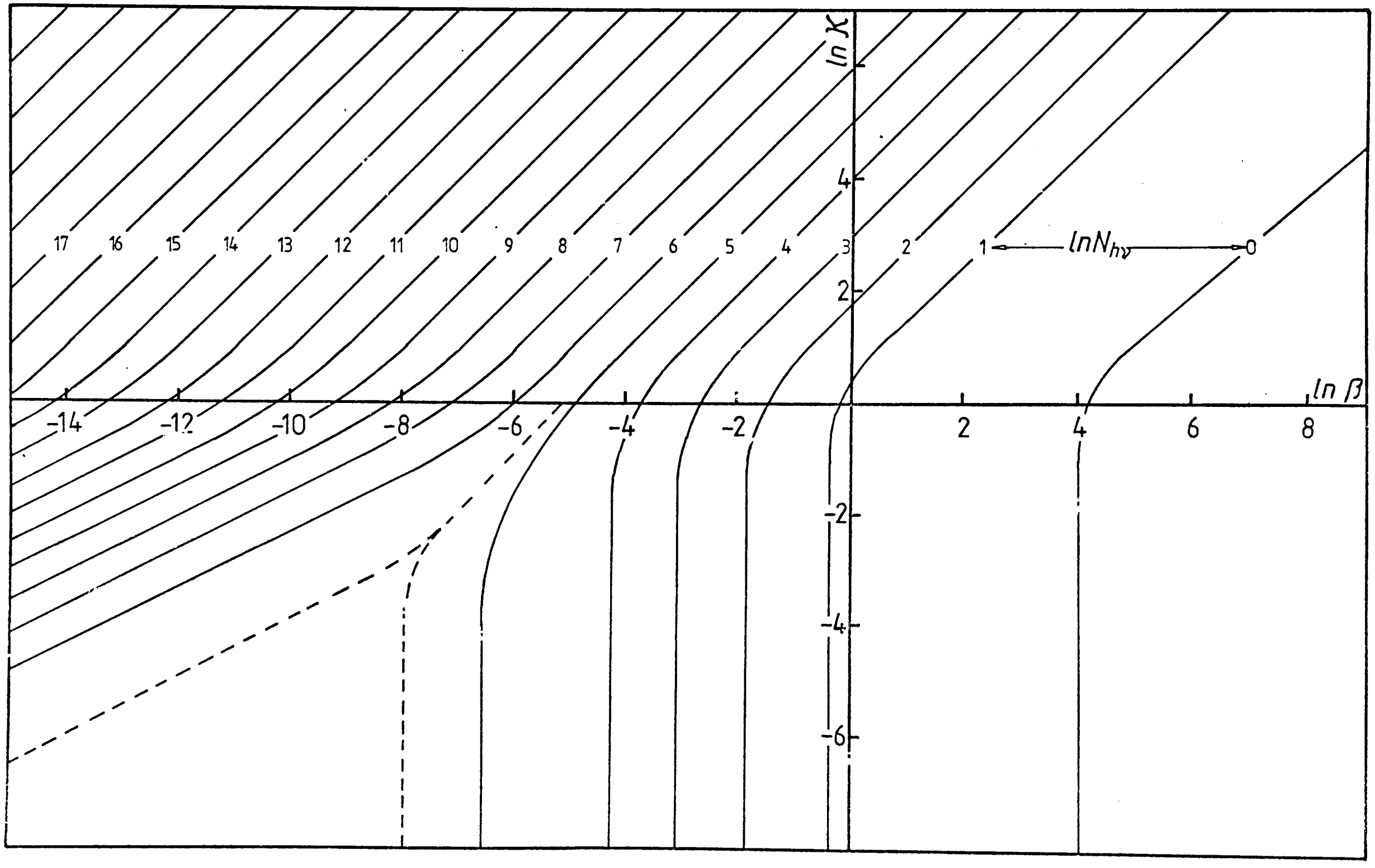

Fig 2 : 5

Photoelectrochemical Collection Efficiency Contour Diagram

FLASH ELECTROLYSIS AT AN OPTICAL DISC ELECTRODE

As described in Chapter 1 a very short pulse of uniform parallel light is flashed through a stationary electrode into the photogalvanic solution. This generates an appreciable concentration of B. In order to set up and solve the differential equation for the transport of B to the electrode a number of assumptions are made:[42-49]

1) The flash is of infinitely short duration and occurs at time $t = 0$.

2) The optical density of the solution is low so that the concentration of B at $t = 0$, $[B]_o$, is constant as a function of distance from the electrode. (If the flash is powerful enough it will bleach the solution, i.e. $X_G << X_k, X_\varepsilon$, and this condition becomes redundant.

3) $[B]_o << [Y]$. This means that after the flash B will undergo a pseudo first order decay in the bulk of the solution, well away from the electrode perturbation. This gives a boundary condition

$$[B] = [B]_o \, e^{-kt} \quad \text{as} \quad x \to \infty \qquad (2:50)$$

where $k = k_{-2}[Y]$.

4) The X/Y couple is completely inactive at the electrode so that the concentrations of Z and Y remain constant for all x throughout the experiment.

5) The electrode is held at a potential where all the B reaching it is converted to A. This gives the boundary condition

$$[B] = 0 \quad \text{at} \quad x = 0$$

Equation (2:4) thus becomes

$$\frac{\partial [B]}{\partial t} = D \frac{\partial^2 [B]}{\partial x^2} - k[B] \qquad (2:51)$$

The time dependent term is kept in this equation as a steady state is not invoked. There are no convective terms as the electrode is stationary and all transport is by diffusion.

The equation is now normalised by defining

$$u = ([B]_o \, e^{-kt} - [B])/[B]_o \qquad (2:52)$$

$$\tau = kt \qquad (2:53)$$

$$\chi = x/X_k \qquad (2:54)$$

where $X_k = (D/k)^{\frac{1}{2}}$.

Equation (2:51) becomes

$$\frac{\partial u}{\partial \tau} = \frac{\partial^2 u}{\partial \chi^2} - u \qquad (2:55)$$

and the boundary conditions become

$$u = 0 \qquad \text{at } \tau = 0 \qquad (2:56)$$

$$u = e^{-\tau} \qquad \text{at } \chi = 0 \qquad (2:57)$$

$$u = 0 \qquad \text{as } \chi \to \infty \qquad (2:58)$$

Solution by Laplace transform gives

$$\left(\frac{\partial u}{\partial \chi}\right)_o = - \frac{1}{(\pi\tau)^{\frac{1}{2}}} e^{-\tau} \qquad (2:59)$$

Thus $$j = (D/\pi)^{\frac{1}{2}} \cdot [B]_o \; t^{-\frac{1}{2}} . e^{-kt} \qquad (2:60)$$

or $$\ln(it^{\frac{1}{2}}) = -kt + Q \qquad (2:61)$$

where Q is a constant.

The $t^{-\frac{1}{2}}$ term is the simple solution for semi-infinite linear diffusion of B to the electrode. The e^{-kt} term describes

the first order decay of B. Figure 2:6 shows concentration profiles for B and current-time transients. Thus if the kinetics are infinitely slow the current time transient is given by $t^{-\frac{1}{2}}$. The bulk concentration stays at $[B]_o$ and ordinary semi-infinite linear diffusion is observed. However if the kinetics are significant the bulk concentration falls exponentially with increasing τ(Figure 2:6) and the current time transient includes this exponential term.

This theory predicts that at $t = 0$ $i \to \infty$. This is impossible. In order to understand the early part of the transient the equivalent circuit for the system must be considered. This is shown in Figure 2:7.[47]

The important feature of this circuit is that the double layer capacitance of the working electrode is included. The resistance of the solution between the reference electrode and working electrode is given by R_s. Further it is assumed that potentiostat has an infinitely fast response and therefore that the potential between reference and working electrodes is fixed at E_p. The instantaneous generation of B at $t = 0$ is considered as a current generator across the double layer capacitance. It generates a current, i_*, which is known from equation (2:60) to be

$$i_* = a(\pi t)^{-\frac{1}{2}} e^{-kt}$$

where a is a constant.

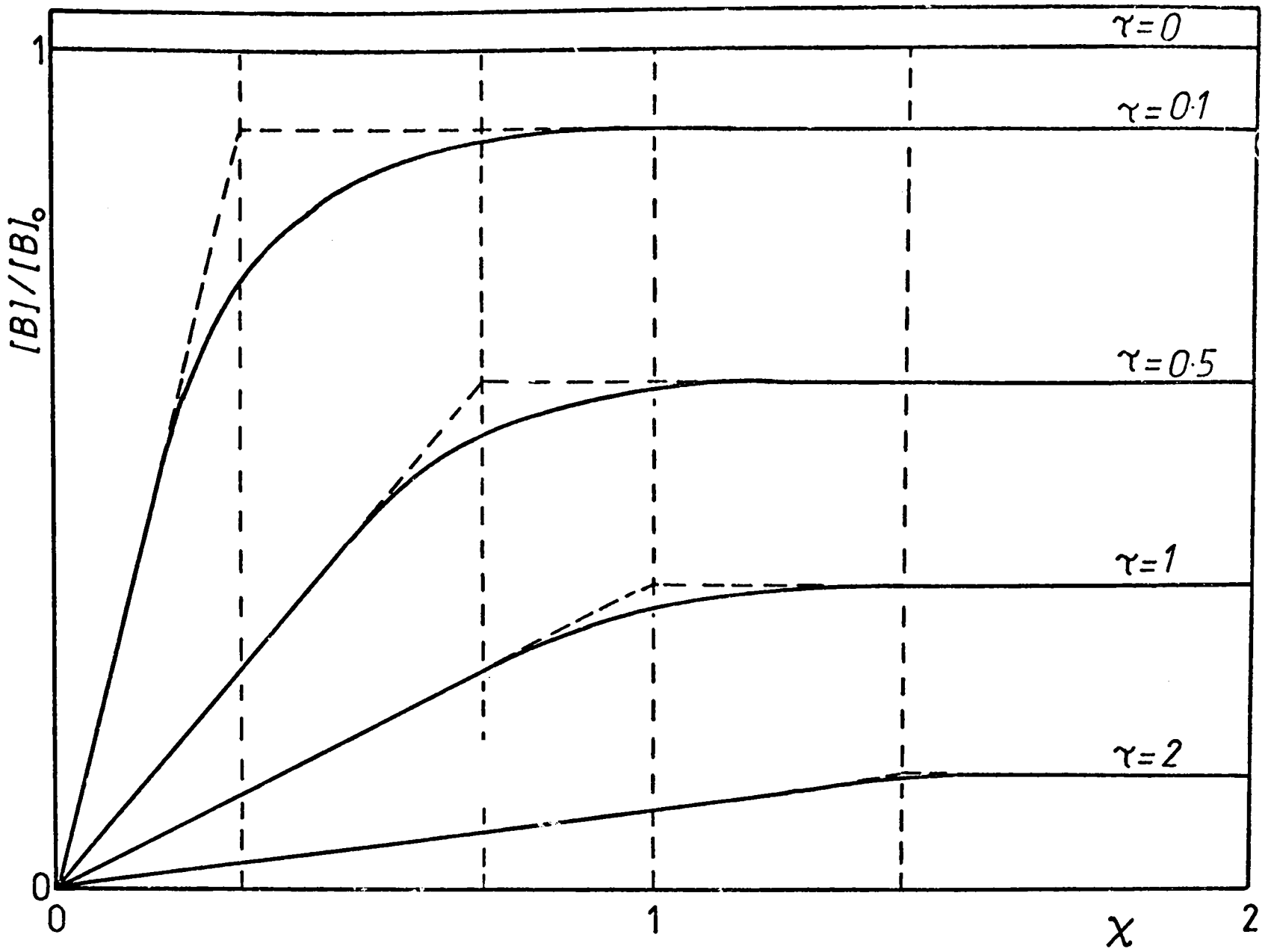

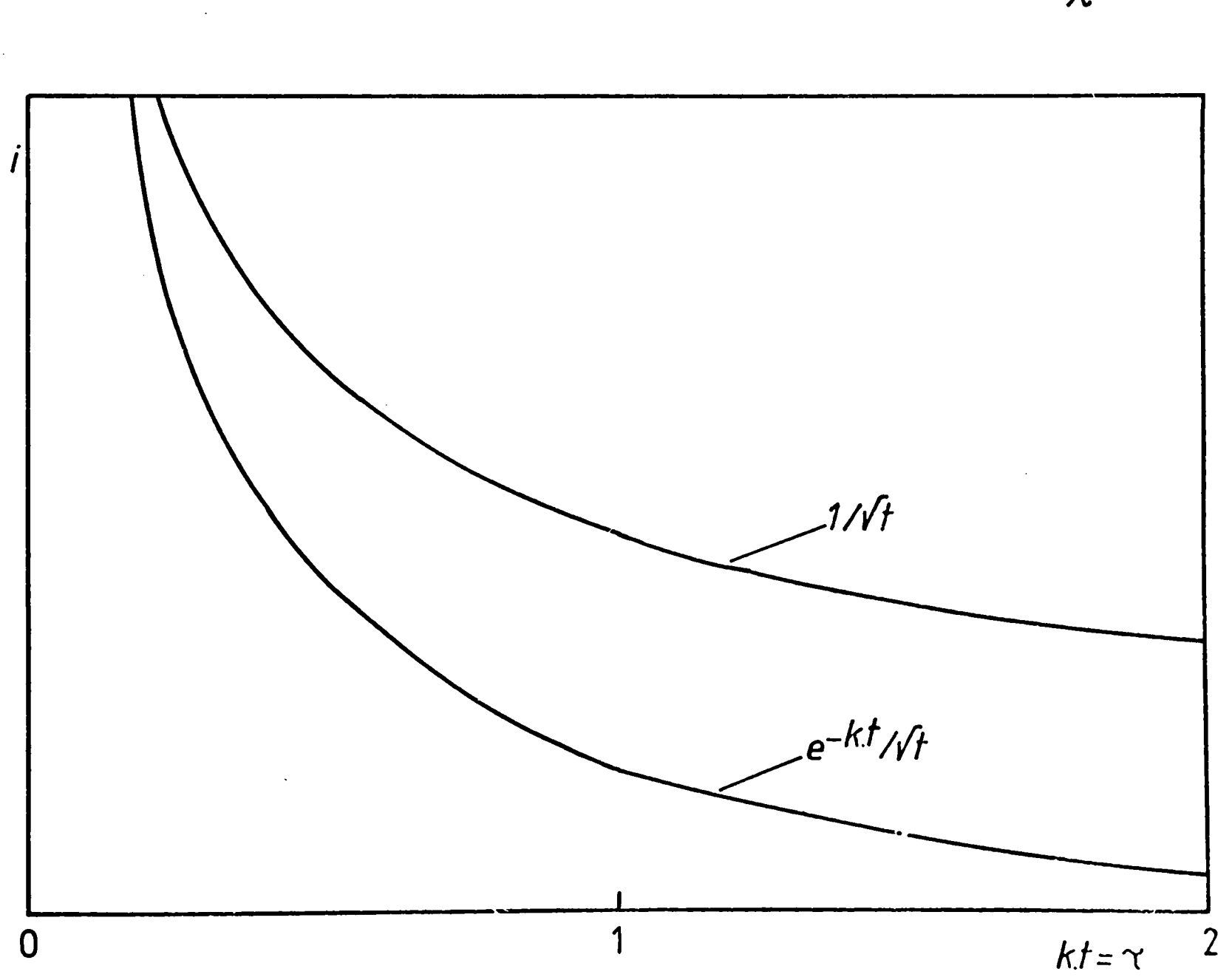

Fig 2 : 6

Concentration Profiles and Current-Time Transients for Flash Electrolysis

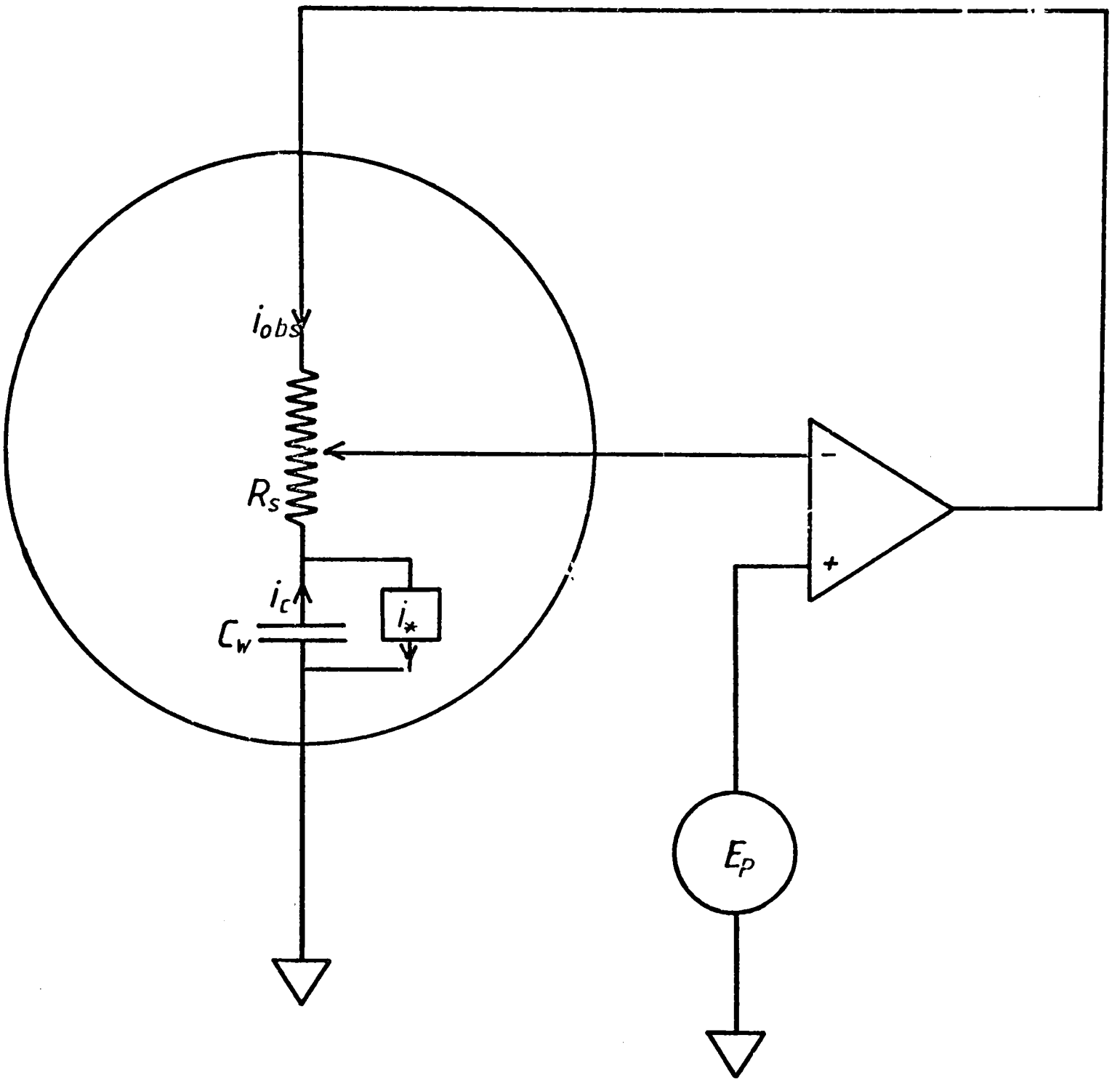

Fig 2 : 7

Equivalent Circuit for Flash Electrolysis

As the potential E_p remains fixed throughout

$$\delta E_p = 0 = i_{obs} R_s - \frac{1}{C_w} \int_o^t (i_* - i_{obs}).dt$$

Solution of this equation by Laplace transform for $k < 1/R_s C_w$ gives

$$i_{obs} = \frac{a\, e^{-kt}}{\sqrt{\pi}\, R_s C_w (1/R_s C_w - k)} \cdot F\left[\frac{1}{R_s C_w} - k\right]^{\frac{1}{2}} t^{\frac{1}{2}} \qquad (2:62)$$

where F(x) is Dawson's Integral[55]. The condition that $k < 1/R_s C_w$ is likely for most experimental situations. F(x) and $F(t^{\frac{1}{2}})$ are both plotted in Figure 2:8. For large values of x

$$F(x) \rightarrow 0.5/x$$

and thus

$$i_{obs} \rightarrow \frac{a}{(\pi t)^{\frac{1}{2}}(1 - k/R_s C_w)} \cdot e^{-kt}$$

This is the same as the previous solution with the exception of the small $k/R_s C_w$ term. This term represents the slow discharge of the double layer capacitance after the initial rapid charging.

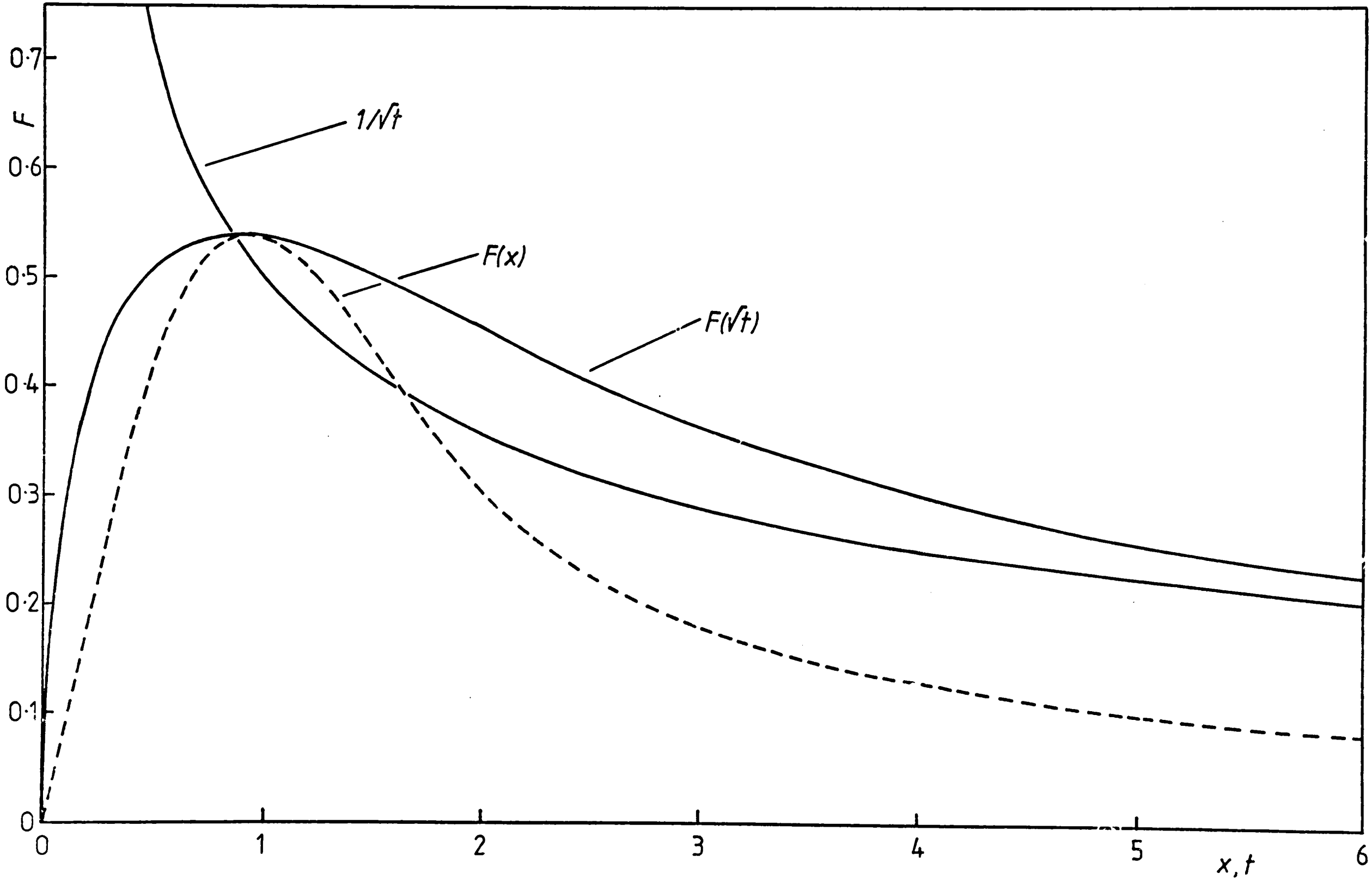

Fig 2 : 8

Dawson's Integral

Flash electrolysis is thus a composite of three effects. The first is the double layer charging described by the Dawson Integral. The second is the diffusion of the species to the electrode described by the $t^{-\frac{1}{2}}$ term and the third is the decay of [B] in the solution by pseudo first order kinetics.

CHAPTER 3

APPARATUS AND EXPERIMENTAL

This Chapter describes the design and development of apparatus for the ORDE and flash electrolysis experiments. It also describes the procedures used in RDE, ORDE and Stopped Flow experiments.

THE ORDE APPARATUS

The first ORDE apparatus was designed by Field[56] and developed by Archer and Turner[57]. It had a number of limitations. A new design was undertaken in which the important improvements were:

1) The provision of a more versatile light source.
2) The provision of more versatile electronics.
3) The reduction of electronic, and electromechanical noise.
4) The streamlining of the mechanical design for ease of operation.

The general layout of the apparatus is shown in Plate 3:1 and the various components are now described.

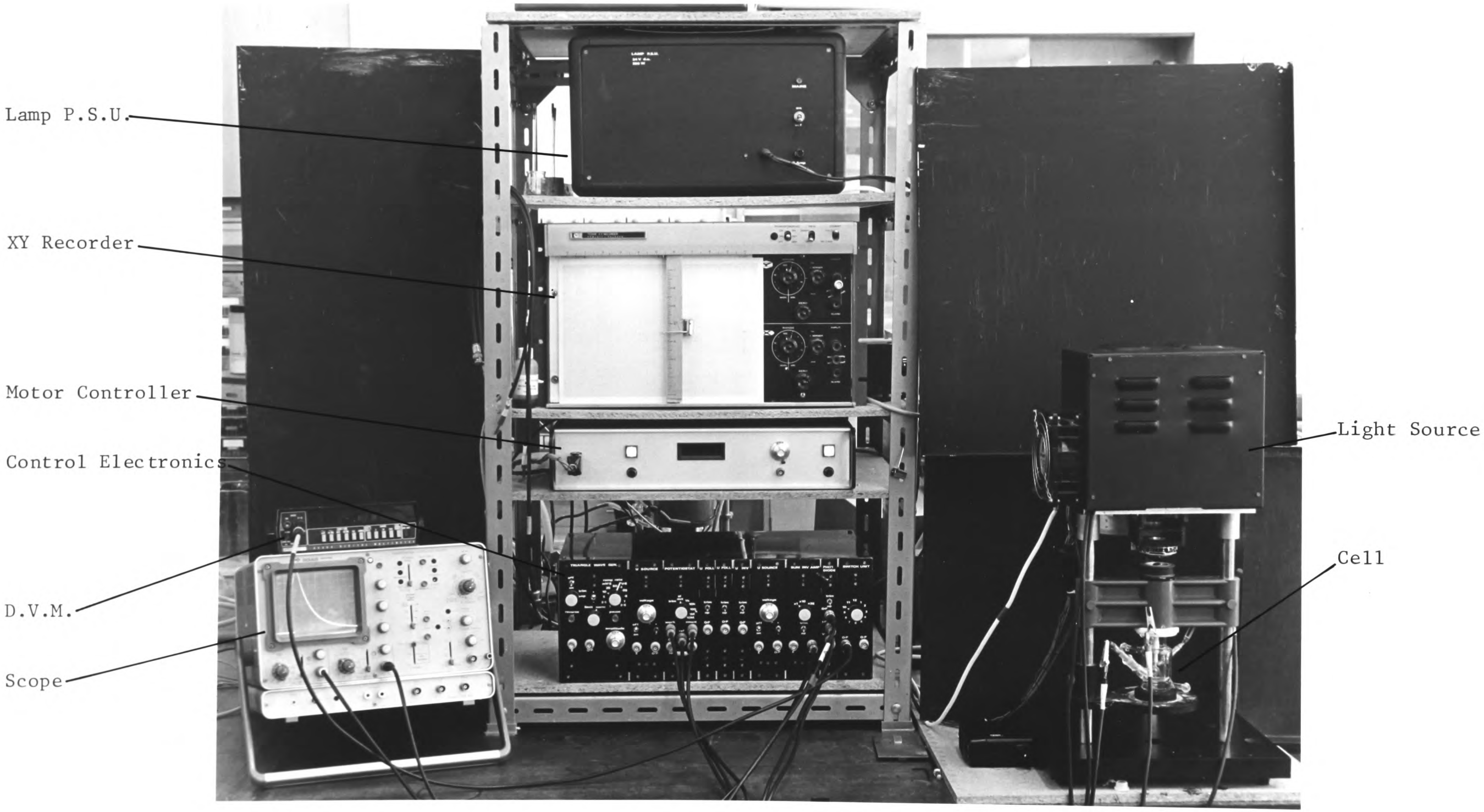
Lamp P.S.U.
XY Recorder
Motor Controller
Control Electronics
D.V.M.
Scope
Light Source
Cell

Plate 3 : 1

The Light Source

In the past ORDE experiments were performed with a polychromatic light source (a medium pressure mercury lamp). This made calculation of the expected photocurrents very difficult. Convolution of the lamp spectrum with the absorption spectrum of the dye and the equation for the mass transport and homogeneous kinetics was tedious and inaccurate. However monochromatic light allows accurate measurement of its intensity and defines a unique extinction coefficient at any wavelength.

The requirements for a light source are that it should be

1) Monochromatic and variable over the whole spectrum.
2) Collimated and uniform to give an even parallel light distribution at the electrode.
3) Of high intensity : typically 0.1 - 1.0 mA photons in a 15 nm waveband. (It was found convenient to express a flux of photons as a current of photons. An amp of photons is

$$\frac{\text{Number of photons/s}}{\text{Number of electrons/Coulomb}}$$

The unit has the advantage that the photoelectrochemical collection efficiency, $N_{h\nu}$, is simply the ratio of the electron current to the photon current.)

The lower limit of photocurrent detection was ~ 1 nA. With a photon current of 1 mA this allowed photoelectrochemical collection efficiencies as low as 10^{-6} to be measured.

A tunable dye laser would have met these conditions handsomely but happily a cheaper solution presented itself. The system used was developed around an A1/223, 250W, 24V, quartz-iodine projector lamp. This had a filament temperature of 3,350^{o}K. The spectral output in terms of photons before (dotted line) and after the heat filter (solid line) is shown in Figure 3:1. The bulb was chosen to have as near round and uniform a filament as possible as the filament image was to be focussed onto the top of the electrode. The bulb is shown in Plate 3:2. Clearly the proportions of the filament were not perfect and an attempt was made to change the shape of the filament image by using cylindrical lenses (Figure 3:2a). Poor results were achieved.

Coles[58] then suggested that the optimum design of a condensing lens unit had already been achieved for slide projectors. It was soon found that a Leitz "Pradovit-Color" projector had a suitable bulb mounting and condensing lens unit. This unit is shown in Figure 3:3 with the addition of a further condensing lens to focus the light onto the top of the electrode. The filament image focussed on the electrode is shown in Figure 3:2b. The system had the advantage that the rear reflector produced an inverted image (dotted) which increased the intensity and the uniformity

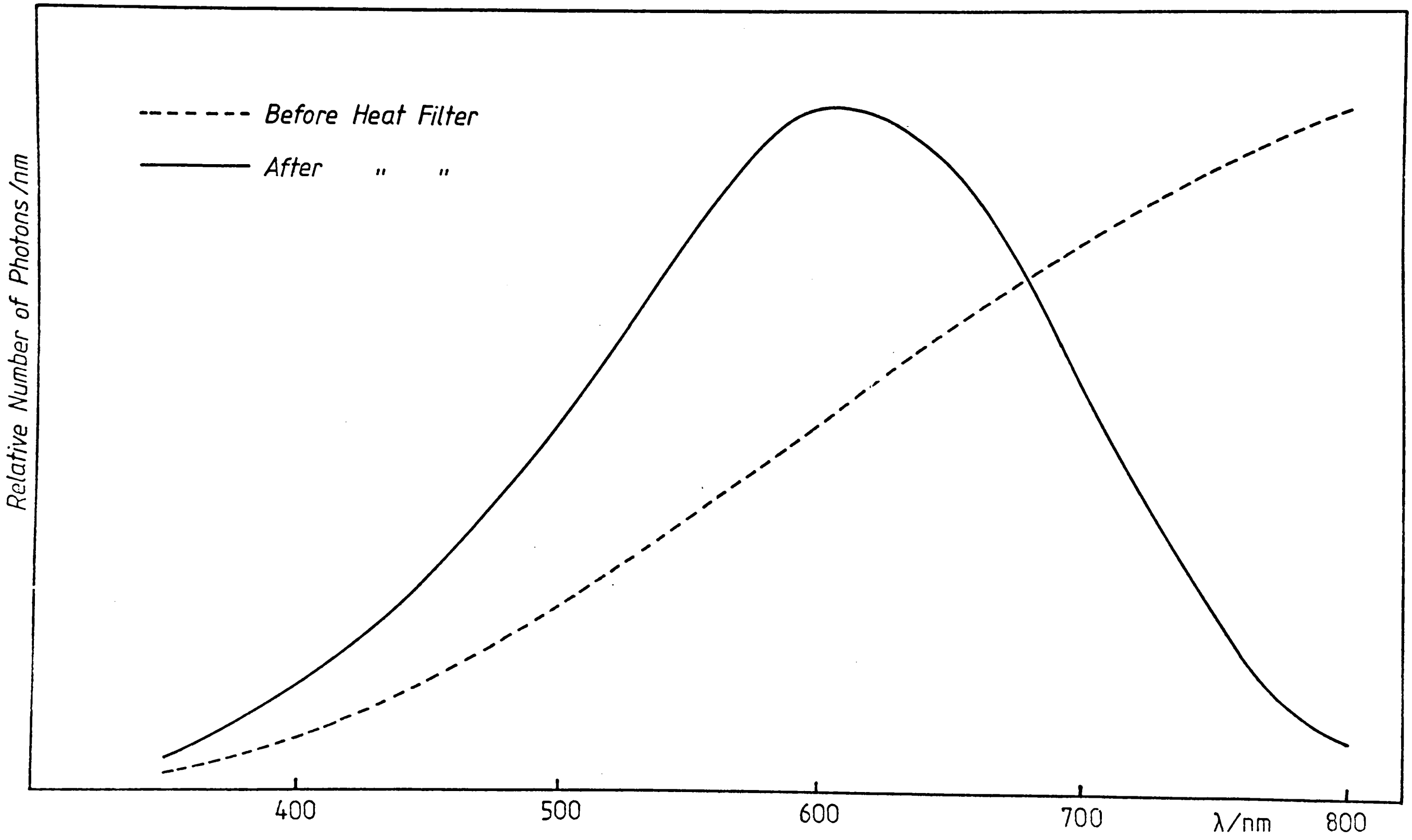

Fig 3 : 1

Lamp Output Spectrum

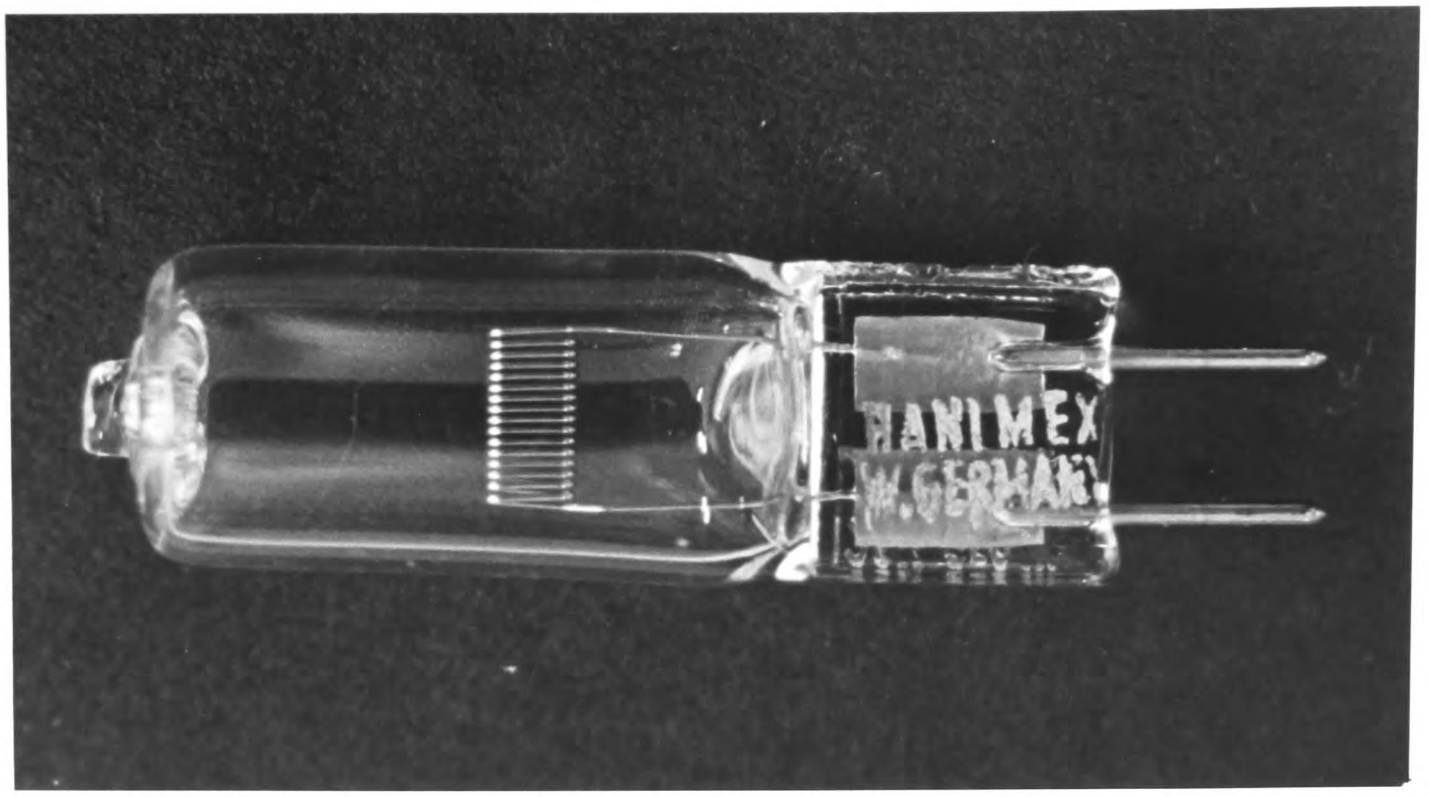

Plate 3 : 2

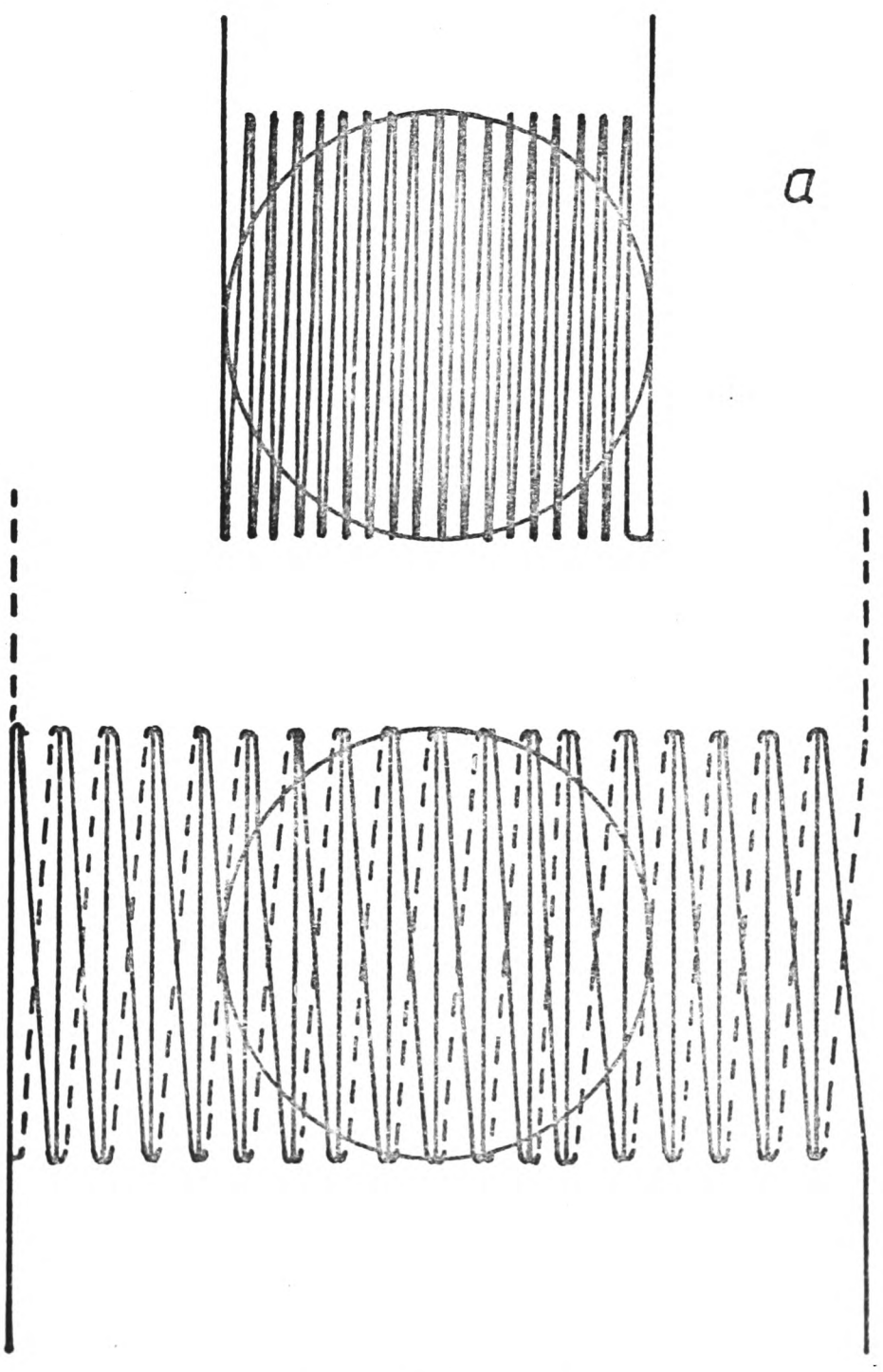

Fig 3 : 2

Filament Images

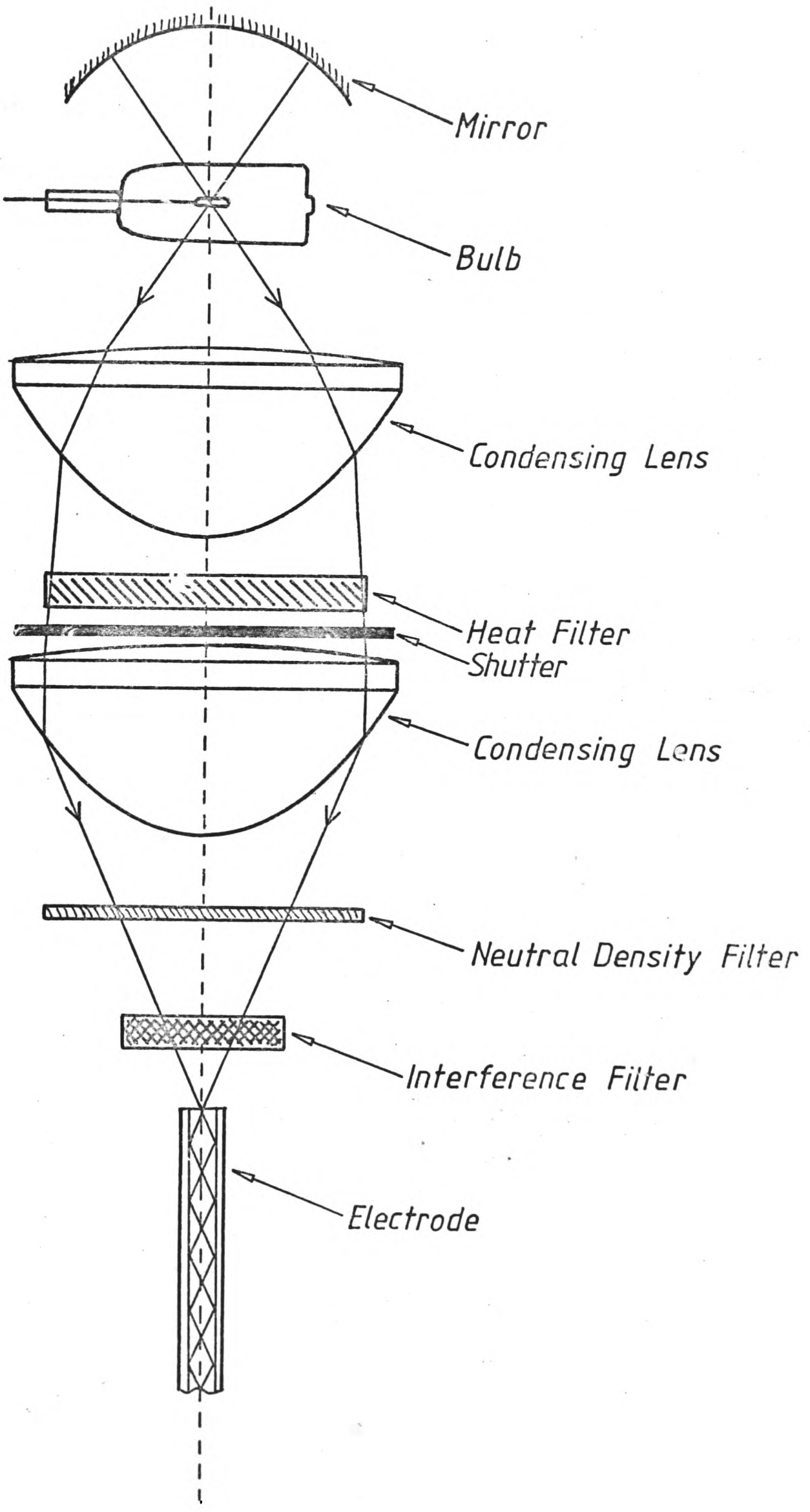

Fig 3 : 3

The Light Source

of the filament image on the electrode. Although more than 50% of the light was wasted because of the difference in filament and electrode shapes the light gathering power of the Leitz system more than compensated for this shortcoming.

The bulb was designed to run off 24V A.C. in projectors. However measurement of the light intensity with a photodiode showed that there was a 5 to 10% ripple in the output at 100 Hz. This was unacceptable for a steady state ORDE experiment, so a 10A, 24V power supply was built. Figure 3:4 shows the circuit diagram for this unit. This reduced the ripple in the light intensity to <<1%.

Between the second condensing lens and the electrode provision was made to hold Ealing neutral density filters to vary the light intensity. These were reasonably uniform in absorbance across the visible spectrum. Typical spectra are shown in Figure 3:5 (measured on a Cary 14 spectrophotometer). A holder was also made for Ealing-IRI 25mm interference filters to provide monochromatic light. A typical spectrum for one of these filters is shown in Figure 3:6. The spectra are measured for light perpendicular to the filter and the band width is ~10nm. However the light source provides converging light which affects both the nominal wavelength, λ , of the interference filter and the bandwidth, $\delta\lambda$. The expression for the shift in wavelength is

$$\lambda_{\phi} = \lambda \left(1 - \frac{\sin^2\phi}{n^2}\right)$$

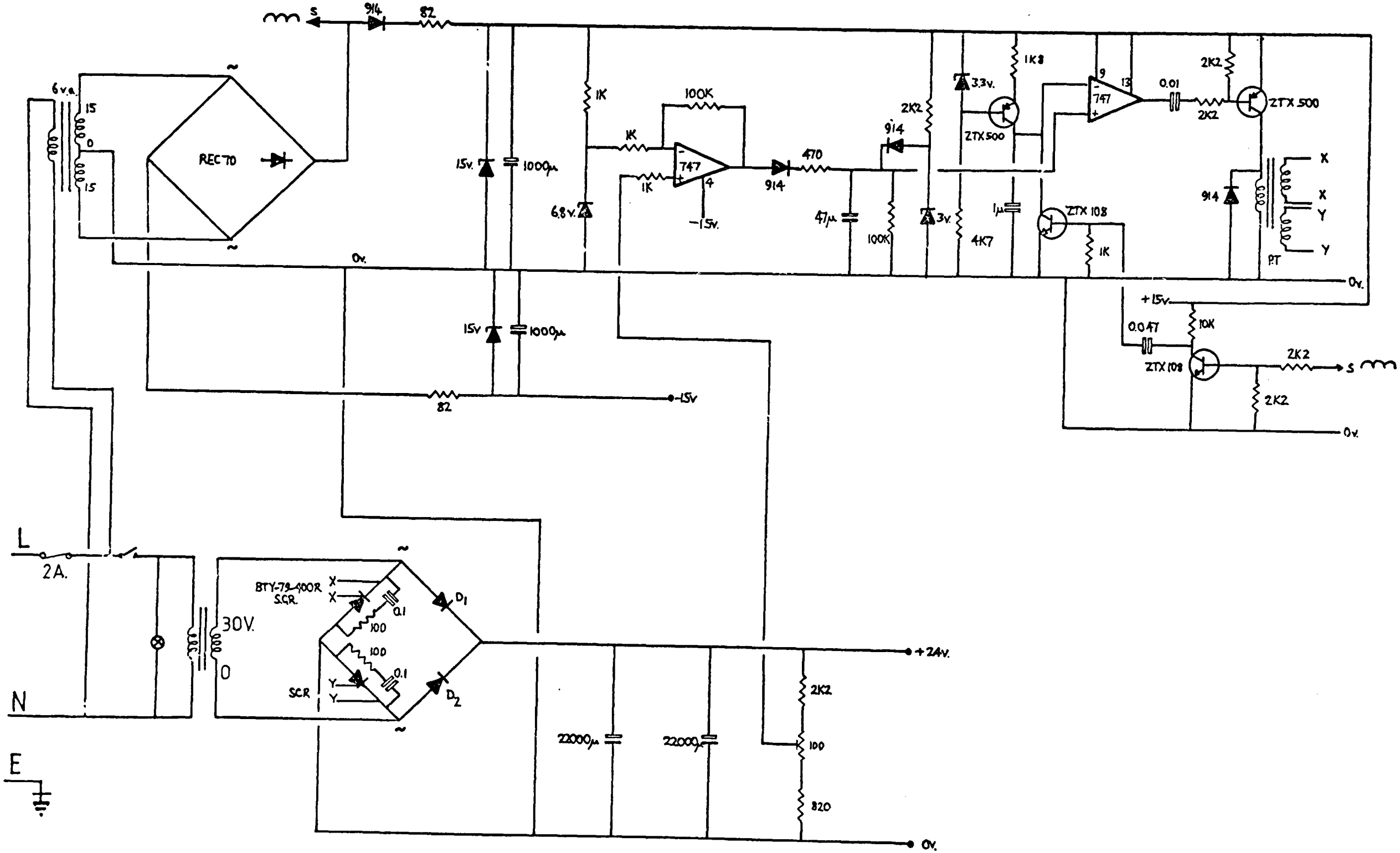

Fig 3 : 4

250W. Lamp Power Supply Unit

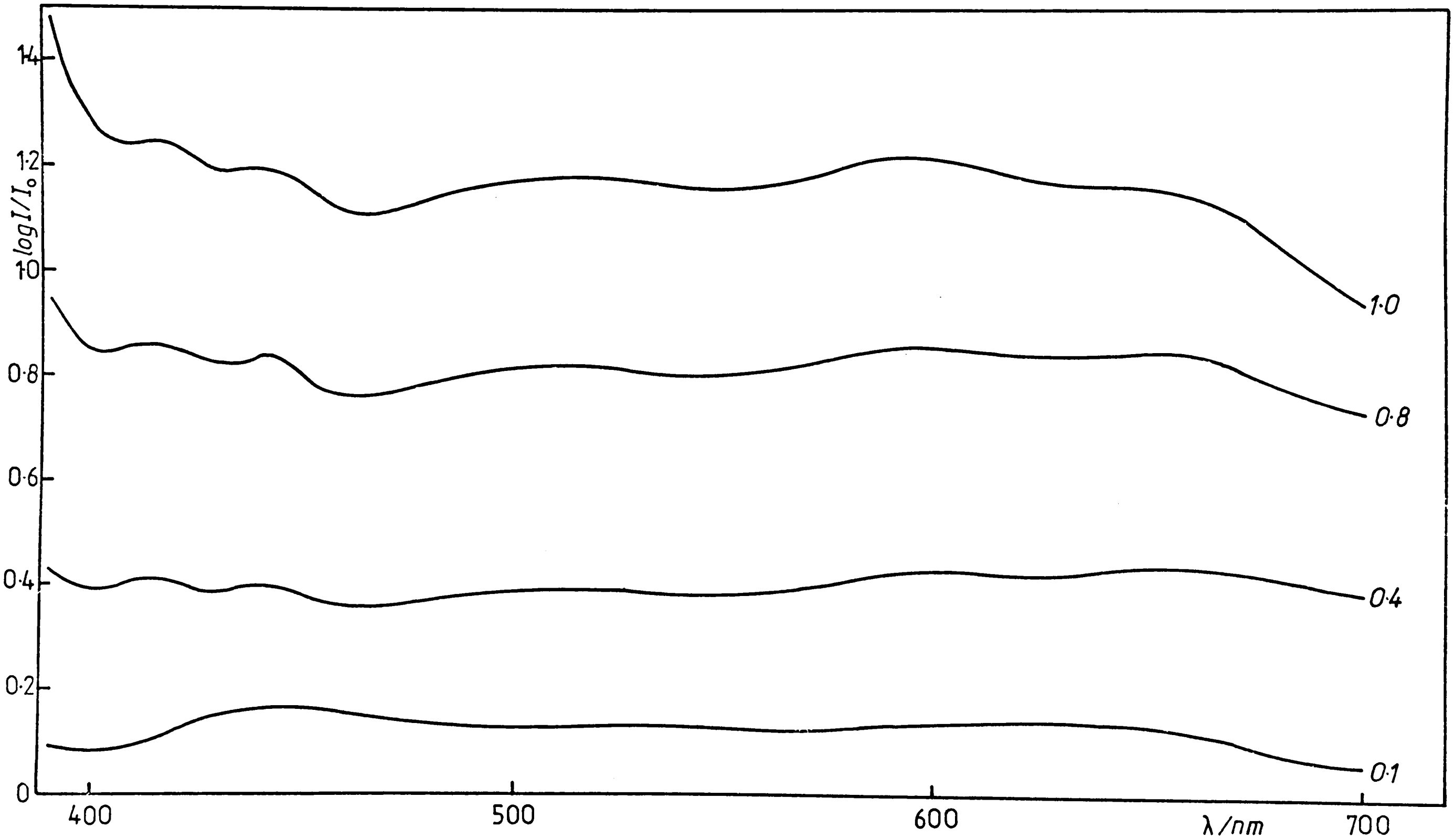

Fig 3 : 5

Neutral Density Filters

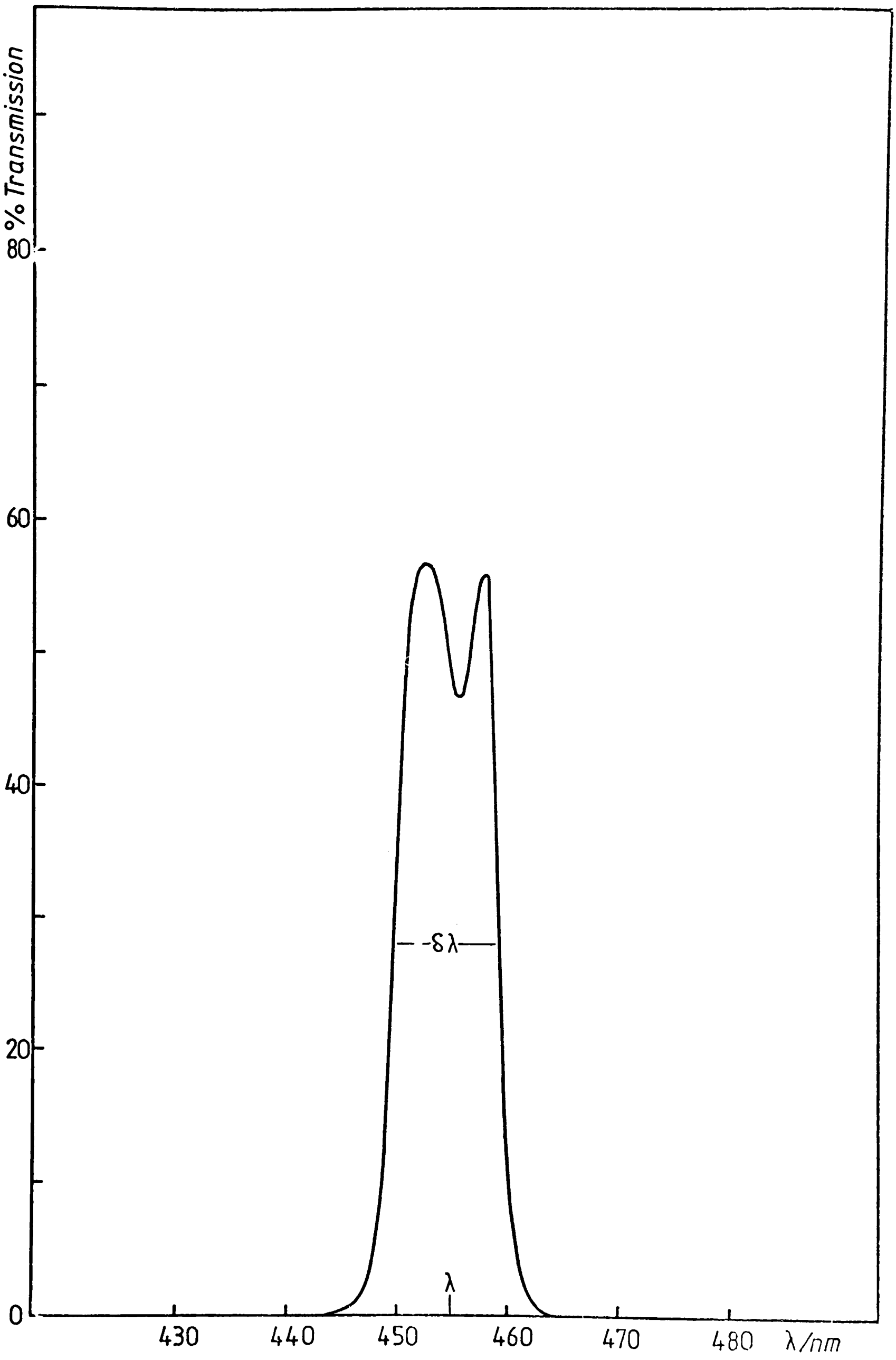

Fig 3 : 6

Interference Filter Spectrum

where λ_ϕ is the mean wavelength for an angle of incidence of $(90 - \phi)^o$.

λ is the mean wavelength for perpendicular light and n is the refractive index of the filter. Thus small deviations from the perpendicular would produce only minor variations in λ. However the maximum ϕ for the light source was 20^o due to the large aperture lenses used. It was therefore important to check the average wavelength in this converging beam and also estimate the bandwidth. A simple method was devised to do this.

A coloured glass filter with a reasonably linear change in absorbance in the appropriate wavelength range was used. The light intensity, with and without this filter, was measured and the absorbance obtained was compared with the absorbance measured on the spectrophotometer. Table 3:1 shows the perpendicular specifications for the interference filter and the experimental values found by this method. The deviations from λ are small.

TABLE 3:1

Interference Filters

λ /nm	Band Width / nm	n	λ_ϕ/nm	Band Width$_\phi$ / nm
404.2	11.0	1.45	400	16
436.2	11.2	1.45	432	16
442.1	11.0	1.45	438	16
455.0	8.8	1.45	452	13
485.5	10.0	2.00	484	12
508.0	9.6	2.00	507	11
546.0	10.0	2.00	545	11
576.4	8.0	2.00	576	9
588.6	10.2	2.00	588	11
599.1	10.0	2.00	599	11
632.0	9.4	2.00	632	10

The Electrodes

The semi-transparent ORDE was first developed by Field[56]. These electrodes consisted of thin films of Pt deposited on quartz. However the poor transmittance to resistance ratio and the very large surface effects (surface factors were found to be >6) made them unsuitable for the photogalvanic measurements made in this thesis.

The design of the SnO_2 electrodes used in this thesis was first perfected by Egdell[59]. A complete electrode is shown in Plate 3:3 and Figure 3.7.

Both ends of a 4mm quartz rod (Spectrosil B, Thermal Syndicate) were polished in stages, starting with 180 and 320 grit Bramet carborundum discs (Engis Ltd.) with water as a lubricant. The next stage was performed with a glycerol/carborundum (600 grit) slurry on a Hyprocell Pellon, type PSV, polishing pad (Engis Ltd.). Finally a water/cerirouge (grade 90) slurry, on a similar pad, was used until there were no scratches or distortions visible with a × 7 jewellers' eyepiece.

The rods were then very carefully cleaned and a coat of Johnson Matthey PBC 2532 platinum paint was applied to the side of the rod for the end 2cm and to a 0.2mm anulus around the face of the electrode. This was to ensure a good electrical contact between the face and the side of the rod. The paint was fired

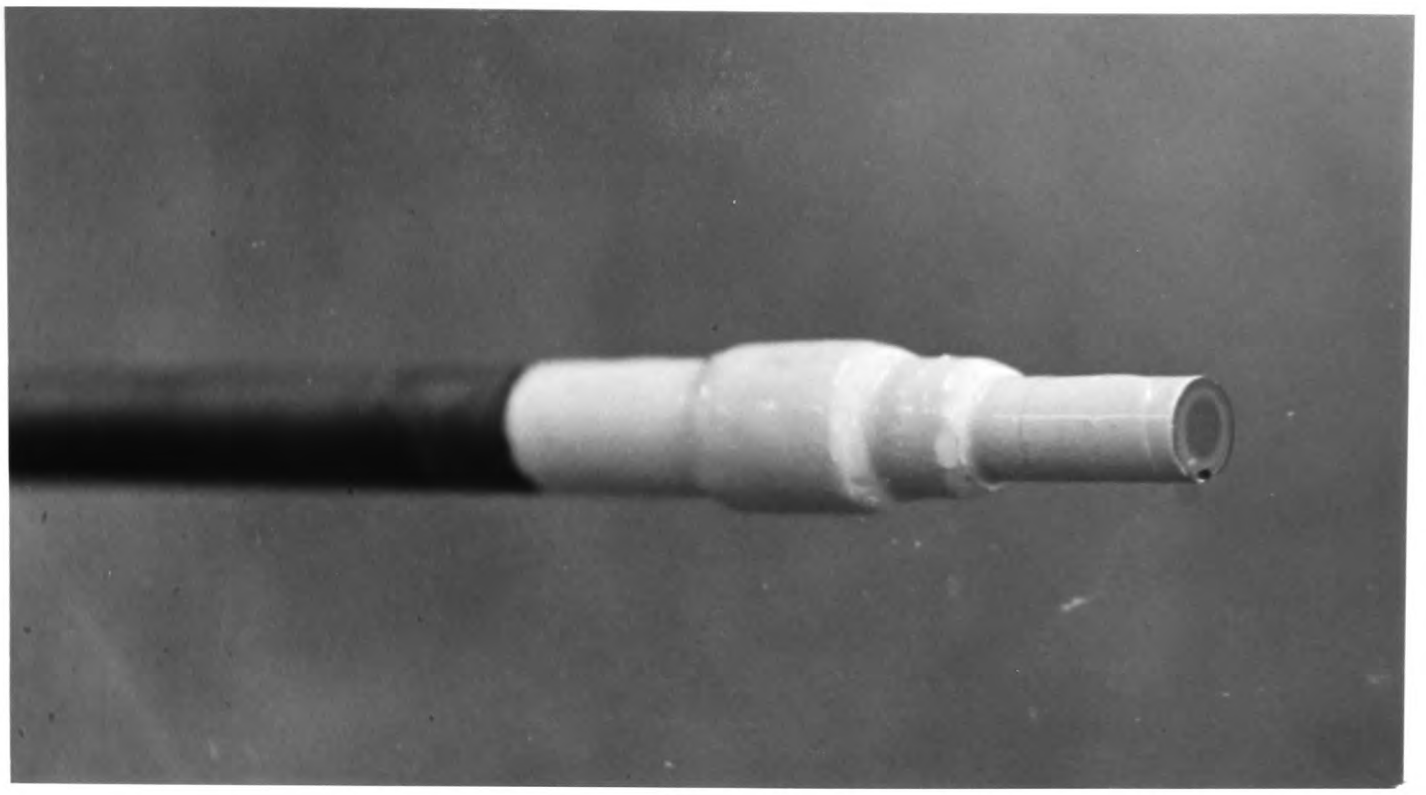

Plate 3 : 3

The Electrode

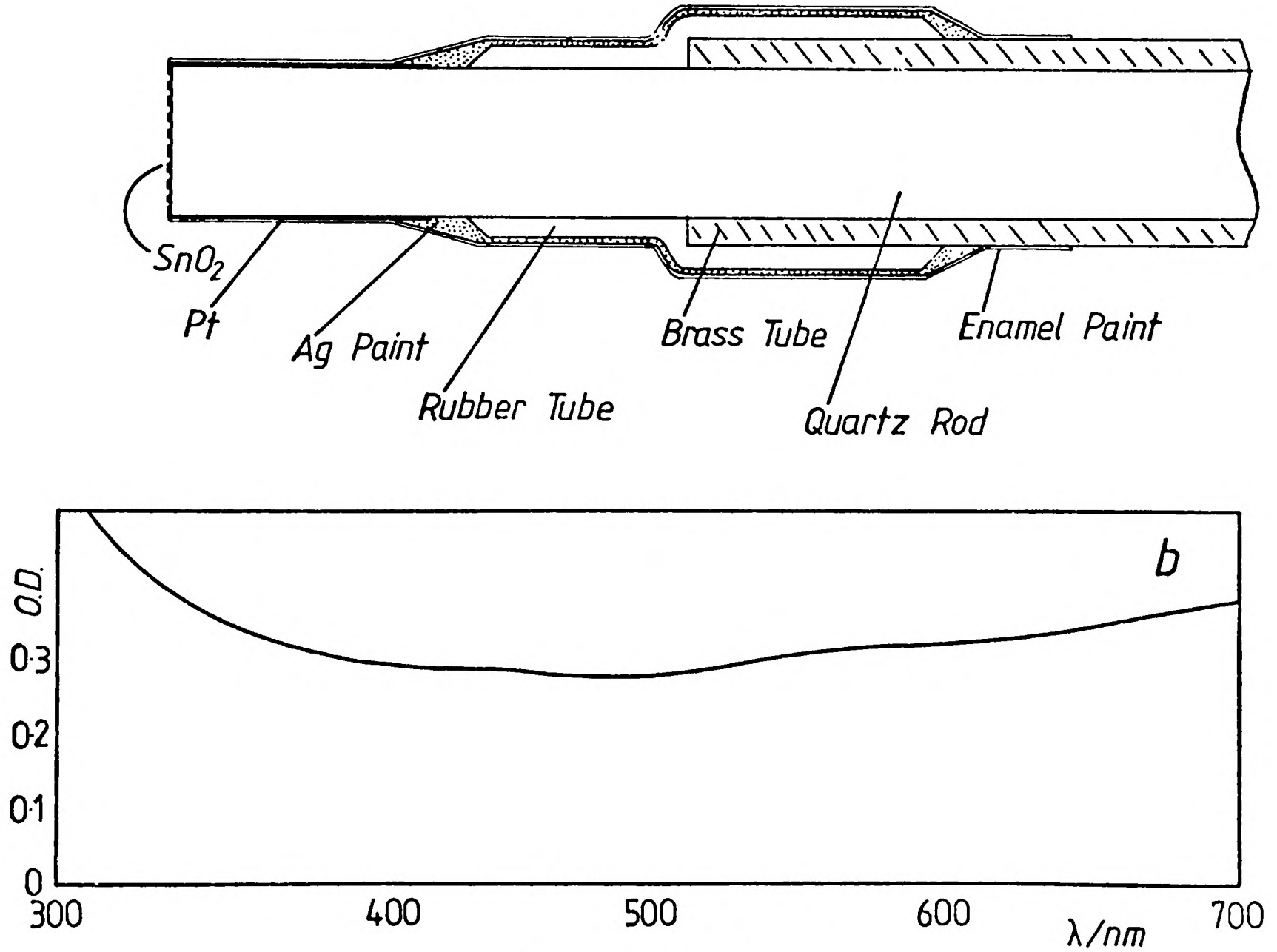

Fig 3 : 7

The Tin Oxide O.R.D.E.

up to 800°C in a Carbolite MF3 furnace to remove the organic components of the paint leaving a thin Pt layer.

The tin oxide was then deposited on the face of the electrode by spraying a solution of $SnCl_4/SbCl_5$ in ethyl acetate onto the red hot rod. The spraying solution was prepared by slow addition of 16.7 cm^3 of $SnCl_4$ and 1 cm^3 of $SbCl_5$ to 33.3 cm^3 of ethyl acetate in a dry glove box. The mole ratio of Sn:Sb was 95:5 giving the maximum film conductivity[60]. The pale yellow solution matured to a deep brown after several weeks and was then sprayed onto the rod, just previously heated to red heat in an oxygen natural gas flame, with a DeVilbis spray gun using compressed air. The rod was rotated at ~5 Hz during the 1-2 second spraying. Reflected interference rings showed that the thickness of the film was 400-700 nm. Figure 3:7b shows the absorption spectrum of the film.

The high doping concentration was chosen to produce an electrode as close to a transparent metal as possible. Semiconductor effects due to low carrier concentrations were not desired. Schottky-Mott[61] experiments by Hillman and Bartlett[62] showed the carrier concentrations to be between 1 and 3 x 10^{21} carriers cm^{-3} which was more than adequate to prevent any drop in potential across the space charge layer of the semiconductor for the current densities measured in this thesis.

Light focussed onto the top of the electrode was trapped by internal reflection and passed through the tin oxide layer at the other end of the rod. Field[56] calculated that this light would have a significantly non uniform radial intensity dependence. He predicted that it would be higher at the centre of the electrode than at the edges. Turner[57] confirmed this experimentally. However Egdell[59] showed that the assumption of uniform light intensity is a good approximation. Three factors are favourable.

1) The thickness of the SnO_2 films was greater in the centre of the disc. As the films absorbed light evenly across the visible spectrum this evened out the non-uniformity in the light intensity for all wavelengths.

2) Radial convection is much faster than diffusion towards the electrode inside the diffusion layer and rapidly evens out any non uniformity in the concentration of photoproducts.

3) All the experiments in this thesis were carried out in region B of Figure 2:4 where $X_k < X_D$ and the radial dependence of the light intensity does not affect the photoelectrochemical collection efficiency.

The Mechanical Design

The general layout is shown in Plate 3:4. The light source, electrode and electrochemical cell were all mounted coaxially and supported on two 18 mm stainless steel rods set in a cast iron baseplate. The electrode was rotated by a servo motor connected by a toothed drive belt and two toothed pulleys to the bearing assembly.

The bearing block was built to a design by Heslop[63]. The important feature of this unit is the mercury contact. This was intended to reduce the noise well below the level generated by the previously used silver carbon brushes. Initially the mild steel mercury cup and the rotor were nickel plated so that the mercury would wet the metal surfaces and provide a good contact. However the nickel dissolved in the mercury and oxides formed which broke the contact. The final solution, which provided very low noise levels, was to put clean mercury into the highly polished cup and rotor.

The electrode was held inside the central shaft by a collet and the whole assembly rotated using toothed belts and pulleys (Aurora Ltd.).

The motor was a printed armature, DC servo motor with integral tachometer made by Printed Motors Ltd. It was controlled by an Oxford Electrodes motor controller with digital readout of the

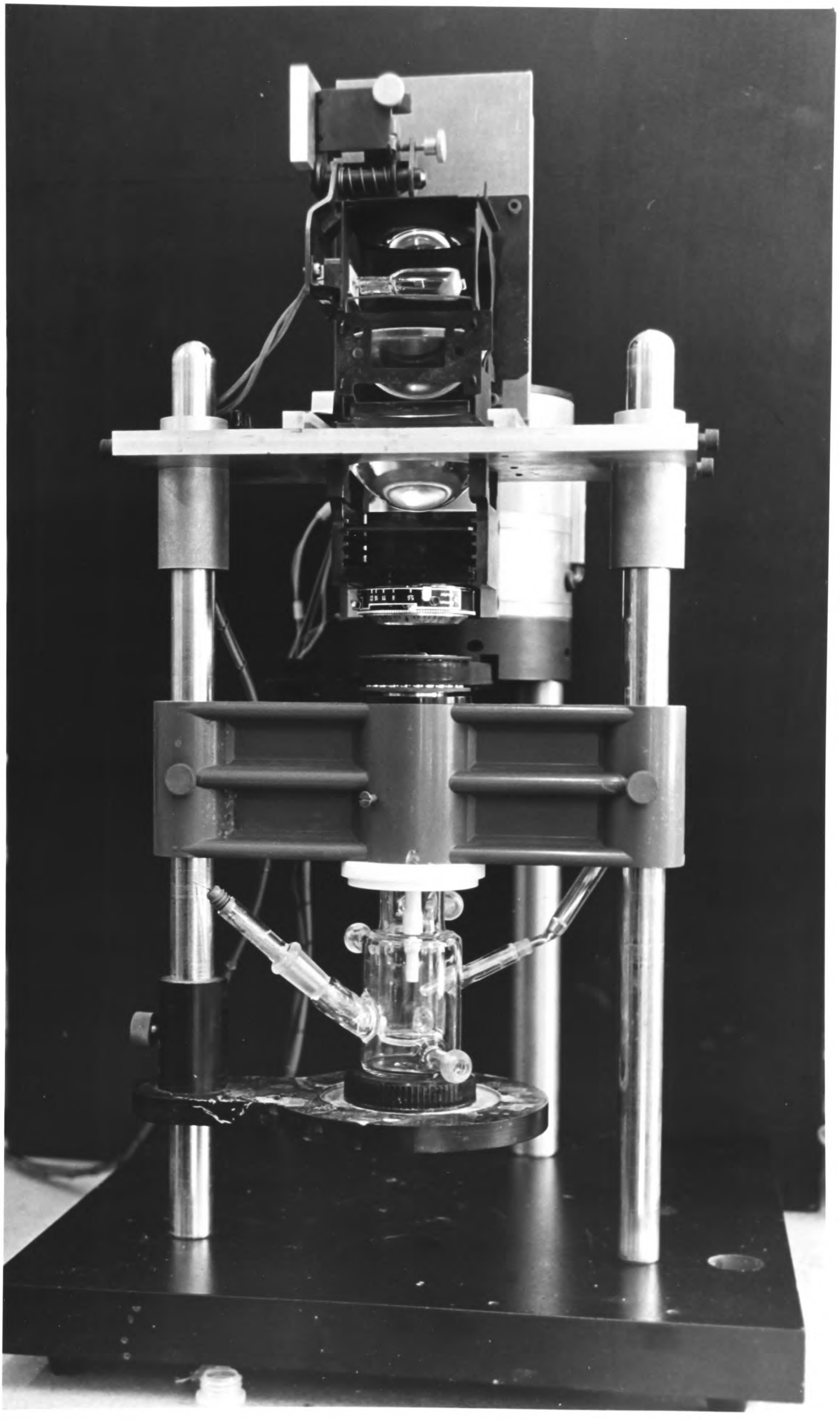

Plate 3 : 4

rotation speed to $\pm$ 0.01 Hz. The servo feedback for the controller was provided by the integral tachometer. The rotation speed of the motor shaft was measured using a toothed wheel and slotted opto-switch (RS components 306-061) providing 100 pulses per revolution. A frequency counter and digital display provided the output. As the rotation speed could only be measured on the motor shaft the toothed belt and pulleys were used to avoid any difference in rotation speed between motor and electrode.

The cell was mounted on a platform, supported above the baseplate, so that it could readily be lowered and removed to allow the electrode to be changed without disturbing the bearing block and optics. Figure 3:9 shows the cell arrangement. Because of the high cost of the compounds studied and the small quantities available a low volume cell was designed. The minimum volume of solution required for this cell was 15 cm^3.

The cell was thermostatted with water to $\pm$ 0.2^oC of the desired temperature (usually 25^oC). White spot nitrogen was further purged of O_2 by passing through three Dreschel bottles containing a caustic solution of anthraquinone-2-sulphonate in contact with Zn/Hg amalgam. The oxy-free nitrogen was then used to deoxygenate solutions in the cell.

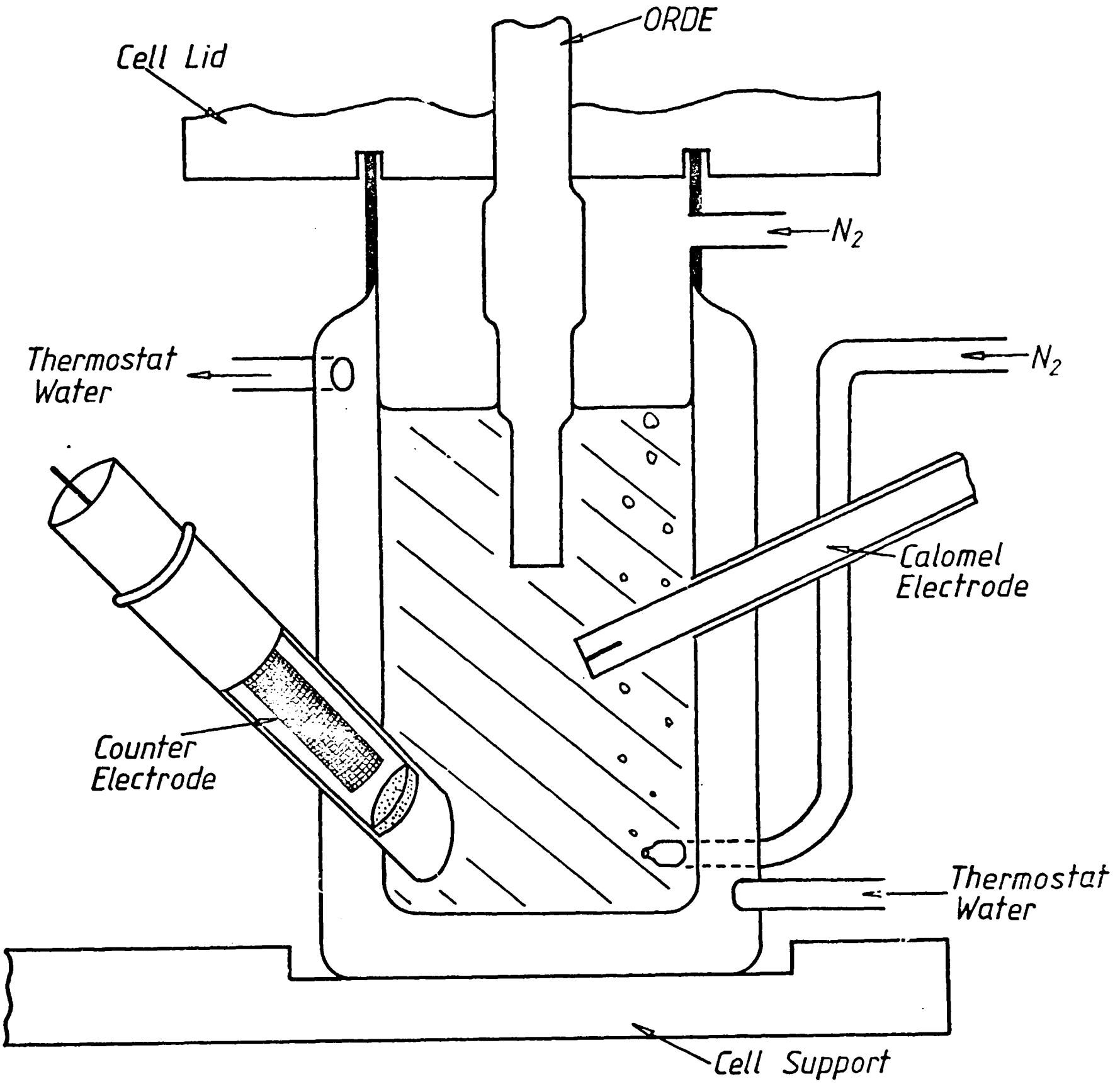

Fig 3 : 9

The Electrochemical Cell

Electronic Control and Measurement

The electronics were built with various modifications to a design by Chadwick[64]. The basic electronic unit used is the operational amplifier (op. amp).

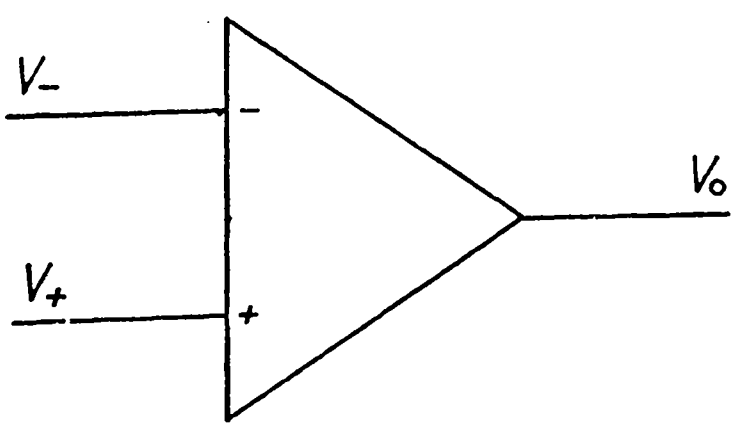

This has two inputs, inverting (-) and non inverting (+), and an output. The properties of the ideal op. amp. are

i) The op. amp. draws zero current at the inputs.

ii) $V_+ = V_-$ if there is a closed feedback loop, i.e. a path of finite resistance between the inverting input and the output.

In practice these conditions are almost fulfilled. Typical input resistances of ~ $10^{12}\Omega$ and input bias currents of <20 pA

are found for FET op. amps. satisfying condition i). Condition ii) is also met as open loop gains of $>10^5$ are found for most op. amps.

$$dV = (V_+ - V_-) = 10^5 V_o$$

A number of modules were constructed.

1) Potentiostat : Figure 3:10a. The non-inverting input and thus by condition ii) the inverting input are held at a potential V_s by the voltage source, S. The working electrode, held at earth, is thus at a potential $-V_s$ relative to the reference electrode. In order to maintain this condition current, i, is passed through the counter and working electrodes. The current is measured by measuring ΔV and applying Ohms law.

Various values of resistor, R_p were used (1k, 10k and 100k). The op. amp. output voltage is limited by the supply to $\pm$ 15V and it can only supply 2-5mA at this potential. The resistor R_p is chosen so that the op. amp. does not saturate (i.e. reach its maximum output voltage). Thus for high currents, e.g. 1-2 mA, a low value of R_p is used. The advantage of using a high value of R_p for low currents (1 nA - 10 µA) is that this amplifies ΔV directly and it was found that this gives a much better signal: noise ratio than using a low value of R_p and subsequent amplification of ΔV. Thus for R_p = 100 k a factor of 20 improvement in the

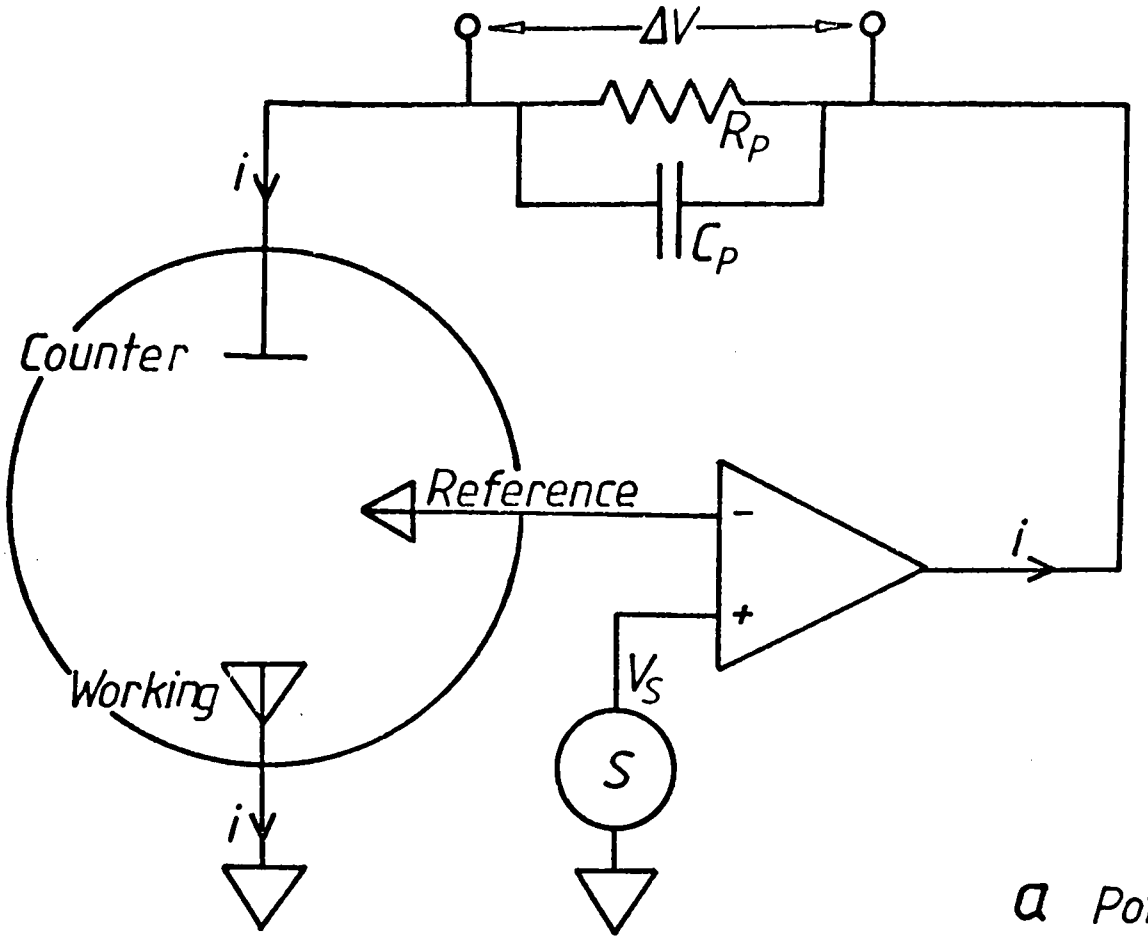

a Potentiostat

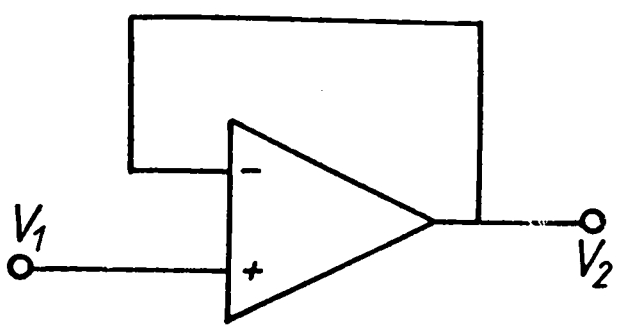

b Voltage Follower

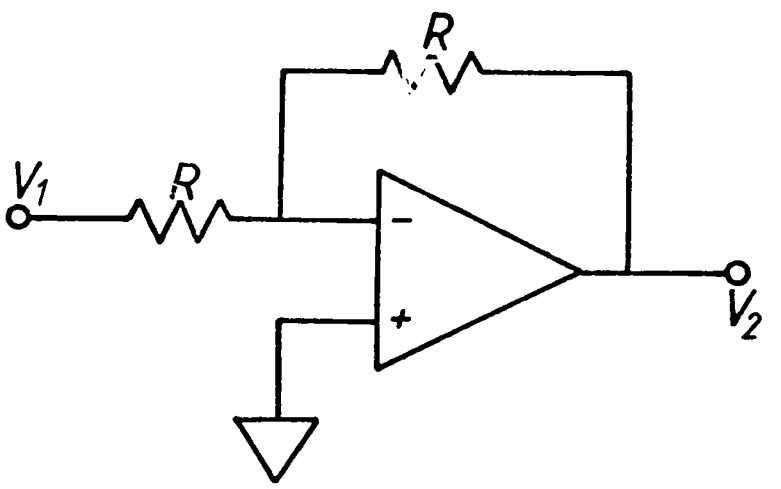

c Voltage Inverter

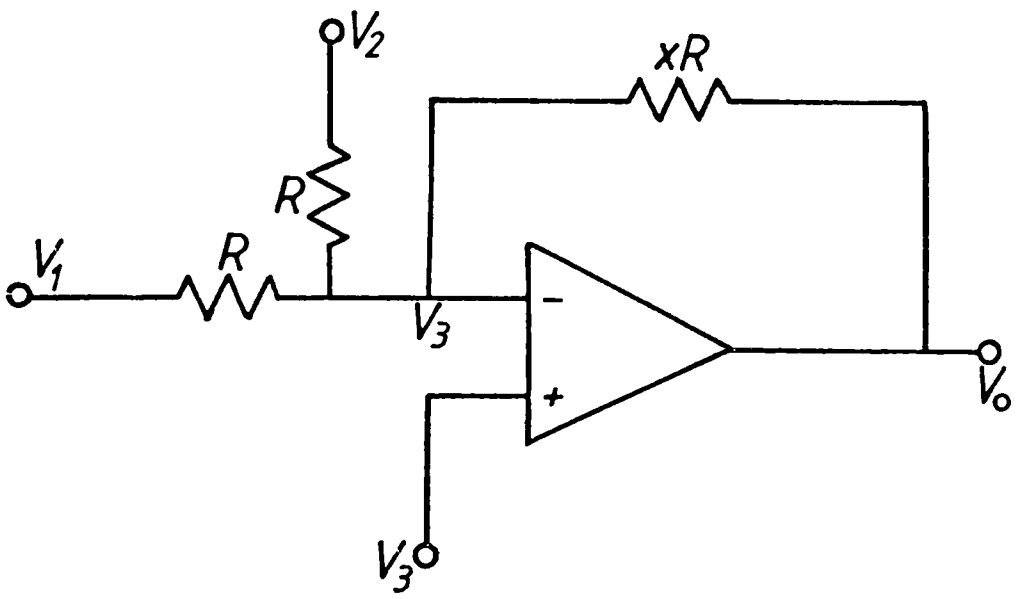

d Summing Inverting Amplifier

Fig 3 : 10

Electronic Modules

signal to noise ratio over R_p = 1 k was found.

A further improvement in the signal:noise ratio was made with the capacitor, C_p, for time dependent measurement. The time constant for the simple $R_p C_p$ filter being chosen to be much less than the time constant of the measured current change to avoid distortion.

2) Voltage Follower: Figure 3:10b. Using conditions i) and ii)

$$V_1 = V_2$$

This circuit provides a means of drawing zero current at the input, V_1, and giving a low impedance output of the same voltage.

3) Voltage inverter : Figure 3:10c. In this case

$$V_1 = -V_2$$

and the circuit is used for just this purpose.

4) Summing inverting amplifier : Figure 3:10d. In this case

$$(V_1 - V_3) + (V_2 - V_3) = \frac{(V_3 - V_o)}{x}$$

and $$d(V_1 + V_2) = - \frac{dV_o}{x}$$

This unit is used to add voltages and then amplify the sum by a factor $-x$ (x = 1, 10 or 25).

5) Voltage Source: Figure 3:11a. This provides a voltage V_s where $-2V < V_s < +2V$ in steps of <1 mV.

6) Triangle wave generator : Figure 3:12. This unit gives a triangle wave with

$$\frac{dV}{dt} = \begin{matrix} 1, 2.5, 5, 10, 25, 50 \text{ mV/s} \\ 0.1, 0.25, 0.5, 1.0 \text{ \& } 2.5 \text{ V/s.} \end{matrix}$$

The peak to peak voltage is variable between 0 and 5 V.

7) Photodiode Circuit : Figure 3:11b. The voltage output, V_o, is proportional to the incident light intensity, I_o. The response time is < 250 ns.

By combining these modules the circuit shown in Figure 3:13 was constructed for photogalvanic measurements. The potentiostat is as described in 1). The potential difference, ΔV, can be

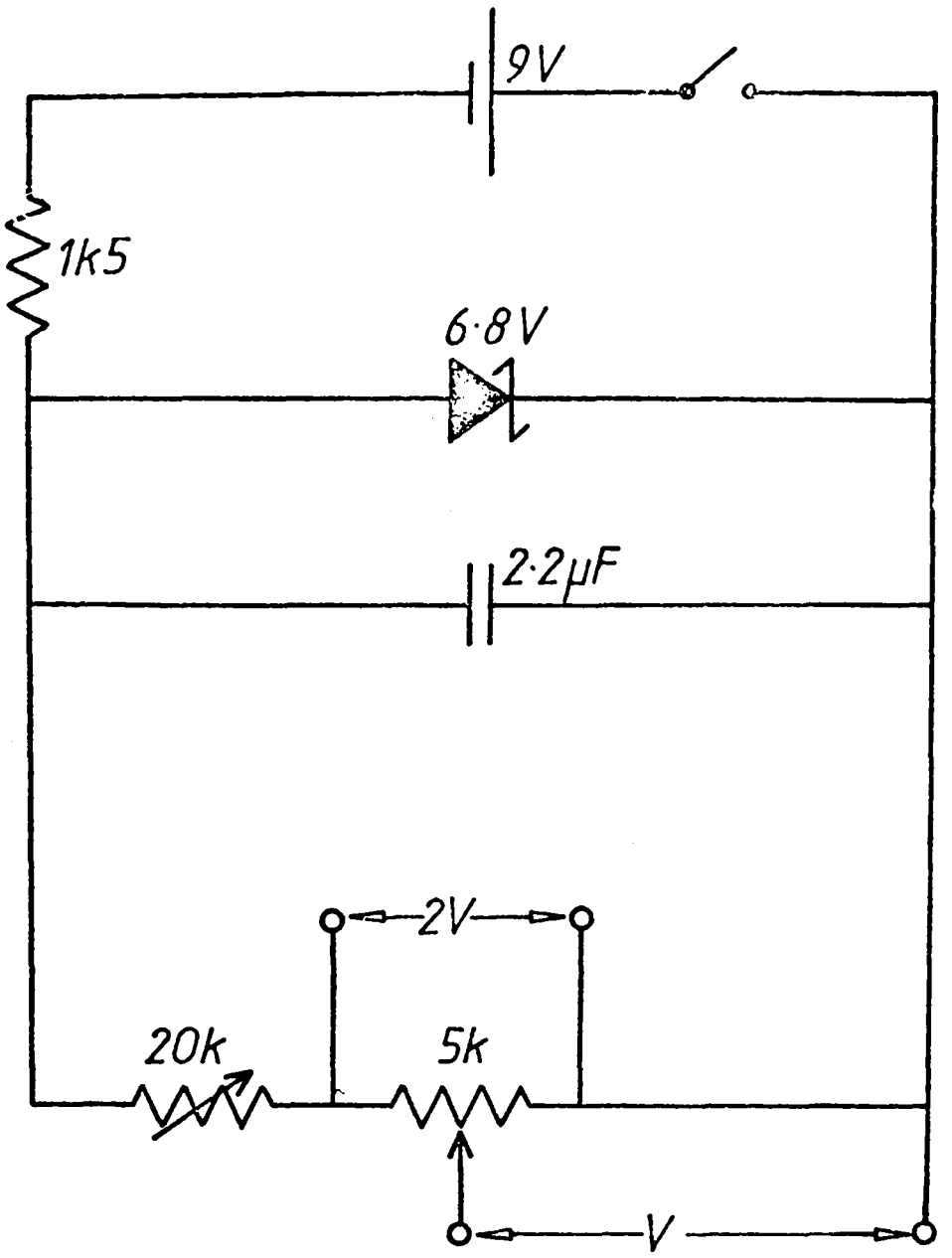

a Voltage Source

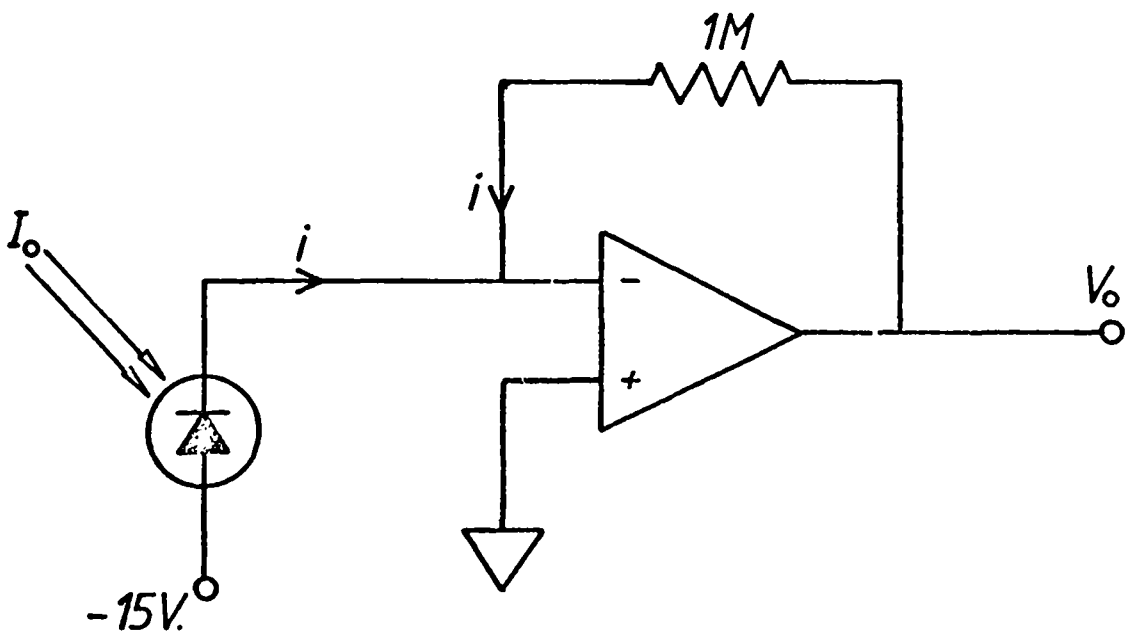

b Photodiode Circuit

Fig 3 : 11

Electronic Modules

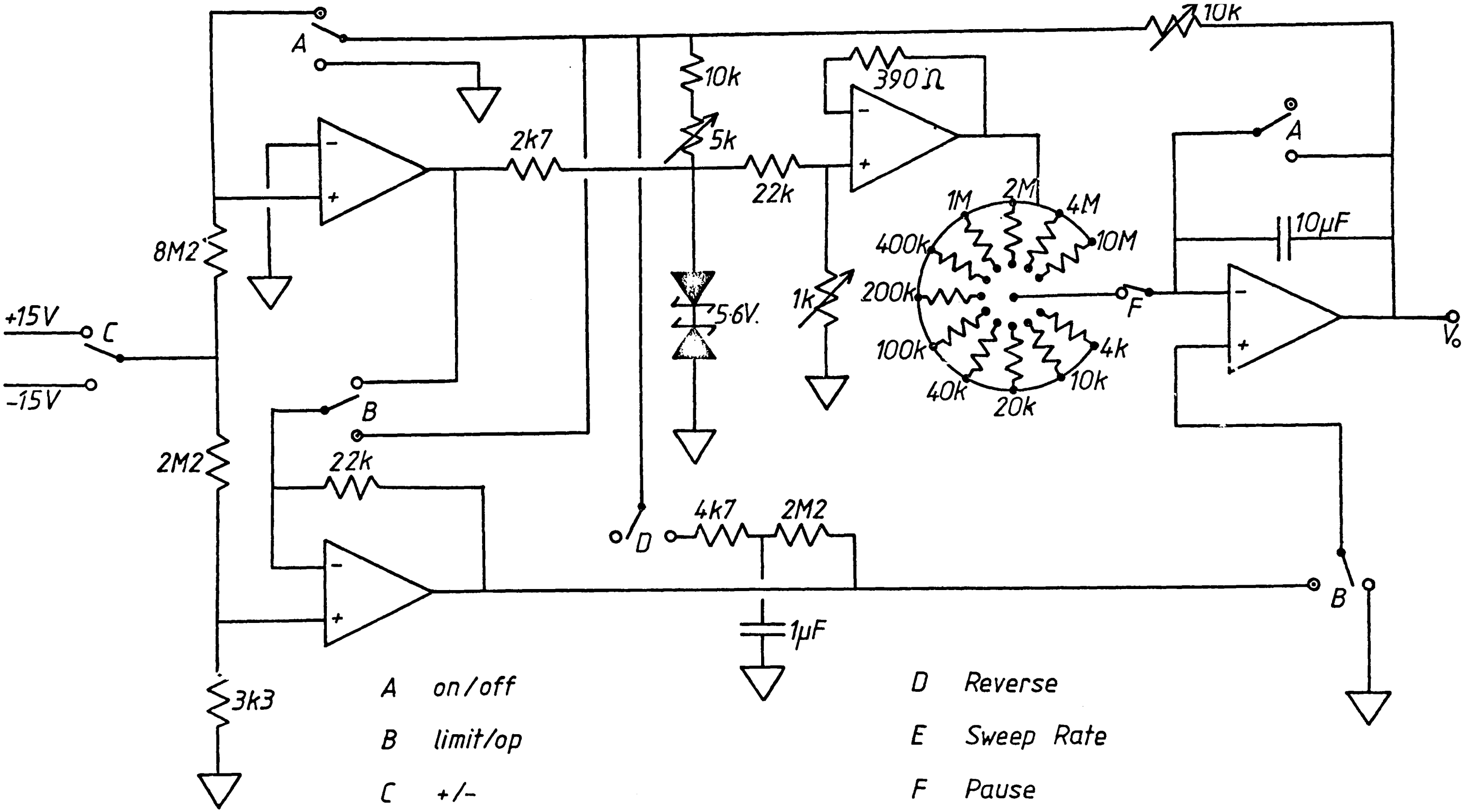

Fig 3 : 12

Triangle Wave Generator

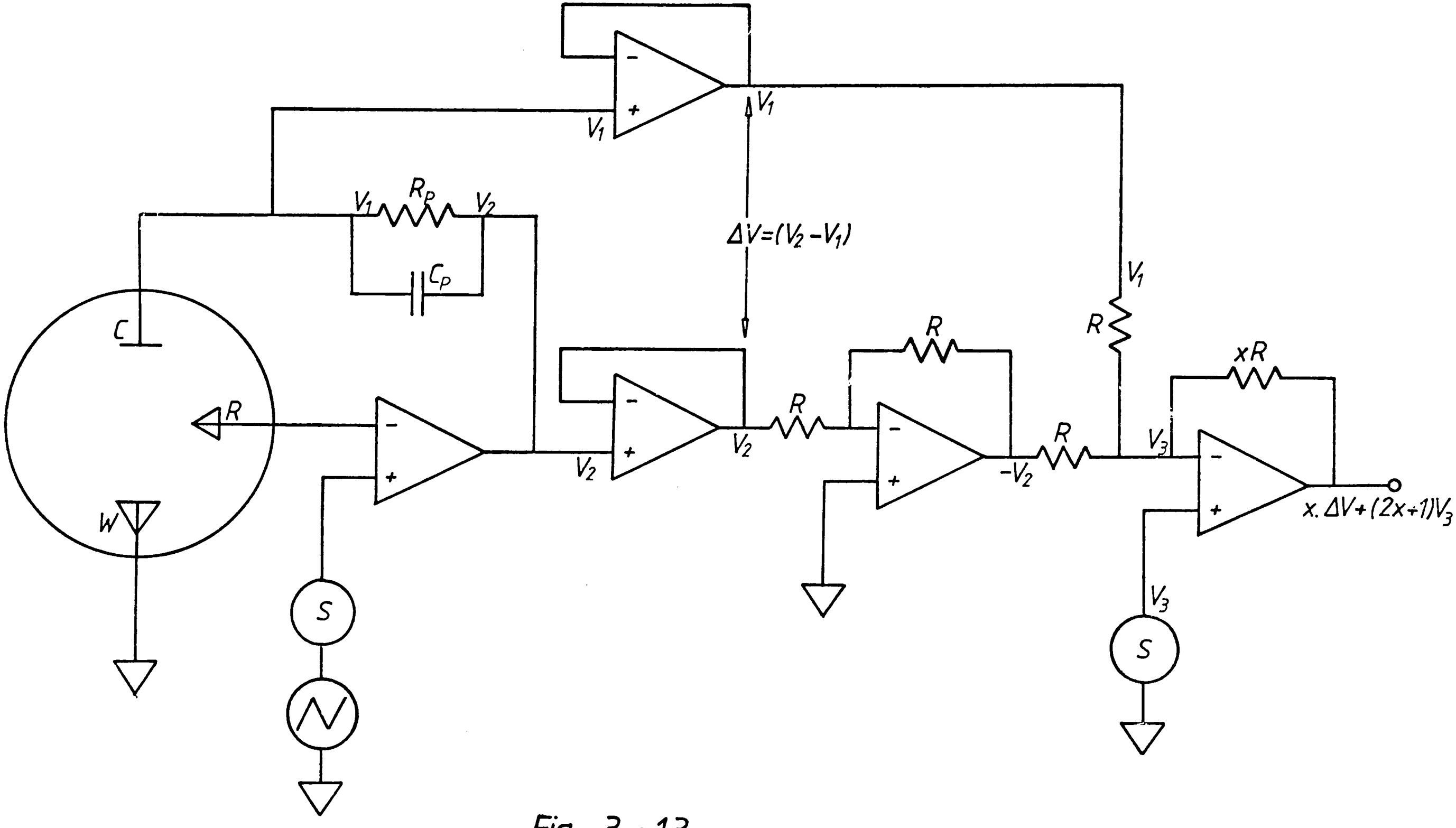

Fig 3 : 13

Circuit for ORDE Measurements

measured after the voltage followers and then the current found by Ohms law

$$i = \frac{\Delta V}{R}$$

However when making photogalvanic measurements it is sometimes necessary to measure small increases in the current on top of a large background. For this reason the output is converted by the inverting amplifier and the summing inverting amplifier to

$$V_o = x \cdot \Delta V + (2x + 1)V_3$$

and $$dV_o = x \cdot d\Delta V$$

Thus by choosing a value of V_3 so that

$$x\Delta V \approx -(2x + 1)V_3$$

the output V_o will be ≈ 0 and a small change in ΔV, $d\Delta V$, may be amplified by the factor x and measured on the most sensitive scale of the voltmeter. (Fluke 8000A Digital Multimeter).

ACTINOMETRY

Measurements of light intensities were made using the method of Hatchard and Parker[65] for ferrioxalate actinometry as a standard. Light was passed through an ORDE into a ferrioxalate solution of sufficient optical density to trap 99% of the light. The quantity of Fe(II) generated was measured spectrophotometrically after complexation with 1:10 phenanthroline and the light intensity calculated given the absolute quantum yield measured by Hatchard and Parker[65].

A Metrologic 60-535 Radiometer was then calibrated to this standard (at 452 nm). The spectral response of the radiometer is shown in Figure 3:14a. Using this response curve the radiometer readings can be corrected to give the true light intensities for the various wavelengths selected by the interference filters. These are shown in Figure 3:14b for a typical electrode. The light intensities are expressed as photon currents. By a suitable choice of neutral density filter an approximately constant photon current may be obtained across the visible spectrum which is useful for measurements of action spectra. This is shown in the figure with the appropriate neutral density filter number marked.

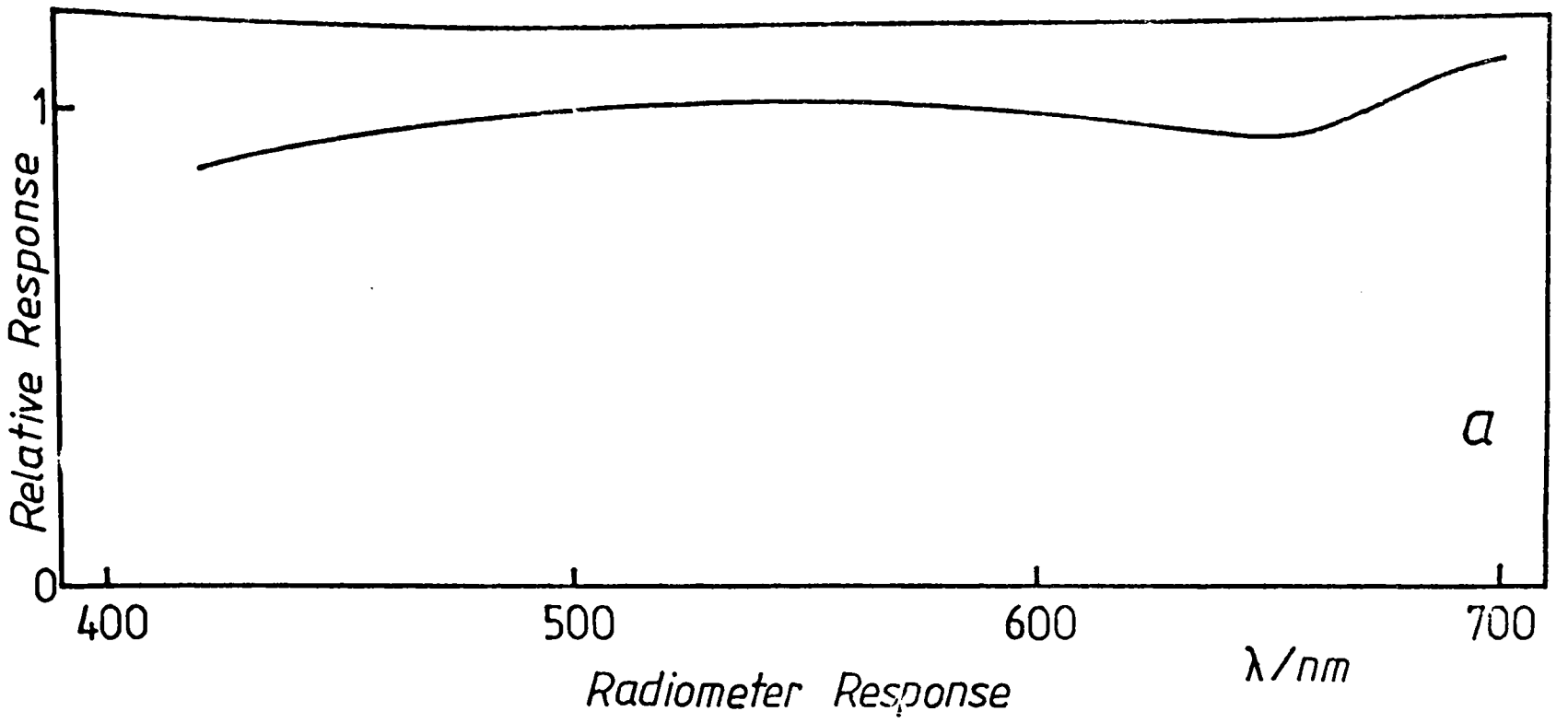

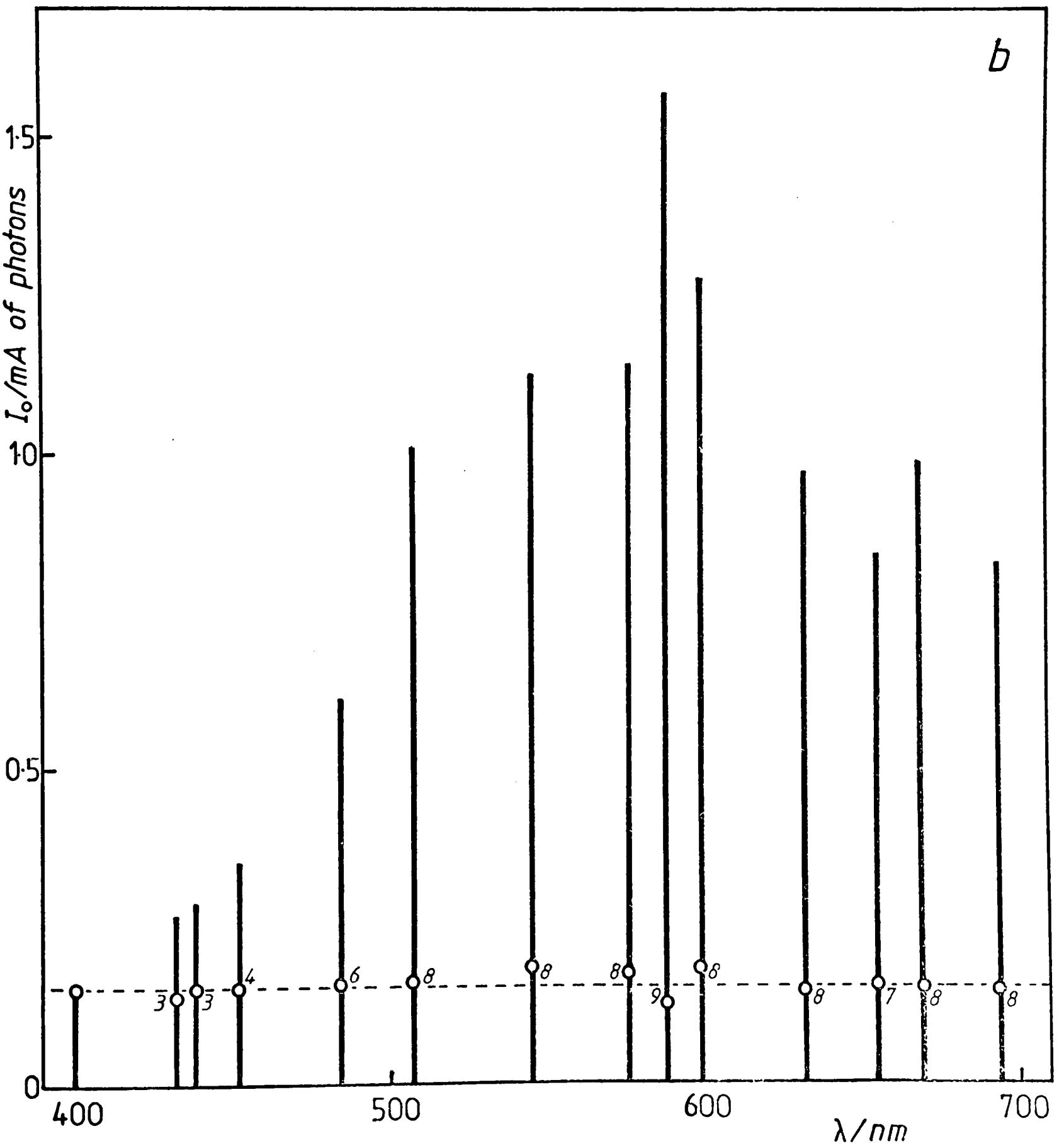

Fig 3 : 14

Light Intensity through Electrode

CHEMICALS

1) All simple inorganic chemicals were of Analar grade and used without further purification. All water used was deionised and then doubly distilled.

2) Ruthenium complexes:

a) $Ru(bipy)_3Cl_2.6H_2O$ was prepared by the method of Burstall[14]. $Ru(III)Cl_3.xH_2O$ (B.D.H.) was heated with excess 2 2' bipyridyl at 250-260°C for several hours. The cooled melt was then extracted with benzene to remove excess organics and the $Ru(bipy)_3Cl_2$ recrystallised three times from water.

		C	H	N	Cl
Analysis	Calc.	48.15	4.85	11.23	9.47
	Found	49.53	4.79	11.64	9.96

b) All other Ru(II) complexes were prepared by Anderson[66] who took great pains to prepare the more soluble chlorides and to avoid the phosphinic acid route[67] to these complexes. The phosphinic acid route invariably leaves trace phosphate impurities with the complex . Egdell[59] and others have shown that phosphate poisons electrode processes at semiconductor surfaces.

3) Substituted Thionines:

These were prepared by Suoto Bachiller[37] by the routes shown in Figure 3:15. Only very small quantities were prepared and they have not as yet been fully characterised.

FLASH ELECTROLYSIS APPARATUS

This apparatus is only a slight modification of the ORDE apparatus. The major differences are

1) The projector light source is replaced by a camera flash gun.

2) An oscilloscope is used to store the transient photocurrents as they are too rapid for an X-Y recorder.

Coles[58] suggested the use of a camera flash gun for the investigation of transient photogalvanic effects, for which it has proved very useful.

A Prinz 770C was used for all flash electrolysis experiments. In such a flash gun the D.C. power from batteries (4 x 1.25V Nickel-Cadmium AA rechargeable cells) is converted to A.C. by an oscillator, transformed up to several hundred volts and then rectified to give a high voltage direct current. This is in turn used to charge up a capacitor where the energy is stored until released across the flash tube. The flash tube is a "Daylight type, colour coated Xenon tube with a colour temperature of 5,600 K".

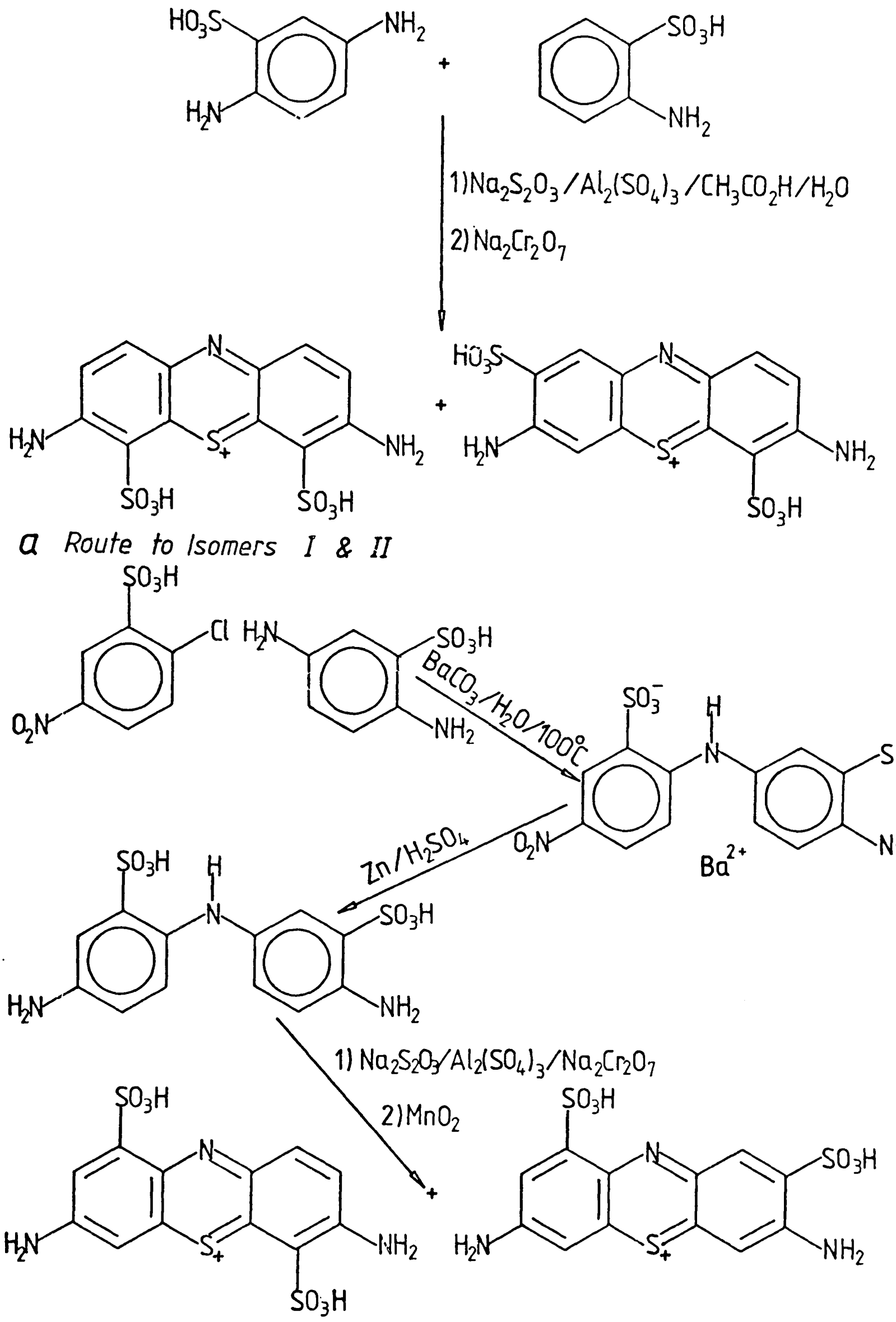

a *Route to Isomers I & II*

b *Route to Isomers III & IV*

Fig 3 : 15

Synthesis of Sulphonated Thionines

Figure 3:16 shows the output light intensity as a function of time and the integrated light intensity. More than 78% of the light is delivered in the first 0.5 ms. The dotted lines show how the flash can be cut short after a given time. This proved a useful feature both to reduce the time duration of the flash and to reduce the total amount of light delivered. It was achieved by using the flash gun on its "auto" setting. In this mode a photocell on the front of the flash gun is connected to an integrator which cuts the flash off when a given integrated light intensity is reached. By reflecting different amounts of light back onto the photocell, by adjusting the position of a small piece of paper close to the flash gun, the flash could be cut off at any time.

Figure 3:17 shows a block diagram of the flash apparatus. The optical electrode is potentiostatted and the current transient stored on a Gould Advance OS 4000 Digital Storage Oscilloscope with a 4001 output unit. The oscilloscope was triggered at the beginning of the flash using the signal from a separate photodiode with a response time of 250 ns. Once stored the transient could be rolled out of the output unit slowly onto a Bryans 29000 XY,t recorder to obtain hard copy.

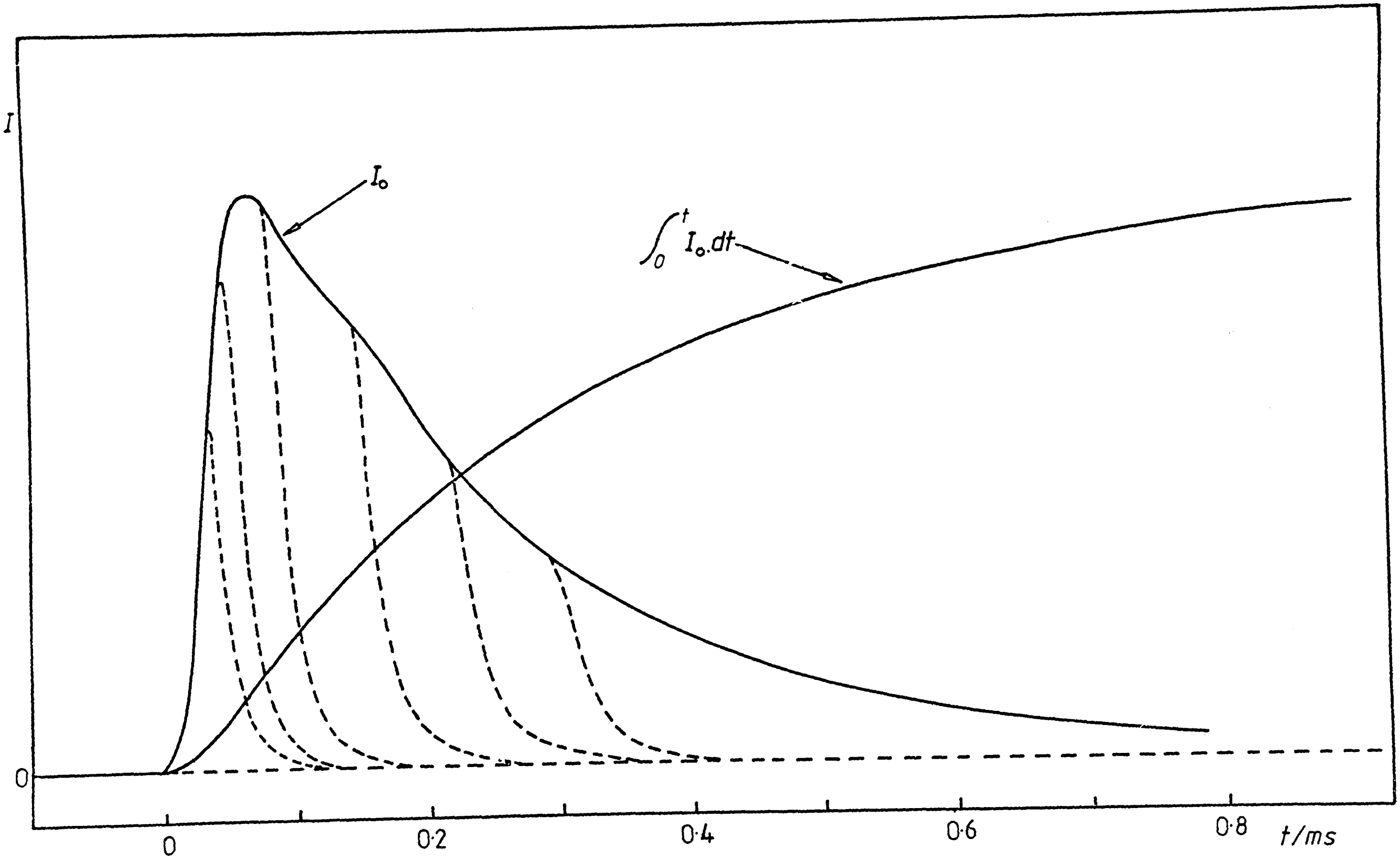

Fig 3 : 16

Flash Profiles

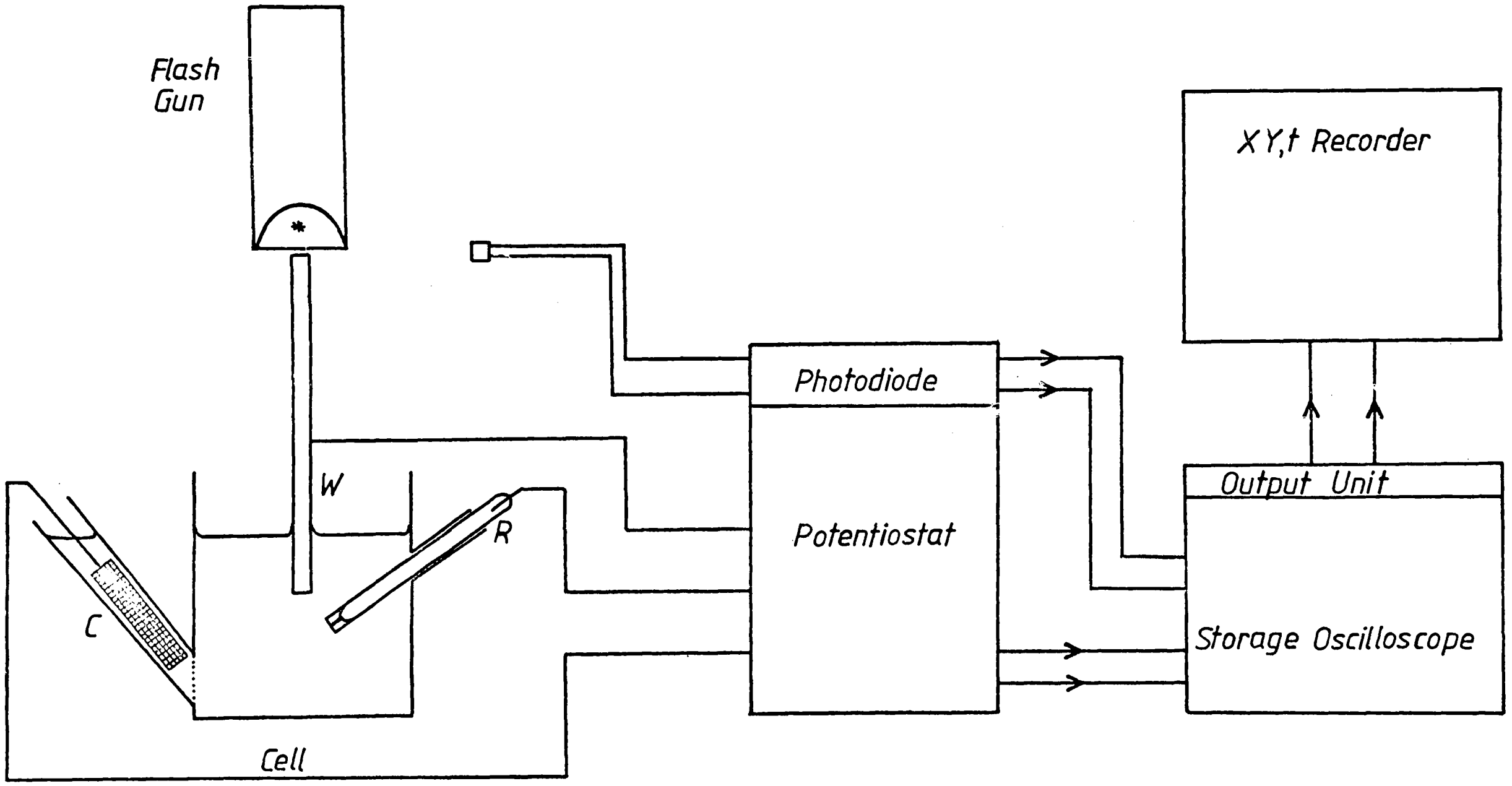

Fig 3 : 17

Flash Electrolysis Apparatus

PROCEDURES

Formal Electrode Potentials

Various methods were used to measure the formal electrode potentials of the couples studied. The method used depended on the electrode kinetics and the stability of the oxidation states. Polarograms were recorded, under potentiostatic control, at a slow sweep rate (~ 5 mV/s) to screen compounds quickly for reversible electrode kinetics.

(a) Reversible Systems : If a compound was found to be reversible the formal electrode potential, E', is equal to the half wave potential and may be obtained by simple analysis. Measurements were made at a rotating tin oxide electrode. The electrode was potentiostatted at various points on the wave and the current and potential noted. A correction was made for the small background currents at the electrode. The very small surface effects made the tin oxide electrode ideal for measuring polarograms at low concentrations as many of the compounds were in short supply and/or sparingly soluble. Figure 3:18 shows the behaviour of the electrodes in 0.5M H_2SO_4 and 0.5M HCl. In H_2SO_4 they behave as ideal polarised electrodes between -0.2 and +1.3 V (v S.C.E.) and, in HCl, between -0.2 and +1.1V (v S.C.E.). In both media use of the electrodes at potentials more negative than -0.3V causes reduction of the Sn(IV) to Sn(II) and dissolution

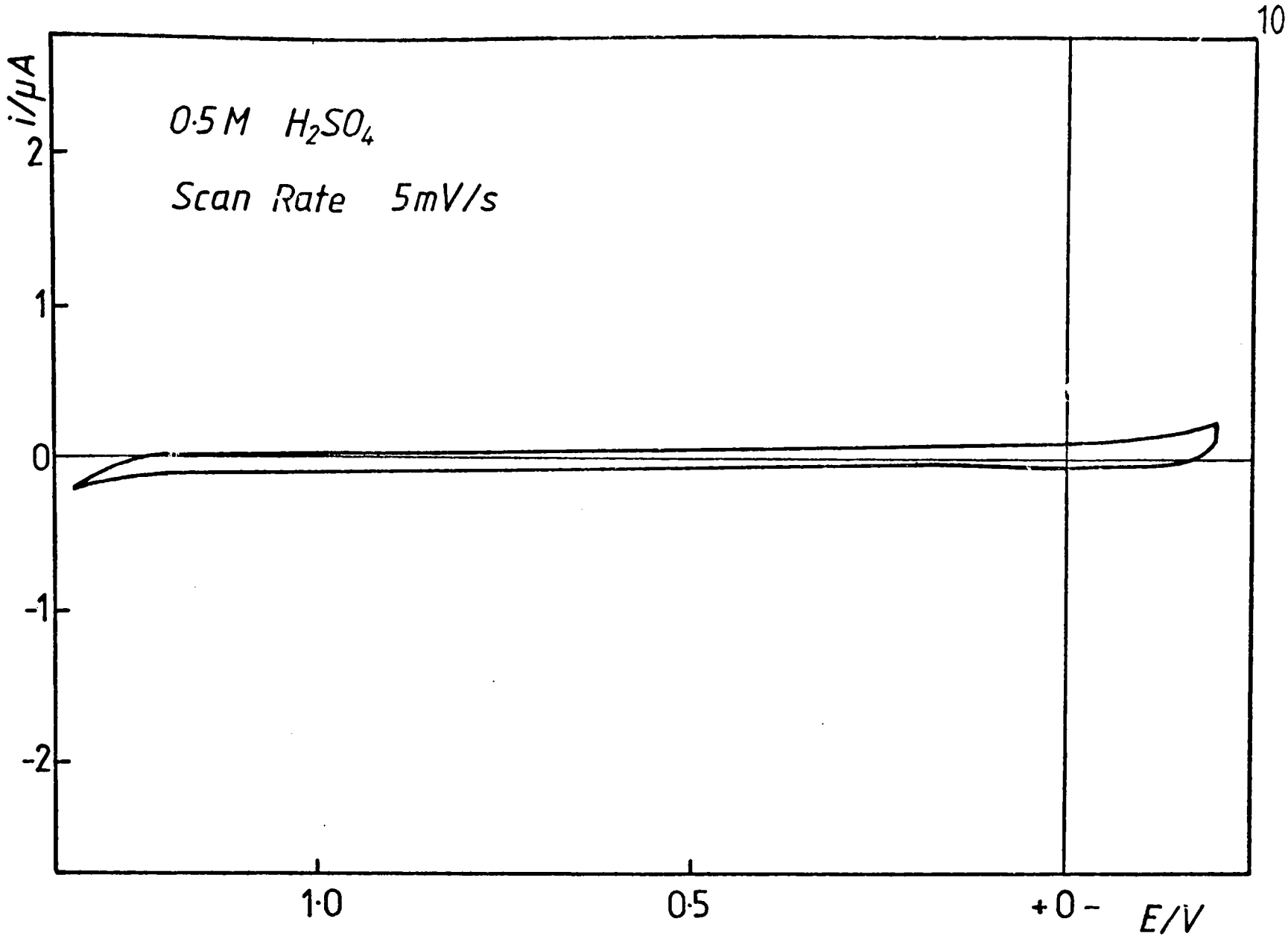

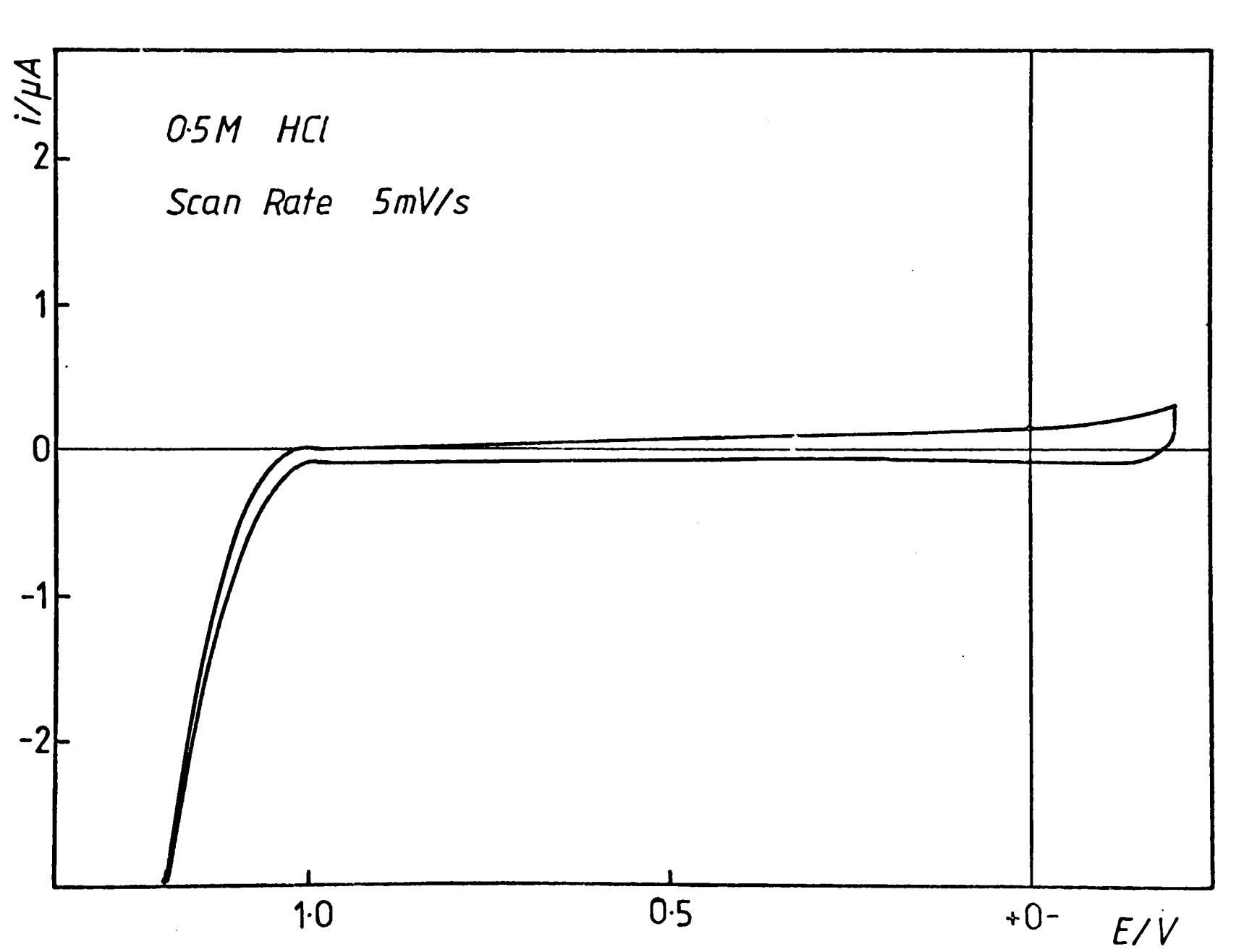

Fig 3 : 18

Behaviour of SnO_2 Electrode in Background Electrode

of the electrode. At positive potentials solvent decomposition was found to occur at > +2.0 V. But use of the electrode at > +1.3 V caused a marked deterioration in performance.

(b) Stable irreversible systems : The formal electrode potentials for the Fe(II)/Fe(III) couple were measured by potentiometric titration. A known concentration of Fe(II) was added in small aliquots to a known concentration of Fe(III) and the potential of zero current was measured. A simple Nernst plot then gave E'.

(c) Unstable irreversible systems : Some of the Ru(II) compounds did not have reversible electrode kinetics and Ru(III) was unstable with respect to reduction by water. The formal electrode potentials were therefore measured by electrogenerating Ru(III) from Ru(II) in situ and then measuring the potential of zero current and the limiting currents of the two species. This was repeated several times for different proportions of Ru(II) and Ru(III). Each measurement could be made in <30 secs. This was much faster than the reduction of Ru(III) by the solvent which had a half-life ranging from 10^3 - 10^4 secs. at room temperature. A Nernst plot could then be constructed as the limiting currents for the two species are proportional to their concentrations.

Diffusion Coefficients

Measurements of diffusion coefficients were made using the Levich relation for the limiting current at a rotating disc electrode (equation (2:13)). Using known concentrations of the pure samples the limiting current was measured at various rotation speeds and the gradient of i_L v $W^{\frac{1}{2}}$ was used to find the diffusion coefficient.

$$D = (n.A.F.c_\infty \nu^{-1/6}. i_L^{-1} W^{\frac{1}{2}} . 1.554)^{-3/2} \qquad (3:1)$$

The electrode was under potentiostatic control for these measurements and the cell was thermostatted at 25°C.

Some diffusion coefficients were also measured as a function of temperature. For these experiments the cell was simply thermostatted at different temperatures and measurements of the limiting current as a function of rotation speed were made as above.

In equation (3:1) the kinematic viscosity, ν, also has a temperature dependence and measurements of ν were thus necessary in order to obtain the diffusion coefficient. These measurements were made using an Oswald Viscometer thermostatted at temperatures between 20 and 50°C. Calibration of the viscometer was made using the literature values[68] for H_2O.

The Albery-Hitchman method[69] for measuring the diffusion coefficient by exhaustive reduction or oxidation of the relevant

ion at a rotating disc was not suitable, despite the advantage that the concentration of the ion need not be known. The time of the experiment (typically 1 hour) is comparable with the rate of reduction of Ru(III) by the solvent. This means that the electrode cannot exhaustively oxidise all the Ru(II) and the method thus fails. The method was, however, used successfully by Foulds and Bartlett[70] to measure the diffusion coefficients for some of the newly synthesised substituted thionine dyes, quoted in Chapter 5.

Photogalvanic Measurements at the ORDE

Various experiments were conducted with the ORDE apparatus all under potentiostatic control. The change in current, Δi, when the shutter was opened was usually measured by the method described in the electronics section of this chapter. However in some cases it was possible to run polarograms with the shutter open and observe the photocurrent as a function of potential directly on the X-Y recorder without amplification by the summing inverting amplifier.

Light intensities and wavelengths were varied with the neutral density filters and interference filters respectively as described. The Metrologic Radiometer was used to measure the light intensities for every electrode as both the areas and the transmittances of the electrodes varied from one to another.

In many of the experiments it was necessary to change the concentration of one component of the solution, while keeping the others constant. Rather than change the whole solution for each concentration a titration technique was developed. To a known volume of solution in the electrochemical cell small aliquots of a solution, of the same composition in all components but the one to be increased, were added. A syringe drive was built to add volumes from 0.01 cm^3 upwards. A 2.5 cm^3 1002 LT Hamilton syringe was mounted in an aluminium support and driven by a micrometer screw gauge graduated in 0.01 mm. A Hamilton teflon needle of internal diameter 0.6 mm was used to introduce the solution into the cell.

Stopped Flow Measurements

A number of rate constants were measured using a Nortech Laboratories Stopped Flow apparatus developed by Caldin[71]. This apparatus was a composite of two models. The basic apparatus was the SF-2A model, however this was improved by the use of a grating monochromator and the control system for the SF-3A model (Plate 3:5). All the experiments in this thesis were conducted under pseudo first order conditions.

One useful feature of the apparatus was a "ratio arm". This pivoted lever allowed the reactant syringes to be driven in various ratios (1:6, 1:3, 1:2, 1:1, 2:1, 3:1 and 6:1) so that the

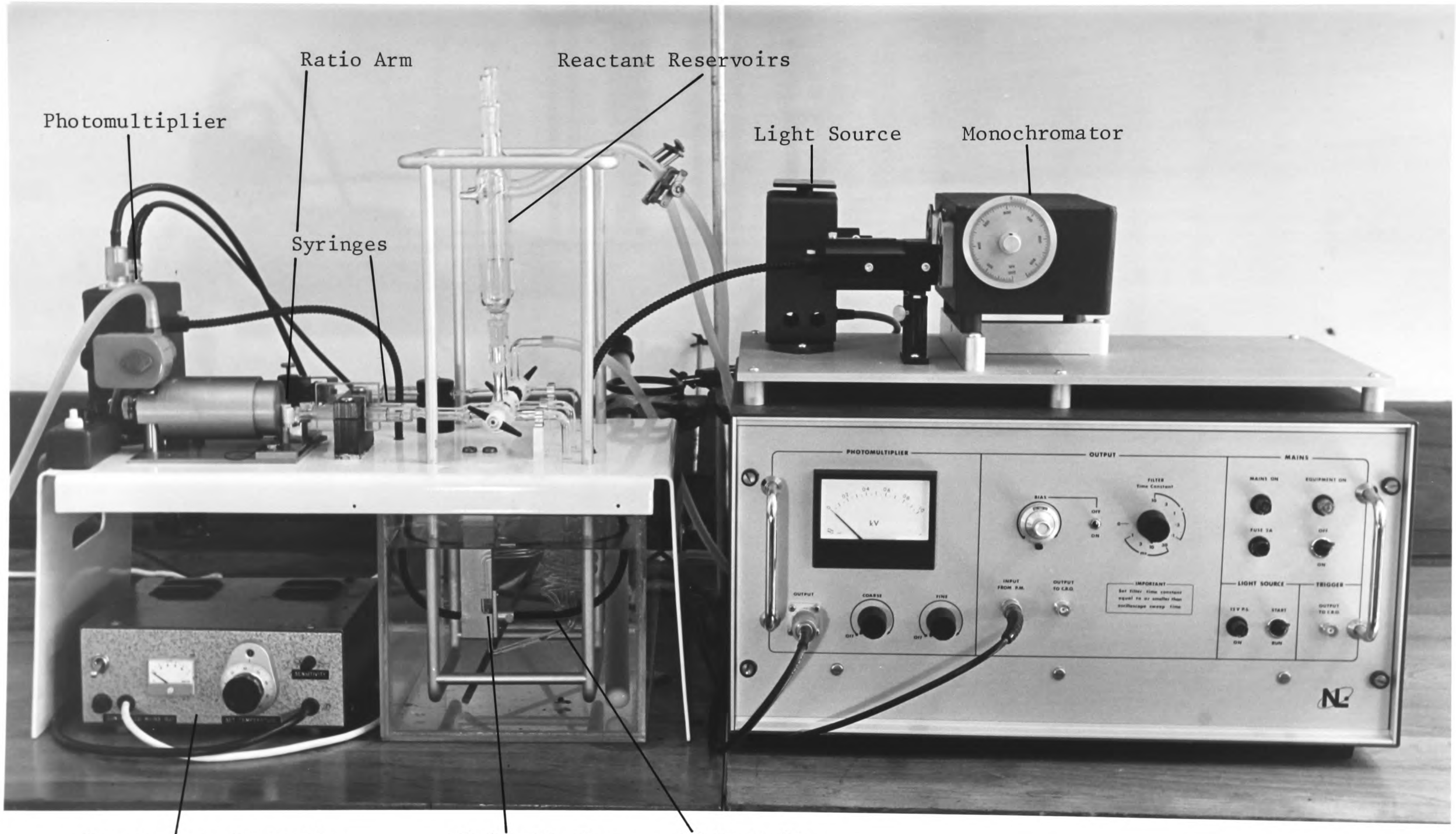
Ratio Arm
Reactant Reservoirs
Photomultiplier
Light Source
Monochromator
Syringes
Temperature Controller
Mixing Chamber
Light Guide

Plate 3 : 5

concentrations of the reactants could be varied without making up solutions at each concentration.

The two general reactions studied were

1) $Ru(III) + Fe(II) \xrightarrow{k} Fe(III) + Ru(II)$.

2) $\text{Substituted leucothionine} + 2Fe(III) \xrightarrow{k} 2Fe(II) + \text{Substituted Thionine}$.

In both cases the reactants, Ru(III) and substituted leucothionines were not stable and were generated electrochemically just prior to the experiment. As already stated the Ru(III) complexes are slowly reduced by water at room temperature and quite rapidly at 50°C. They were thus generated with a large Pt gauze electrode potentiostatted at +1.2 V v SCE and used immediately. The substituted leucothionines were highly sensitive to oxygen and were also generated with a large Pt gauze electrode potentiostatted at 0V v SCE and used immediately. A stream of Argon was used to keep oxygen from entering the reservoirs containing the reactants.

CHAPTER 4

FLASH ELECTROLYSIS

This chapter describes the development of Perone's[42-49] technique to measure transient phenomena at the optical disc electrode. It describes the type of experiment performed and the results used to prove the theory and experimental procedure.

The following diagram rationalises the types of experiment possible with the optical electrode

Light Electrode	Constant	Flash
Rotating	✓	x
Stationary	x	✓

With a constant light intensity the electrode must be rotated to set up well defined hydrodynamics so that a steady photocurrent can be measured. This photocurrent can then be calculated using the ORDE theory. Some of the first transient experiments were attempted at a rotating electrode by using a camera shutter to interrupt the light beam. These experiments proved unsatisfactory because of the noise generated by the peripheral equipment (lamp p.s.u., cooling fans, motor and controller etc.). A flash experiment was therefore developed.

For the flash experiment the electrode is kept stationary as the theory is most easily derived assuming semi-infinite linear diffusion. Rotating the electrode both complicates the theoretical treatment and reduces the observed effect by convective dilution. A further advantage is gained as all of the peripheral equipment required to maintain a steady state in the ORDE experiments can be switched off for the one or two seconds duration of the experiment, greatly reducing the noise level.

EXPERIMENTAL PROCEDURE AND RESULTS

The apparatus developed for these experiments is a slight modification of the ORDE apparatus and is described in the previous chapter. For these experiments the electrode is potentiostatted at a potential where all the photoproducts reaching the electrode will be oxidised (Thionine system) or reduced (Ruthenium system). The flash gun is then fired and the current-time transient recorded on a storage oscilloscope.

Solutions The solutions for these experiments were made up with the following factors in mind.

1) The dye, A. A lower limit on the concentration of the dye is imposed by the need to achieve a measurable signal above the noise. This limit was found to be 5×10^{-5}M for both thionine and ruthenium systems. The upper limit on the concentration

is set by two constraints. The first is that the optical length, X_ε, must be much greater than the length, X'_D, over which photo-porducts diffuse to the electrode in the timescale of the experiment. This is in order to fulfil the assumption made in the theory that the solution is subjected to a constant light intensity as a function of distance from the electrode during the flash. This assumption is not absolutely necessary (a Beer-Lambert profile could be used) but it does simplify the mathematical treatment.

X'_D is given by

$$D = \frac{(X'_D)^2}{t} \qquad (4:1)$$

and assuming values of $D \sim 5 \times 10^{-6}$ cm^2/s and of an empirical maximum t of ~ 2 s.

$$X'_D \approx 3 \times 10^{-3} \text{ cm.}$$

This puts an upper limit on [A] of 2×10^{-4} M assuming that $X_\varepsilon = 10\ X'_D$ and taking $\varepsilon = 1 \times 10^5$ (natural log. extinction coefficient), which is a typical value for the most strongly absorbing thionine compounds. The second requirement concerns the ratio of [A] : [Y] and is discussed in 3).

2) The quencher, Z : The concentration of the quencher was always chosen to give the maximum quantum efficiency, ϕ_1, for the electron transfer quenching

i.e. for the system

$$A \xrightarrow{h\nu} A^* \qquad (4:2)$$

$$A^* \xrightarrow{Z} B + Y \qquad k_q[Z] \qquad (4:3)$$

$$A^* \xrightarrow{k_t} A \qquad k_t \qquad (4:4)$$

$k_q[Z] >> k_t$.

For Ru(II) systems this is 10^{-2} M Fe(III) and for Thionine systems 10^{-2} M Fe(II) although the absolute values of k_q and k_t are different in each case.

3) The Oxidised/Reduced quencher, Y : The concentration of this species was varied to give pseudo first order rate constants, k_{obs}, in the range 1 - 500. The reasons for limits are discussed at the end of this chapter. One further condition imposed is on the ratio of [A] to [Y]. An analytical solution for the flash electrolysis transient can only be found for a first order decay of B. If the flash converts a high proportion of A to B then in order that pseudo first order kinetics for the back reaction

$$B + Y \xrightarrow{k_{-2}} A + Z \qquad (4:5)$$

should hold, we must have [A] << [Y]. This is not an easy

condition to fulfil for $k_{-2} > 10^6\ M^{-1}\ s^{-1}$ as we must also have $k_{obs} < 500$, where $k_{obs} = k_{-2}[Y]$, so we must have

$$[A] << [Y] < 500/k_{-2}$$

or $$10^{-4} M << [Y] < 5 \times 10^{-4}$$

which leaves little room for changing [Y].

4) The background electrolyte: For all measurements of k_{-2} this was standardised as 0.05 M H_2SO_4 for thionine systems and 0.5 M HCl or H_2SO_4 for Ruthenium systems.

The Electrode. The stationary optical electrode was potentiostatted at the potential of zero dark current. This corresponded to potentials in the region of + 0.4 to + 0.5 V for both Ruthenium and Thionine systems as the small exchange currents of the irreversible Fe(II)/(III) couple were sufficient to poise the electrode at these potentials. The electrochemistry of the Fe(II)/(III) couple at SnO_2 electrodes is discussed in the next chapter, however the important points of potentiostatting in this region are.

1) The Fe(II)/(III) couple is almost completely inactive in this region so that the only electroactive species is the photoproduct B, (Ru(III) or Leucothionine) and the potential is such that all the B reaching the electrode is reduced (Ru(III)) or oxidised (Leucothionine)., i.e. the concentration of B at the

electrode surface, $[B]_o$, is zero.

2) The precise selection of the potential of zero dark current ($\pm$ 5 nA) prevents the build up or depletion of Fe(II)/(III) close to the stationary electrode due to the small but none the less significant exchange currents. Furthermore if the electrode is not potentiostatted at the potential of zero dark current there is a slow drift of this current due to the perturbation of [Fe(II)] and [Fe(III)]. This causes errors in the analysis of the transients, which is very sensitive to the change in zero.

3) At potentials + 0.5 V to SnO_2 electrodes showed a transient photoeffect of their own even in background electrolyte. It was therefore necessary to avoid these potentials.

As stated in the introduction to this chapter the electrode was stationary. This allows the thickest diffusion layer possible. This in turn allows the longest time for the assumption of semi-infinite linear diffusion, made in the theory, to hold and thus extends as far as possible the lower limit for the measurement of rate constants. This time is >10s as the electrodes were found to have well behaved rotating disc hydrodynamics, as judged by the limiting currents obtained (Fig. 5:5), at 1 Hz and this rotation speed corresponds to a time of passage across the diffusion layer of ~10s.

The Transient. Just before the flash much of the peripheral equipment (in particular the water pump and temperature controller) was switched off to reduce noise levels and the nitrogen was switched from bubbling through the solution to passing over the top to prevent convection close to the electrode. The flash gun was then fired manually and the light, I_o, and current, i, transients followed on the double-beam storage oscilloscope. The oscilloscope was triggered at the start of the flash as measured by the photodiode. A typical example is shown in Figure 4:1.

The early part of the transient was found to yield no useful information on the rate constant because of the slow potentiostat response and is discussed in a subsequent section of this chapter. The signal was therefore amplified for accurate measurement of the latter part of the transient (Figure 4:2a) and analysed according to the theory (equation 2:60) by plotting $\ln/it^{\frac{1}{2}}$) v t (Figure 4:2b).

It is clear that the shape of the transient is predicted accurately by the theory and the gradient of the line gives the rate constant, k_{obs}. The second order rate constant, k_{-2}, is found by measuring k_{obs} as a function of [Y].

Results

1) Ru(II) systems: In order to obtain quantitative confirmation of the theory a number of $Ru(II)L_3$ systems were studied under the same condition (0.5 M H_2SO_4) as those used by Sutin[26]. The rate constants, k_{obs}, were measured as a

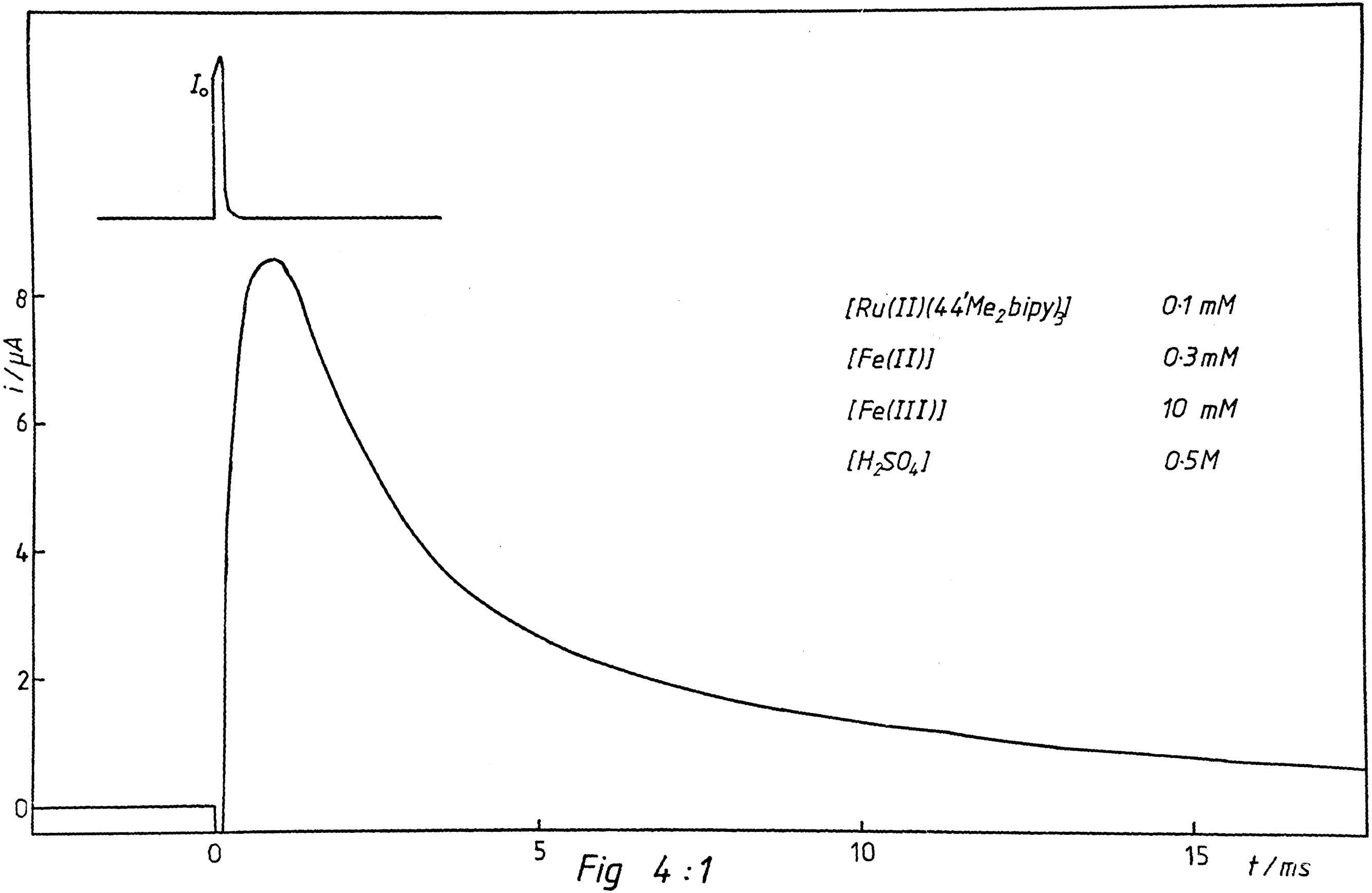

Fig 4 : 1

A Typical Flash Transient

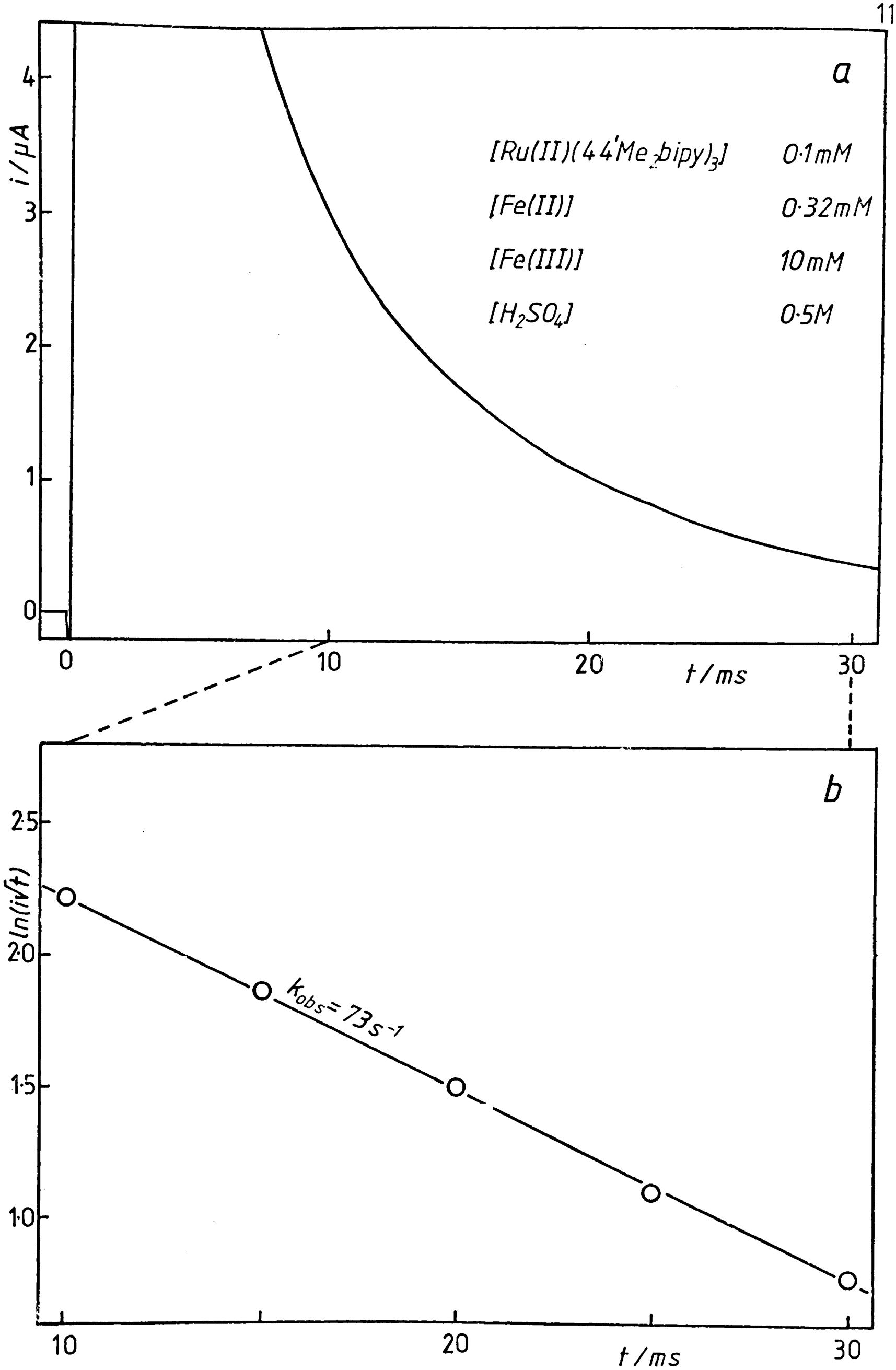

Fig 4 : 2

Flash Transient and Analysis

TABLE 4:1

Compound	$k_{-2}/10^5 M^{-1}s^{-1}$ (This work)	$k_{-2}/10^5 M^{-1}s^{-1}$ (Sutin[26])
$Ru(4,4'Me_2bipy)_3$	1.9 ± 0.1	2.1
$Ru(5,6\ Me_2bipy)_3$	16 ± 1	18
$Ru(4,7\ Me_2phen)_3$	2.5 ± 0.5	3.4
$Ru(3,4,7,8\ Me_4phen)_3$	0.56 ± 0.02	0.61

function of added [Fe(II)]and typical examples of the results are shown in Figures 4:3 and 4:4. The gradients of these lines give the second order rate constant

$$k_{-2} = \frac{\partial k_{obs}}{\partial [Fe(II)]} \qquad (4:6)$$

These results are compared with Sutin's values, which were measured by Stopped Flow, in Table 4:1. The good agreement confirms all of the assumptions made in the theoretical description, and the experimental technique.

One feature of Figures 4:3 and 4:4 which is not predicted is the significant intercept at [Fe(II)] = 0. This is due to significant concentrations of photogenerated and adventitious Fe(II). If the lines are extrapolated back to $k_{obs} = 0$ the intercept on the [Fe(II)] axis might be expected to give an estimate of this photogenerated [Fe(II)] and is 5×10^{-5} M. A theoretical estimation of the photogenerated [Fe(II)] can be obtained from the bulk photogenerated which is given by rearranging equation 2:60

$$C_o = \frac{i(\pi t)^{\frac{1}{2}} e^{kt}}{n.A.F.D^{\frac{1}{2}}} \qquad (4:7)$$

Substitution of measured values for typical transients into this equation gives $C_o \approx 6 \times 10^{-5}$ M. This suggests that most of the intercept is caused by photogenerated [Fe(II)] and that the Ru(II) ($\sim 10^{-4}$ M) is almost entirely converted to Ru(III) by the flash.

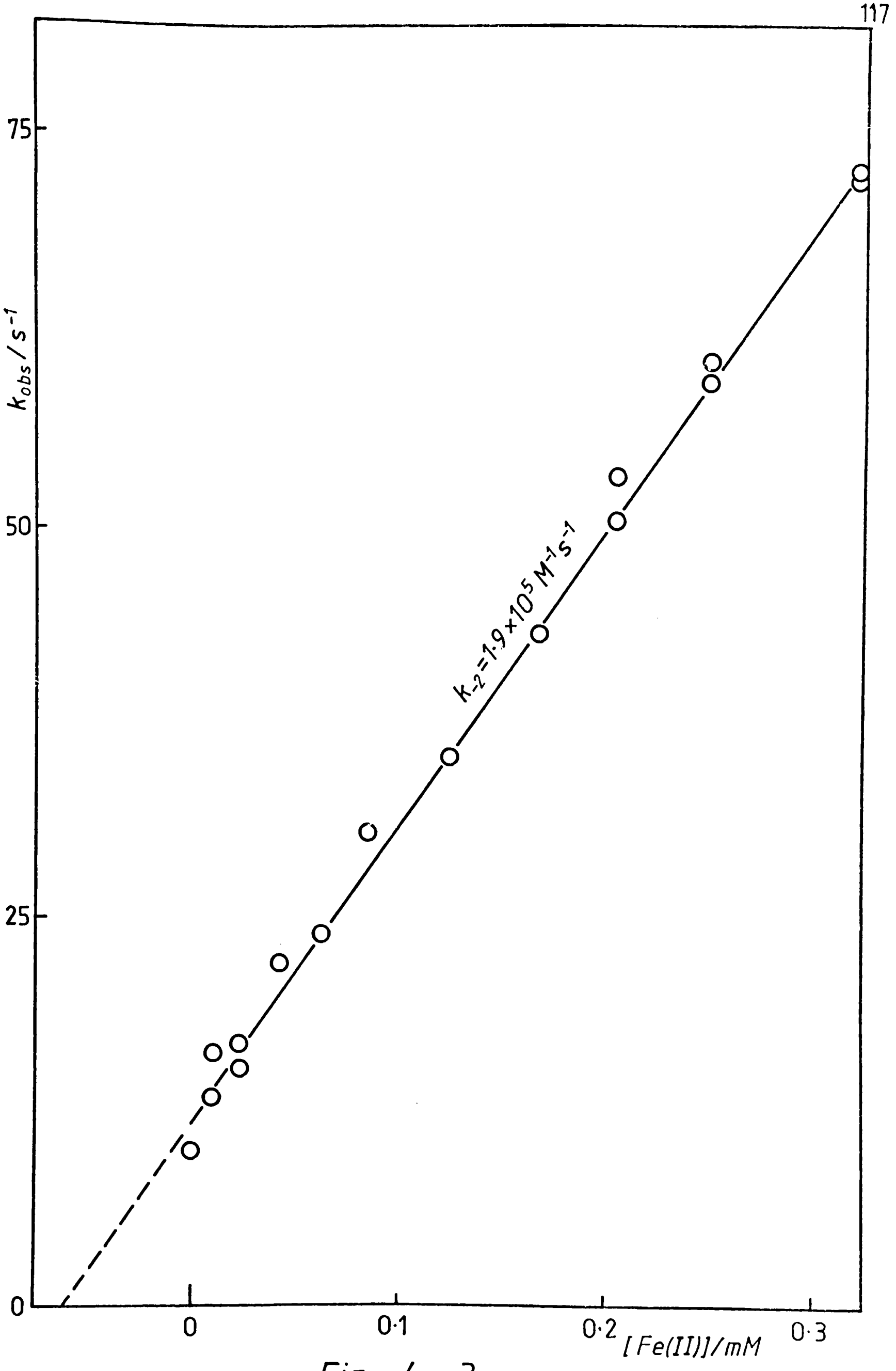

Fig 4 : 3

k_{obs} v [Fe(II)] for Ru(III)(4 4'Me_2bipy)$_3$ in 0·5 M H_2SO_4

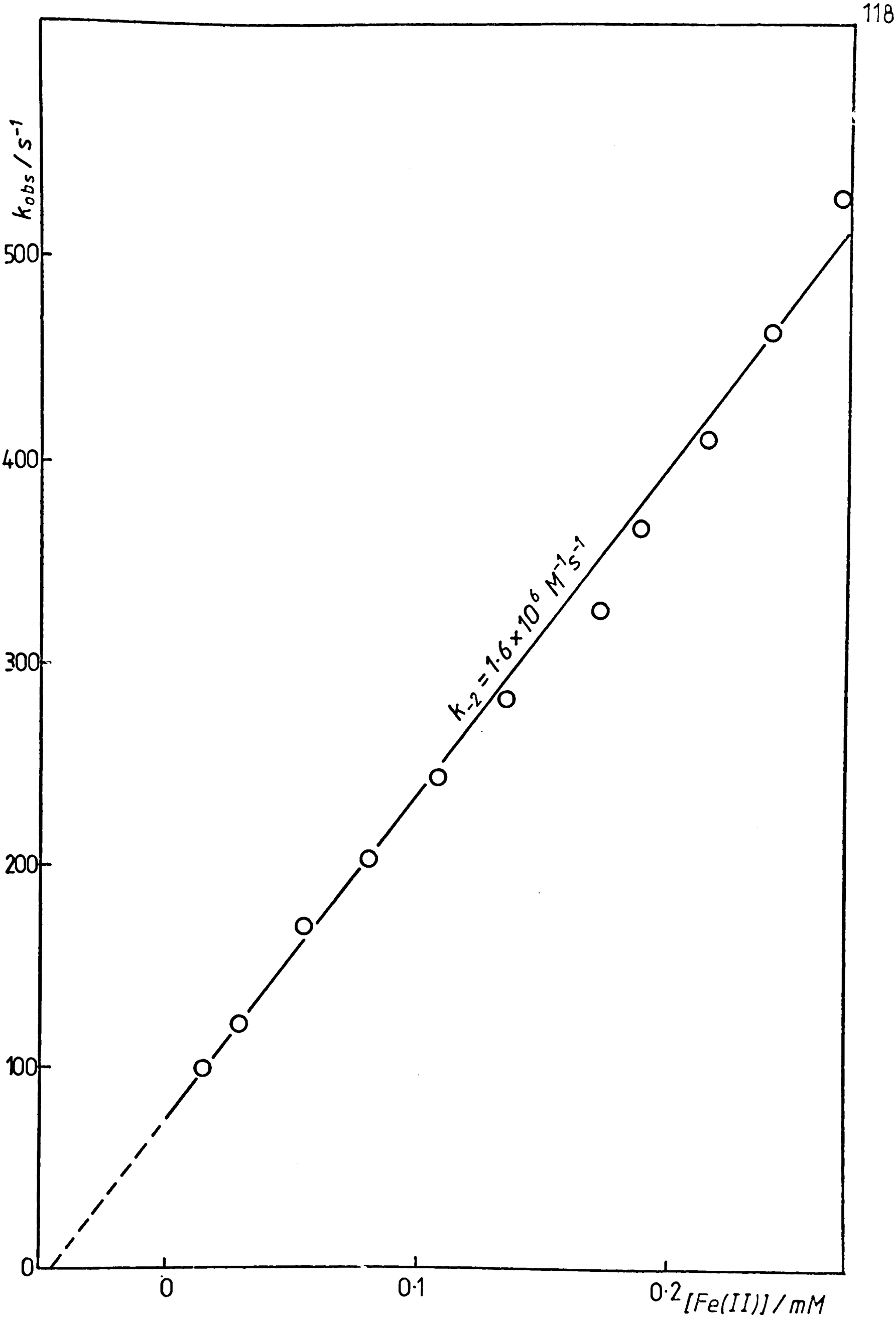

Fig 4 : 4

k_{obs} v [Fe(II)] for $Ru(III)(5,6Me_2phen)_3$ in 0·5M H_2SO_4

It is worth noting that at low added Fe(II) where first order kinetics would no longer be applicable in, for example, a stopped flow experiment the transients still give a reasonable estimate of k_{obs}, and the $\ln(it^{\frac{1}{2}})$ v t plots are still quite linear.

This may be explained in terms of the concentration profiles for the second order case shown in Figure 4:5. The profiles were obtained by Daul[24] by numerical solution of the second order case for $[B]_o = [Y]_o$.

The normalised time variable is

$$\tau = 1/k_{-2}[B]_o$$

the normalised distance from the electrode is

$$\chi = (D.\tau)^{\frac{1}{2}}$$

At $\tau = 0$ equal concentrations of B and Y (Ru(III) and Fe(II)) are generated by the flash. In the bulk of the solution the decay of B is a normal second order process and $[B] = [Y]$. However close to the electrode the electrode perturbation leaves a higher concentration of Y than found in the bulk of the solution. B diffusing through this layer is thus depleted at a faster rate and experiences a less variable concentration of Y than it would in purely homogeneous experiments such as stopped flow or flash photolysis.[72]

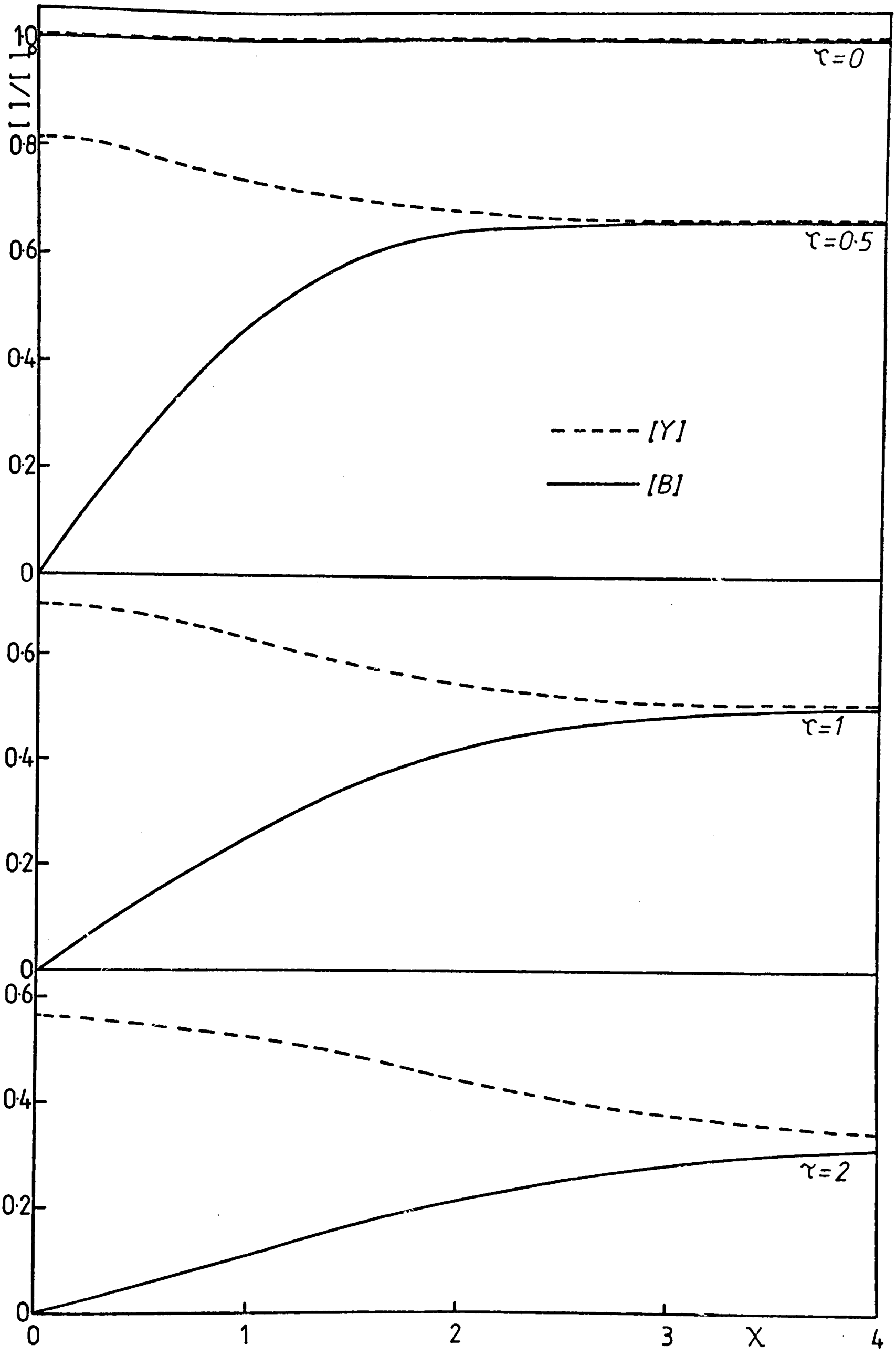

Fig 4 : 5

Concentration Profiles for Second Order Flash Electrolysis

2) Thionine: The back reaction for the thionine/ferrous system was also measured by this technique. In this case both L and S$^{\cdot}$ are electroactive

$$\text{Th} + \text{Fe(II)} \xrightarrow{\text{flash}} \text{S}^{\cdot} + \text{Fe(III)} \qquad (4:8)$$

$$2\text{S}^{\cdot} \xrightarrow{k_3} \text{L} + \text{Th} \qquad (4:9)$$

$$\text{L} + \text{Fe(III)} \xrightarrow{k_{-2}} \text{S}^{\cdot} + \text{Fe(II)} \qquad (4:10)$$

However k_{-2} still governs the decay of the photocurrent transient. During the flash a high proportion of Th is converted to S$^{\cdot}$. However k_3 is so fast (2.4×10^9 M^{-1} s^{-1})[35] that only a very low steady state concentration of S$^{\cdot}$ remains after the first few milliseconds and L accounts for all the electroactive species arriving at the electrode surface. A transient and its analysis are shown in Figure 4:6, again confirming the theoretical description and experimental technique.

Figure 4:7 shows the variation of k_{obs} with Fe(III) and compares the data with stopped flow data obtained by Foulds[73]. The agreement is good and gives a value of k_{-2} at 25^{o}C of 4.3×10^2 M^{-1} s^{-1}. It is worth noting that for the thionine system the pseudo first order condition is fulfilled, [Th](50 μM) << [Fe(III)] (3-30 mM), and, within experimental error, no intercept due to photogenerated Fe(III) is found.

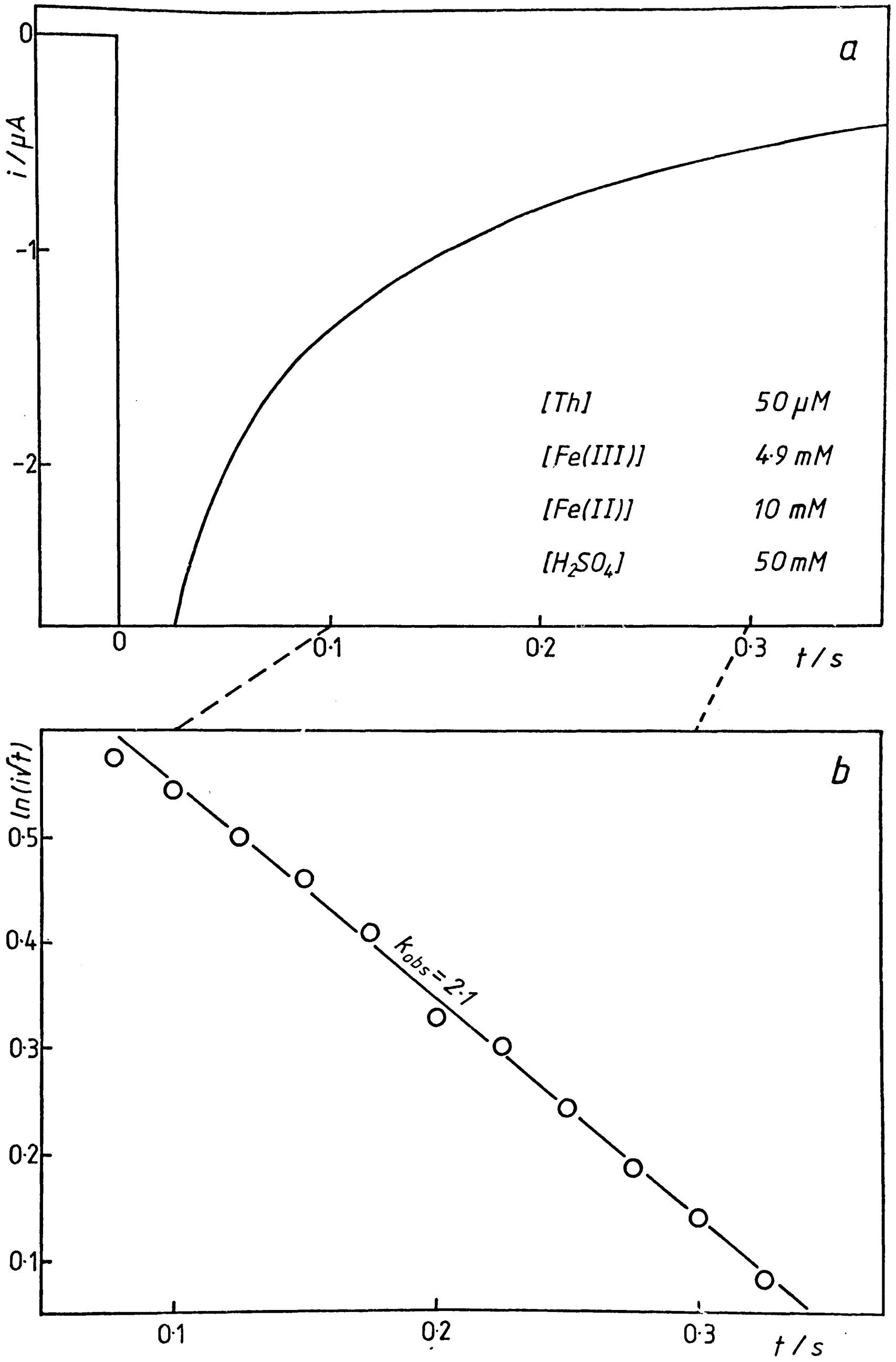

Fig 4 : 6

Flash Transient and Analysis

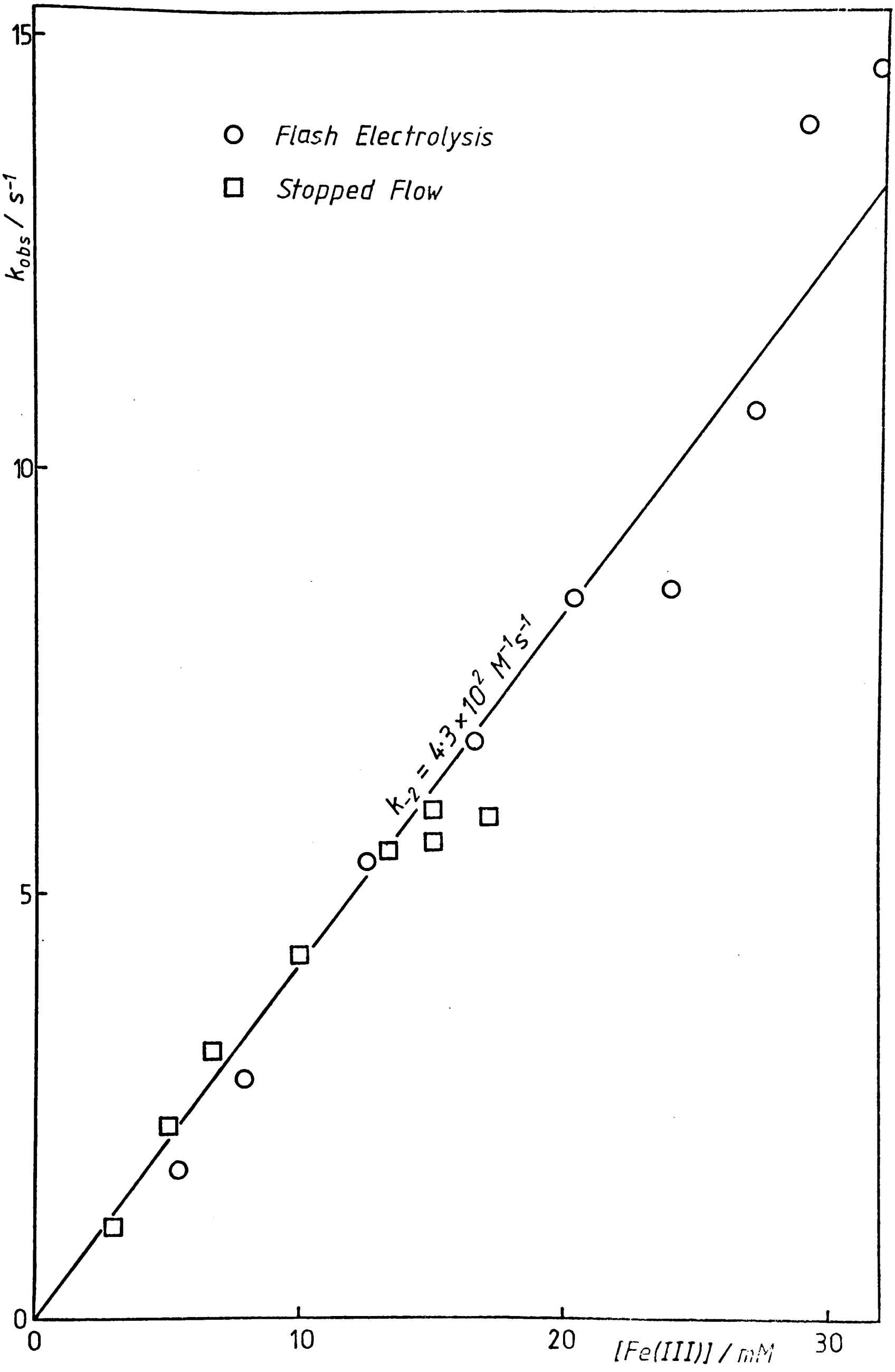

Fig 4 : 7

k_{obs} v [Fe(III)] for Leucothionine in 0·05M H_2SO_4

Flash electrolysis was also used to measure the temperature variation of this rate constant in collaboration with J.P. Davies[74] . The pot was thermostatted at various temperatures between 25 and 55°C. The values of k_{-2} were obtained by measuring the variation of k_{obs} with Fe(III) as in Figure 4:7. The Arrhenius plot is shown in Figure 4:8 and compares very well with results obtained by stopped flow, again in collaboration with Davies. The activation parameters obtained are given in Table 4:2. The value of k_{-2}, estimated from the Arrhenius plot at 22° C is in good agreement with the value of 2.6×10^2 M^{-1} s^{-1} found by Hatchard and Parker[35] in the same conditions.

The technique was used to measure the rate constants for new Ru(II) compounds and some modified thionine dyes. The results for these experiments are given in chapter 5.

THE DOUBLE LAYER CHARGING EFFECTS

It is clear from Figure 4:1 that the early part of the transient does not follow the predicted $i \propto t^{-\frac{1}{2}} e^{-kt}$ behaviour as this would require an infinite starting current. This deviation from the theoretical curve is not due to the finite duration of the flash, as the maximum in the photocurrent occurs after the flash has finished.

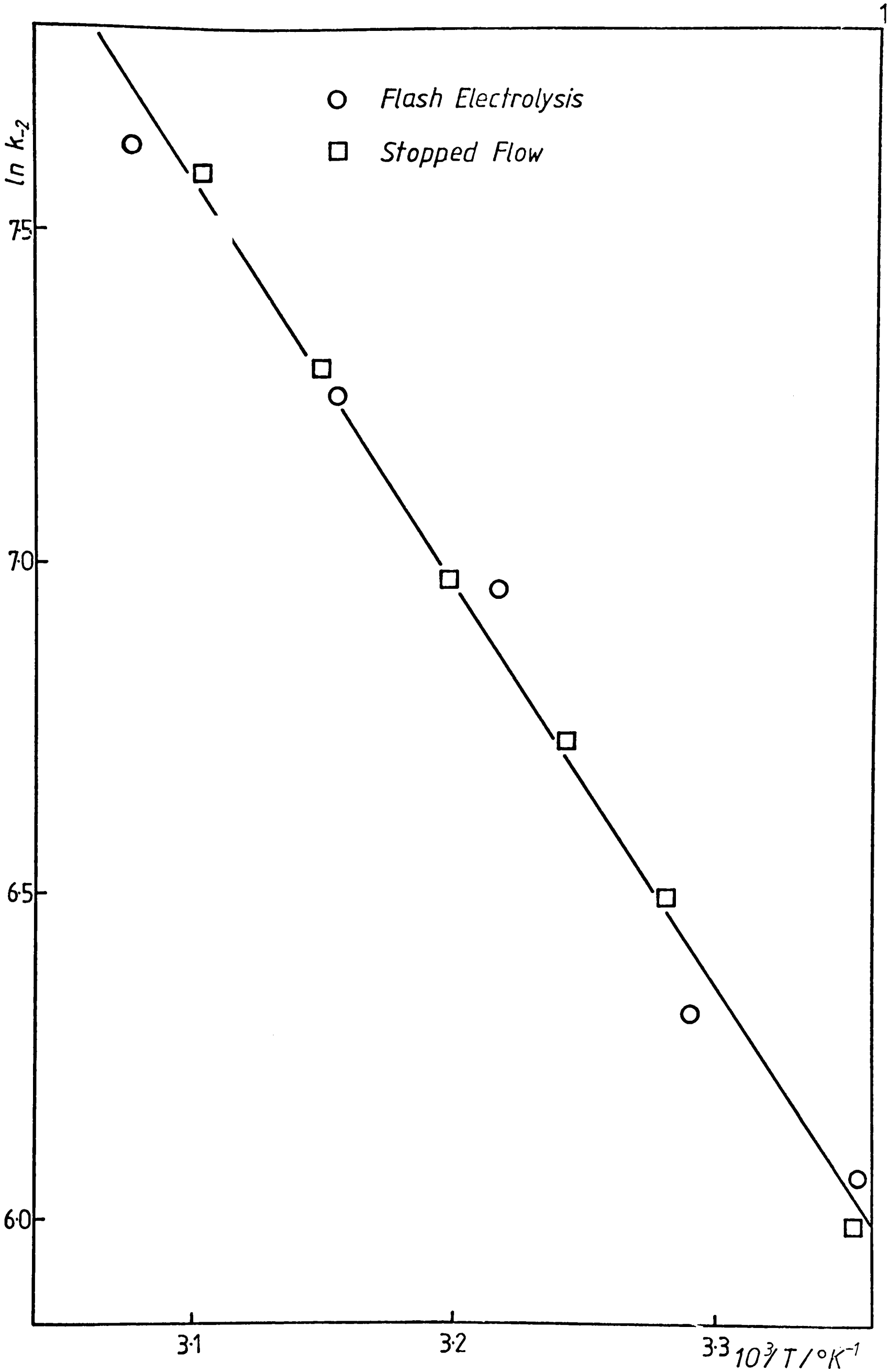

Fig 4 : 8

Arrhenius Plot for L + Fe(III) in 0·05M H_2SO_4

TABLE 4:2

Kinetic Data for Reaction Between Fe(III) and Leucothionine

	Flash Electrolysis	Stopped Flow	Flash Photolysis (Hatchard & Parker)
$k_{-2}(25^{\circ}C)/M^{-1}\ s^{-1}$	4.2×10^2	4.1×10^2	-
$k_{-2}(22^{\circ}C)/M^{-1}\ s^{-1}$	3.4×10^2	3.3×10^2	2.6×10^2
E_A/kJ mol^{-1}	49 ± 4	53 ± 1	-
$\Delta H^{\ddagger}$/kJ $mole^{-1}$	46 ± 4	50 ± 1	-
$T\Delta S^{\ddagger}$/kJ $mole^{-1}$	-12 ± 4	-8 ± 1	-
$\Delta G^{\ddagger}$/kJ $mole^{-1}$	58 ± 4	58 ± 1	-

It was found that with no capacitor, C_p (Figure 3:13), in the feedback of the potentiostat, large oscillations occurred in the early part of the transient which later settled to the predicted behaviour, Figure 4:9. However with a suitable capacitor (~ 2000 pF) these oscillations could be damped out without affecting the latter part of the trace. This had two advantages. The first was to reduce the high frequency noise using this simple $R_p C_p$ filter in the potentiostat. The second was to prevent wild excursions of the operational amplifier output voltage which would saturate. If too large a value of C_p was used the response of the potentiostat was too slow to follow even the latter part of the transient.

The oscillations, with $C_p = 0$, were caused by the inability of the op. amp. to respond to an instantaneous change in the current. This was investigated by imposing a small square wave modulation on the reference potential as shown in Figure 4:10 and clearly demonstrates the limitations of the potentiostat.

The reasons for the behaviour after the flash

$$\frac{di}{dt} \rightarrow \infty \quad \text{at } t = 0$$

were twofold. The first was that the flash gun produced a large electromagnetic spike as the flash tube was fired and then switched off. This spike was picked up by the potentiostat which was thrown well out of equilibrium, Figure 4:11, in 1 μs. The second reason lies in the theoretical description of the early part of the transient given in chapter 2 first observed by Perone.

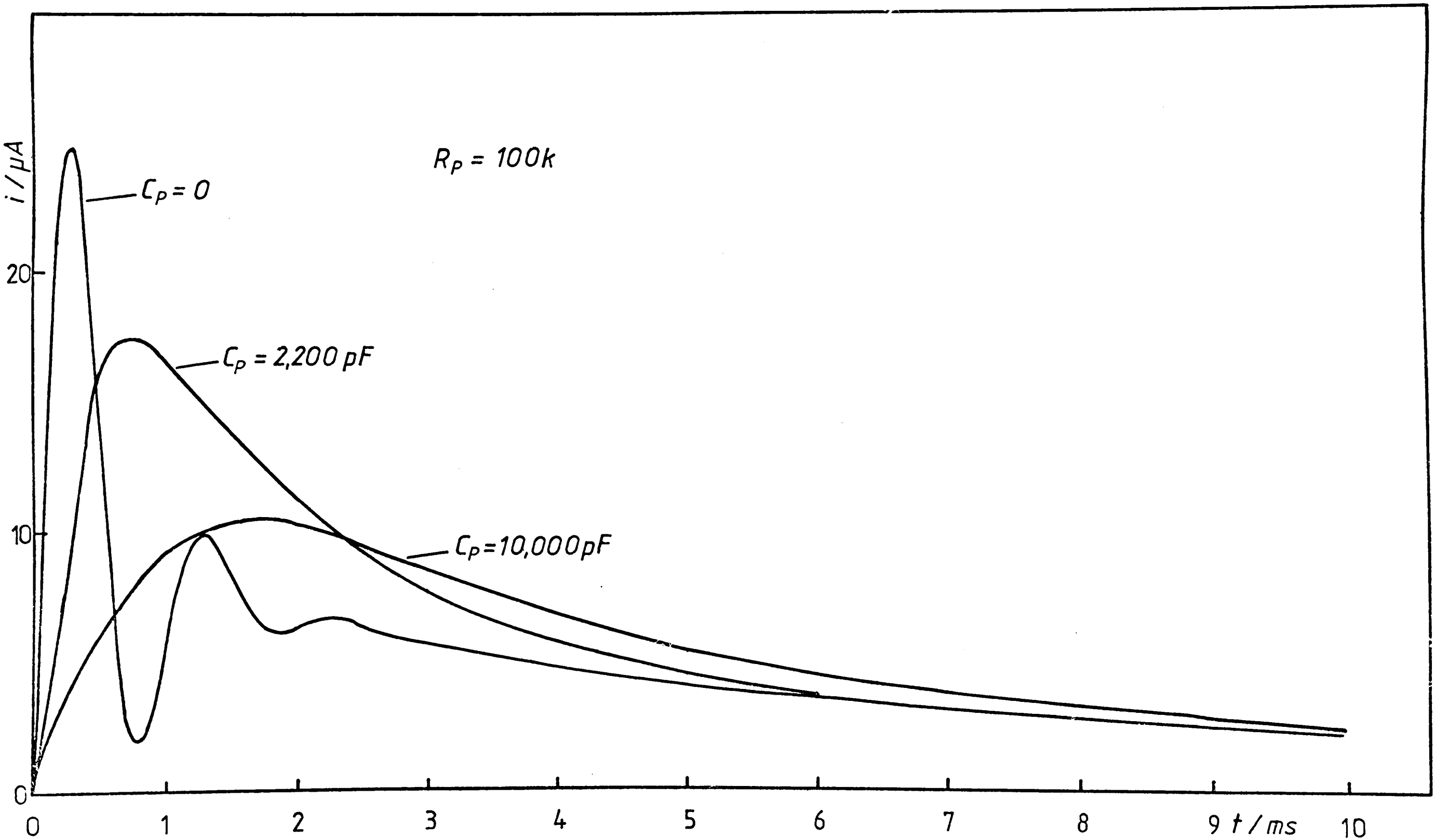

Fig 4 : 9

Flash Transients for Various Potentiostat Response Times

a

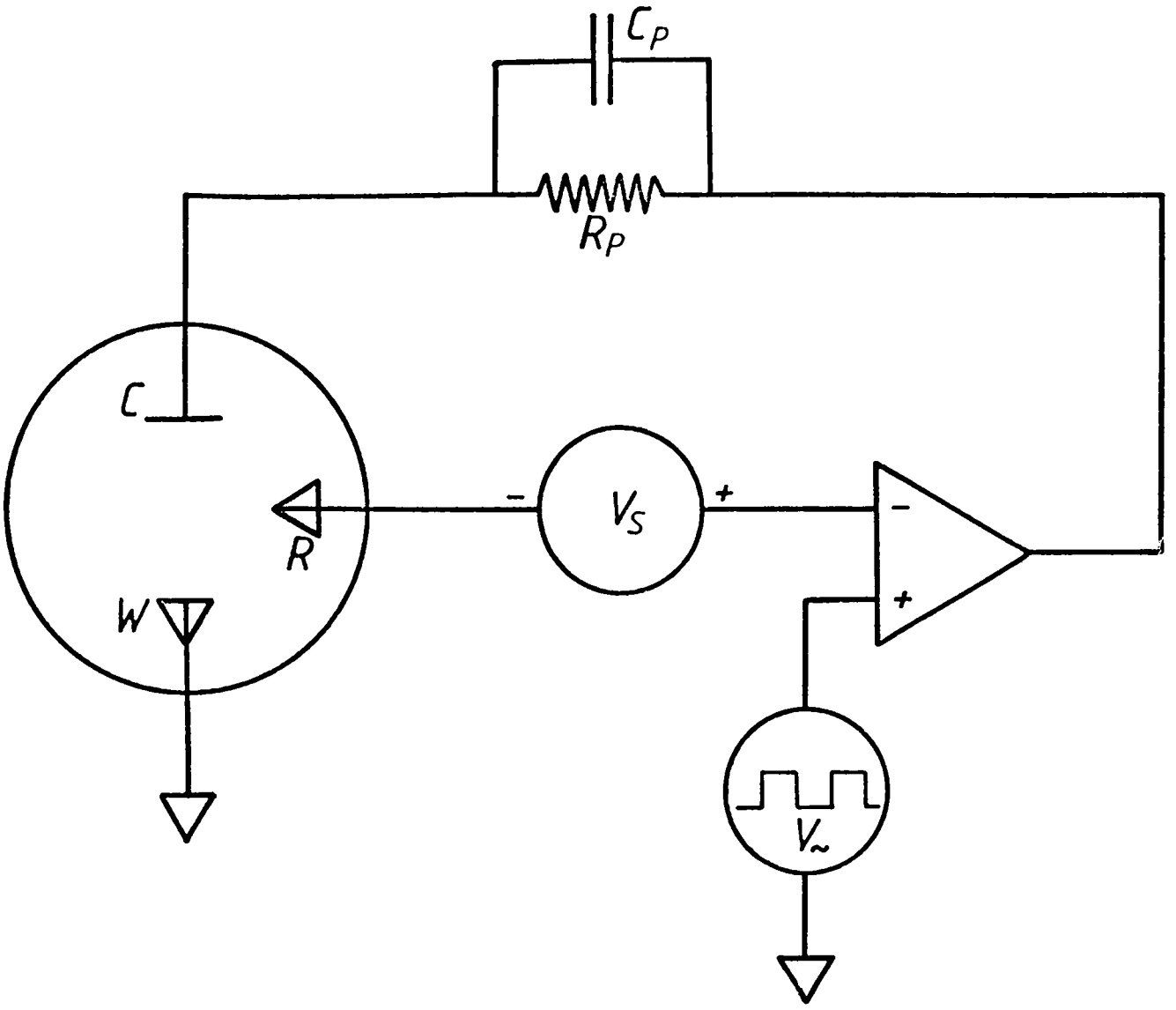

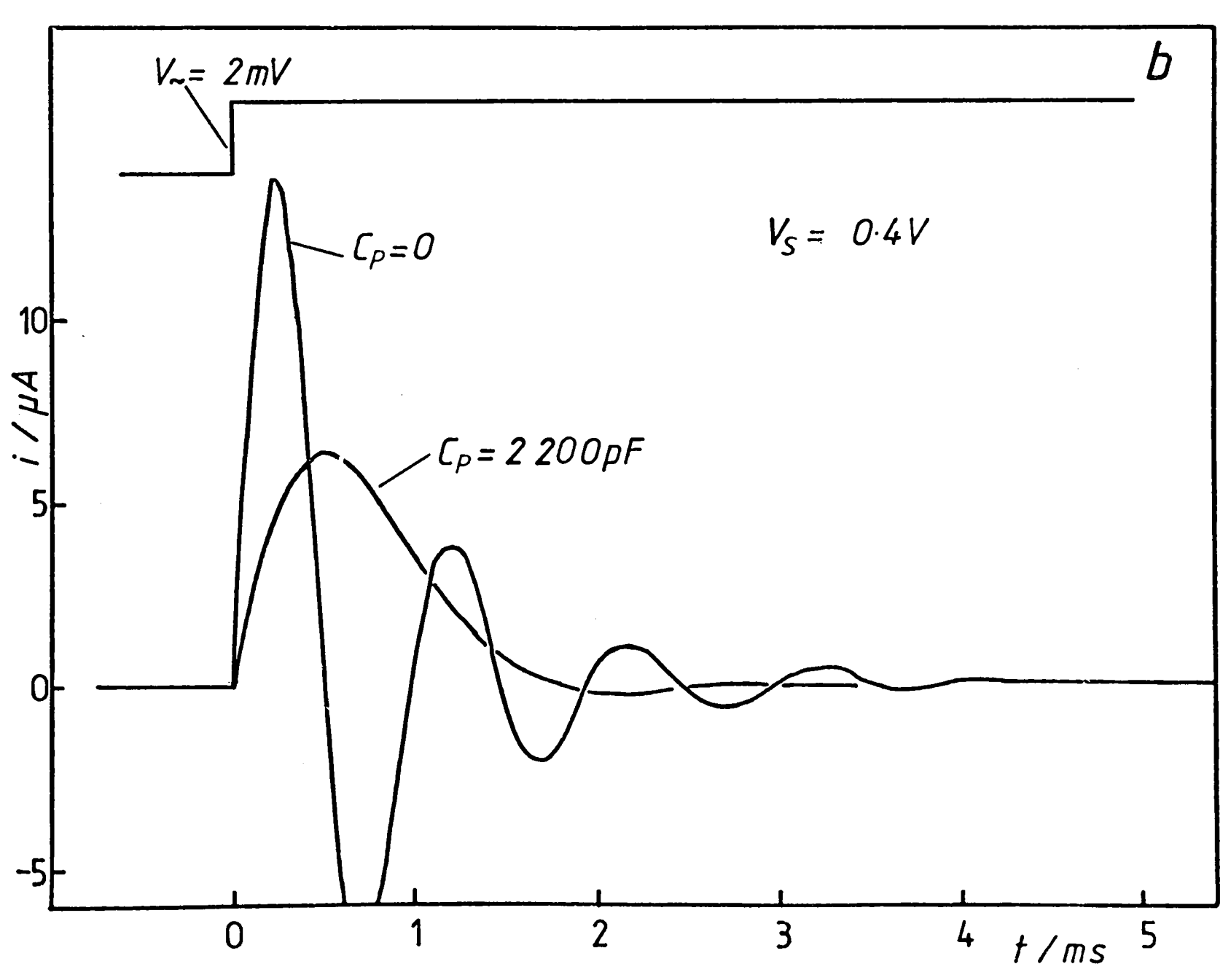

Fig 4 : 10

Potentiostat Response to Voltage Step

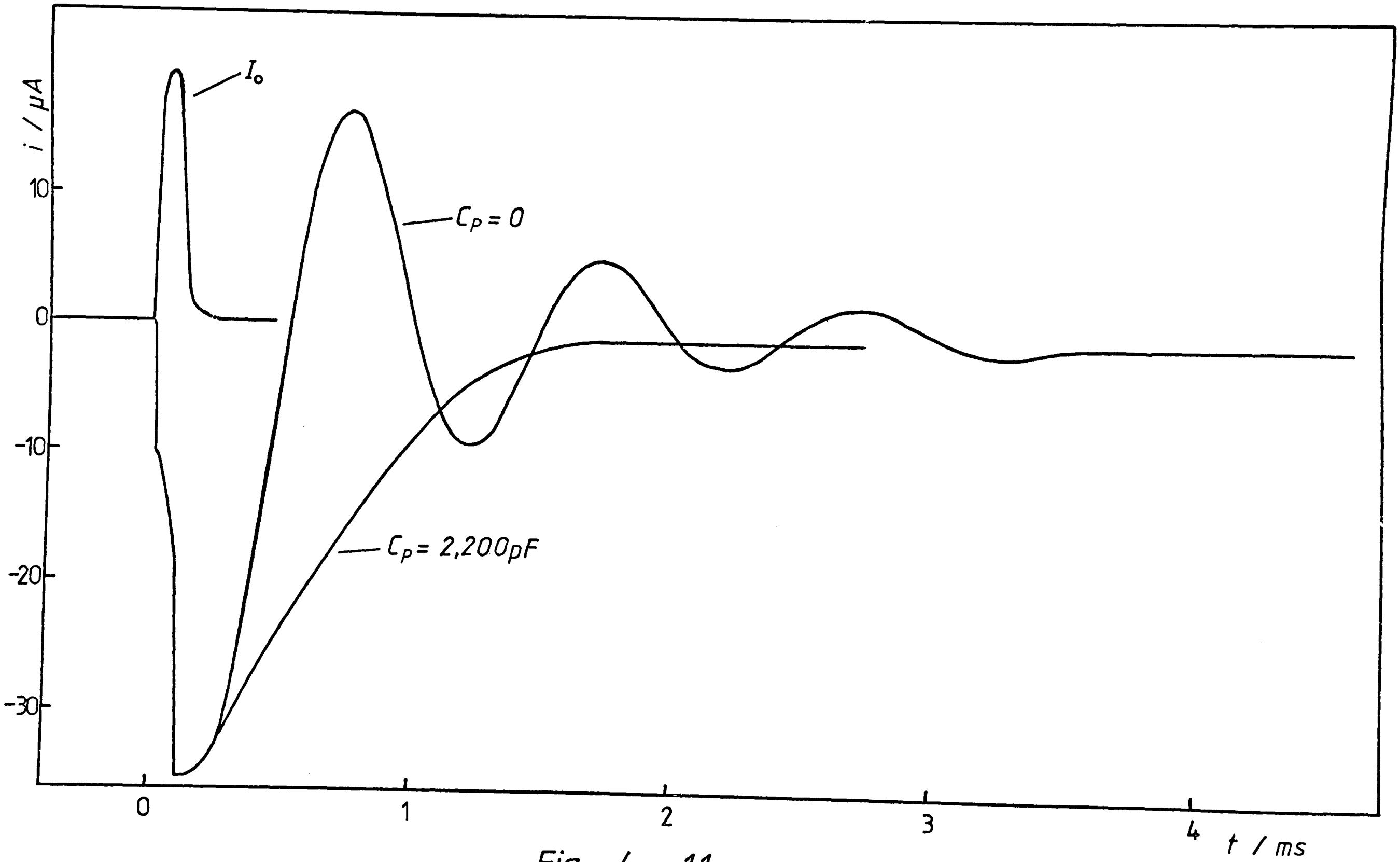

Fig 4 : 11

Potentiostat Pickup from Flashgun

Equation 2:62

$$i = \frac{a\, e^{-kt}}{\sqrt{\pi} R_s C_w (\tau)^{\frac{1}{2}}} \cdot F[(\tau t)^{\frac{1}{2}}]$$

where $\tau = (1/R_s C_w - k)$

and $F(x) = e^{-x^2} \int_o^x e^{t^2}.dt$ (Dawson's Integral)

predicts that at $t = 0$ $\frac{di}{dt} \to \infty$ as $F(t^{\frac{1}{2}}) \to \infty$ as $t \to 0$.

and this very rapid charging of the double layer cannot be followed by the operational amplifier. The theory for the rapid double layer charging, presented in chapter 2, was however confirmed by a suitable experiment.

The problem of electrical interference from the flash gun was solved by removing the flash gun to a suitable distance (~ 0.5 m) and using a $^1/_8$" fibre optic (Ealing Beck) to guide the light to the top of the electrode.

The double layer charging was then slowed down by a large increase in the $R_s C_w$ time constant so that the first part of the transient was slow enough to be followed by the op.amp.

This was achieved by

1) Increasing R_s by reducing the concentration of background electrolyte, HCl, to 10^{-3}M. If $[H^+] < 10^{-3}$M then Fe(III) and Fe(II) would have hydrolysed and precipitated.

2) Changing the cell geometry, again to increase R_s. Figure 4:12a shows a schematic representation of the current density in the solution using the standard cell geometry. Most of the resistance, R_s, between working and reference electrodes is concentrated close to the working electrode where the current per unit area is highest. However by placing a small silicone rubber tube over the end of the electrode, Figure 4:12b, R_s can be greatly increased by concentrating the current in a smaller area over a longer distance from the electrode.

The result of this was to produce the transient shown in Figures 4:13 and 4:14. Figure 4:13 shows the latter part of the transient and from slope of the $\ln it^{\frac{1}{2}}$ v t plot as $t \to \infty$ k_{obs} is determined. The value for k_{obs} may then be used to correct the early part of the observed transient, Figure 4:14, and this is compared with a theoretical curve for F(x) when

$$x = [(^{1}/R_s C_w - k_{obs})t]^{\frac{1}{2}}$$

for a suitably chosen value of $R_s C_w$. The agreement is good. It is encouraging to find that an obscure integral in the Handbook of Mathematical Functions describes the shape of this transient as well. The experiment is also an interesting way of probing

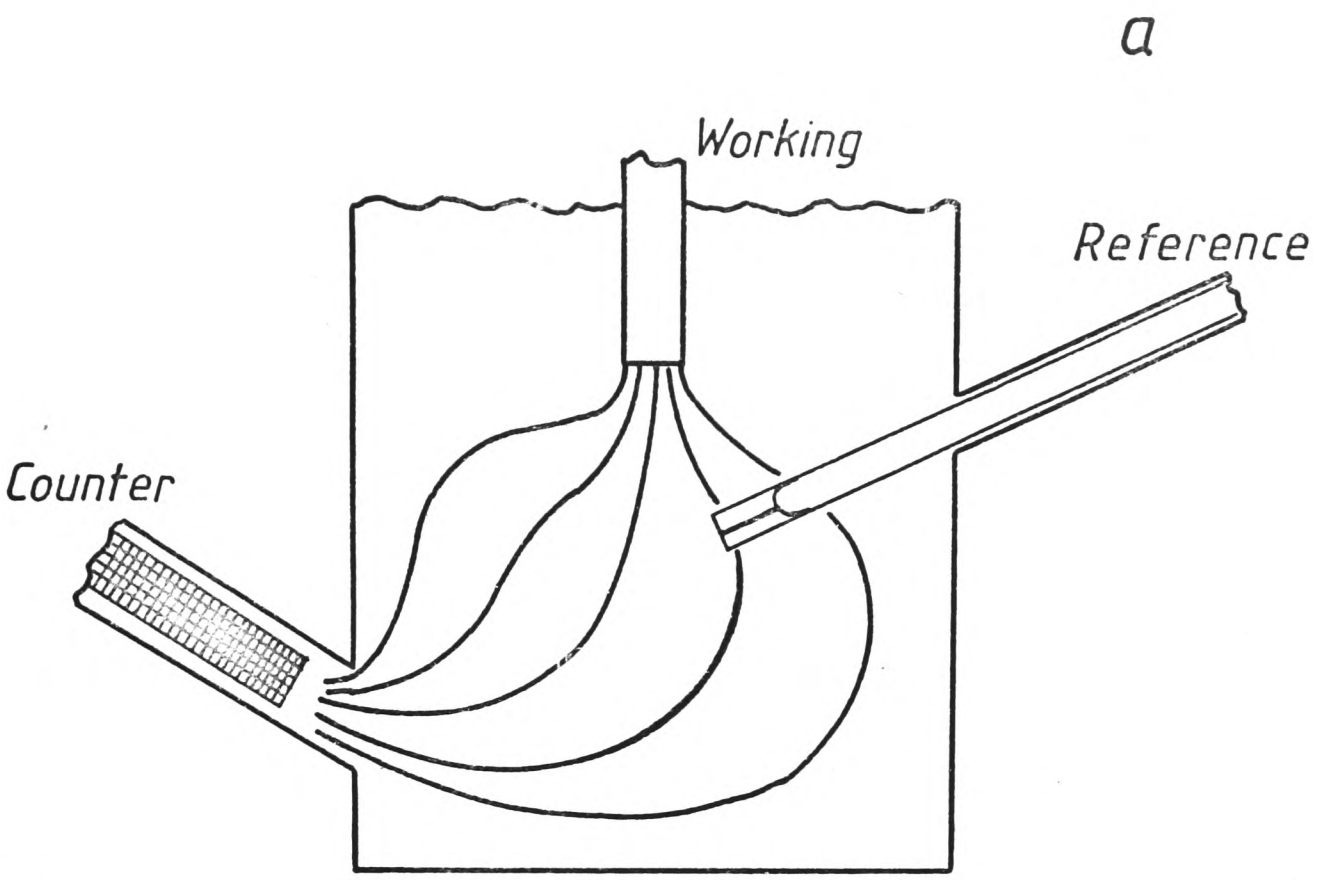

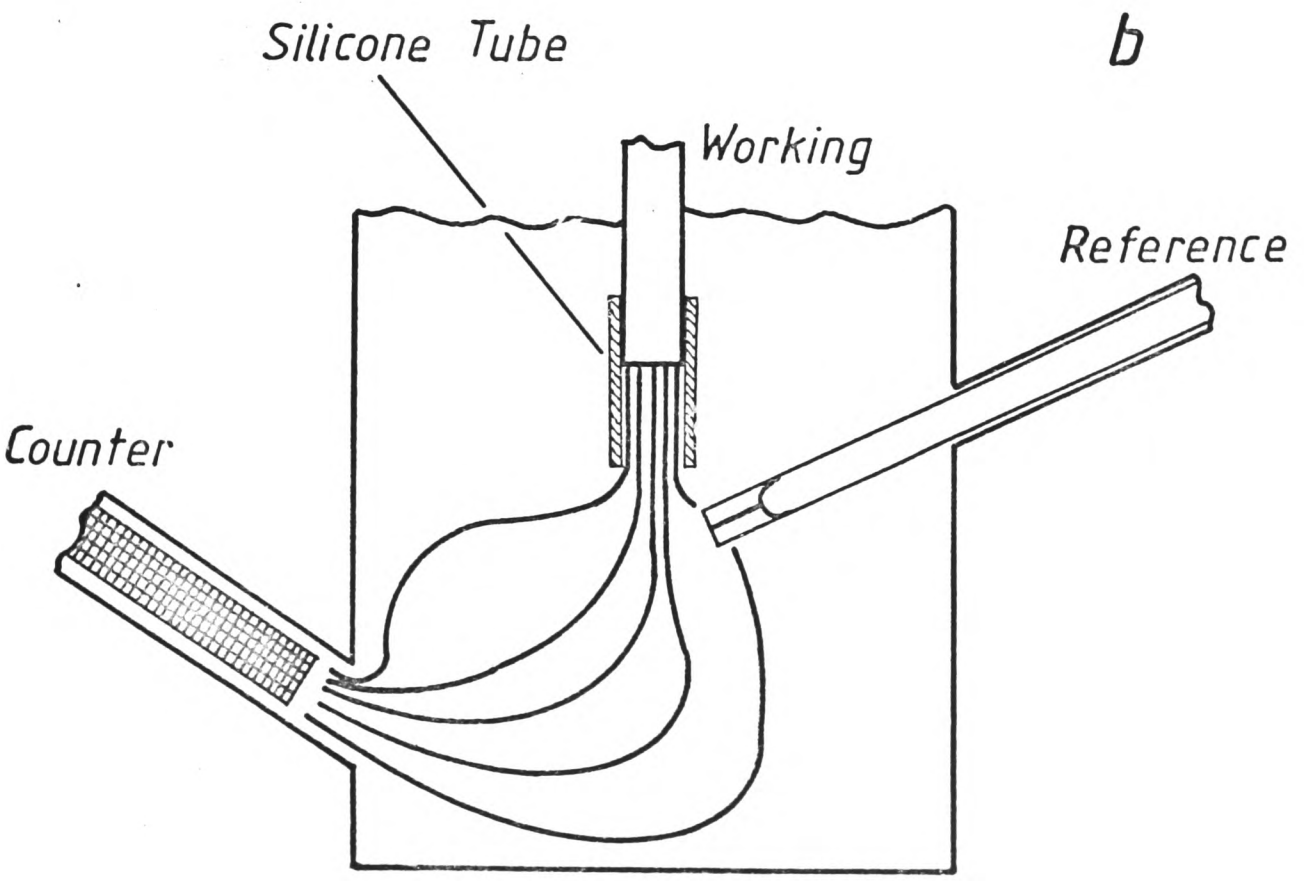

Fig 4 : 12

Schematic Representation of Current Density

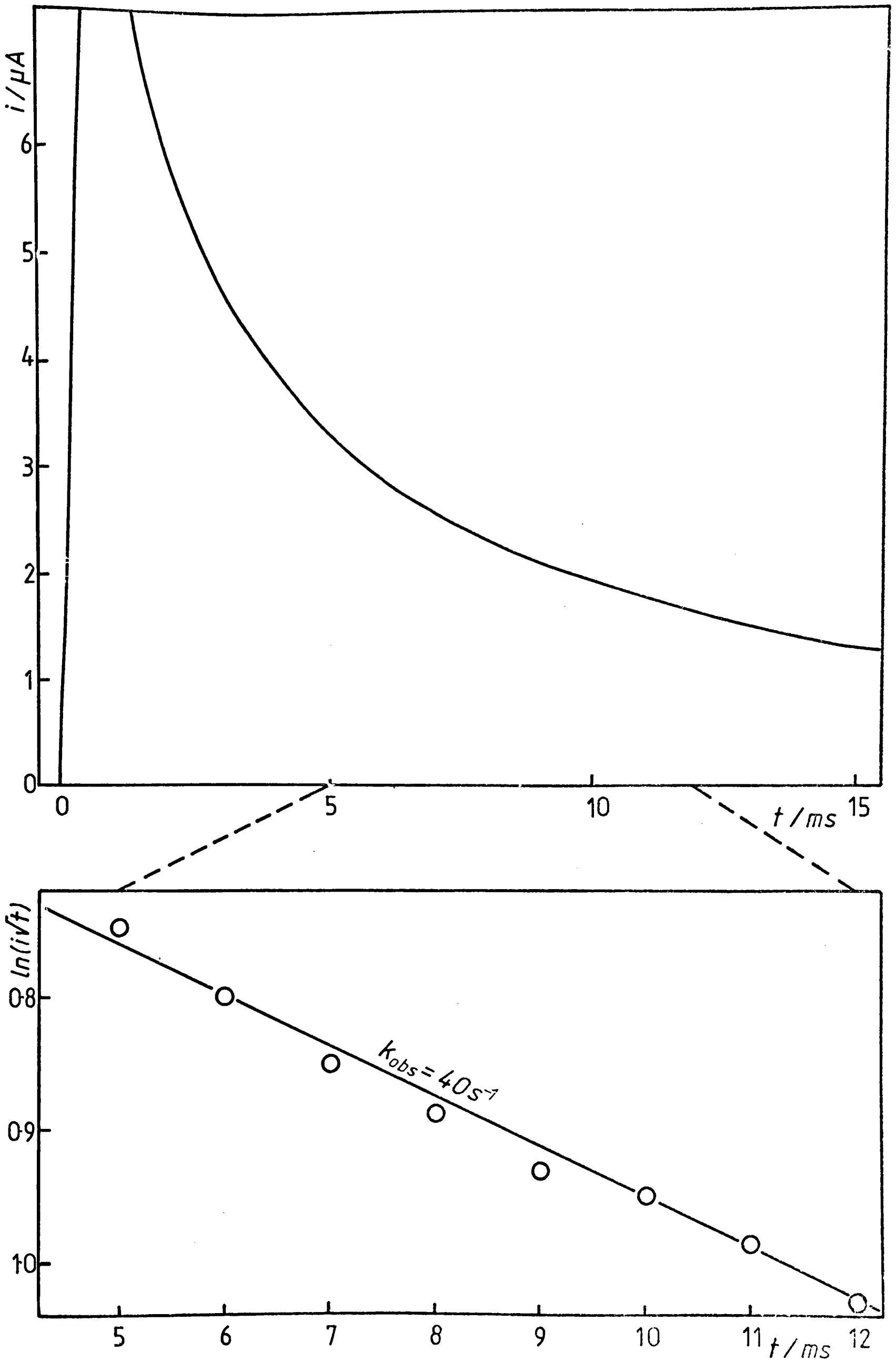

Fig 4 : 13

Flash Transient and Analysis

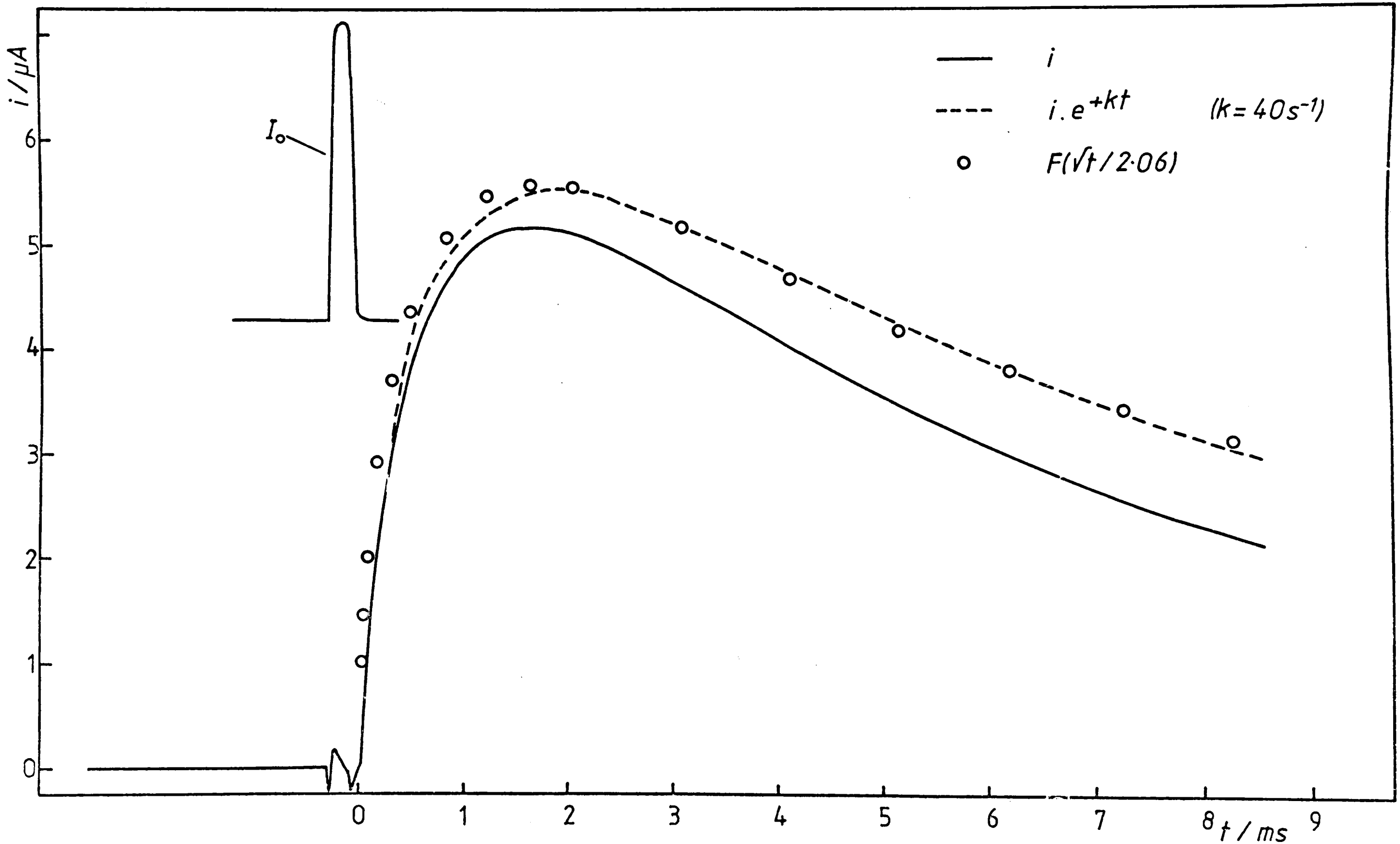

Fig 4 : 14

Flash Transient and Dawson Integral

the double layer. No other method exists of charging and discharging the double layer while at a fixed potential. The change in the double layer charging occurs because the distribution of potential between the solution and the double layer changes. As current flows across the solution resistance ($i_{max} \times R_s$ 0.5 mV) the potential of the electrode moves to accommodate this excursion and leaves the overall potential between working and reference electrodes unchanged.

COMPARISON WITH OTHER TECHNIQUES

Flash electrolysis is simply flash photolysis with electrochemical detection. It is not as versatile in terms of the number of systems which can be studied. Selectively electroactive photoproducts are not as common as the universal uv/visible absorption bands of the photoproducts. The timescale of the experiment is also limited, whereas there is virtually no limit at either end of the timescale for flash photolysis. However for electron-transfer quenching and in particular those systems suitable for photogalvanic cells it is an ideal technique.

It has the advantage that it closely mimics the processes occurring in a photogalvanic cell. And processes occurring outside the range of the technique will also be outside the critical conditions for an efficient photogalvanic cell. It is able to measure the homogeneous kinetics simply, directly and cheaply. A number of comparisons with other techniques may be made.

The Range of Rate Constants

It proved possible to measure first order rate constants in the range

$$k_{obs} = 1 \rightarrow 500\ s^{-1}$$

which in turn gave second order rate constants in the range

$$k_{-2} = 10 \rightarrow 10^{6}\ M^{-1}\ s^{-1}$$

These limits were achieved easily and do not represent the theoretical limits of the technique.

1) The lower limit : This is imposed by two factors. The first is that natural convection in the solution gives an upper limit to the time for which semi-infinite linear diffusion will hold. This is ~ 10 s and if measurements are to be taken over two half-lives implies

$$k_{obs} \approx 0.2$$

and for a typically high value of [Y] (~ 0.1 M) gives

$$k_{-2} \sim 2$$

The second factor is caused by the falling base line. As

$i \propto t^{-\frac{1}{2}}$, for k = 0, the observed signal must eventually fall below the noise level. The noise level for the tin oxide electrodes used was typically 50 nA peak to peak. Now at long times after the flash

$$i_{obs} = n.A.F.[B]_o \cdot D^{\frac{1}{2}}(\pi t)^{-\frac{1}{2}} e^{-kt} .$$

For favourable values of $D(5 \times 10^{-6}\ cm^2/s)$ and $[B]_o$ $(10^{-7}\ mol/cm^3)$.

$$i_{obs} = 2.5\ t^{-\frac{1}{2}} e^{-kt}\ \mu A .$$

For two half lives $e^{-kt} = 0.25$

$$i_{obs} = 0.63\ t^{-\frac{1}{2}}\ \mu A.$$

The noise becomes 20% of the signal at

$$t^{-\frac{1}{2}} = 0.4 \quad \text{or} \quad t \sim 6 \text{ secs.}$$

Thus

$$e^{-k_{obs}t} = 0.25 \quad \text{or} \quad k_{obs} = 0.23,$$

and

$$k_{-2} \sim 2.$$

Both factors lead to approximately the same lower limit for the rate constant. This is not as good as the stopped flow technique which is capable of measuring rate constants down to $k_{-2} \approx 0.1$.

2) The upper limit : In this case the noise problem is removed because the $t^{-\frac{1}{2}}$ factor works to the advantage of the observed signal at short times after the flash. The upper limit imposed in the experiments described was due to the inability of the potentiostat to follow the early part of the transient without oscillation. Perone[49] has shown that, by using a very fast response potentiostat and solving the second order kinetic problem, rate constants > 10^9 M^{-1} s^{-1} may be measured.

Precision. The precision varies with k_{obs} due to the falling base line, although this can be evened out by judicious choice of the potentiostat damping capacitor, C_p, which acts as a filter. Typically the precision was $\pm$ 5% for most of the rate constants measured in the range

$$k_{-2} = 1.6 \times 10^6 \text{ 1 mole}^{-1} \text{ s}^{-1} \text{ } Ru^{II}(5,6\ Me_2phen)_3$$

to $k_{-2} = 4.3 \times 10^2$ 1 mole^{-1} s^{-1} Thionine.

This is comparable with stopped flow and has the advantage that the precision does not vary with the extinction coefficient, as a given concentration of photoproduct will give an integral number of electrons per molecule. The RuL_3 complexes show roughly equal precision with both techniques implying that for an extinction

coefficient change of $<2 \times 10^4$ the stopped flow would be less accurate for these faster rate constants.

Comparison with Steady State Photogalvanic Measurements

Flash electrolysis has a significant advantage over the steady state ORDE technique (also described in this thesis) and the spectrophotometric measurements of photostationary states[75] because the measurement of the rate constant is independent of any light intensity measurements.

If the integrated flash intensity were known, however, the analytical expression for $[B]_{o}^{h\nu,Y}$, would allow the quantum efficiency, ϕ_1, for the process $A \longrightarrow B$ to be calculated.

CHAPTER 5

RESULTS AND DISCUSSION

This chapter is divided into four parts. The first deals with the electrochemistry of the compounds studied. The second describes the photochemical results obtained with the ORDE. The third part describes further kinetic measurements made by flash electrolysis and some kinetic measurements made using the stopped flow technique. Discussion of the implications of all these measurements is left until the end of the chapter.

THE ELECTROCHEMISTRY AND SPECTRA

1) Formal Electrode Potentials: The three methods of measurement and the reasons for using each are described in chapter 3.

(a) Reversible systems: Most of the $Ru(II)L_3$ complexes showed reversible electrode kinetics at tin oxide electrodes. A typical polarogram is shown in Figure 5:1(a) and its analysis is shown in Figure 5:1(b).

For a reversible wave

$$E = E' \pm \frac{RT}{nF} \ln \left(\frac{i_L - i}{i}\right)$$

thus when $i = i_L/2$ (the half-wave point).

$$E = E'$$

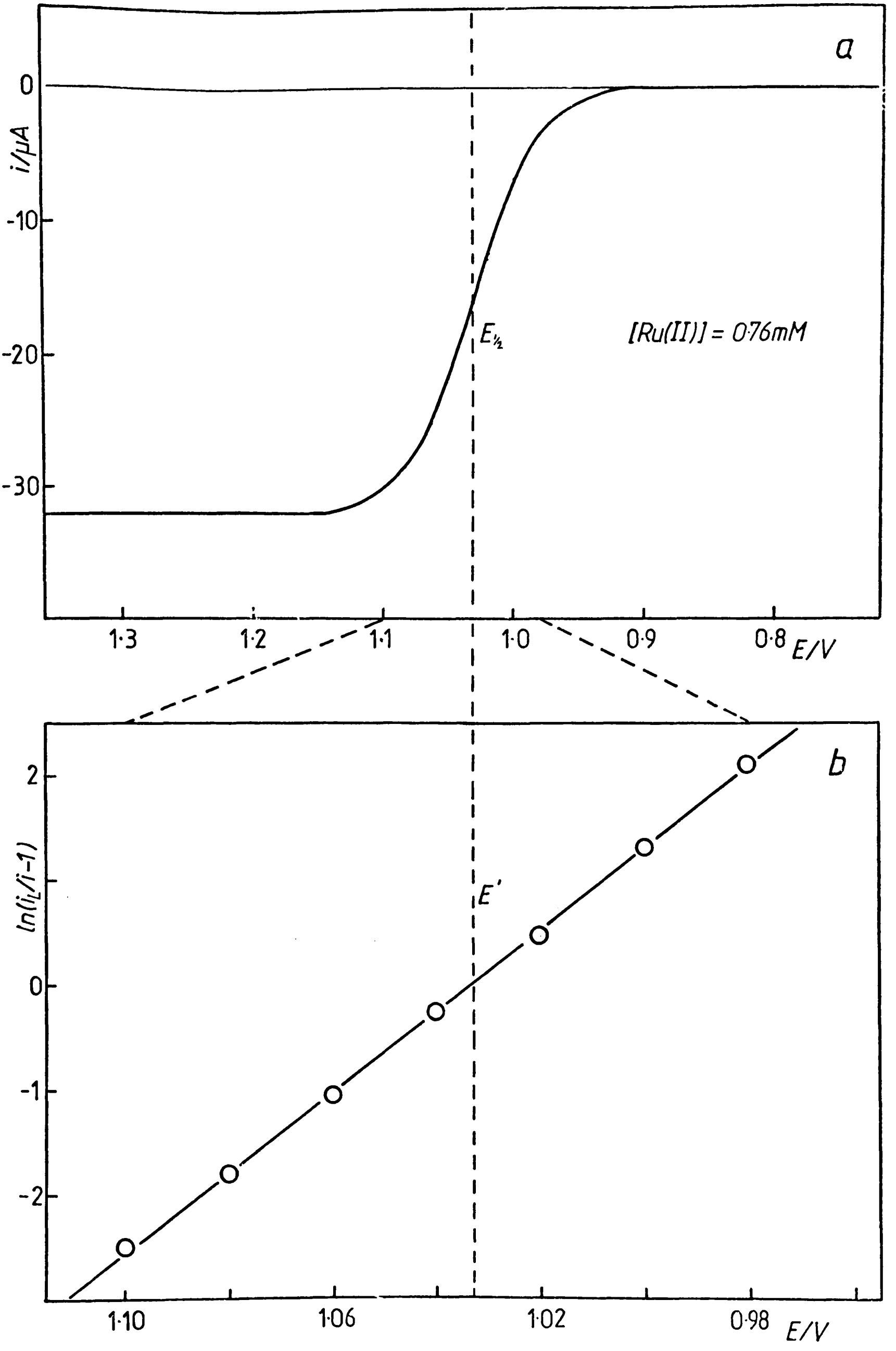

Fig 5 : 1

Polarogram and Analysis for Ru(II)(phen)$_3$ in 0·5M H_2SO_4

Plots of $\ln(i_L/i - 1)$ v E therefore give the formal electrode potential as the E-axis intercept and the gradients were found to be equal to $F/RT = (38.9\ V^{-1})$ confirming the the reversibility of the systems.

(b) Stable irreversible systems: The formal electrode potentials for the Fe(II)/Fe(III) couple in 0.5M HCl and 0.5M H_2SO_4 were measured by potentiometric titration. The Nerst plots are shown in Figure 5:2. The gradients are equal to F/RT as predicted by the Nerst equation.

$$E = E' + \frac{RT}{nF} \ln \frac{[Ox]}{[Red]}$$

(c) Unstable irreversible systems: For those Ru(II) compounds with irreversible electrode kinetics Nernst plots were obtained by measuring the limiting current due to Ru(II). The potential of zero current, E, was plotted against $\ln(i_{Lo} - i_L/i_L)$

where i_{Lo} = the initial limiting current for all Ru as Ru(II)

i_L = the limiting current for Ru(II) at E

and as $i_L\ \alpha[Ru(II)]$

$$\ln \left(\frac{i_{Lo} - i_L}{i_L} \right) = \ln \frac{[Ru(III)]}{[Ru(II)]}$$

Figure 5:3 shows a typical plot and the gradient is again F/RT as predicted.

This method was also used to measure the formal electrode potential of thionine and its derivatives by Foulds, Bartlett,

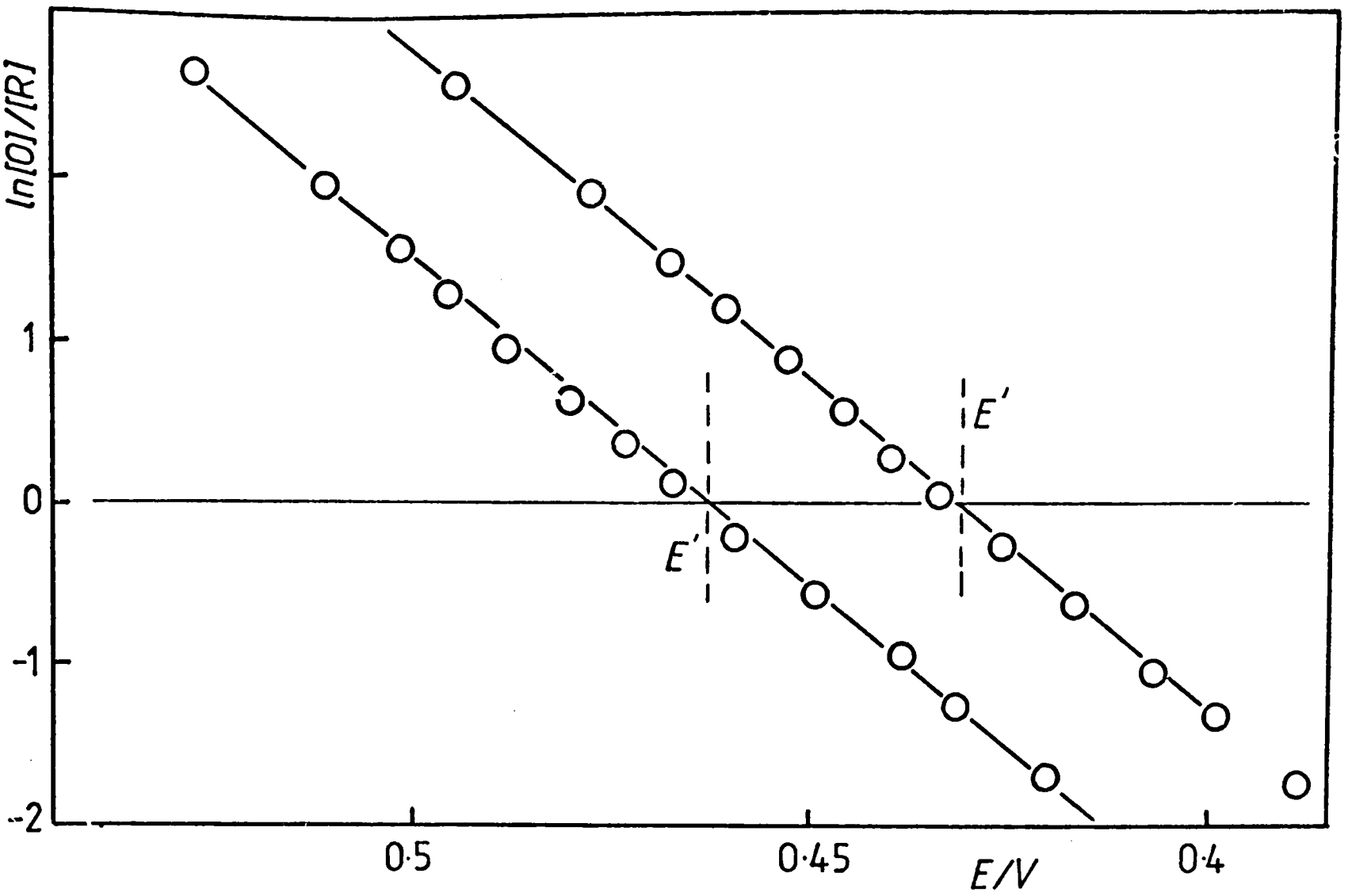

Fig 5 : 2

Nernst Plots for Fe(II)/Fe(III)

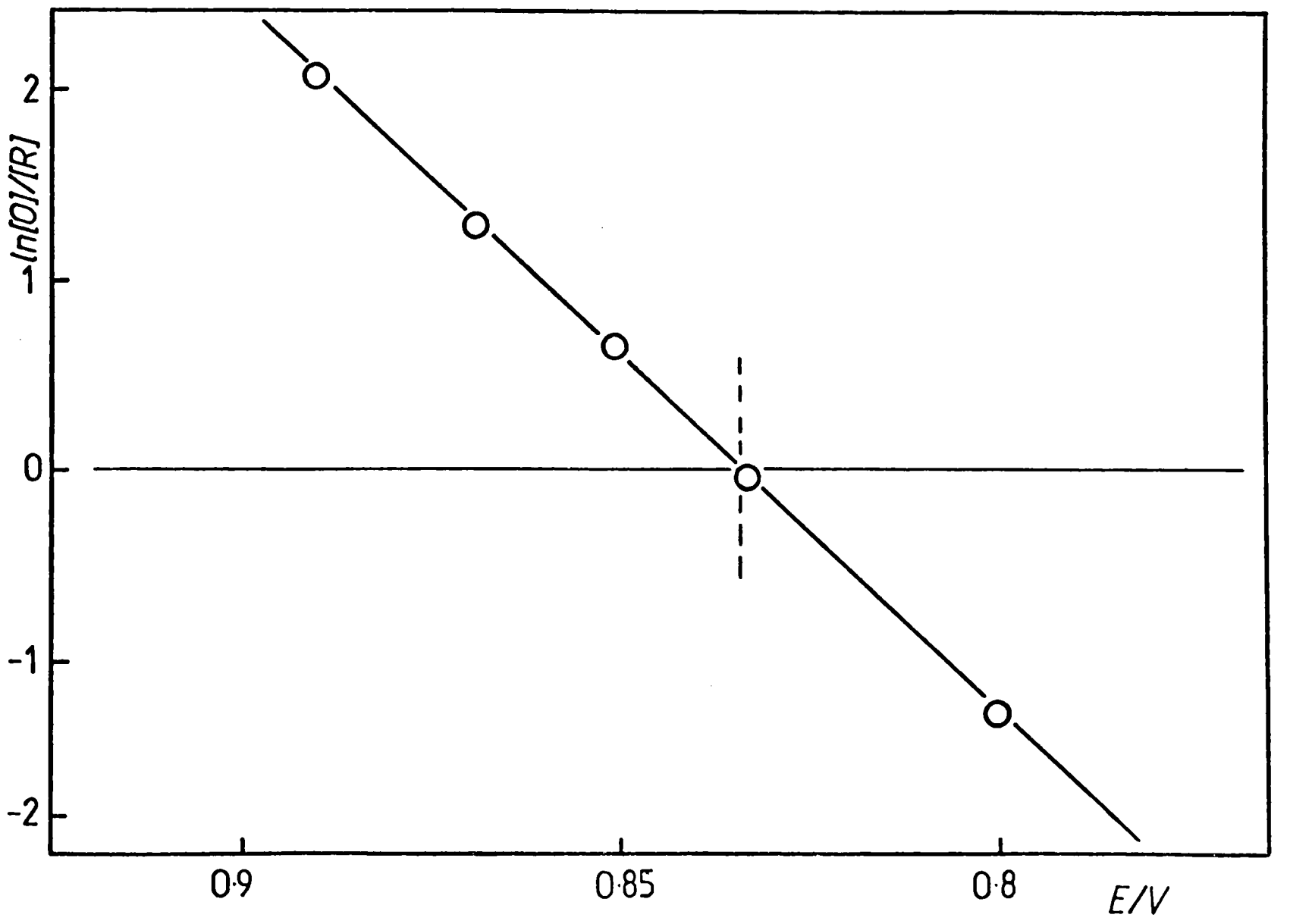

Fig 5 : 3

Nernst Plot for Ru(44'Me bipy) (II)/(III)

TABLE 5:1

Formal Electrode Potentials

Compound	Medium (0.5M)	E'(V)	Method	Sutin*[26]
$Ru(bipy)_3^{2/3+}$	H_2SO_4	1.020 ± 0.002	(a)	1.02
	HCl	1.020 ± 0.005	(a)	
$Ru(bipy)_2(Me_2bipy)^{2/3+}$	H_2SO_4	0.957 ± 0.002	(a)	
$Ru(bipy)(Me_2bipy)_2^{2/3+}$	H_2SO_4	0.896	(c)	
$Ru(Me_2bipy)_3^{2/3+}$	H_2SO_4	0.834	(c)	0.86
	HCl	0.836 ± 0.005	(a)	
$Ru(phen)_3^{2/3+}$	H_2SO_4	1.033	(a)	1.02
$Ru(5,6\ Me_2phen)_3^{2/3+}$	H_2SO_4	0.956	(a)	0.96
$Ru(4,7\ Me_2phen)_3^{2/3+}$	H_2SO_4	0.850	(a)	0.85
$Ru(3,4,7,8\ Me_4phen)_3^{2/3+}$	H_2SO_4	0.793	(a)	0.78
	HCl	0.795 ± 0.005	(a)	
$Ru(3,5,6,8\ Me_4phen)_3$				0.85
$Fe^{2/3+}$	H_2SO_4	0.431	(b)	
	HCl	0.463	(b)	

*Values estimated from measurements in CH_3CN/0.1M $(NPr_4^+)(PF_6^-)$ for 1M H_2SO_4 in H_2O at 25°C, the difference in the two media being 0.03V.

Note: All potentials measured in this thesis are quoted relative to the saturated calomel electrode (0.243 V v NHE)

Hillman and Davies as the leucothionines were easily oxidised by air.

Table 5:1 gives a summary of all the electrode potential measurements.

It is worth noting that in the literature formal electrode potentials for these compounds (other than $Ru(bipy)_3^{2/3+}$ and $Ru(phen)_3^{2/3+}$) have not been measured in water[26]. Because of the reduction of $Ru(III)L_3$ by the solvent, H_2O, measurements were made in acetonitrile and an appropriate correction made by comparing the values for $Ru(bipy)_3^{2/3+}$ in acetonitrile and water. However the timescale, t, of the experiment at a rotating disc electrode is

$$t = X_D^2/D$$

which for a typical D ($\sim 5 \times 10^{-6}$ $cm^2/5$) and X_D (at 9Hz X_D 2×10^{-3} cm) in 1s. This is very much shorter than the observed halflife of $Ru(III)L_3$ in these strongly acidic media which varies from minutes to hours. Thus for reversible systems the polarogram is a good method of measuring E', and for the less reversible systems the limiting current measurements can be made in seconds and again give good results.

There are two important observations to be made on these measurements:

1) The comparison with Sutin's estimated values[26] is very good and shows that E' is not strongly dependent on the medium. The correction which Sutin used from acetonitrile to water was -0.03V.

The values in 0.5M HCl and H_2SO_4 are also very similar whereas those of $Fe^{2/3+}$ are considerably different in the two media. This is to be expected as the strongly bound ligands of the RuL_3 complexes screen the metal centre from large solvent effects and thus the solvent does not greatly affect the redox potential. However in the $Fe^{2/3+}$ system the solvent plays a much more important part, being directly bound to the metal centre and being partially displaced by the ligands SO_4^{2-} and Cl^-, and thus strongly influencing the redox potential.

2) Ligand substituent effects on the complexes: The effect of introducing the Me group into the ligand is to donate charge density to the metal centre and thus stabilise the +(III) state with respect to reduction. The redox process is between a d^6 and a d^5 configuration with the relevant d electron localised on the metal centre. (The d orbitals are split by the D_3 ligand field into a_1 and e bonding orbitals and e^* anti-bonding orbitals. The configuration is thus $e^4a_1^2$ for the +(II) state and $e^4a_1^1$ for the +(III) state). A withdrawing group, such as -Cl, has the opposite effect E' $Ru(5Cl\text{-}phen)_3^{2/3+}$ = 1.12V[26].

Both the number and the position of the substituents are important. Thus:

(a) in the series of complexes $Ru(bipy)_3^{2/3+}$, $Ru(bipy)_2(Me_2bipy)^{2/3+}$, ... $Ru(Me_2bipy)_3^{2/3+}$ there is a steady decrease in E' as the number of Me groups in the molecule is increased. This is shown in Figure 5:4. The linearity of this free energy relationship shows that the effect is additive.

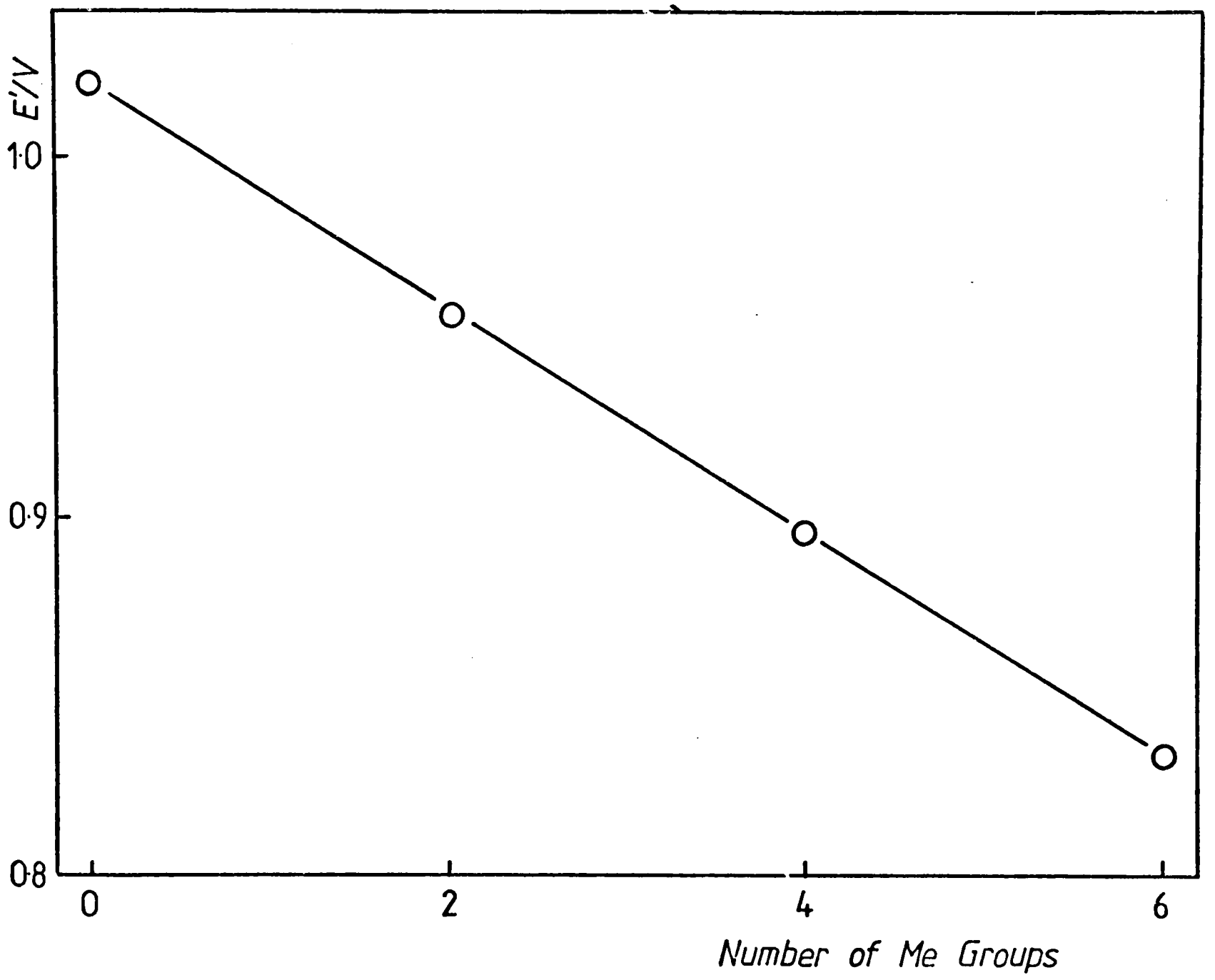

Fig 5 : 4

Electrode Potential Variation with Substituents for $Ru(bipy)_3$ (II)/(III)

(b) Substituents on the aromatic ring of the ligand have more effect that those not on the ring. Compare $Ru(4,7\ Me_2\ phen)_3^{2/3+}$ with $Ru(5,6\ Me_2\ phen)_3^{2/3+}$ and $Ru(3,4,5,8\ Me_4\ phen)_3^{2/3+}$ with $Ru(3,5,6,8\ Me_4\ phen)_3^{2/3+}$. The 5 and 6 positions clearly affect the potential less than the 3,4,7 and 8 positions because the 5,6 double bond is not delocalised over the whole π system. This observation is supported by the small difference in the E' between $Ru(bipy)_3^{2/3+}$ and $Ru(phen)_3^{2/3+}$.

Thus the charge density in the ligand π systems can be used to modify the redox properties of the complexes.

2) Diffusion coefficients:

Typical Levich plots for $Ru(II)L_3$ and for Fe(II) and Fe(III) are shown in Fig. 5:5. The diffusion coefficients are calculated from the gradient using equation (2:13) and are shown in Table 5:2.

Also shown in Table 5:2 are the activation energies, E_D, for the diffusion process. Taking equation

$$D = (n.F.A.\ c_\infty\ \nu^{-1/6}.\ i_L^{-1}.\ W^{\frac{1}{2}}.\ 1.55)^{-3/2} \qquad (5:1)$$

and using $D = D_o e^{-E_D/RT}$ (5:2)

and $\nu = \nu_o e^{-E_\nu/RT}$ (5:3)

where D_o and ν_o are the prexponential factors for diffusion and viscosity respectively and E_ν is the activation energy for viscosity.

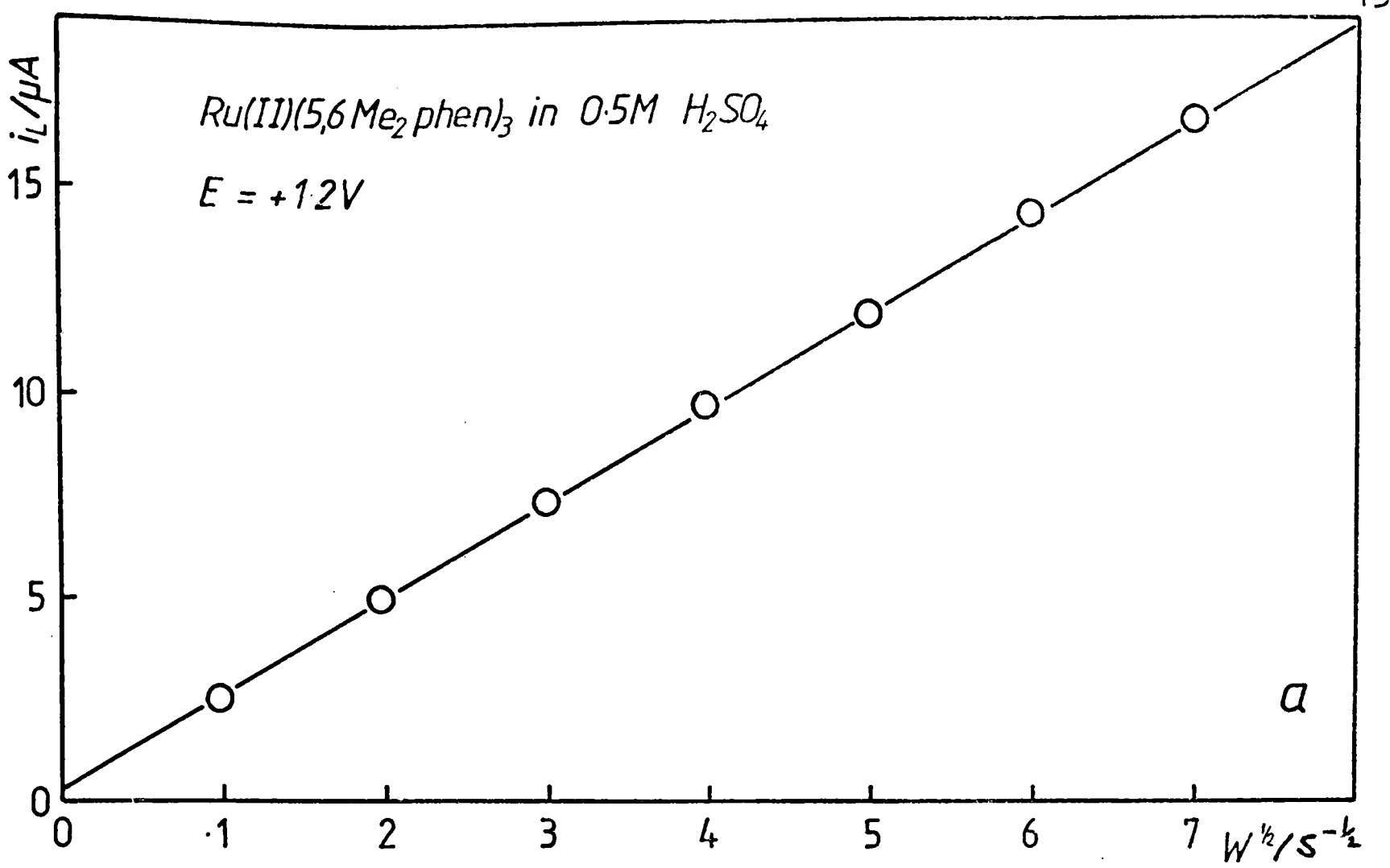

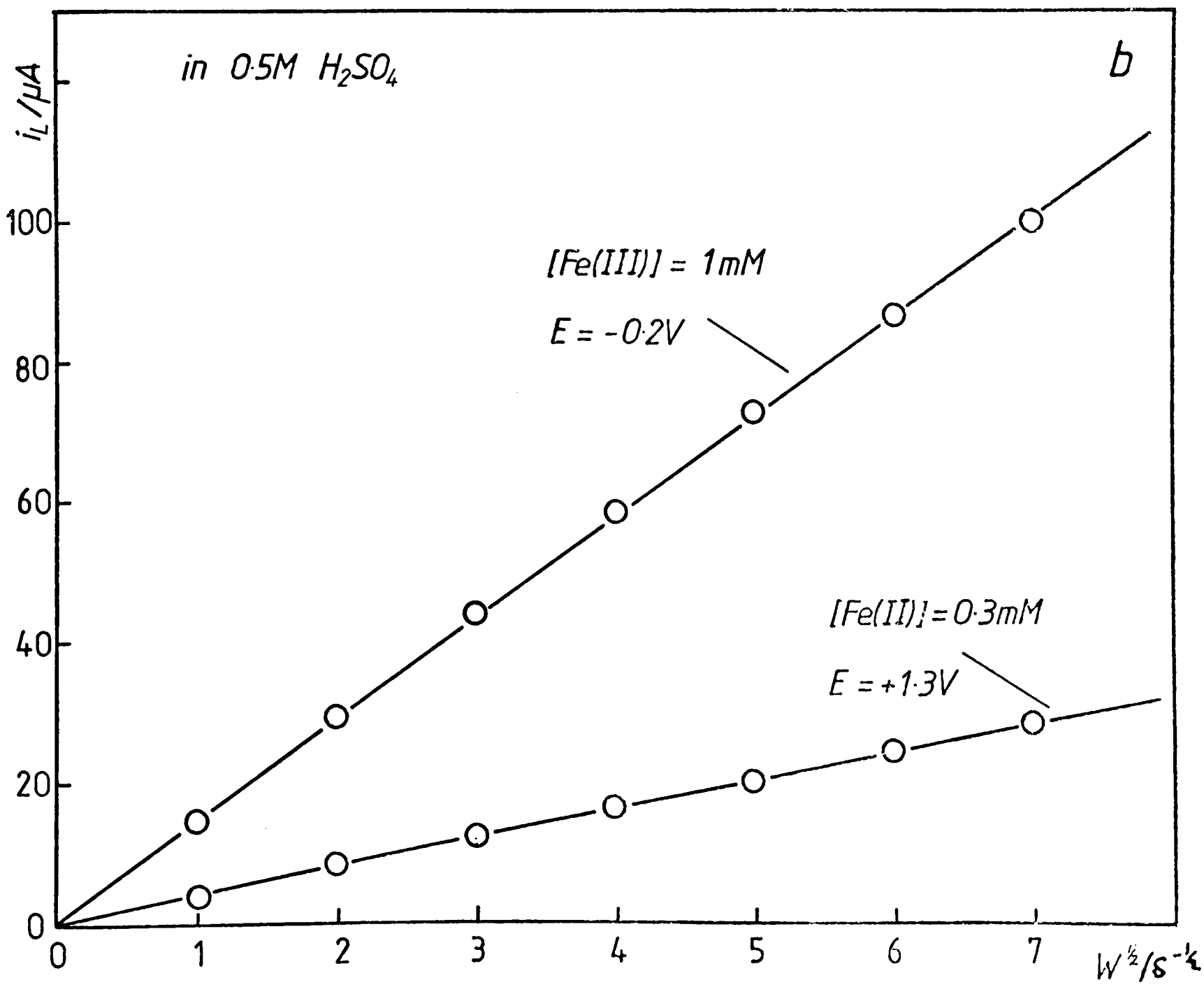

Fig 5 : 5

Levich Plots

TABLE 5:2

Ion	Medium	$D^{25^{\circ}C}/cm^2s^{-1}$	E_D kJ/mol
$Ru(bipy)_3^{2+}$	H_2SO_4	$(4.0\pm0.3)\times10^{-6}$	17.4 ± 0.2
$Ru(bipy)_2(Me_2bipy)^{2+}$	"	$(3.2\pm0.3)\times10^{-6}$	
$Ru(bipy)(Me_2bipy)_2^{2+}$	"	$(2.5\pm0.5)\times10^{-6}$	
$Ru(Me_2bipy)_3^{2+}$	"	$(1.7\pm0.4)\times10^{-6}$	
$Ru(phen)_3^{2+}$	"	$(2.7\pm0.3)\times10^{-6}$	
$Ru(5,6\ Me_2pehn)_3^{2+}$	"	$(2.9\pm0.3)\times10^{-6}$	18.3 ± 0.6
$Ru(4,7\ Me_2pehn)_3^{2+}$	"	$(2.0\pm0.2)\times10^{-6}$	
Fe^{2+}	H_2SO_4	$(4.6\pm0.2)\times10^{-6}$	
	HCl	$(5.7\pm0.1)\times10^{-6}$	
Fe^{3+}	H_2SO_4	$(4.3\pm0.2)\times10^{-6}$	
	HCl	$(5.7\pm0.1)\times10^{-6}$	

Substituting (5:2) and (5:3) in (5:1) and taking natural logs.

$$\frac{E_D}{RT} = -\frac{3}{2}\left(\ln i_L - \frac{E_\nu}{6RT}\right) + \text{const.}$$

Thus E_D is obtained from the gradient of $\ln i_L$ v $^1/T$. Examples of this plot are shown in Figure 5:6. (Measurements of E_ν as described in chapter 3 were

	E_ν/kJ/mol
0.5M HCl	15.2 ± 0.3
0.5M H_2SO_4	15.4 ± 0.1
H_2O	15.6 ± 0.2 (lit 15.7)[68]

A number of conclusions may be drawn from these results:

1) The absolute values of the diffusion coefficients are in line with those predicted by the Stokes-Einstein equation

$$r = kT/(6\pi\eta D)$$

where r is the molecular radius

k is the Boltzmann constant

and η is the viscosity of the medium.

For values of D between 2 and 4 x 10^{-6} cm^2 s^{-1} this equation predicts radii between 5 and 10 Å. The radius of $Ru(bipy)_3^{2+}$ is ~6.5 Å and that of $Ru(Me_2\ bipy)_3^{2+}$ is estimated to be ~8 Å.

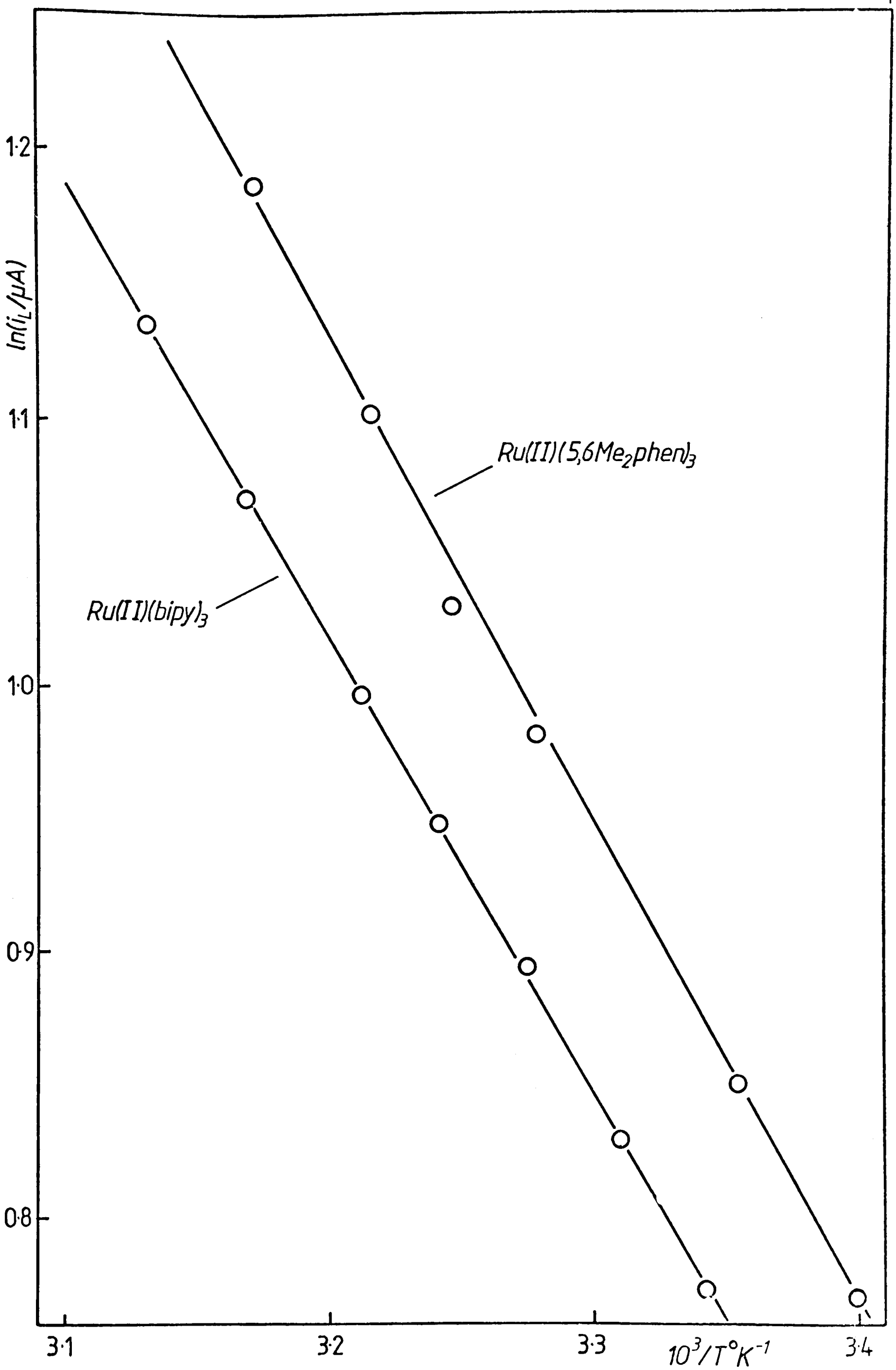

Fig 5 : 6

Temperature Variation of Limiting Current

The variation in D is thus a bit larger than might be predicted from the ionic radii, however the trends are much as would be expected. Thus as the ionic volume increases from $Ru(bipy)_3^{2+}$ to $Ru(Me_2\ bipy)_3^{2+}$ as Me_2 bipy ligands are added stepwise so too does the diffusion coefficient decline monotonically. Simiarly the difference between $Ru(bipy)_3^{2+}$ and $Ru(phen)_3^{2+}$ may also be explained by the greater volume of phen than bipy. There are some slight anomalies apparent. Thus one might expect $Ru(4,7\ Me_2\ phen)_3^{2+}$ and $Ru(5,6\ Me_2\ phen)_3^{2+}$ to be very similar in molecular volume and thus diffusion coefficient but there is a sizeable difference. However the overall trend and the fact that the RuL_3^{3+} ions showed little or no difference in diffusion coefficient from their $Ru\ L_3^{2+}$ equivalents suggests that the ions move as discrete ions and little or none of the solvent is strongly associated with them. This might be predicted from their large size, low surface charge density and hydrophobic surface. (Contrast the trend in the alkali metals Li^+, Na^+, ...).

2) The temperature dependences of the diffusion coefficients are as predicted by Walden's rule.

$$\text{e.g.} \quad D.\eta \text{ or } D.\nu \approx \text{const.}$$

$$\text{i.e.} \quad E_D \approx E$$

This is important for the prediction of the behaviour of a practical photogalvanic cell which will not of course be used under conditions of constant temperature.

ELECTRODE KINETICS

Earlier discussion of the ideal selective electrodes suggest that the Fe(II)/(III) couple should have very slow kinetics at the illuminated electrode. This requirement also applies to the measurement of the photogenerated Ru(III) at the ORDE.

The observed electrode kinetics for Fe(II)/(III) at the SnO_2 electrode approach the ideal and allow measurement of the photoeffects.

In H_2SO_4 at SnO_2

Figures 5:7 and 8 show polarograms for the Fe(II) and Fe(III) oxidation and reduction respectively in 0.5M H_2SO_4. They are typical of the electrodes used for subsequent photochemical experiments, although some electrodes, when first prepared, show slightly faster electrode kinetics. The electrode kinetics generally become slower with use and the working life of an electrode was thus limited. It is important to notice that there are still appreciable exchange currents at $E = E'$ and in the range $+0.4 < E < +0.6V$, where measurements of photocurrents were made.

The analysis of the two waves, using equation (2:27), is also shown in Figures 5:7 and 8. The values of k'_* and α and β obtained from the analyses are given in Table 5:3.

The values of k' are given as k'_* and not k'_o as they were obtained by extrapolation of the analysis from the potential region in which the polarograms were measured and not from measurement of

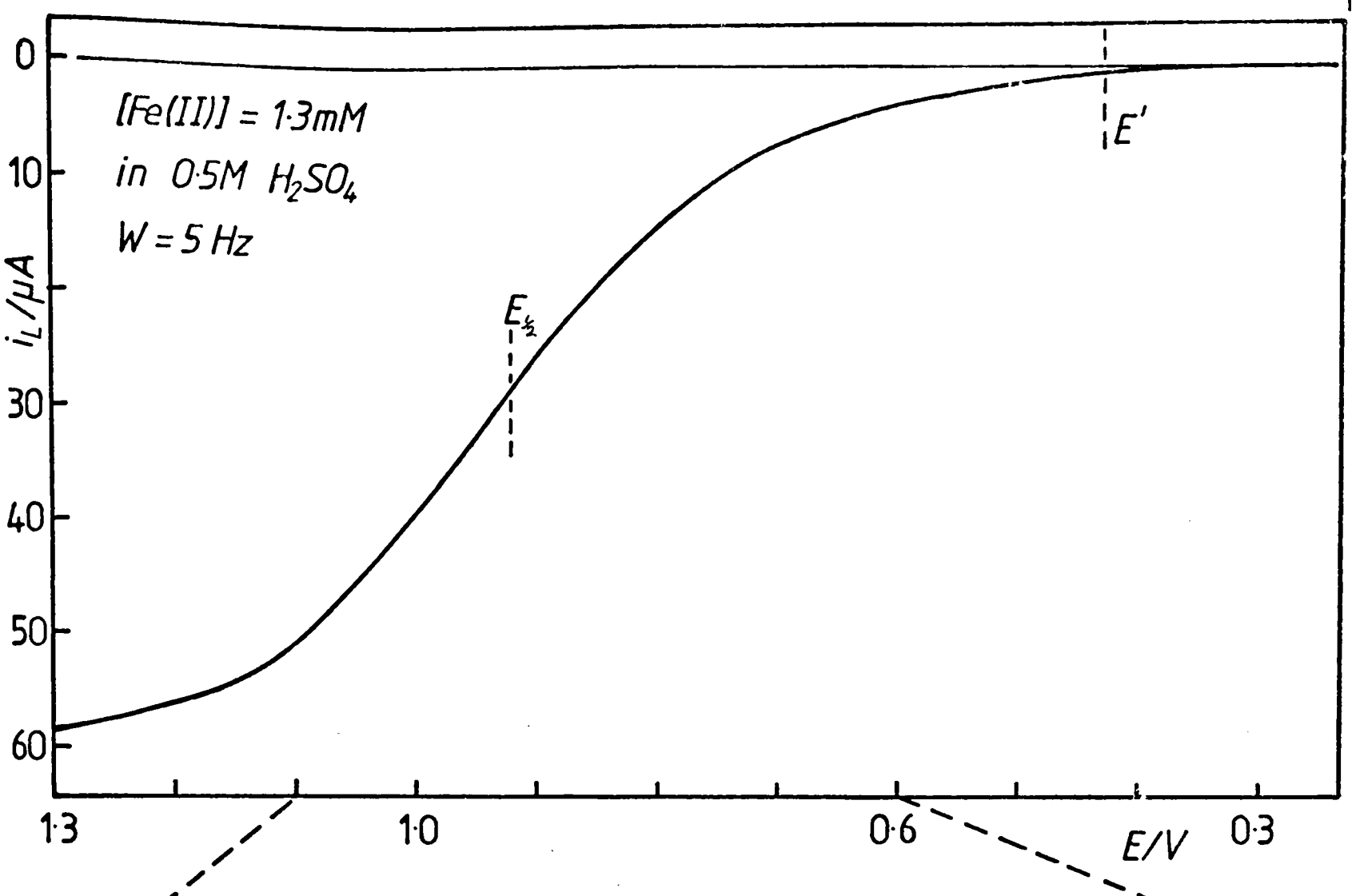

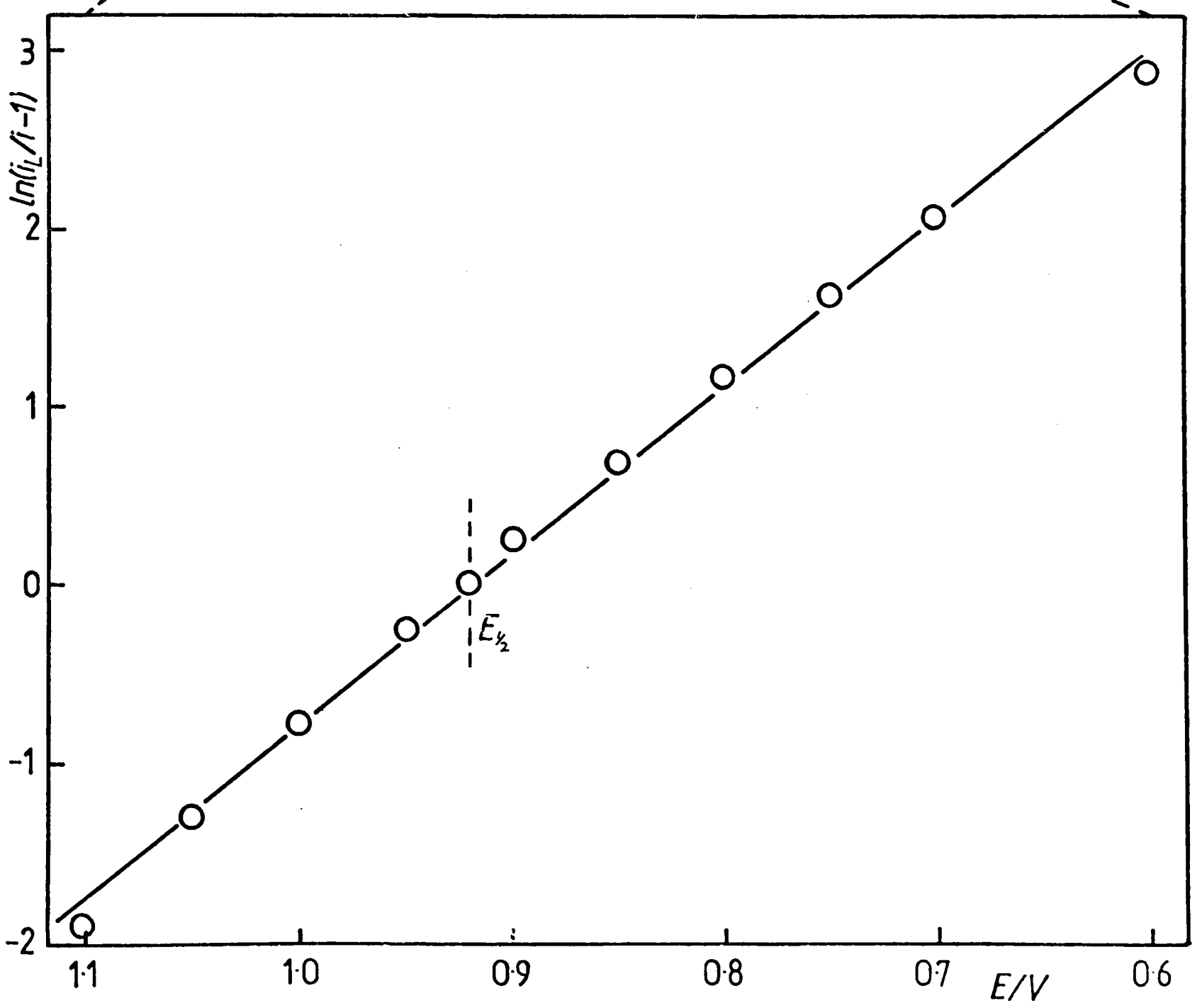

Fig 5 : 7

Oxidation of Fe(II) at SnO_2

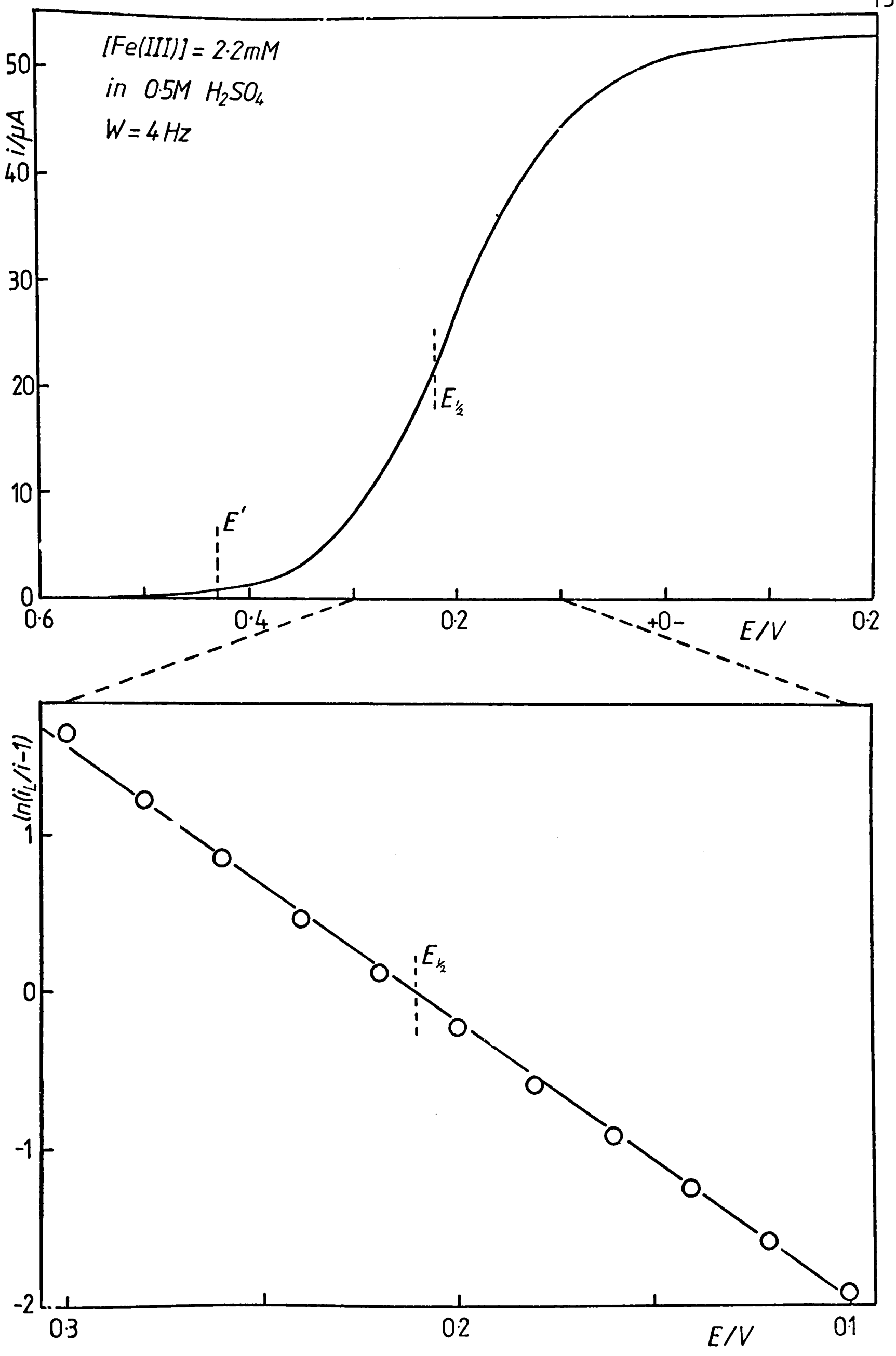

Fig 5 : 8

Reduction of Fe(III) at SnO_2

the exchange currents at E = E'.

In HCl at SnO_2

In Figures 5:9 and 10 are shown the polarograms and analyses for Fe(II) (this Work) and Fe(III) (Hillman[76]) in 0.5M HCl. The values of k'_* and α and β, obtained from the analyses, are given in Table 5:3.

There are a number of important features in these two polarograms.

1) The reduction wave for Fe(III) in HCl is significantly slower (by a factor of ~ 6.5) than in H_2SO_4. This makes quantitative measurement of photo-galvanic effects much easier as it means that, when potentiostatted in the region + 0.6 to + 0.4V, the electrode does not generate Fe(II) from the Fe(III) in solution which artificially increases the back reaction rate close to the electrode.

2) The oxidation wave for Fe(II) shows more complex behaviour. The region of interest is when E < + 1.1V. The rate constant k'_* is thus found using the early part of the analysis where $\beta = 0.1$. (The β value changes with potential but not in the direction usually found for electrochemical reactions. The sum of the α and β values $\neq 1$ for these reactions. Neither of these two observations breaks the law of microscopic reversibility as the whole potential energy surface is changed as the potential is changed and the reactions at, e.g. E = + 0.1V and E = + 1.1V, may be quite different in mechanism.

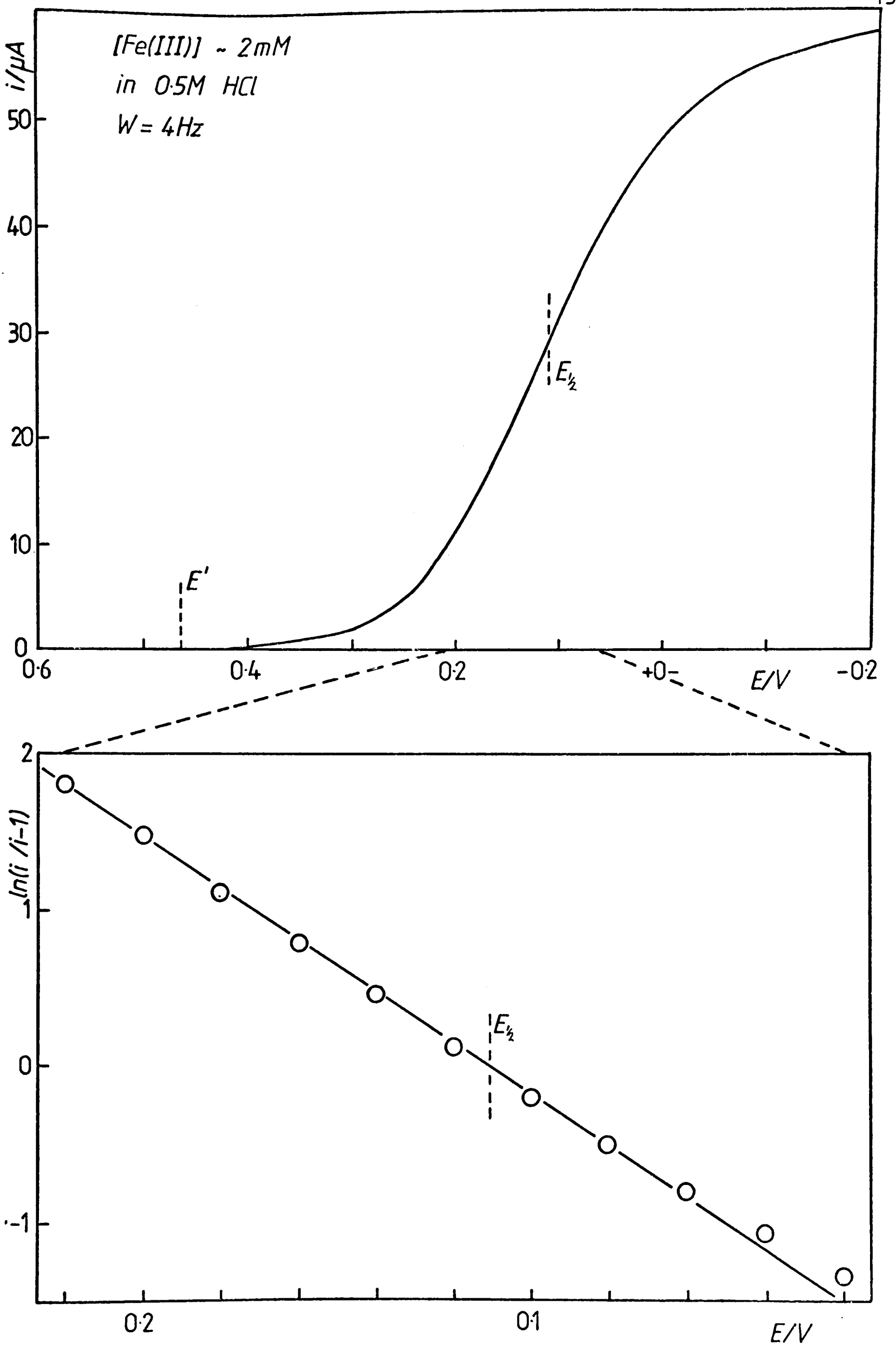

Fig 5 : 9

Reduction of Fe(III) at SnO_2

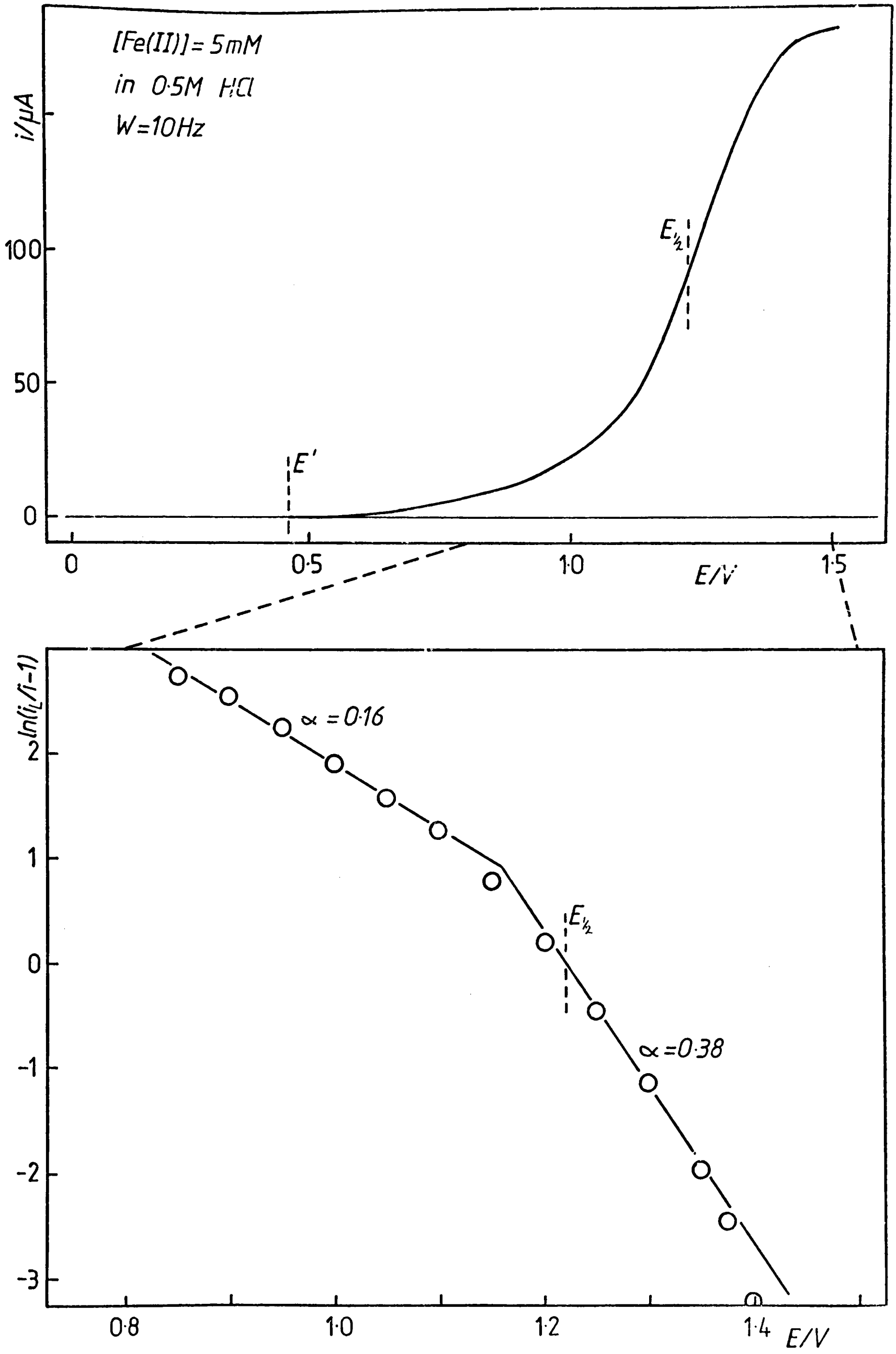

Fig 5 : 10

Oxidation of Fe(II) at SnO_2 (ref 76)

TABLE 5:3

Ion	Electrode	Medium/ 0.5M	E'/(V)	k_*'/cm s^{-1}	α/β
Fe(II)	SnO_2	H_2SO_4	0.431	1.8×10^{-5}	0.25(β)
Fe(III)	"	"	"	3.5×10^{-5}	0.46(α)
Fe(II)	"	HCl	0.463	1.7×10^{-5}	0.16(β)
Fe(III)	"	"	"	6.3×10^{-6}	0.43(α)
				k_o'/cm s^{-1}	
Fe(II)	Pt	HCl	0.463	3.4×10^{-5}	0.45(β)
Fe(III)	"	"	"	"	0.55(α)

α refers to reduction

β refers to oxidation

The value of k'_* for Fe(II) is very similar to that in H_2SO_4. However the dramatic difference in the β value means that the observed rate constant k' (equation 2:27) is very much slower in HCl. This means that a very good potential "window" is available for photogalvanic measurements. Figure 5:11 shows the two complete polarograms for Fe(II)/(III) in HCl and H_2SO_4.

In HCl at Pt

Just as the Fe(II)/(III) couple must be irreversible at the illuminated electrode in a photogalvanic cell, so must it be reversible at the dark electrode. A polarogram measured by Hillman[76] of equimolar Fe(II) and Fe(III) at Pt is shown in Figure 5:12. It is not perfectly reversible and so must be described fully using equation 2:24 which when combined with equations 2:15 and 16 gives

$$\ln\left(\frac{k_D}{k'_o}\right) + \frac{\alpha F}{RT}(E-E') = \ln\left(\frac{i_o}{i} - 1\right) + \exp\frac{n(E-E')F}{RT}\left(\frac{i_R}{i} + 1\right) = y$$

In Figure 5:11 y is plotted against E and values of α and k'_o are obtained. In this case classical behaviour is observed $\alpha + \beta = 1$ in the potential range measured.

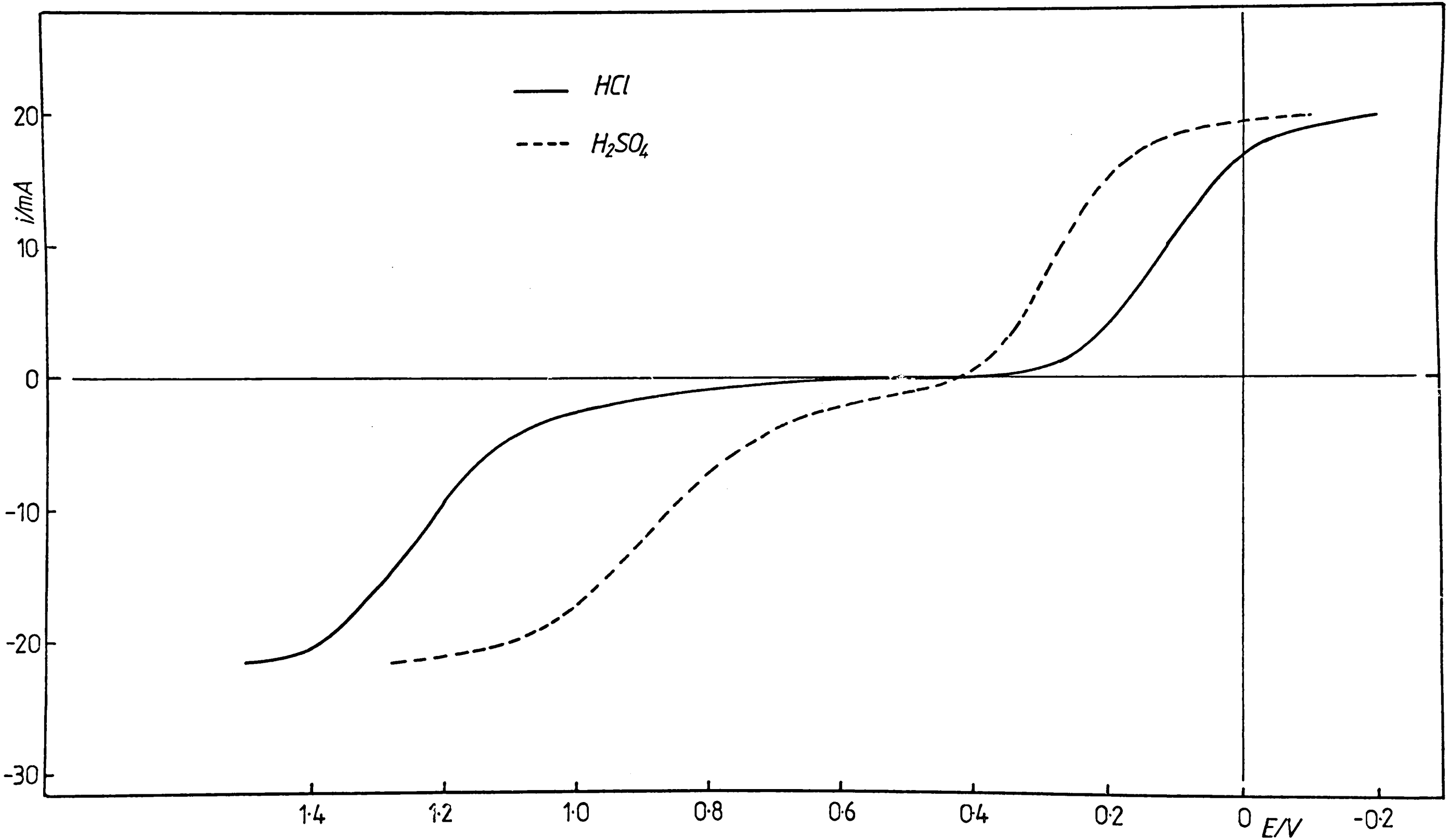

Fig 5 : 11

Polarograms of Fe(II)/(III)

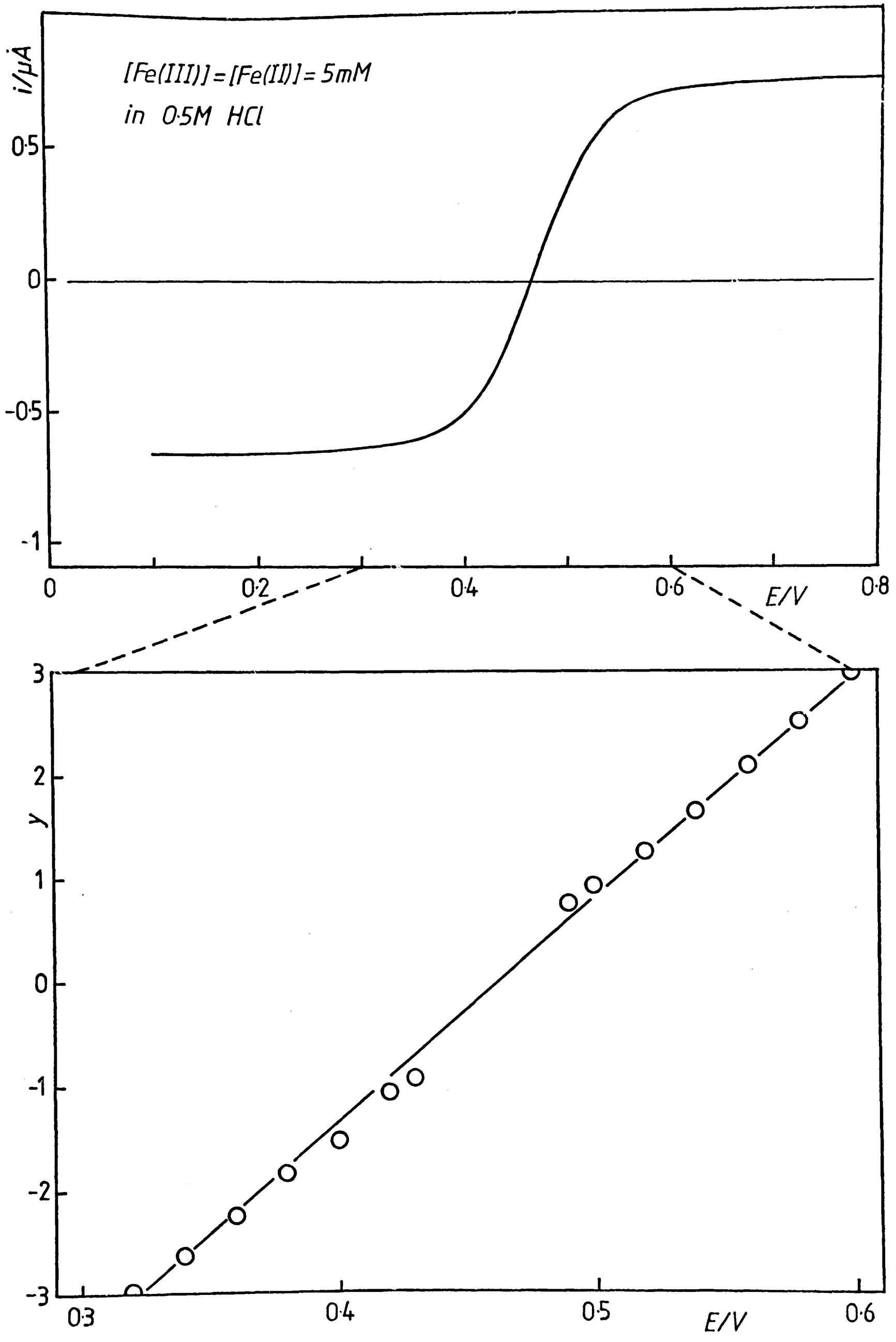

Fig 5 : 12

Reaction of Fe(II)/(III) at Pt(ref 76)

OPTICAL ROTATING DISC ELECTRODE

Two Ruthenium systems, $Ru(II)(bipy)_3$ and $Ru(II)(44'Me_2bipy)_3$ were investigated with the ORDE. They were used to confirm much of the theory for the ORDE and to establish reliable methods for the investigation of new photogalvanic systems.

Note: In all photogalvanic measurements at the ORDE the light used was of wavelength λ = 452 nm with intensity I_o ~ 150 μA of photons through electrodes of area A ~ 0.15 cm^2.

1) The "window" of measurement

In order to measure photogalvanic effects ideally it is required that

$$[Ru(III)] = 0 \quad at \quad x = 0 \tag{5:4}$$

and

$$\frac{\partial[Fe(II)]}{\partial x} = 0 \quad at \; x = 0 \tag{5:5}$$

so that accurate calculation of $N_{h\nu}$ is possible.

The range of this window is determined by the electrode kinetics of the Fe(II)/(III) couple and the shape of the photocurrent, Δi v E, potential curves is determined by the electrode kinetics of the two couples and the ratio of the diffusion coefficients, (Δi is defined as the difference between the currents when the light is on, $i_{h\nu}$, and

when the light is off i_D. $\Delta i = (i_{h\nu} - i_D)$.

Figure 5:13 and 5:14 show typical examples of the potential dependences of the photocurrent for various $Ru(II)L_3$ complexes. In both Figures 5:13 and 5:14 the concentration of Fe(III) was sufficient to quench all the $Ru(II)^*$ and the concentration of Fe(II) was $< 10^{-6}$ M.

Note: High concentrations of H^+ (0.5M) were used in all studies on $Ru(II)L_3$ complex as Ru(III) is rapidly reduced by OH^-.

Considering first Figure 5:13 a and b and 5:14, the difference observed between the electrode kinetics of the Fe(II)/(III) couples in 0.5 M HCl and 0.5 M H_2SO_4 is quite apparent in the plots of Δi v E. In HCl in this range +0.7 to +0.45 V both the above conditions (5:4) and (5:5) are satisfied and $N_{h\nu}$ may be calculated accurately using the ORDE theory in Chapter 2. In H_2SO_4, however, there is a sharp maximum in this region which may be predicted from the significant exchange currents at SnO_2 for the Fe(II)/(III) couple. At potentials $>+$ 0.5 V this fall in photocurrent is due to the reaction of both photogenerated species, Fe(II) and Ru(III), at the electrode and their respective effects cancelling out. At potentials $> +0.9$ V this effect actually changes sign because the diffusion coefficient of the Ru(III) species is significantly less than that of Fe(II). At potentials $<+$ 0.5 V the effect decreased because the electrode generates Fe(II) from the high concentration (10^{-2} M) of Fe(III) present in solution. This Fe(II) generated at the electrode

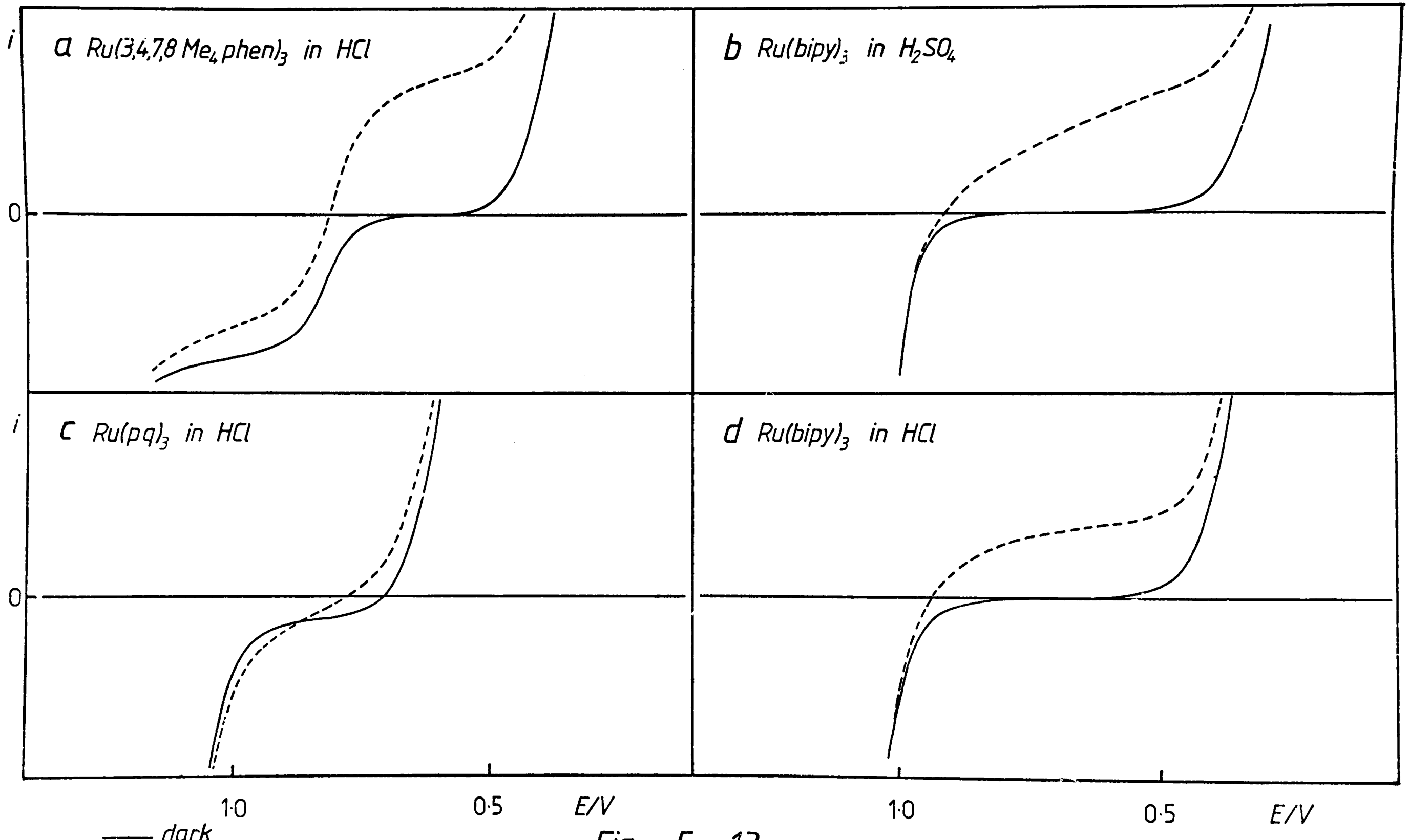

Fig 5 : 13

The Photogalvanic Effect

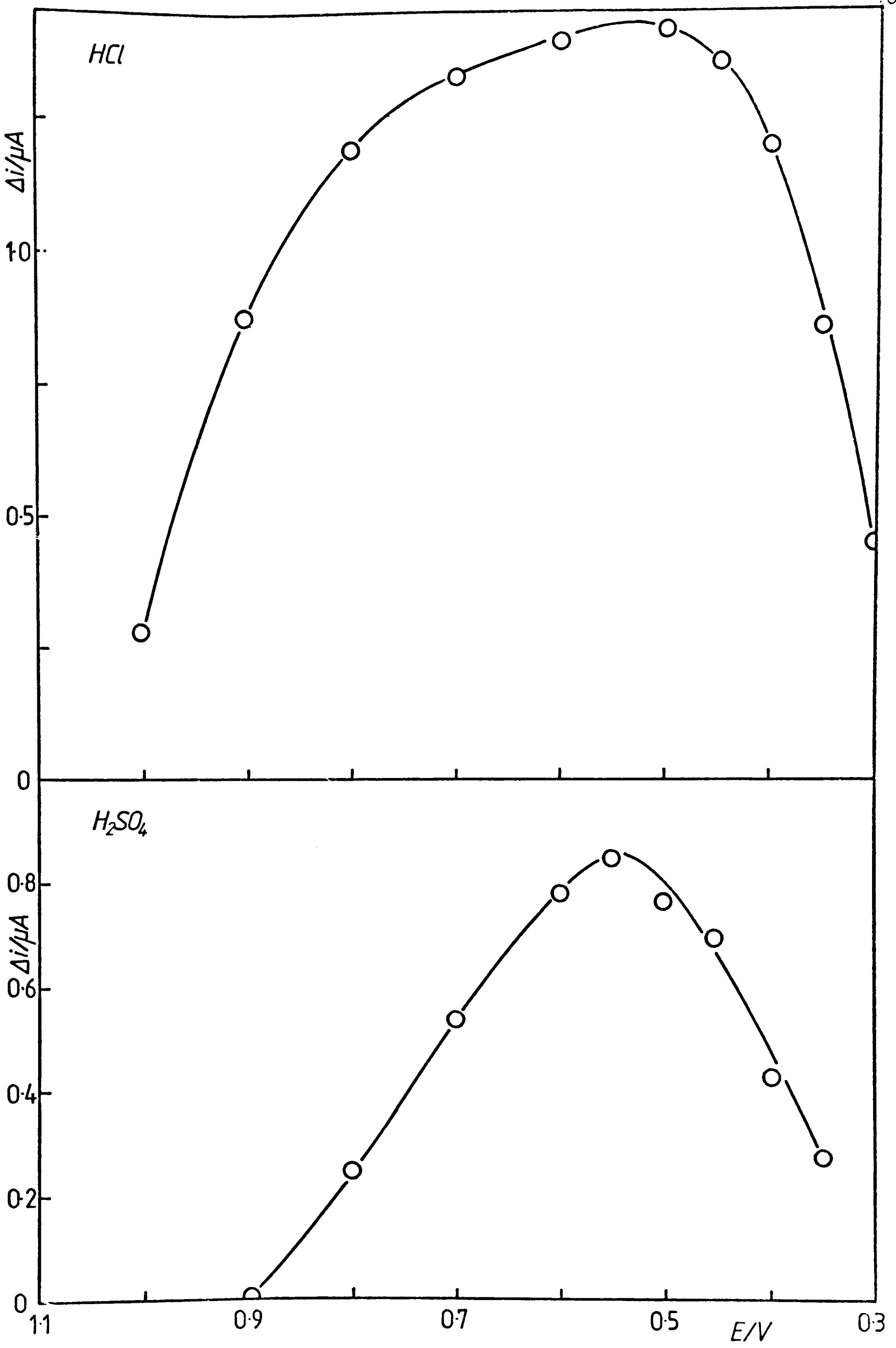

Fig 5 : 14

Comparison of Photocurrent in HCl & H_2SO_4

increases the rate of the back reaction and thus decreases the photoelectrochemical collection efficiency.

In HCl all of these effects occur but there is a range of potential (+ 0.7 V to + 0.45 V) where they are not important.

In Figure 5:13a the effect for Ru(II) $(3,4,7,8\ Me_4\ phen)_3$ is shown. This compound has a much slower back reaction so that the effect is comparable with the limiting dark current. The same features are still seen however and the effect disappears at high positive potentials when Fe(II) begins to react at the electrode.

Figure 5:13c shows the photogalvanic effect for Ru(II) $(2,2'$ pyridyl quinoline$)_3$. In this case the change in sign of the photocurrent occurs at ~+ 0.9 V because of the small diffusion coefficients of the Ru(II) compound.

2) Variation of the Photoeffect with [Fe(III)]

In order to investigate the [Fe(III)] dependence of the photoeffect region B of Figure 2:4 is most suitable as

$$N_{h\nu} = \phi \frac{\beta}{\kappa} \quad \text{for} \quad \kappa >> \beta$$

If β and κ are kept constant (i.e. [Ru(II)] and [Fe(II)] constant) ϕ may be investigated.

$$A + h\nu \longrightarrow A^* \qquad \text{Absorption}$$

$$A^* \xrightarrow{k_M} \qquad \text{Non E-T Deactivation}$$

$$A^* + Fe(III) \xrightarrow{k_q} B + Fe(II) \qquad \text{E-T Quenching}$$

ϕ is the quantum efficiency for the production of B, and thus

$$\phi = \frac{k_q[Fe(III)]}{k_M + k_q[Fe(III)]}$$

or $$1/\phi = 1 + \frac{k_M}{k_q[Fe(III)]}$$

Figure 5:15 shows the variation of Δi with [Fe(III)] and the Stern-Volmer analysis below.

When $\phi = \frac{1}{2}$

$$[Fe(III)] = \frac{k_M}{k_q} = (8.2 \pm 1) \times 10^{-4} \text{ M.}$$

This is in reasonable agreement with Sutin's[26] work. The fluorescence decay, k_f, was measured in 0.5 M H_2SO_4 and HCl as 1.66×10^6 s^{-1} and k_q as 2.7×10^9 M^{-1} s^{-1} in 0.5 M H_2SO_4

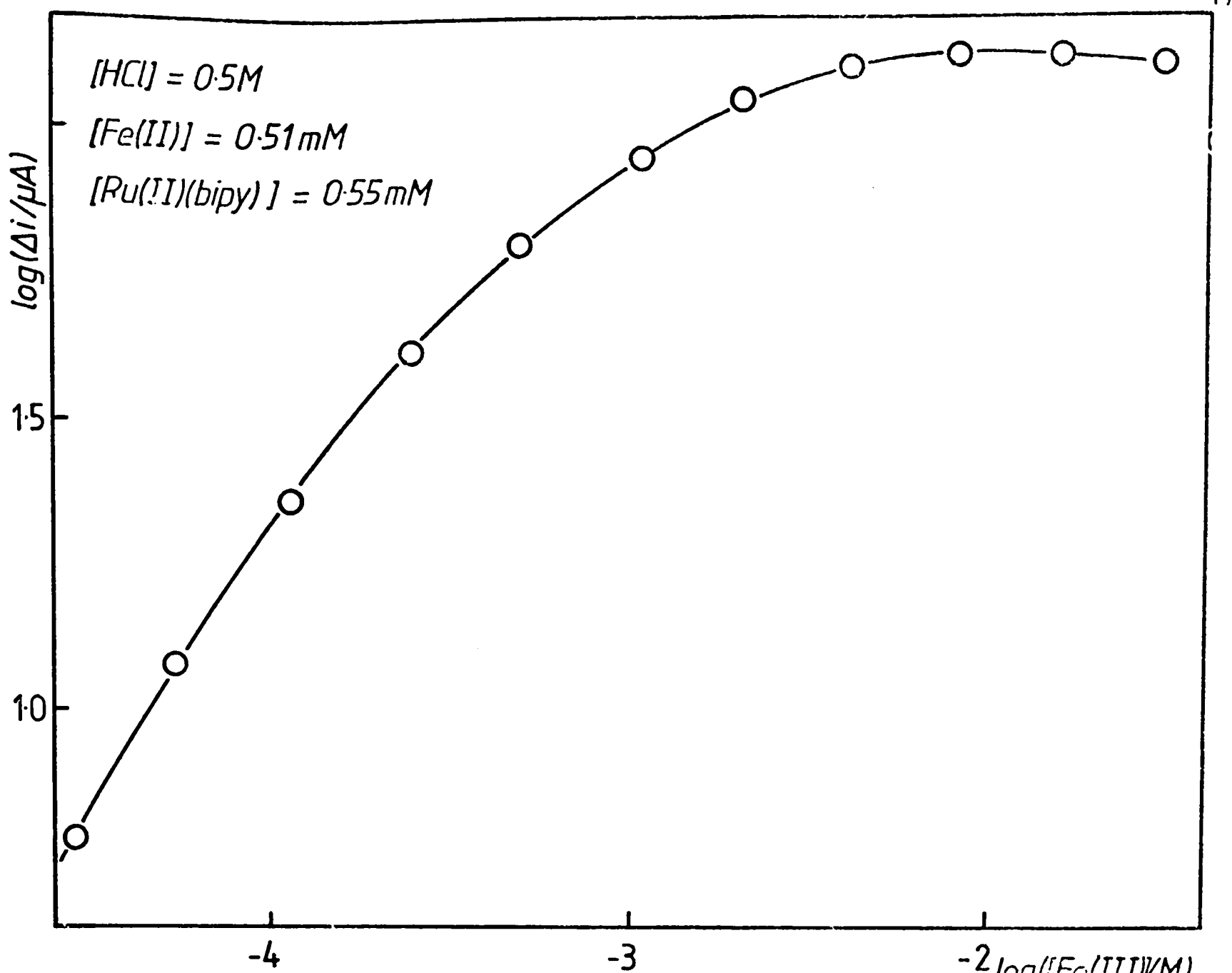

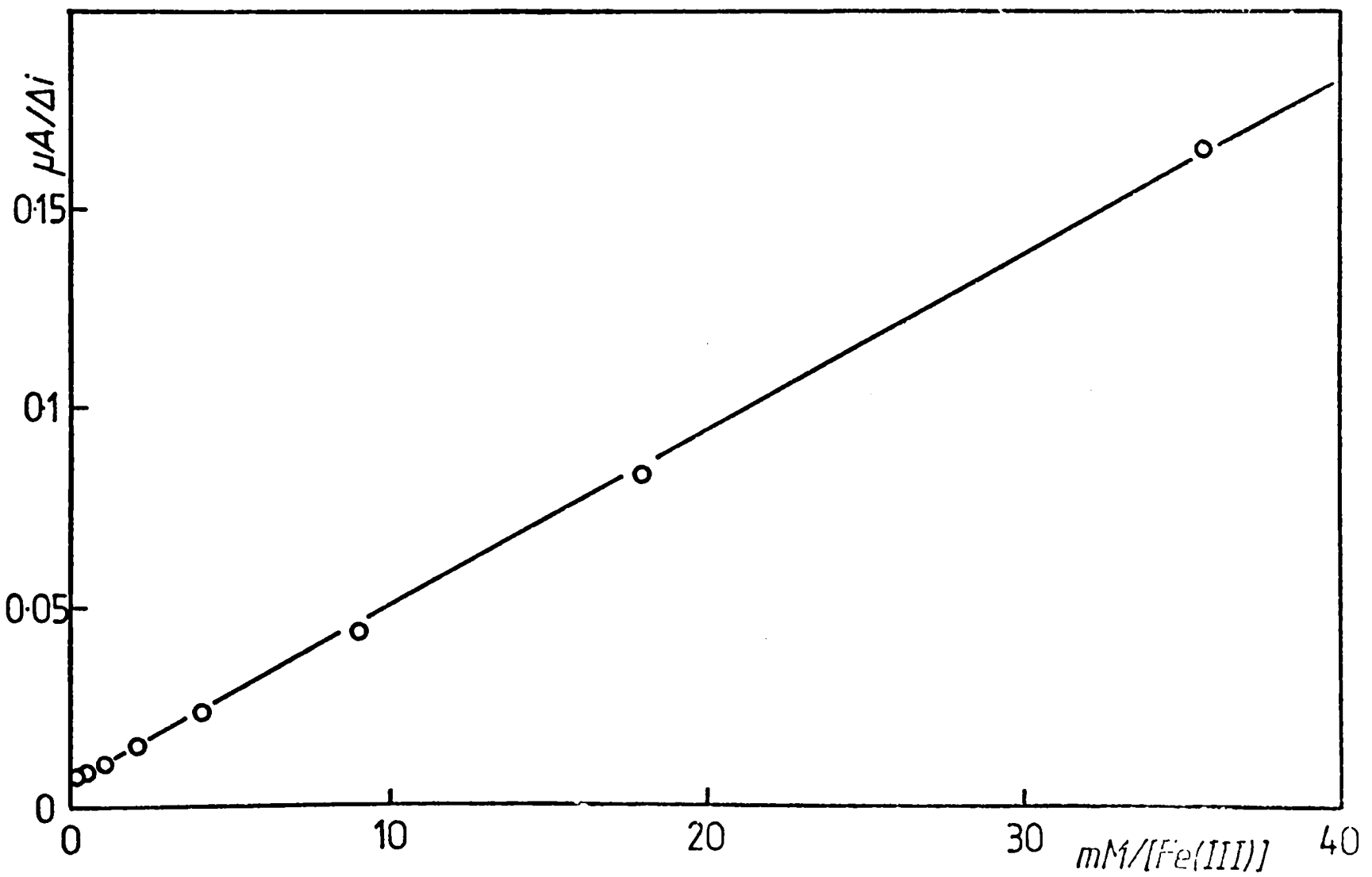

Fig 5 : 15

Variation with [Fe(III)]

$$\text{thus} \qquad \frac{k_f}{k_q} = 6.1 \times 10^{-4}\ \text{M} \ .$$

The small difference can be attributed to the variation of k_q between the two media.

The identical experiment for Ru(II)(44'Me_2bipy)$_3$ gives

$$\frac{k_M}{k_q} = (1.8 \pm 0.5) \times 10^{-4}\ \text{M}$$

whereas Sutin's[26] value for k_f and k_q are

$$k_f = 3 \times 10^6\ s^{-1} \quad \text{in } H_2O, \quad 0.5\text{M HCl and } 0.5\text{M } H_2SO_4$$

and $$k_q = 2.9 \times 10^9\ M^{-1}\ s^{-1} \quad \text{in } 0.5\text{M } H_2SO_4$$

giving $$k_f/k_q = 1.04 \times 10^{-3}\ \text{M}.$$

The factor of 5 difference must be due to the variation of k_q between HCl and H_2SO_4 as it is impossible for the substitution of HCl for H_2SO_4 to enhance the luminescence lifetime.

The rate of the quenching reaction agrees well with that calculated for the simple Smoluchowski equation for diffusion

controlled rates. The very high ionic strength of the media used means that the Debye correction for the coulombic forces between the reactants is small. A second factor which makes the Debye correction small in this case is that, although the reaction is between Fe(III) and Ru(II), the charge on the Fe(III) is not 3 +. In 0.5 M HCl the predominant species is $FeCl_4^-$ and thus one might expect only a small enhancement in rate. In 0.5M H_2SO_4 the important species are $Fe(SO_4)^+$ and $Fe(SO_4)_2^-$ in comparable quantities so that any enhancement of the rate between oppositely charged species is fortuitiously cancelled out by the slower reaction of the like charged species.

Having investigated the variation of the effect with Fe(III) all further experiments were caried out with [Fe(III)] > 10^{-2} M so that the electron transfer quenching of $Ru(II)^*$ was of maximum efficiency.

3) Variation of the Photoeffect with [Fe(II)]

Working again in region B of Figure 2:4

$$N_{h\nu} = \phi \frac{\beta}{\kappa} = \phi \varepsilon[A] \left(\frac{D}{k_{-2}[Y]}\right)^{\frac{1}{2}} \qquad (5:6)$$

Thus $N_{h\nu} \propto [Fe(II)]^{-\frac{1}{2}}$ and is independent of rotation speed. However Figure 5:16a shows that for [Fe(II)] < 1 mM this is not true.

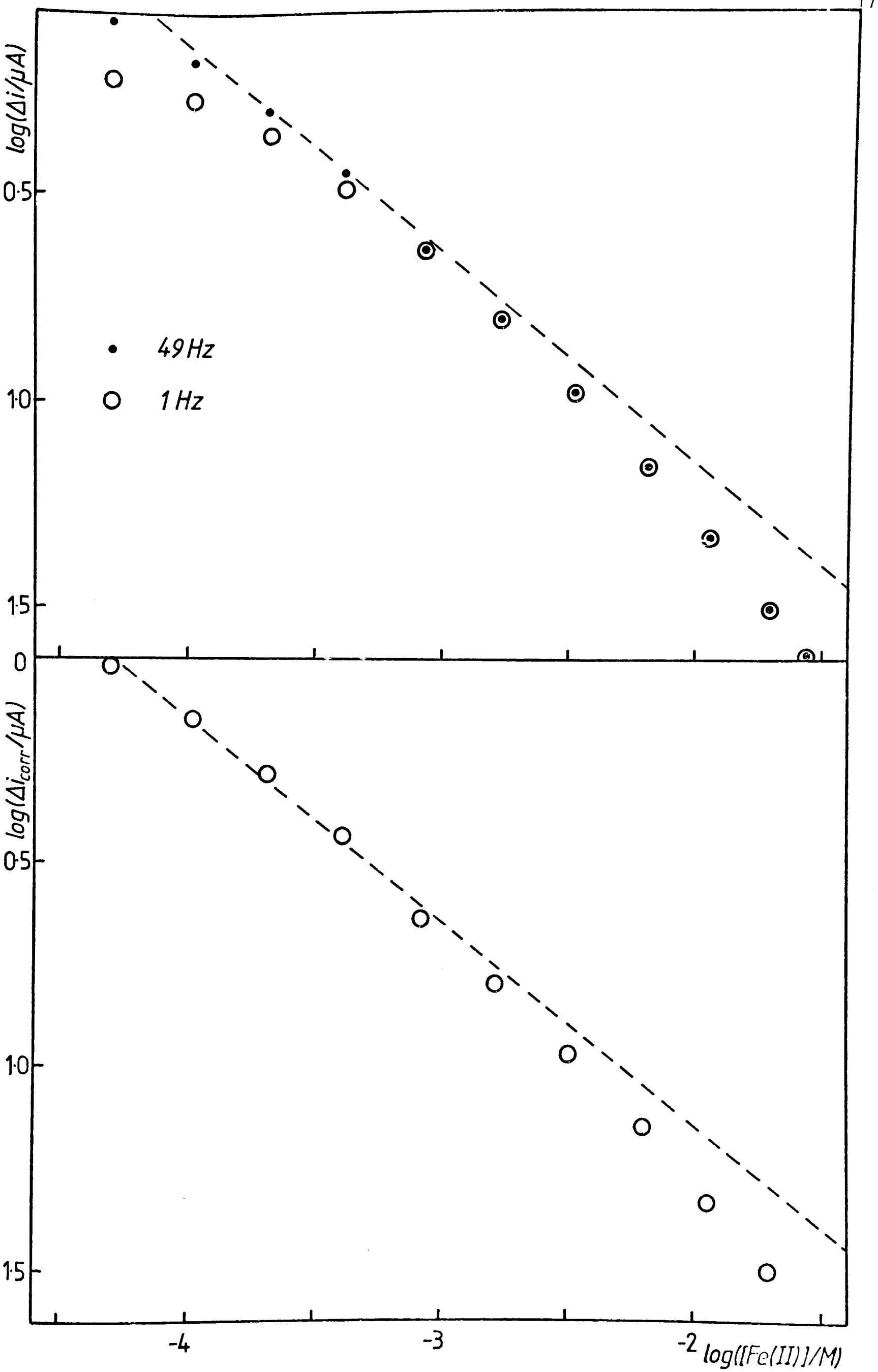

Fig 5 : 16

Variation of Photocurrent with [Fe(II)]

The deviation from the expected behaviour may be explained in terms of a simple model represented in Figure 5:17. The important feature of this model is that, although $X_k < X_D$ and equation (5:6) is expected to hold, the photogenerated Fe(II) must diffuse away from the electrode across the diffusion layer and thus builds up close to the electrode.

In this model the assumptions made are

(a) X_ε is long (>> X_D) so that at $x \to \infty$ a photostationary state is produced with a constant concentration of B, dependent on the light flux and the bulk concentration of Y in the dark.
i.e. $[B]_{PSS} = [Y]_{PSS} << [Y]_{Dark}$ at $x = \infty$.

(b) $X_k << X_D$ so that, inside the diffusion layer, while B is converted to A at the electrode having diffused across the short distance X_k, Y must diffuse out to the bulk of the solution across the distance $(X_D - X_k) \approx X_D$. As the flux of B and Y must be identical it is clear that [Y] will build up close to the electrode due to the constant concentration gradient acting over a longer distance.

Now

$$[Y]_o = [Y]_k = [Y]_\infty + [Y]_{PSS} + \frac{j_{h\nu} X_D}{D} \qquad (5:7)$$

where j is the flux of material at the electrode

o refers to the electrode surface, x = 0

k refers to $x = X_k$

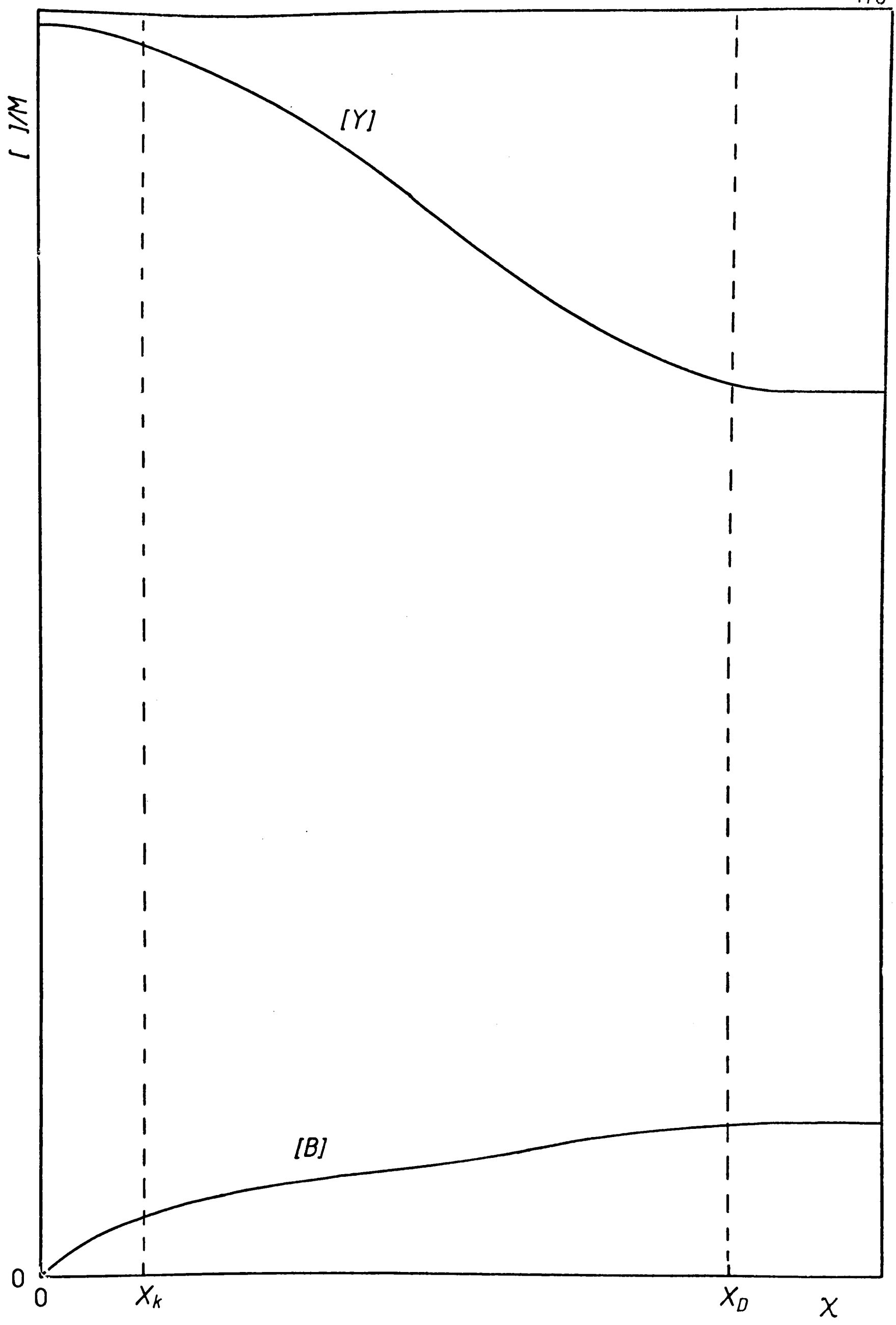

Fig 5 : 17

Concentration Profiles for Half Buffered Case

∞ refers to the bulk of solution, $x = \infty$

PSS is a photostationary state

$h\nu$ refers to a light induced effect

$j_{h\nu}$ is the limiting flux of B diffusing across X_k and is thus

$$j_{h\nu} = \frac{D[B]_{PSS,k}}{X_k} = D\ k\ [Y]_o \cdot [B]_{PSS,k}$$

Considering now the boundary layer flux at X_k the light flux, $j_{h\nu,k}$, is equated with the back reaction giving a photostationary state.

$$j_{h\nu,k} = k[Y]_k\ [B]_{PSS,k} \qquad (5:9)$$

Substituting (5:0) in (5:8)

$$j_h = \frac{j_h \sqrt{D}}{\sqrt{k[Y]_o}}$$

$$[Y]_o = \left(\frac{f_{h\nu}}{j_{h\nu}}\right)^2 \frac{D}{k} \qquad (5:10)$$

Equating (5:7) and (5:10)

$$\frac{f_{h\nu}^2}{j_{h\nu}^2} \cdot \frac{D}{k} = [Y]_\infty + [Y]_{PSS,} + \frac{j_{h\nu} X_D}{D} \qquad (5:11)$$

$$\approx [Y]_\infty + \frac{j_{h\nu} X_D}{D}$$

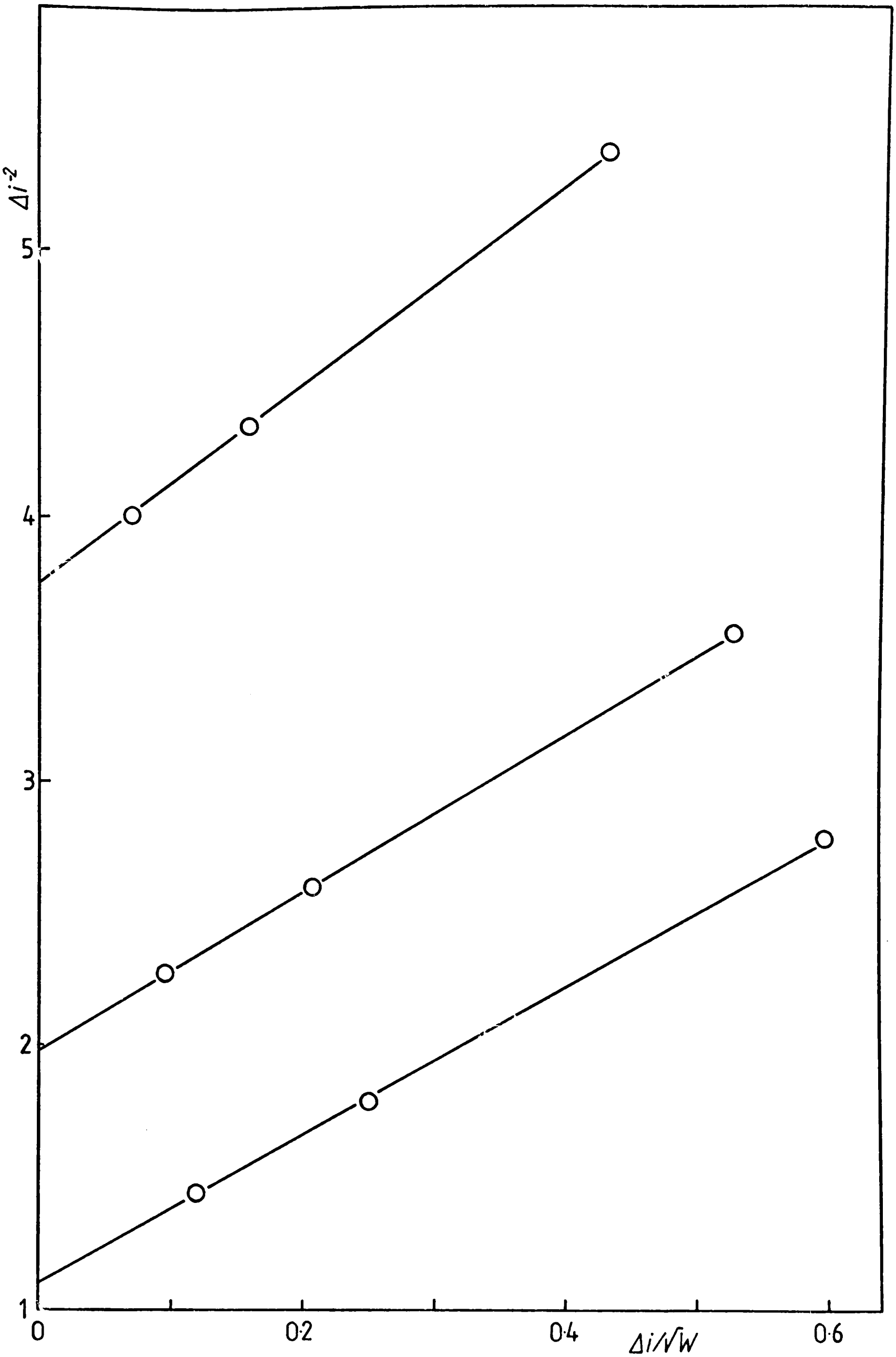

Fig 5 : 18

Variation of Photocurrent with Rotation Speed

Now for constant f and with $X_D \propto W^{-\frac{1}{2}}$

$$\frac{1}{\Delta i^2} \propto \frac{\Delta i}{\sqrt{W}}$$

Plotting this relation the intercept on the $1/\Delta i^2$ axis corresponds to an infinitely thin diffusion layer ($W \rightarrow \infty$) and thus no build up of Y.

Δi_{corr} is thus defined as Δi as $W \rightarrow \infty$ and is obtained from Figure 5:18. The plot of log Δi_{corr} v log[Fe(II)] in Fig. 5:16b is now well behaved for [Fe(II)] < 1 mM

i.e. $$N_{h\nu,corr} \propto [Fe(II)]^{-\frac{1}{2}}$$

A similar analysis for Ru(II) (44'Me_2bipy), is shown in Figure 5:19. The agreement with the theory is not quite as good in this case, but is reasonable for [Fe(II)] < 3 mM.

At high concentrations of Fe(II) the experimental results again deviate from those predicted. One explanation for this is that Fe(II) quenching of $Ru(II)^*$ begins to compete with Fe(III) quenching.

Assuming a simple model

$$A^* + Fe(III) \xrightarrow{k_q} Fe(II) + B$$

$$A^* + Fe(II) \xrightarrow{k_s} A + Fe(II) + \Delta$$

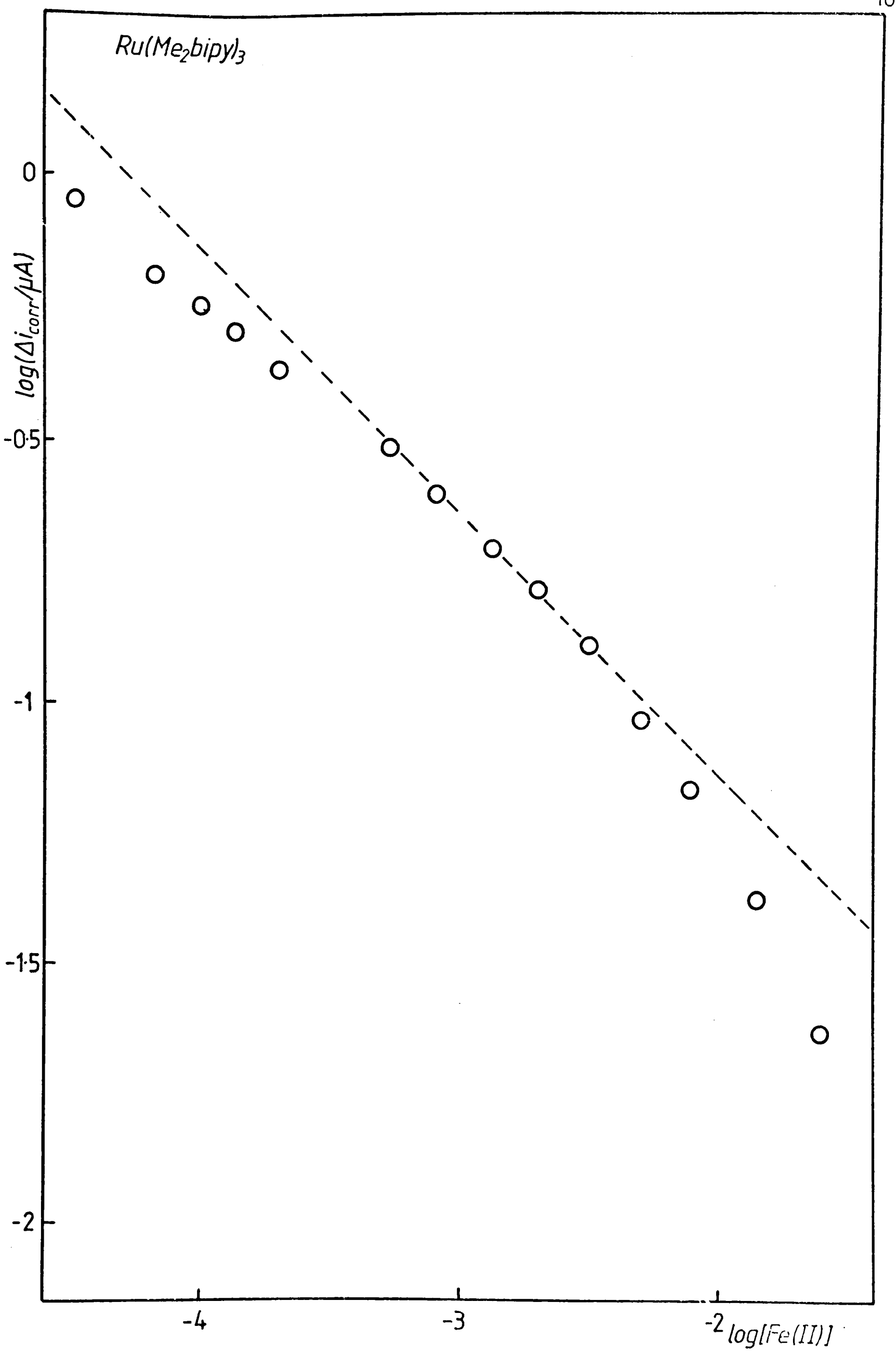

Fig 5 : 19

Variation of Photocurrent with [Fe(II)]

Thus

$$\phi = \frac{1}{1 + K_Q \frac{[Fe(II)]}{[Fe(III)]}} \qquad (5:12)$$

where $K_Q = \frac{k_s}{k_q}$

and ϕ is the quantum efficiency for the production of B.

In region B of figure 2:4

$$N_{h\nu} = \phi \beta/\kappa$$

or $$\Delta i[Fe(II)]^{\frac{1}{2}} = \phi(I_o \varepsilon [A] \sqrt{D/k}) \qquad (5:13)$$

Combining (5:12) and (5:13)

$$\frac{1}{\Delta i[Fe(II)]^{\frac{1}{2}}} \propto 1 + K_Q \frac{[Fe(II)]}{[Fe(III)]}$$

when $\phi = \frac{1}{2}$ (assuming $\phi = 1$ for $[Fe(II)] = 0$)

then $$K_Q \frac{[Fe(II)]}{[Fe(III)]} = 1$$

Thus when

$$\frac{1}{\Delta i\ Fe(II)^{\frac{1}{2}}} = 2 \times \text{Intercept of (5:13)}$$

$$K_Q = \frac{[Fe(III)]}{[Fe(II)]} \qquad (5:14)$$

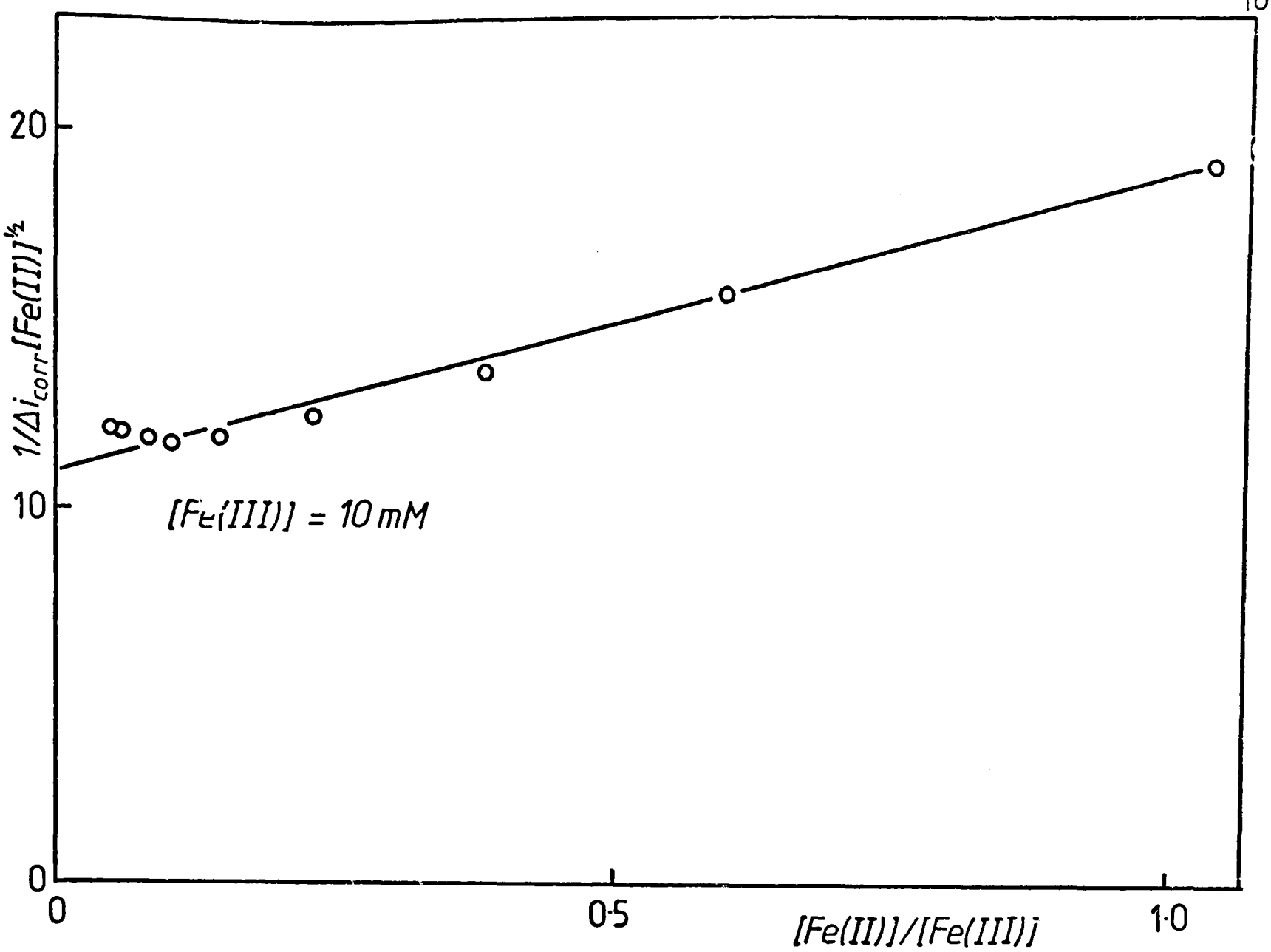

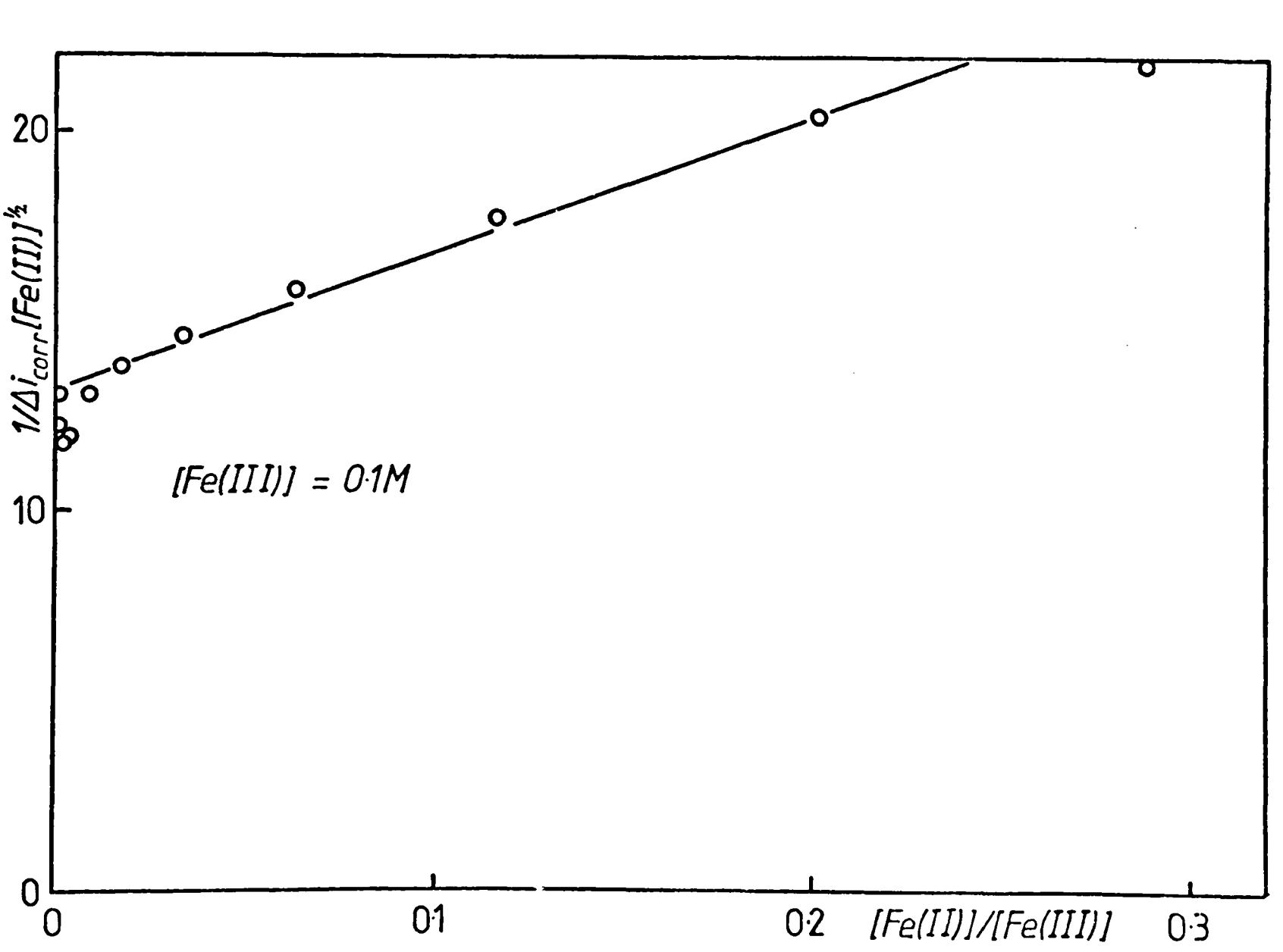

Fig 5 : 20

Variation of Photocurrent with [Fe(II)]

For $Ru(II)(bipy)_3$

Figure 5:20a gives $K_Q = 0.73$

and Figure 5:20b gives $K_Q = 2.8$

But according to Sutin[26]

$$K_Q = \frac{k_s}{k_q} = 10^{-3} \quad \text{in } 0.5M\ HClO_4.$$

This large discrepancy may be explained in part by two factors.

(1) The Fe(II) may quench $Ru(II)^*$ by an electron transfer mechanism. If this is the case then the model becomes

$$Ru(II)^* + Fe(III) \xrightarrow{k_q} Ru(III) + Fe(II)$$

$$Ru(II)^* + Fe(II) \xrightarrow{k_s} Ru(I) + Fe(III)$$

If Ru(I), either by reaction with Ru(III) or by reaction at the electrode, reduces the photocurrent then ϕ becomes

$$\phi = \frac{k_q[Fe(III)] - k_s[Fe(II)]}{k_q[Fe(III)] + k_s[Fe(II)]} \qquad (5:15)$$

$$= \frac{1 - \alpha}{1 + \alpha} \qquad (5:16)$$

where $$\alpha = K_Q \frac{Fe(II)}{Fe(III)} \qquad (5:17)$$

For small amounts of Fe(II) quenching i.e. $\alpha << 1$

$$\phi \approx 1/(1 - 2\alpha)$$

Thus Figures 5:20 a and b will give values for $2K_Q$ so that the K_Q values are 0.37 and 1.4 respectively.

In fact some of the Ru(I) produced may undergo a thermal back reaction with Fe(III) so that the values obtained for K_Q will lie between the two extremes given and will vary with Fe(III) as is found.

(2) The change in medium between Sutin's work (0.5M $HClO_4$) and this work (0.5 M HCl) causes some change in k_s (although not in k_q[26]). Given an electron transfer mechanism for the Fe(II) quenching the rate of the reaction should correlate with the oxidation potential of Fe(II).

E' in 0.5M HCl = 0.461 V (v S.C.E.)

E' in 0.5 - 1 M $HClO_4$ = 0.50 V (v S.C.E.)

The difference of only 40 mV, although in the right direction, is too small to explain such a large change in k_s.

These two factors combined do not explain completely the differences between this work and that of Sutin. However the deviations from the predicted behaviour

$$\Delta i \propto [Fe(II)]^{-\frac{1}{2}}$$

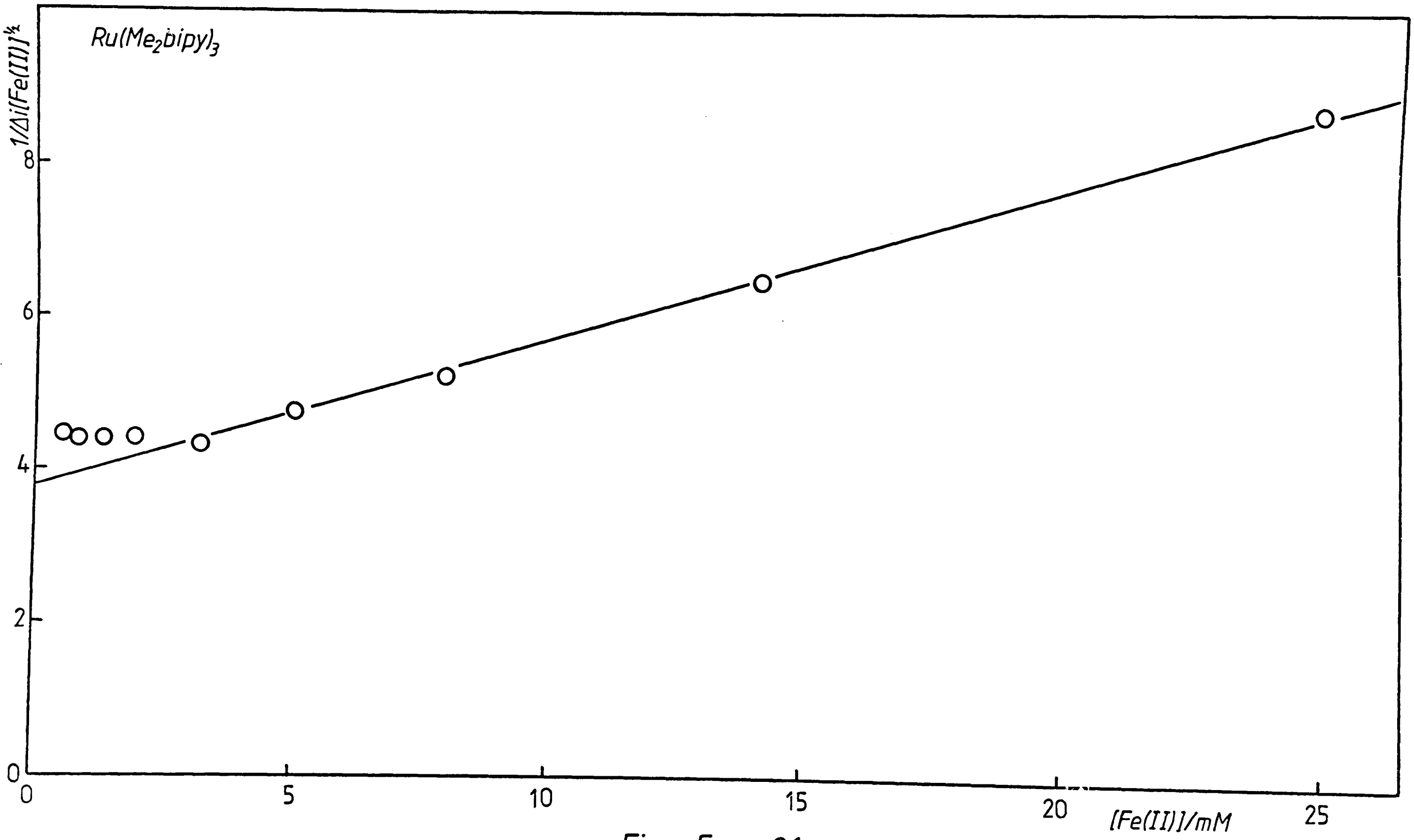

Fig 5 : 21

Variation of Photocurrent with [Fe(II)]

are not large (< a factor of 2) at the concentrations measured.

Figure 5:21 shows a similar result for Ru(II)(44'Me_2bipy)$_3$ giving $K_Q = 0.52$.

However no values of k_s are available for comparison in this case.

4) Variation of Photoeffect with Light Intensity

Working still in region B of Figure 2:4

$$N_{h\nu} = \phi \frac{\beta}{\kappa} = \phi \varepsilon[A]\sqrt{\frac{D}{k_{-2}[Y]}} \qquad (5:18)$$

By definition $N_{h\nu} = \frac{\Delta i}{I_o}$.

Thus $\Delta i \propto I_o$ for constant [A] and [Y]

and

$$k_{-2}/\phi^2 = \frac{\varepsilon^2[A]^2 D}{N_{h\nu}^2[Y]} \qquad (5:19)$$

Given an independent measure of k a value of ϕ may be obtained and vice versa.

Figure 5:22 shows a plot of Δi v I_o with gradient $N_{h\nu} = 1.68 \times 10^{-3}$.

This is now corrected for the small deviation caused Fe(II) quenching discussed in the previous section (14% from Figure 5:16) to give

$$N_{h\nu} = 1.92 \times 10^{-3}$$

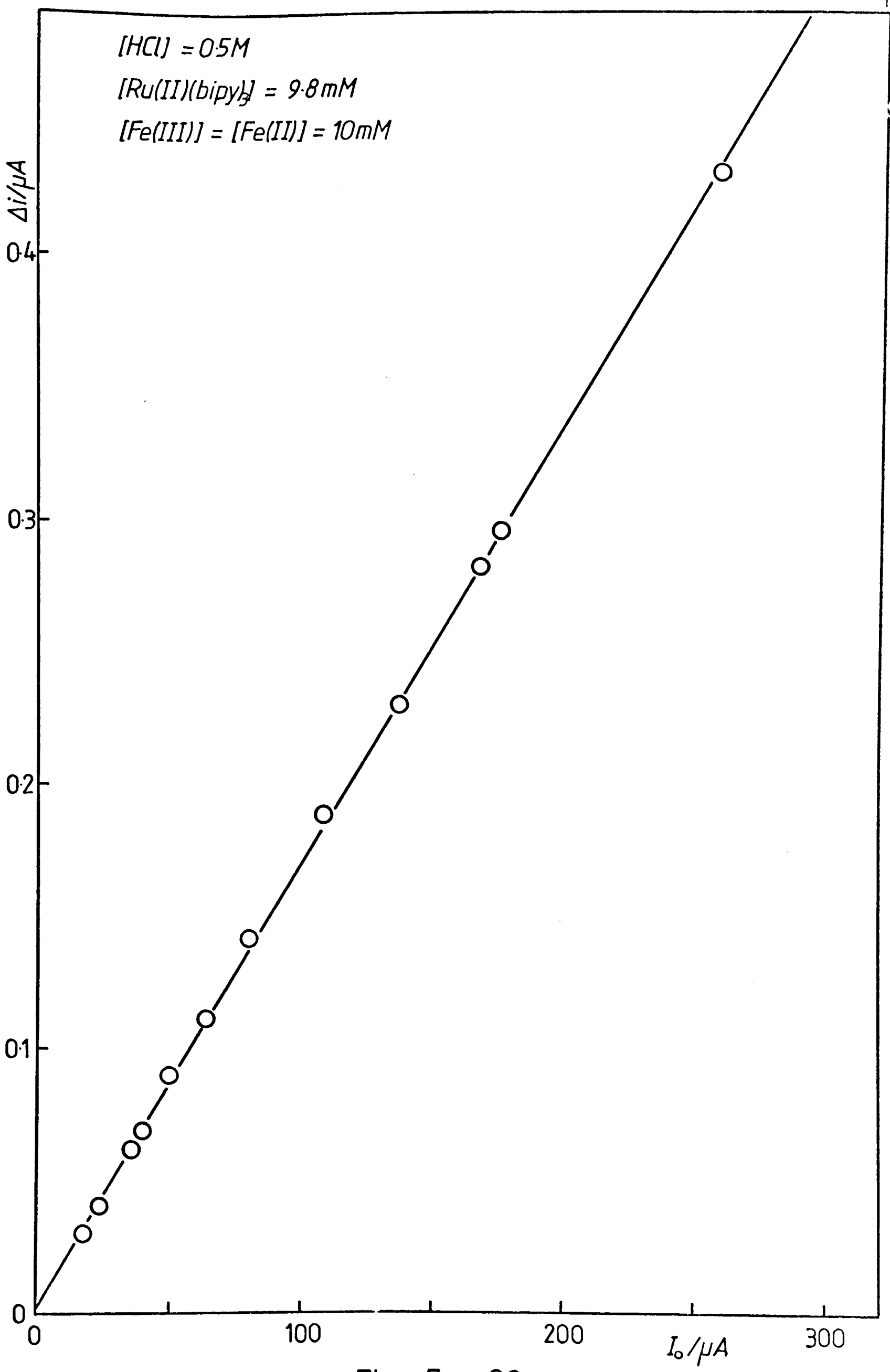

Fig 5 : 22

Variation of Photocurrent with Light Intensity

giving $k_{-2}/\phi^2 = 9.3 \times 10^6\ M^{-1}\ s^{-1}$

Sutin's work in 0.5M H_2SO_4[26] gives

$$k_{-2} = 5 \times 10^6\ M^{-1}\ s^{-1}$$

and $$\phi \approx 1$$

From results described later in this chapter, obtained by stopped flow and flash electrolysis for other $RuL_3^{2/3}$ complexes, it is apparent that the change from H_2SO_4 to HCl increases k_{-2} by a factor of 2-3 at 25°C. It therefore seems likely that in 0.5 M HCl

ϕ is still 1

and k_{-2} is ~ $9 \times 10^6\ M^{-1}\ s^{-1}$.

A similar experiment for Ru(II) $(44'Me_2bipy)_3$ gives a value of $1.1 \times 10^5\ M^{-1}\ s^{-1}$ for k_{-2}/ϕ^2. Again anticipating the result for k_{-2} presented later in this chapter

$$k_{-2} = 6.5 \times 10^5\ M^{-1}\ s^{-1}$$

and thus $$\phi = 0.77 \pm 0.2$$

The ORDE thus provides a useful method of obtaining ϕ given a knowledge of k_{-2}.

5) Action Spectra

Again in region B of Figure 2:4 it is predicted that

$$N_{h\nu} \propto \varepsilon_{\lambda}$$

and thus the photocurrent action spectrum should match the absorption spectrum.

Figure 5:23 and 5:24 show action spectra for $Ru(II)(bipy)_3$ and $Ru(II)(Me_2bipy)_3$ respectively. The action spectra and absorption spectra were normalised to λ = 452 nm. The agreement between the two is good except at λ = 400 nm where there was some doubt about the accuracy of calibration of the laser power meter.

Such action spectra are very important in assessing the interaction of various dyes on multi-component systems, which are essential for practical photogalvanic cells.

6) Variation of the Photoeffect with [Ru(II)]

Having performed most of the ORDE experiments with dilute solutions of Ru(II) (< 1 mM), it is important to confirm that there is no drop in quantum efficiency as the concentration is raised e.g. by self quenching

$$Ru(II)^{*} + Ru(II) \rightarrow 2\ Ru(II) + \Delta$$

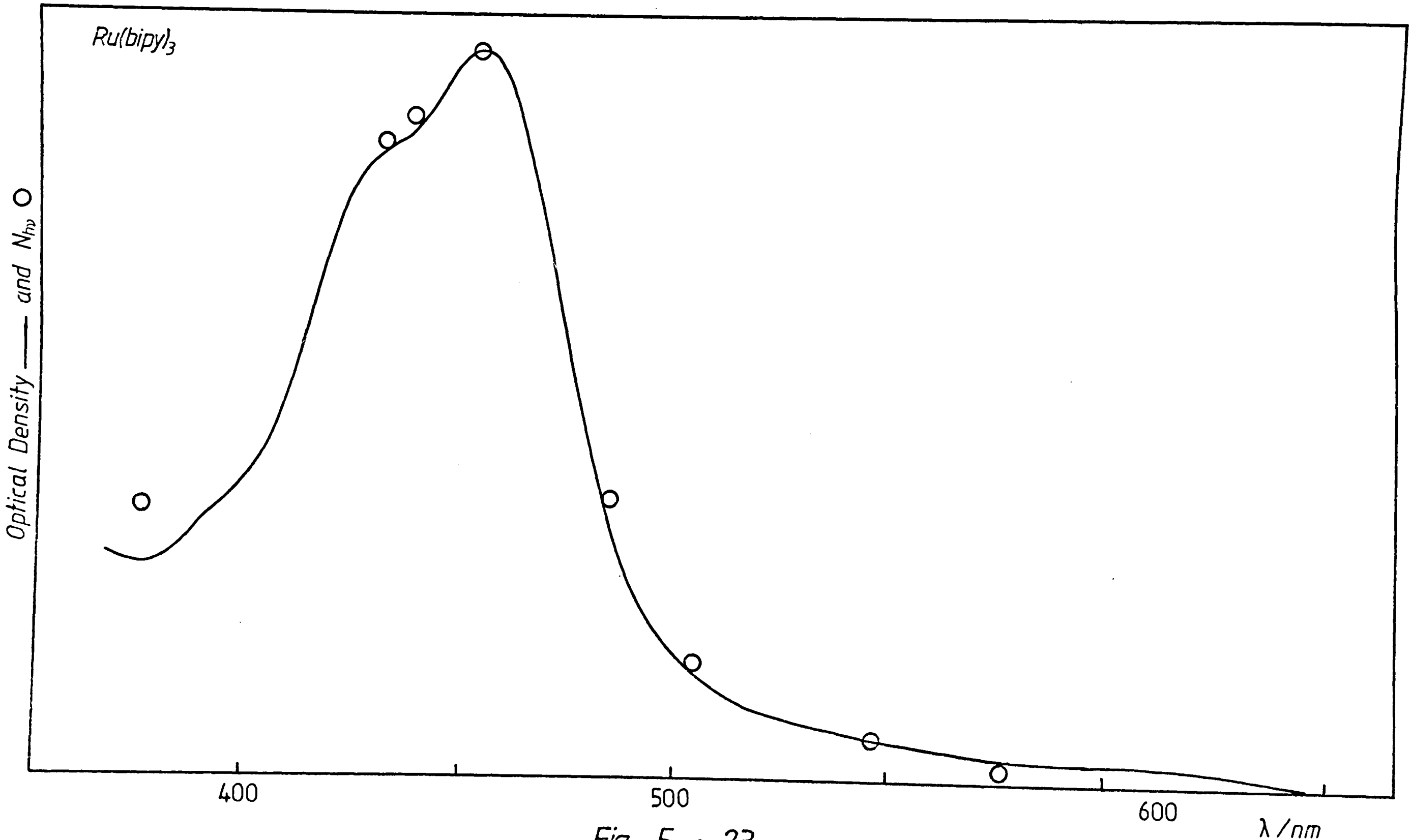

Fig 5 : 23

Action Spectrum

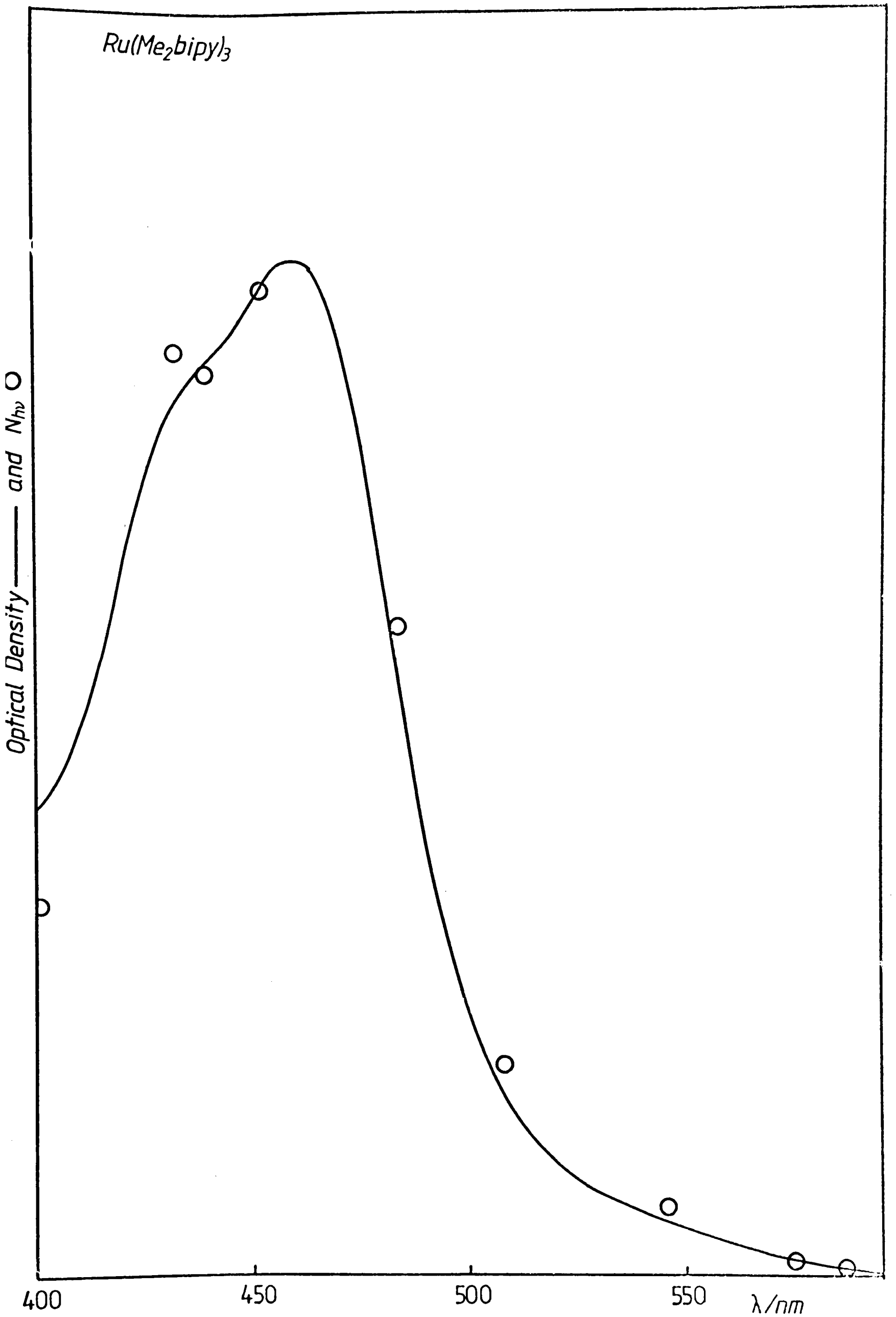

Fig 5 : 24

Action Spectrum

Figure 5:25 shows the results of an experiment in which $Ru(II)(bipy)_3$ was titrated up to 10 mM. There is no detectable deviation from the quantum efficiency found at high dilution i.e.

$$N_{h\nu} \propto [Ru(II)]$$

over the whole concentration range.

This is confirmed by the results of Pilling[77] who found < 13% luminescence self-quenching of $Ru(II)(bipy)_3$ at [Ru(II)] = 50 mM.

One further high concentration experiment was performed. The solubility of $Ru(II)(bipy)_3Cl_2$ in H_2O at 25°C was measured as 0.14 ± 0.02 M. A solution was therefore prepared which was almost saturated in Ru(II) given the other components present.

$$[Ru(II)] = 70 \text{ mM}$$

$$[HCl] = 0.1 \text{ M}$$

$$[Fe(III)] = 10 \text{ mM}$$

$$[Fe(II)] = 0 \rightarrow 10 \text{ mM}.$$

Figure 5:26 shows the region of the β v κ plane which these concentrations imply. As expected at very low light intensities and [Fe(II)] ~ 0 the collection efficiency was high (~ 0.35), confirming that there were no serious loss processes at these high concentrations.

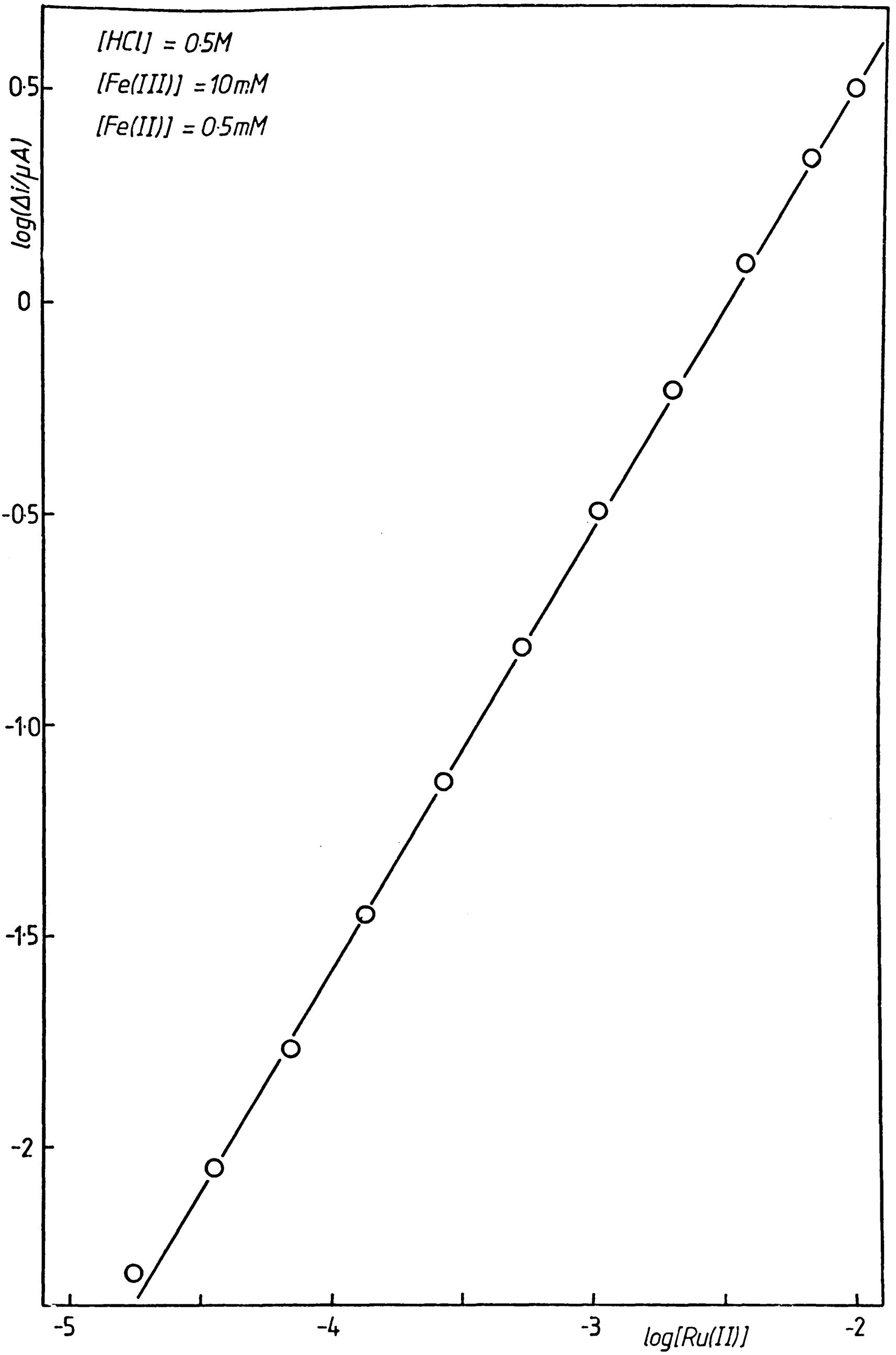

Fig 5 : 25

Variation of Photocurrent with [Ru(II)]

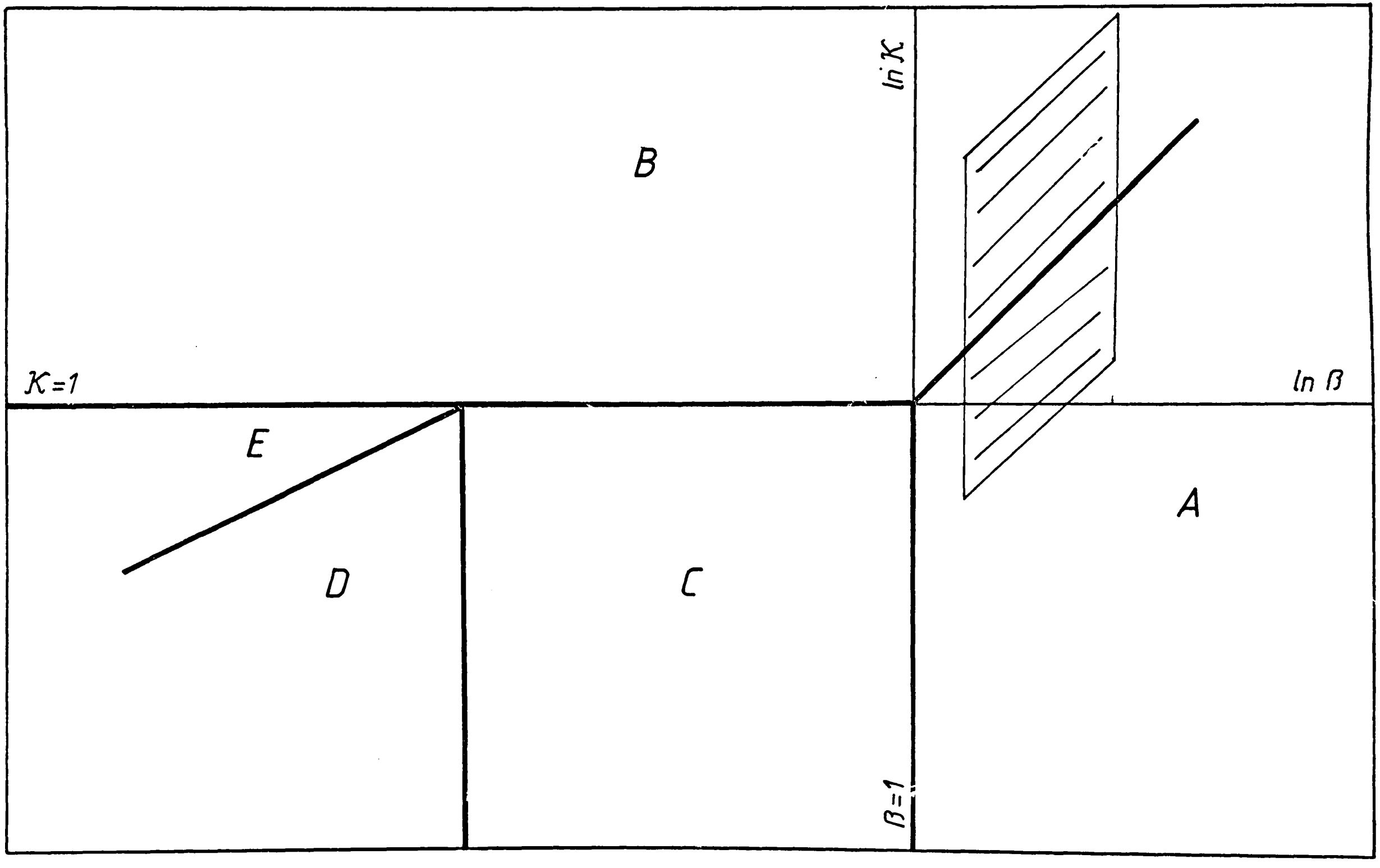

Fig 5 : 26

The βK Plane

Figure 5:27 shows these results for [Fe(II)] ~ 0 in a plot of log Δi v log I_o.

In Figure 5:28 is shown the variation of the photocurrent with [Fe(II)] for various light intensities. There are important general features to be noted. At low light intensities and high [Fe(II)] (bottom right of the diagram) the kinetics for the thermal back reaction should be pseudo first order. It is then expected (1) that the photocurrent should be rotation speed independent and (2) that points on the right of the diagram should be linear in light intensity. Both of these qualitative predictions are confirmed.

In this region of the β v κ plane $\beta \approx \kappa$ and thus

$$N_{h\nu} = \phi \frac{\beta}{\beta + \kappa} = \phi \frac{X_k}{X_k + X_\varepsilon} \qquad (5:20)$$

X_ε is known from the [Ru(II)] to be 4.8×10^{-4} cm. An experimental point is therefore chosen at low light intensity (I_o = 0.1 μA) and intermediate [Fe(II)] (~ 1mM) to check the theory. Substituting $X_\varepsilon = 4.8 \times 10^{-4}$ cm, ϕ = 1 and $N_{h\nu}$ = 0.2 into equation (5:20) gives a value of 1.2×10^{-4} cm for X_k. This however leads to a value of k_{-2} of 2.8×10^5 M^{-1} s^{-1} which is rather lower than that measured in 0.5M HCl. Figure 5:28 shows the theoretical $\beta/(\beta + \kappa)$ lines (dotted) using the fitted value of X_k. The agreement is reasonable at low light intensities and the deviation at high [Fe(II)] is in line with earlier experiments which indicated some quenching by [Fe(II)].

Experiments with the ORDE have thus allowed an extensive investigation of the photogalvanic processes of the Ru(II)$(bipy)_3$/Fe(III) system.

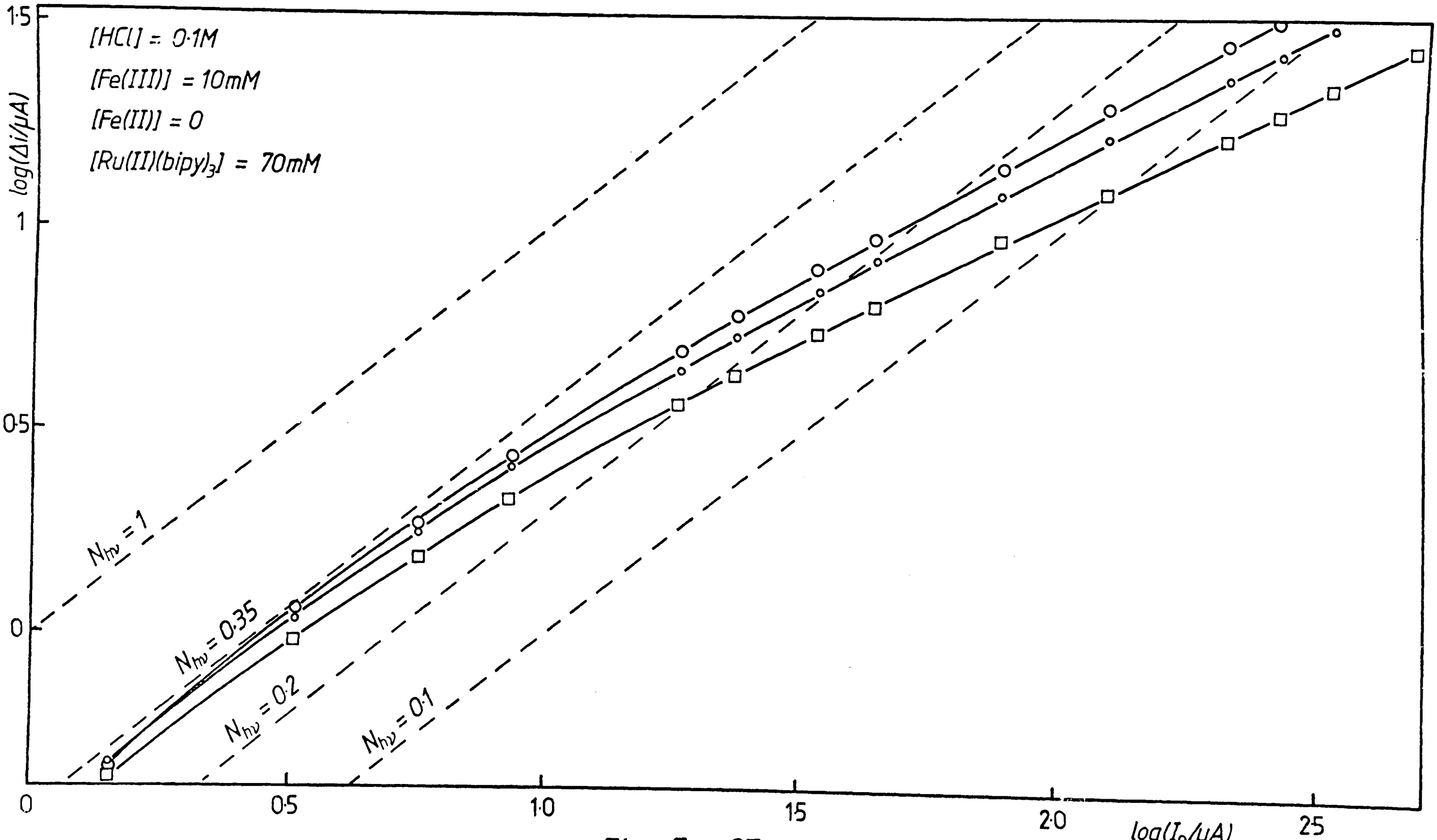

Fig 5 : 27

Variation of Photocurrent with Light Intensity

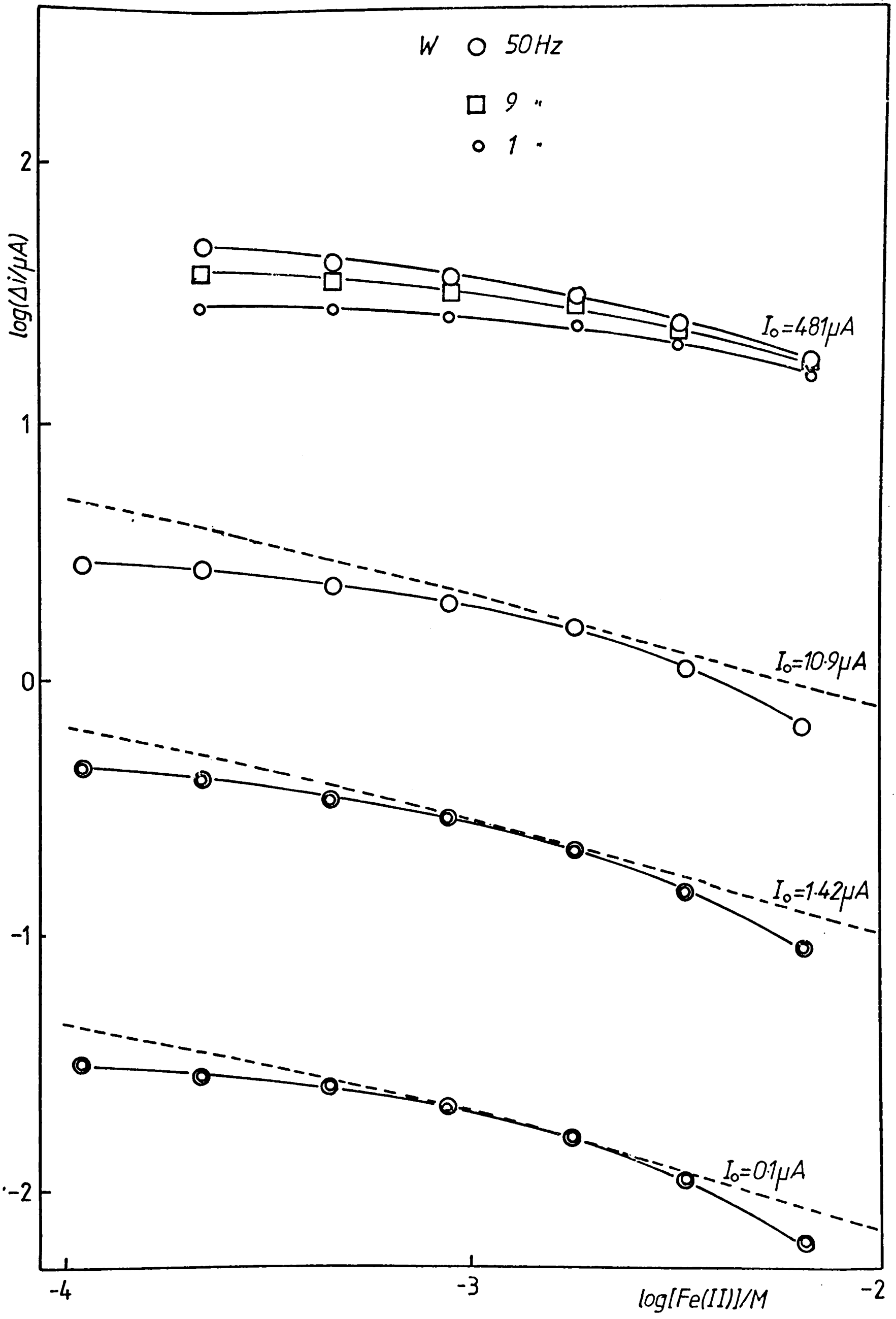

Fig 5 : 28

Variation of Photoeffect with I_o and [Fe(II)]

SULPHONATED THIONINES

A number of disulphonated thionines have also been investigated using flash electrolysis and stopped flow techniques. The reaction investigated is

$$L + Fe(III) \xrightarrow{k_{-2}} S^{\cdot} + Fe(II) \qquad (5:21)$$

where L is the substituted Leucothionine

and S is the substituted Semithionine.

For these systems it is assumed that the reactions

$$S^{\cdot} + S^{\cdot} \xrightarrow{k_3} L + Th \qquad (5:22)$$

and

$$S^{\cdot} + Fe(III) \xrightarrow{k_{-1}} Th + Fe(II) \qquad (5:23)$$

are much faster than (5:21) which is thus always rate determining. For the flash electrolysis experiment it is also assumed that just after the flash the predominant process is (5:22)

i.e. $$k_3[S^{\cdot}]^2 \gg k_{-1}\, Fe(III)$$

so that an appreciable concentration of L is generated which then reacts comparatively slowly with Fe(III) (5:21).

Two types of behaviour have been observed:

(1) Figure 5:29 shows the flash electrolysis measurements of k_{obs} v [Fe(III)] for an isomer of disulphonated thionine prepared by route a in Figure 3:15. The linear behaviour suggests a simple second order reaction

$$Fe(III) + L \xrightarrow{k_{-2}} S^{\cdot} + Fe(II)$$

with $$k_{-2} = 1760 \pm 90\ M^{-1}\ s^{-1}$$

(2) Figure 5:30 shows the flash electrolysis measurements of k_{obs} v [Fe(III)] for an isomer of disulphonated thionine prepared by route b in Figure 3:15. The rise of k_{obs} to a constant limit suggests a mechanism of the form

$$Fe(III) + L \underset{}{\overset{K}{\rightleftharpoons}} [Fe(III).L] \xrightarrow{k} S + Fe(II)$$

in which there is a rapid preequilibrium forming a complex [Fe(III).L] and then a slow first order electron transfer within the complex.

In the flash electrolysis experiment the observed rate will be

$$\frac{d[L] + [Fe(III).L]}{dt} = -k[Fe(III).L] = \frac{d(X - [Th])}{dt} \qquad (5:24)$$

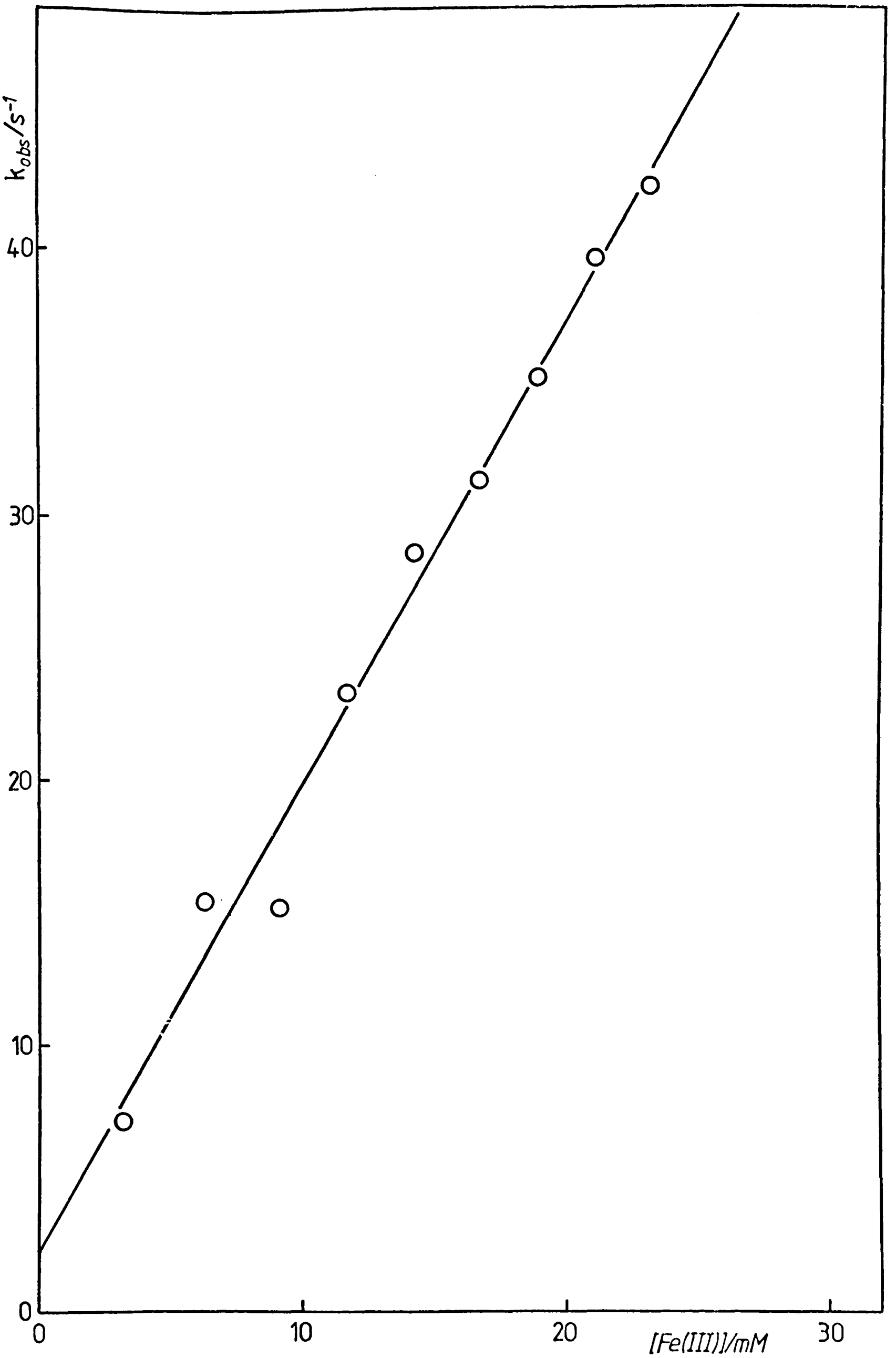

Fig 5 : 29

Variation of k_{obs} with [Fe(III)]

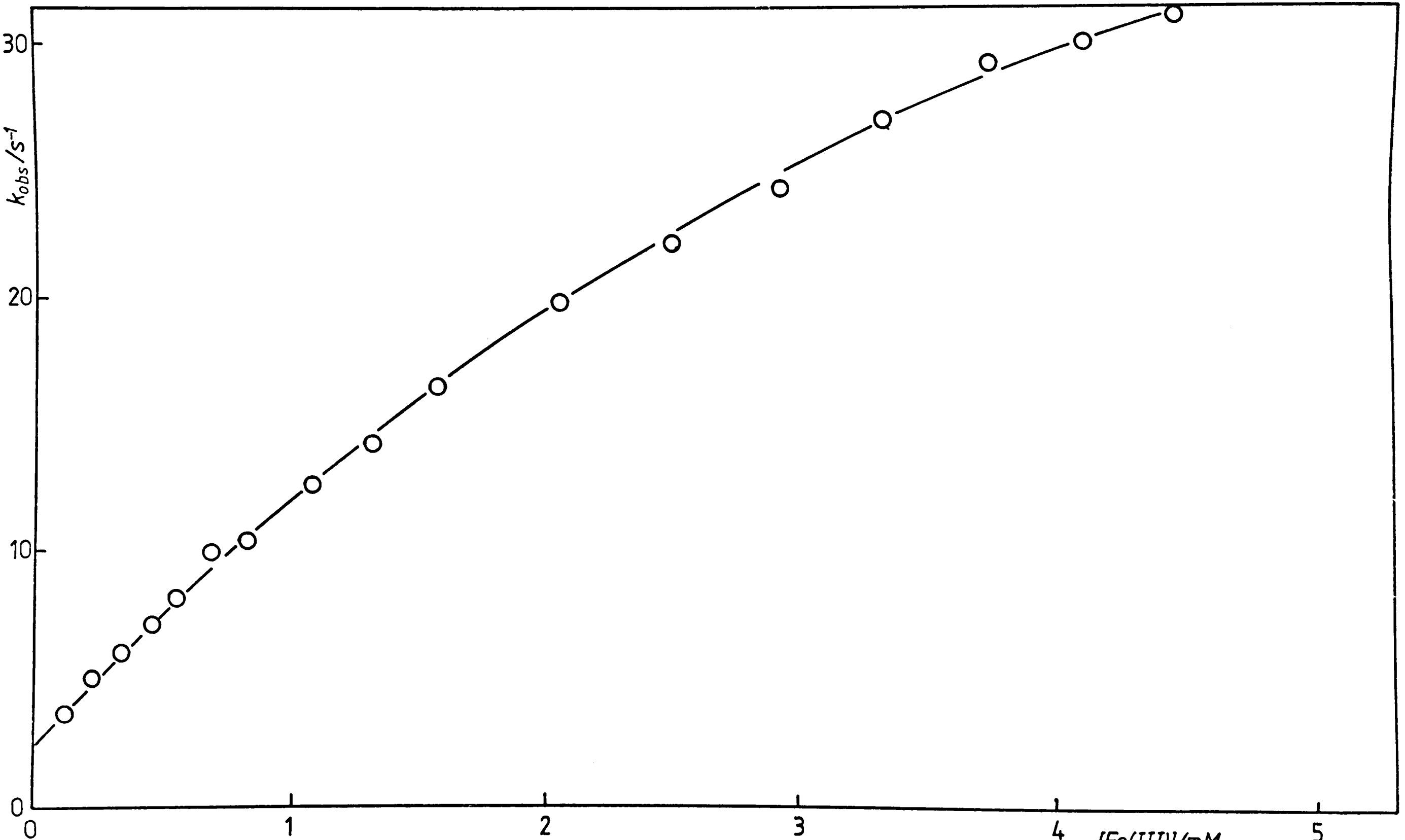

Fig 5 : 30

Variation of k_{obs} with [Fe(III)]

where

$$X = [Th] + [L] + [Fe(III).L] \qquad (5:25)$$

and

$$K = \frac{[Fe(III).L]}{[Fe(III)][L]} \qquad (5:26)$$

(It is assumed that the concentration of $S^{\cdot}$ is negligible while the above conditions hold.)

Combination of (5:24), (5:25) and (5:26) gives

$$\frac{1}{k_{obs}} = \frac{1}{k.K[Fe(III)]} + \frac{1}{k} \qquad (5:27)$$

Figure 5:31 shows a plot of $1/k_{obs}$ v $1/[Fe(III)]$. (The Fe(III) concentration is corrected for the small amount of photogenerated Fe(III) $\approx 2 \times 10^{-4}$ M.) From the slope $(1/K.k)$ and the intercept $(1/k)$ of this line

$$k = 93 \pm 15 \ s^{-1}$$

$$K = 120 \pm 2 \ M^{-1}$$

Such behaviour has also been observed for the reaction of Fe(III) with leucothionine by Lichin[78].

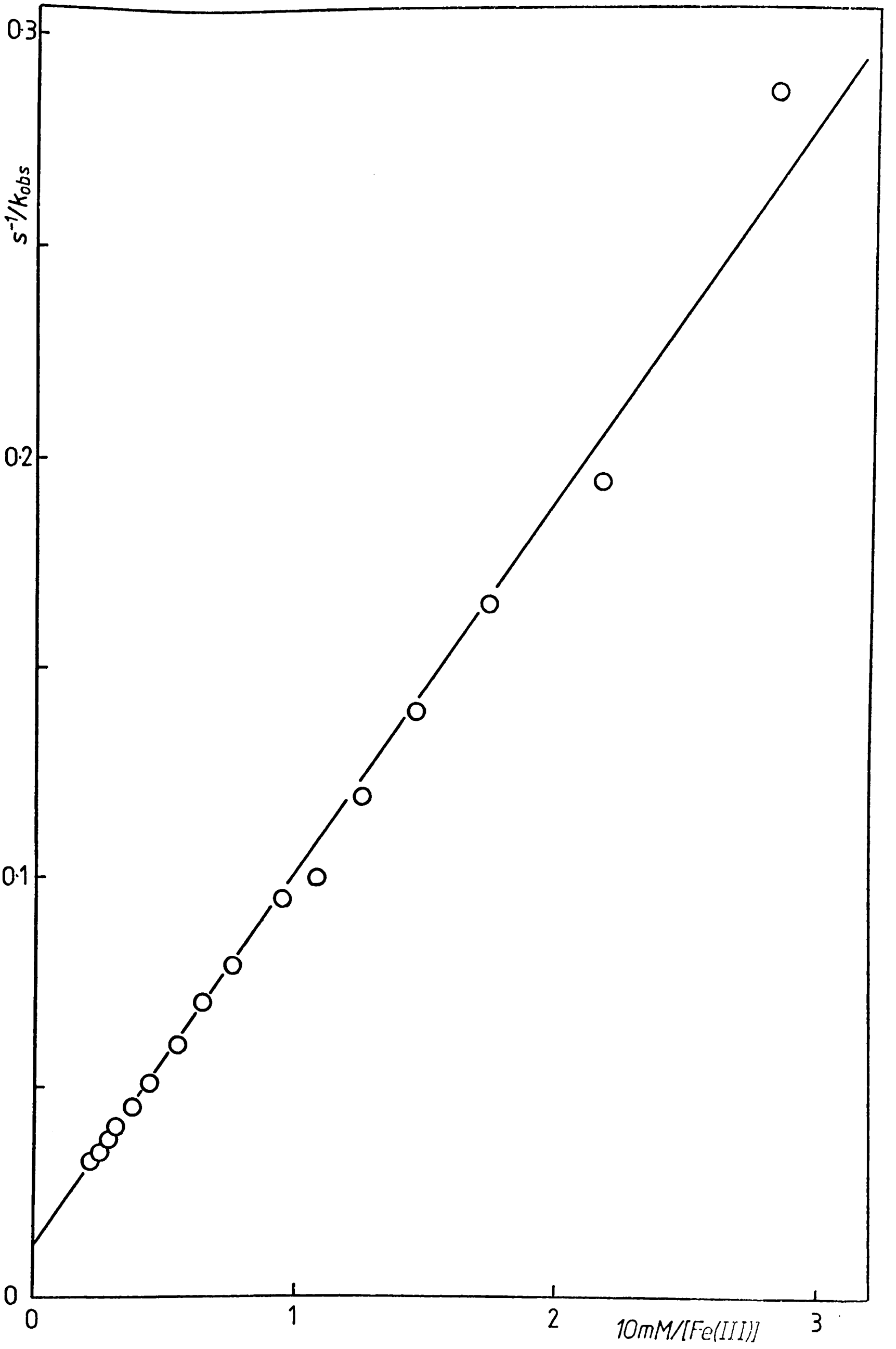

Fig 5 : 31

Analysis of Fig 5 : 30

The temperature dependence of the reaction was also investigated for another isomer prepared by route a in Figure 3:15 but different from the isomer described in (1) above. Figure 5:32 shows an Arrhenius plot for the stopped flow results. Table 5:4 compares the values of the activation parameters obtained from this experiment with those obtained in Chapter 4 for thionine.

TABLE 5:4

	Thionine	Disulphonated Thionine
E_A/kJ mol^{-1}	53 ± 1	53 ± 1
$\Delta H^{\dagger}$/kJ mol^{-1}	50 ± 1	51 ± 1
$T\Delta S^{\dagger}$/kJ mol^{-1}	-8 ± 1	-1 ± 1
$\Delta G^{\dagger}$/kJ mol^{-1}	58 ± 4	52 ± 1
E'/V	+0.21	+0.18 ± 0.01[70]

The differences are small and almost within experimental error as would be expected for two compounds of such similar structure and electrode potential.

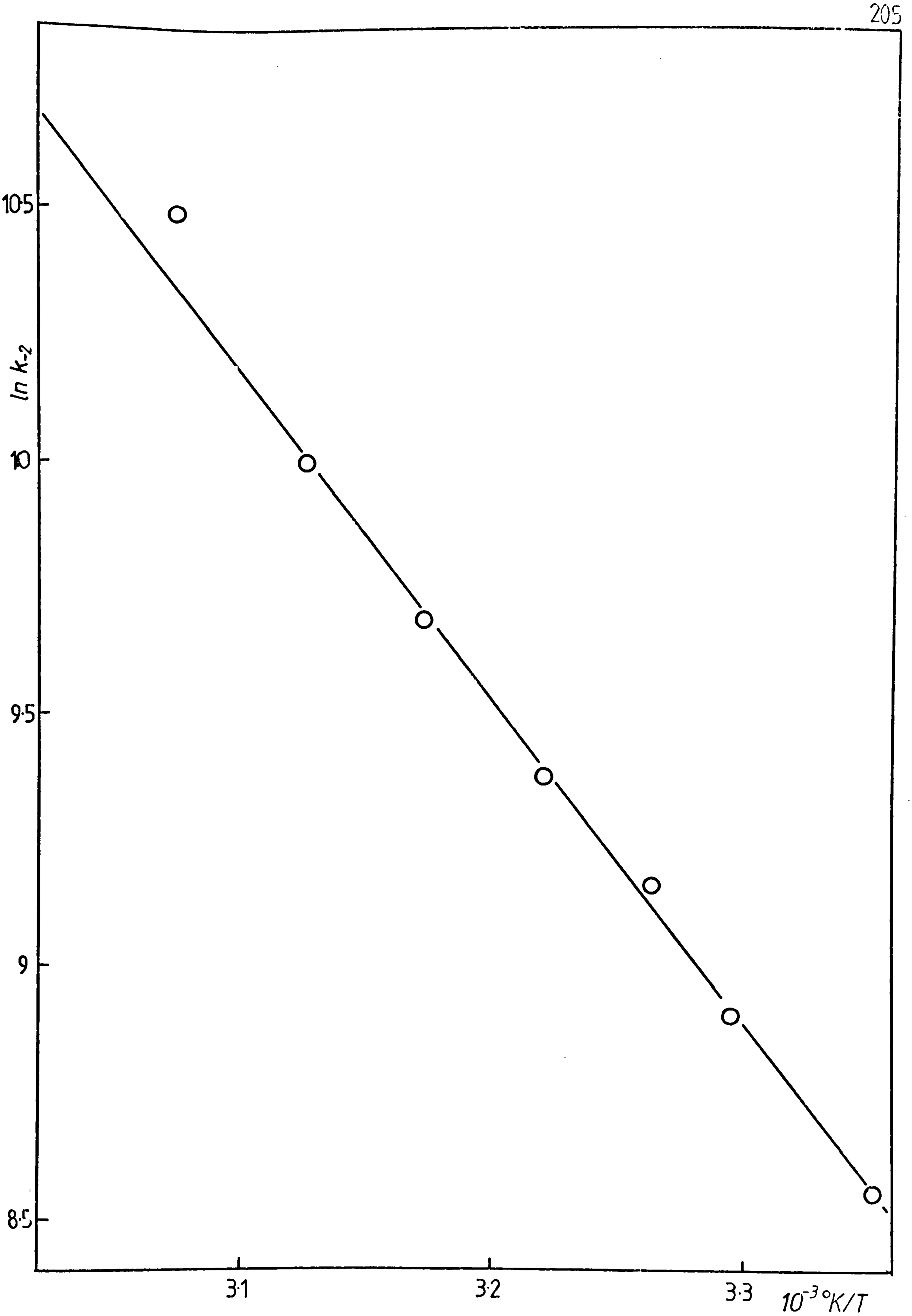

Fig 5 : 32

Arrhenius Plot for a Disulphonated Thionine

Ru(III)/Fe(II) KINETICS

In this section the flash electrolysis and stopped flow results for the Ru(III)/Fe(II) thermal back reaction are described.

The flash electrolysis results were obtained by the method described in Chapter 4 and the results are given in Table 5:5.

The stopped flow technique is described in Chapter 3. Figure 5:33 shows a typical stopped flow transient with the analysis of the pseudo first order change in the optical density. Measurements of the rate constants were made in 0.5M H_2SO_4 or HCl at temperatures between 20 and 50°C with 50 μM Ru(III) and with [Fe(II)] > 5[Ru(III)].

From transition state theory

$$k_{-2} = \frac{k_B T}{h} \; e^{-\Delta H^{\ddagger}/RT} \; e^{\Delta S^{\ddagger}/R} \qquad (5:28)$$

where

k_{-2} is the second order rate constant

k_B is the Boltzmann constant

h is Planck's constant.

Thus

$$\frac{\partial(\ln k_{-2})}{\partial(1/T)} = -T - \frac{\Delta H^{\ddagger}}{R} = -\frac{E_A}{R} \qquad (5:29)$$

TABLE 5:5

Ru(III) complex	$k_{-2}/10^5$ $M^{-1}s^{-1}$ (25°C)			$\Delta H^{\dagger}$/kJ/mol			$T\Delta S^{\dagger}$/kJ/mol (25°C)			$\Delta G^{\dagger}$/kJ/mol (25°C)		
	HCl	$HClO_4$	H_2SO_4	HCl	$HClO_4$	H_2SO_4	HCl	$HClO_4$	H_2SO_4	HCl	$HClO_4$	H_2SO_4
1. $(bipy)_3$	90*	6.4	50		-1.3±0.2			-41±4			+40±4	
2. $(44'Me_2bipy)_2(bipy)$			3.0			+3±1			-39±1			+42±1
3. $(44'Me_2bipy)_3$	6.8 6.2 0.3(f)		2.1 1.9(f)	+26±3		+0.6±1	-14±3		-42±1	+40±3		+43±1
4. $(4,7Me_2phen)_3$			3.0 2.7(f)			+ 6±1			-38±1			+42±1
5. $(3,4,7,8Me_4phen)_3$	3.5 3.1 0.5(f)		0.6 0.5(f)	+38±3		+19±1	- 3±3		-27±1	+41±3		+46±1
6. $(phen)_3$		8.0	56		- 6±2			-45±5			+39±5	
7. $(terpy)_3$		7.2			- 12			-51			+39	
8. $(bipy)_2py_2$		6.4			+ 1			-39			+40	

*ORDE Measurement, (f) flash electrolysis measurement, and all others by Stopped flow.

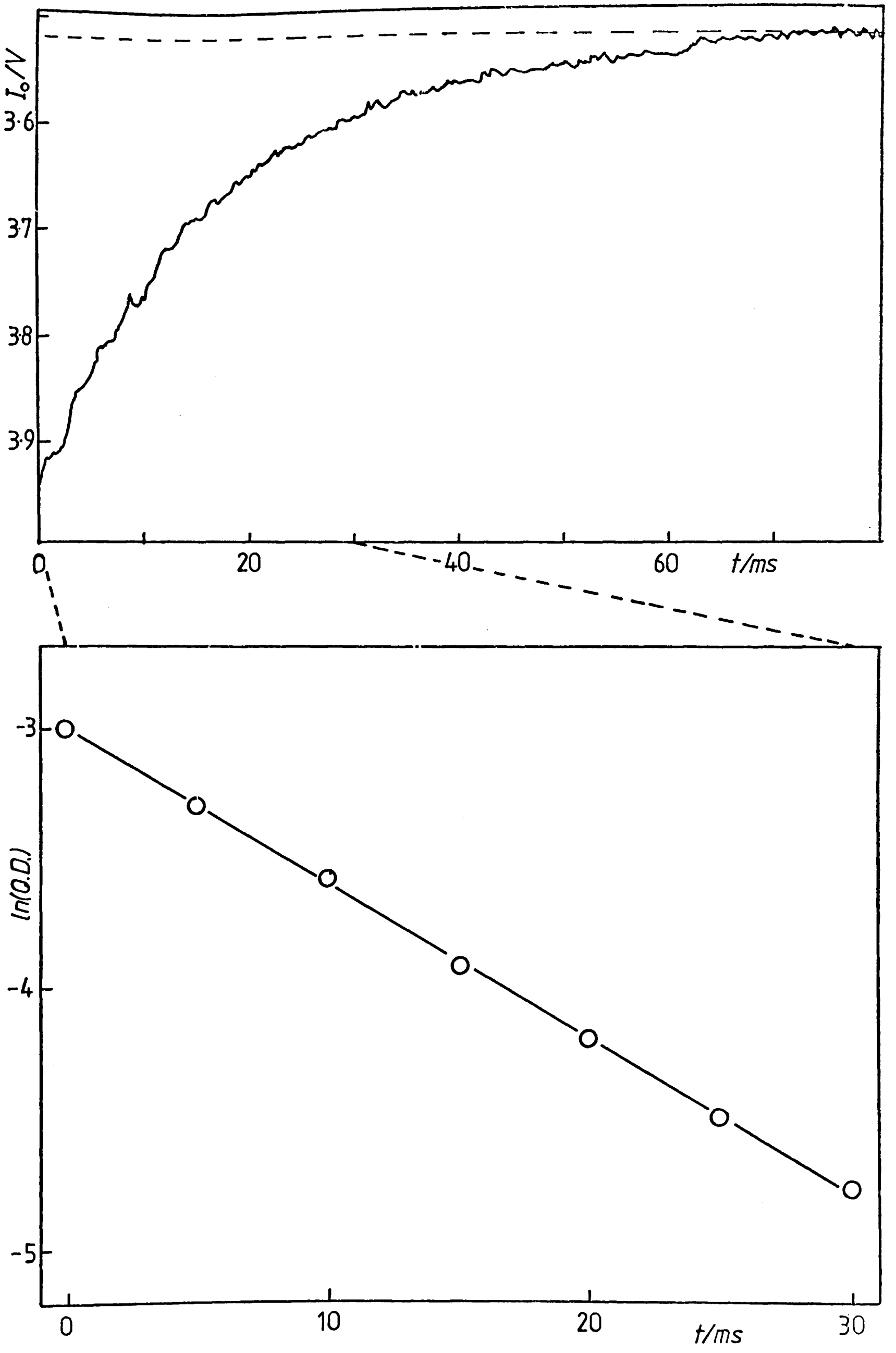

Fig 5 : 33

Stopped flow Transient and Analysis

$$\Delta H^{\ddagger} = E_A - RT \qquad (5:30)$$

$$T\Delta S = RT\ \ln[k_{-2}/(k_B T/h)] + \Delta H^{\ddagger} \qquad (5:31)$$

and

$$\Delta G^{\ddagger} = \Delta H^{\ddagger} - T\Delta S^{\ddagger} = RT\ \ln[k_{-2}/(k_B T/h)] \qquad (5:32)$$

From typical Arrhenius plots such as those in Figure 5:3 the various activation parameters are obtained. They were calculated using the classical transition state theory collision number $k_B T/h = 6.2 \times 10^{12}$ and are given in Table 5:5. (If instead the solvent frequency factor, $\nu_S \sim 10^{11}\ s^{-1}$, had been used, as recommended by Marcus, all the $T\Delta S^{\ddagger}$ values would be greater by 10 kJ/mol and those of $\Delta G^{\ddagger}$ smaller by 10 kJ/mol.)

The rate constants, k_{-2}, measured in 0.5 M H_2SO_4 are in good agreement ($\pm$ 10%) with those measured by Sutin[26] in the same medium. There is also good agreement between the flash electrolysis and stopped flow results.

There are two important correlations which allow all the data in Table 5:5 to be rationalised. The first and larger of these effects is the compensation of $\Delta S^{\ddagger}$ and $\Delta H^{\ddagger}$. As the ligand, L, is changed in the $Ru(III)L_3$ complex causing a small change in ΔG^{o} for the electron transfer with Fe(II) larger but compensating changes are found in $\Delta H^{\ddagger}$ and $\Delta S^{\ddagger}$. The second effect is the resultant change in $\Delta G^{\ddagger}$,

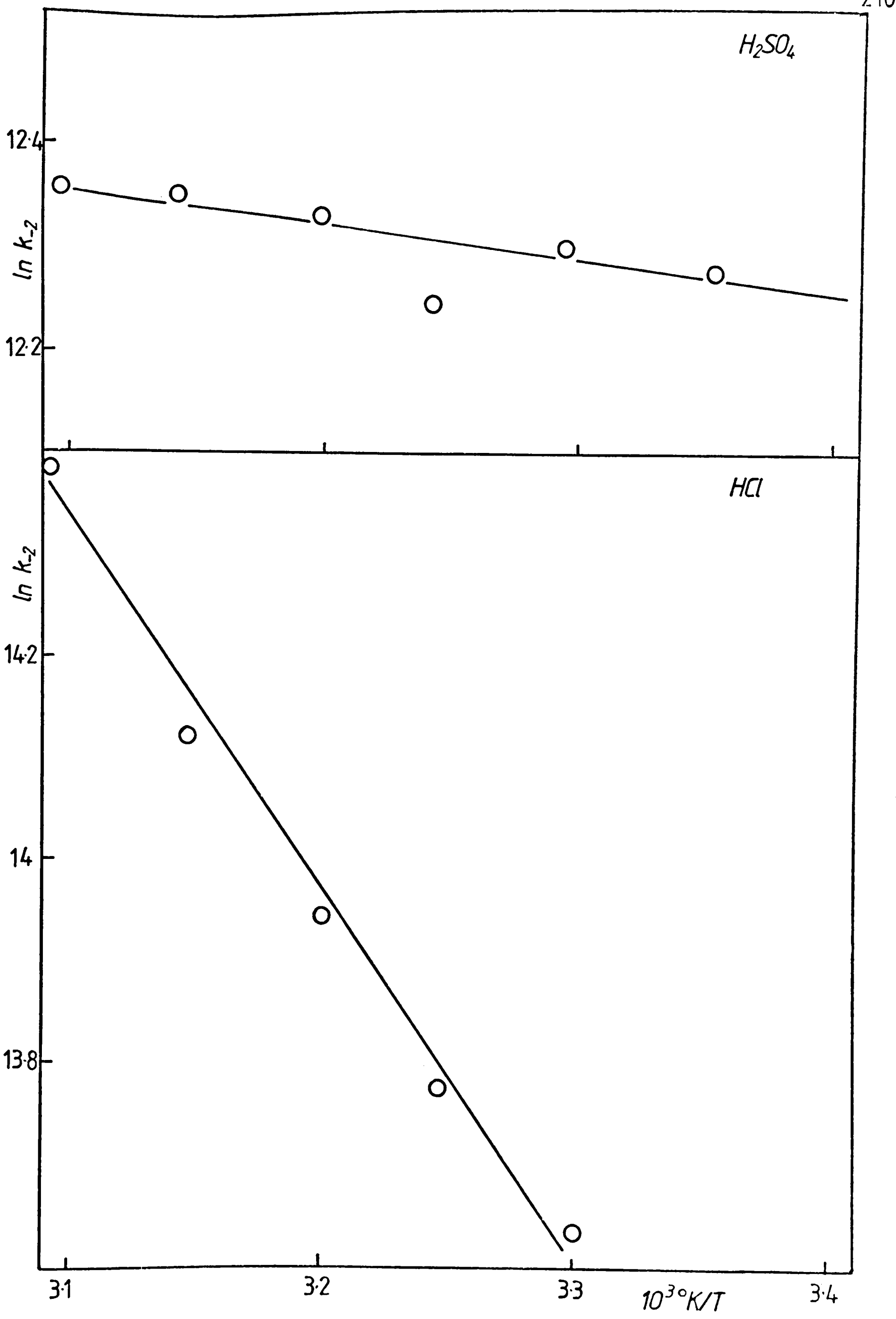

Fig 5 : 34

Arrhenius Plots for $Ru(Me_2bipy)_3$

$$\Delta G^{\ddagger} = \Delta H^{\ddagger} - T\Delta S^{\ddagger},$$

observed as ΔG^{o} is changed. This is the correlation between $\Delta G^{\ddagger}$ and ΔG^{o} predicted by the Marcus-Levich theory.

The changes in $\Delta H^{\ddagger}$ and $\Delta S^{\ddagger}$ are described by the Isokinetic Relationship of Leffler[79], which describes "compensation effects". This has the form

$$\delta\Delta H^{\ddagger} = \beta\, \delta\Delta S^{\ddagger} \qquad \beta > 0 \qquad (5:26)$$

where δ refers to small changes in the reaction centre e.g. the changes in a series of $Ru(III)L_3$ complexes.

The reason for this compensation is that $\Delta H^{\ddagger}$ and $\Delta S^{\ddagger}$ cannot be considered independently. In this type of electron-transfer reaction the rate is limited by the solvent/ligand reorganisation around the reaction centre. If strongly bonded ligands must change conformation to allow reaction then it is expected that $\Delta H^{\ddagger}$ will be large. However the strong binding of these ligands implies that they are well ordered and have low entropy so that there can only be a small entropy barrier, $\Delta S^{\ddagger}$, to reaction.

If the ligands are weakly bonded then reorganisation is easy and $\Delta H^{\ddagger}$ small. However the weak bonding implies more degrees of freedom and a higher entropy in the ground state so that reorganisation to a more ordered transition state implies a large compensating energy barrier.

Now

$$\delta\Delta G^{\ddagger} = \delta\Delta H^{\ddagger} - T\delta\Delta S^{\ddagger} \qquad (5:27)$$

and combination of (5:26) and (5:27) gives

$$\delta\Delta G^{\ddagger} = (1 - \frac{T}{\beta})\ \delta\Delta H^{\ddagger}$$

β has the units of absolute temperature and is a measure of the degree of compensation as the reaction centre is changed. Good compensation is found when β is close to the temperature of measurement and there is poor compensation when β is far from the temperature of measurement.

Figure 5:35 shows the Isokinetic relationship plotted for the data in Table 5:5. The various isokinetic temperatures are

Medium	T_β
0.5M H_2SO_4	101^o C
0.5M HCl	52^o C
0.5M $HClO_4$	48^o C

These temperatures are virtual temperatures and do not represent temperatures at which the differences in rate disappear altogether, or above which the rates actually decrease as the driving force increases.

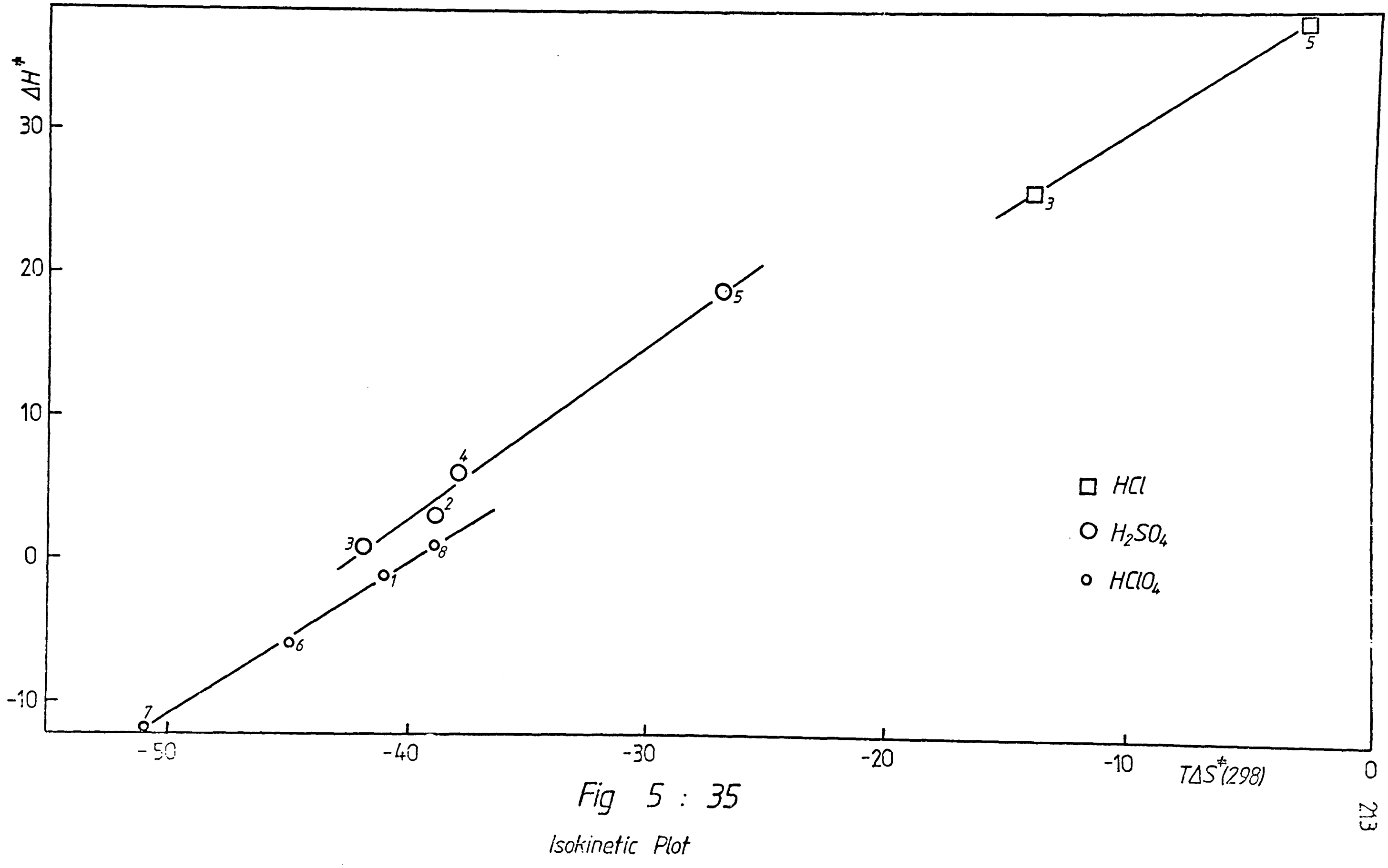

Fig 5 : 35

Isokinetic Plot

In H_2SO_4 the rates do indeed approach each other as the temperature is raised. However both $\Delta H^{\ddagger}$ and $\Delta S^{\ddagger}$ will change with temperature due to heat capacity changes in the reactants and transition state. It would thus be wrong to extrapolate the measurements made between 25 and 50°C to 100°C. If the rate constants were measured accurately at 100°C a small variation in $\Delta G^{\ddagger}$ would still be expected although it would diminish as the temperature was raised. This is expected as reactions usually become less selective at higher temperatures.

In HCl only two sets of measurements of $k_{-2}(T)$ were made for complexes with very similar ΔG^{o}. The errors in T are therefore large and the individual measurements of k_{-2} are not sufficiently accurate to confirm the isokinetic temperature or to detect changes in $\Delta H^{\ddagger}$ and $\Delta S^{\ddagger}$ as a function of temperature. However behaviour similar to that in H_2SO_4 is most likely.

The data in $HClO_4$ are taken from the literature[80-81] and it is not known over what range of temperature measurements were made or if they were sufficiently accurate. However it seems likely that the differences between complexes will not vanish at T_β but rather decrease as the temperature is raised and the reaction progressively loses selectivity.

Similar isokinetic relationships have been found in a great many organic reactions where solvent reorganisation is important (e.g. displacement and elimination reactions, decomposition and association reactions and solvolysis reactions). Leffler and

Grunwald[80] have compiled 96 different examples. One of the most significant is that dielectric relaxation shows an isokinetic relationship in the range 300 to 400°K. The process of orientation of a molecule in an external electric field is a good model for the orientation of a molecule in the field of an ion in solution[80].

It is clear from this work that the major effect observed in this electron transfer reaction is that of compensation and that the isokinetic relationship is accurately obeyed.

Although Sutin[82] has calculated all the activation parameters for

$$Ru(III)(bipy)_3 + Fe(II) \rightarrow Ru(II)(bipy)_3 + Fe(III)$$

in 0.5M $HClO_4$ using equations (1:2), (1:3), (1:4) and (1:5), the good agreement he finds between theory and experiment must be fortuitous. The equations appear to be able to describe this one reaction, but they are quite unable to account for the large changes in $\Delta H^{\ddagger}$ and $T\Delta S^{\ddagger}$ as the driving force of the reaction is changed by changing the ligands.

The changes in $\Delta G^{\ddagger}$ are 4 to 5 times smaller than the corresponding changes in $T\Delta S^{\ddagger}$ and $\Delta H^{\ddagger}$. This can be seen by comparing the linear free energy relationship (LFER) for $\Delta G^{\ddagger}$ and ΔG^{o} plotted in Figure 5:3b with isokinetic plot in Figure 5:3c. The LFER is as predicted by the Marcus theory, but it is quite clear that for this system the Marcus theory described only the free energy changes in the reaction and that the $\Delta S^{\ddagger}$ and $\Delta H^{\ddagger}$ terms cannot be

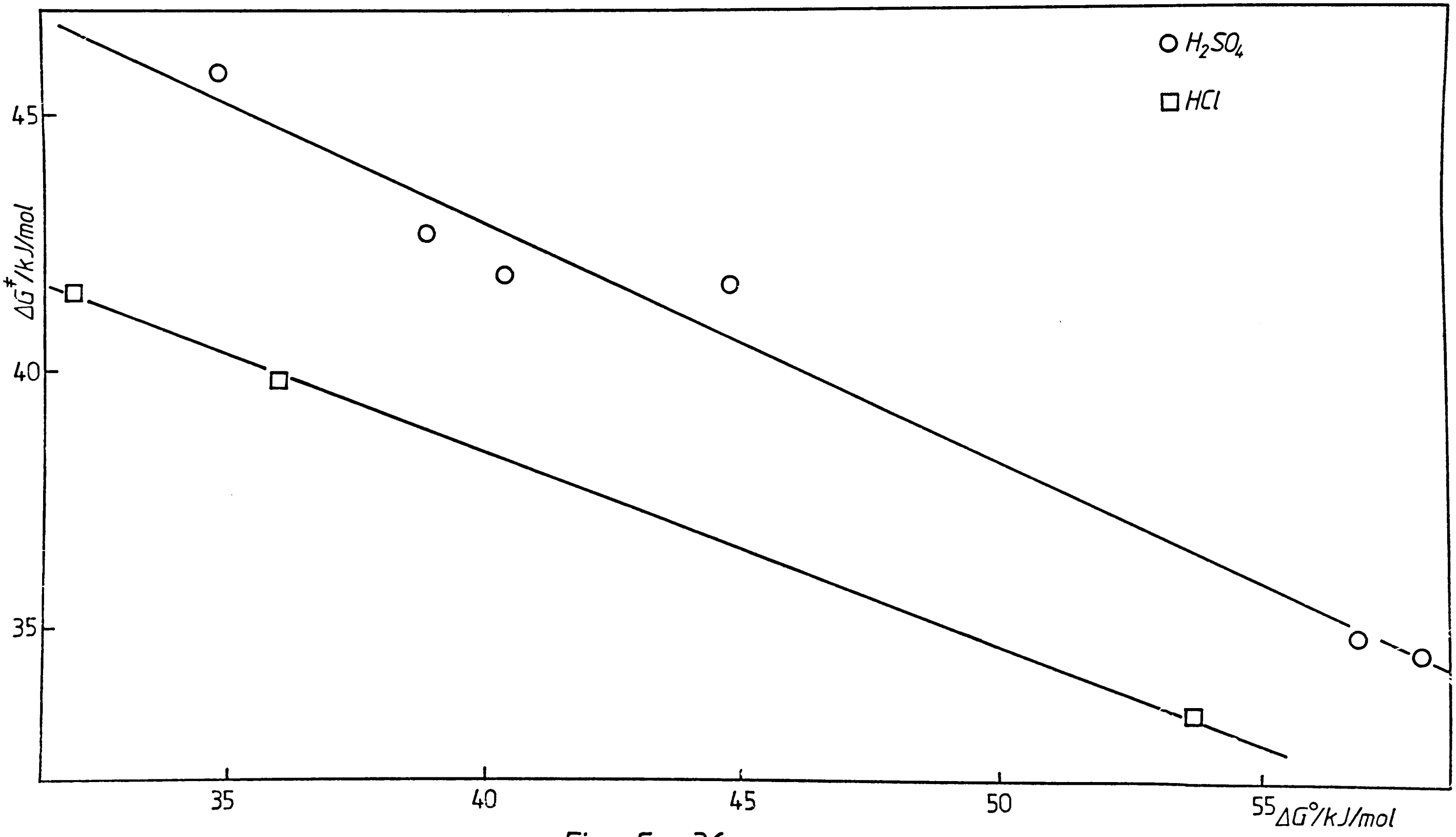

Fig 5 : 36

LFER for $Ru(III)L_3$/Fe(II)

separated out. One implication of this observation is that the reactants, $Ru(III)L_3$ and Fe(II), cannot be thought of separately in their ligand/solvent reorganisation. They must be thought of as a single unit undergoing a complex reorganisation for which only the overall rate and driving force may be correlated and consideration of the individual changes of enthalpy and entropy for the separated reactants leads to no sensible conclusions.

Thus Sutin [26] has calculated the slope for the LFER and reasonable agreement is found between experiment and theory.

	This Work	Sutin
Calc.		0.41
H_2SO_4	0.46	0.51
HCl	0.38	

It is also worth noting that although the driving force for this reaction is larger in H_2SO_4 than in HCl the rate of reaction is significantly slower in H_2SO_4. However this is not in contradiction to the Marcus theory which predicts a correlation between $\Delta G^{\ddagger}$ and ΔG^{o} for a series of similar complexes e.g. $Ru(III)L_3$. But by changing the medium the whole reaction centre has been altered as Cl^- ligands are substituted for SO_4^{2-} ligands on Fe(II) and there is a change in reorganisation energy associated with this.

This change will not necessarily correlate with the change in ΔG^{o} for the reaction.

Thus summarising, it is found that the Marcus theory is well obeyed for this reaction. However the major effect is not that described by the Marcus theory ($\Delta G^{\ddagger}$) but rather that of compensation which describes both $\Delta H^{\ddagger}$ and $\Delta S^{\ddagger}$. It is important to avoid the use of the Marcus theory to describe these two parameters as the theory was only designed to describe the total free energy changes of solvent reorganisation.

DISCUSSION

Having gathered together information on a number of different properties of the $Ru(II)L_3$ system it is now possible to assess their potential for solar energy conversion. It is important to point out immediately that Ruthenium systems would not be practicable on a large scale because of the shortage of Ru in the earth's crust. Mason[83] estimates that Ru is the rarest of the stable elements in the earth's crust at ~ 1 ppb. However it is a good,and one of the only,model systems with which to assess the feasibility of a photo-galvanic cell.

One important factor in considering the performance of a cell is that most of the incident solar energy will be absorbed in the electrolyte and then dissipated as heat. This means that in direct

sunlight the working temperature of the cell will be > 60°C. It is therefore important to measure the temperature dependence of the various properties of photogalvanic systems.

It is now helpful to discuss the relevance of the various properties to the four characteristic lengths.

1) X_L (the cell length). This is an engineering problem. Temperature changes should leave it unaffected - unless the electrolyte boils!

2) $X_\varepsilon = 1/\varepsilon[A]$. [A] must be as high as possible for a photogalvanic cell and higher temperatures will favour higher solubilities. However if the cell is subjected to cold, precipitation and/or freezing may present problems. Only the solubility of $Ru(II)(bipy)_3Cl_2$ has been measured in this thesis. At 25° a saturated solution corresponds to $X_\varepsilon \sim 2 \times 10^{-4}$ cm. This is close to the theoretical ideal of 10^{-4}cm. It also has a significant temperature coefficient of solubility as it may be recrystallized in good yield from hot water.

It is important to note that chloride is the only medium for which the $Ru(II)L_3$ complexes have been found to be appreciably soluble. This in turn affects other properties of the system (e.g. k_{-2} and k'_*).

3) $$X_G = \left(\frac{D}{\phi\varepsilon I_o}\right)^{\frac{1}{2}} = \left(\frac{D_o}{\phi\varepsilon I_o}\right)^{\frac{1}{2}} e^{-E_D/2RT}$$

E_D is ~15 kJ/mol and the temperature variation of the generating length is thus quite small.

$$4) \qquad X_k = \left(\frac{D}{k_{-2}[Y]}\right)^{\frac{1}{2}} = \left(\frac{D_o}{[Y]}\right)^{\frac{1}{2}} A^{\frac{1}{2}} e^{-(E_D - E_A)/2RT}$$

E_D is again ~15 kJ/mol and works in favour of a higher photo-electrochemical collection efficiency at higher temperatures. This is a general feature of all systems. However it is not possible to consider E_A on its own. As has been shown, in measurements of the activation parameters of the $Ru(III)L_3/Fe(II)$ reaction, there is a complex relation between the individual activation parameters and the overall driving force for the reaction, ΔE.

Considering first the relation between $\Delta G^{\ddagger}$ and ΔE it is clear from the LFER in Figure 5:32 that

$$\Delta E \propto \ln(k_{-2})^m$$

where m = 0.38 (HCl).

If this equation is substituted into the equation for the power of a photogalvanic cell[11] and then differentiated to find the maximum, the condition found is

$$W_{max} \text{ is at } \Delta E \approx \frac{RT}{F} \left(\frac{2}{m}\right)$$

0.31 V for m = 0.38.

Not only is this well below the voltage of 1.1 V sought for the ideal cell but the rate of the back reaction for ΔE = 0.31 V

is ~ 3 x 10^5 M^{-1} s^{-1} (corresponding to Ru(II)(3,4,7,8 Me_4phen)$_3$) which is much faster than the value of 4 x 10^3 M^{-1} s^{-1} required. This argument is a very important general point for all photogalvanic cells in which there is a correlation between ΔE and k_{-2}.

If now the temperature variation is considered it is clear that Ru(II)(3,4,7,8 Me_4phen)$_3$ is the least fabourable of the series as it has the largest $\Delta H^{\ddagger}$ and thus the largest increase in k_{-2} with temperature. From earlier discussions the rates are expected to converge at higher temperatures and the differences between the complexes will decrease. Thus unless exceptions to the combined theories of compensation and Marcusian electron-transfer can be found there seems little hope of achieving a large ΔE and small k_{-2} for the Ru(III)L_3 back reaction.

It is worth noting one good feature of the RuL_3/Fe system which is that as the solubility of the RuL_3 complex forces the use of chloride so does it also provide good differential electrode kinetics. The Ru(II)/(III) couple is reversible (although the exact rate constant has not been measured) at SnO_2 electrodes but the Fe(II)/(III) couple is highly irreversible at SnO_2 in chloride. A Pt electrode would provide a suitable dark electrode as the Fe(II)/(III) electrode kinetics are very much faster at this electrode (Table 5:3).

Ruthenium systems are not however going to produce an efficient cell and there are other extensive areas of investigation which may provide yet more conclusive reasons. Thus photoannation has been

observed at 95° for $Ru(bipy)_3$ [84]. Any such degradation process would have to be of extremely low quantum efficiency ($< 10^{-6}$) for the cell to last an appreciable time.

The way to further improvements in cell efficiency is thus in developing the thionine dyes. The problem of differential electrode kinetics for these systems has been solved[85]. The back reaction rates are significantly slower than for Ruthenium systems. Another important feature of the back reactions of some sulphonated thionines (Figure 5:30) is that the formation of a complex places an upper limit on the rate of the back reaction, which is insensitive to further increases in [Fe(III)]. The solubility problem has also been solved by sulphonation of thionine and at present these systems seem to be the most promising for the development of an efficient cell.

REFERENCES

1. Gleria M. and Memming R., J. Electroanal. Chem., 65, 164 (1975)
2. Weiss J., Nature, 136, 794 (1935).
3. Rabinowitch E., J. Chem. Phys. (i) 8, 551 (1940);
   (ii) 8, 560 (1940).
4. Albery W.J., Electrode Kinetics, Oxford Chemistry Series, p 174.
5. Marcus R.A., J. Chem. Phys., 24, 966 (1956).
6. Marcus R.A., Ann. Rev. Phys. Chem., 15, 155 (1966).
7. Marcus R.A., Discuss. Faraday Soc., 29, 21 (1960).
8. Marcus R.A. and Sutin N., Inorg. Chem., 14, 213 (1975).
9. Albery W.J. and Archer M.D., Electrochimica Acta, 21, 1155 (1976).
10. Albery W.J. and Archer M.D., J. Electrochem. Soc., 124, 688 (1977).
11. Albery W.J. and Archer M.D., J. Electronanal. Chem., (i) 86, 1, (1978); (ii) 86, 19 (1978).
12. Albery W.J. and Archer M.D., Nature, 270, 399 (1977).
13. Data from proposed AM2 spectral distribution in Interim Solar Cell Testing Procedures for Terrestrial Applications, 13 (NASA, 1975).
14. Burstall F.H., J. Chem. Soc., 173 (1936).
15. Crosby G.A., Perkins W.G. and Klassen D.M., J. Chem. Phys., 43, 1498 (1965).
16. Paris J.P. and Brandt W.W., J.A.C.S., 81, 5001 (1959).
17. Paris J.P., Ph.D. Thesis, Purdue University (1960).
18. Porter G.B. and Schläfer H.L., Ber. Bunsenges. Physik. Chem., 68, 316 (1964).
19. Klassen D.M. and Crosby G.A., J. Chem. Phys., 48, 1853 (1968).
20. Demas J.N. and Addington J.W., J.A.C.S., 98, 5800 (1976).

21. Harrigan R.W. and Crosby G.A., J. Chem. Phys., 59, 3468 (1973).

22. Hager G.D. and Crosby G.A., J.A.C.S., 97, 7031 (1975).

23. Klasson D.M., Inorg. Chem., 15, 3166 (1976).

24. Daul C., Private communication.

25. Gafney H.D. and Adamson A.W., J.A.C.S., 94, 8238 (1972).

26. Lin C-T., Böttcher W., Chou M., Crentz C. and Sutin N., J. Am. Chem. Soc., 98, 6536 (1976).

27. Sutin N. and Crentz C., Adv. Chem. Ser., 168, 1 (1978).

28. Crentz C. and Sutin N., Inorg. Chem., 15, 496 (1976).

29. Saji T. and Aoyorgni S., J. Electronal. Chem., 58, 401 (1975).

30. Crentz C., Inorg. Chem., 17, 1046 (1978).

31. Bock C.R., Meyer T.J. and Whitten D.G., J.A.C.S., 96, 4710 (1974).

32. Laurence G.S. and Balzani V., Inorg. Chem., 13, 2139 (1974).

33. Hoselton M.A., Lin C-T., Schwarz H.A. and Sutin N., J.A.C.S. 100, 2383 (1978).

34. Bock C.R., Meyer T.J. and Whitten D.G., J.A.C.S., 97, 2909 (1975).

35. Hatchard C.G. and Parker C.A., Trans. Faraday Soc., 54, 1093 (1961).

36. Inaoka W., Harada S. and Yasunaga T., Bull. Chem. Soc. Japan 51, 1701 (1978).

37. Suoto Bachiller F., Private communication.

38. Lichtin N.N., Solar Power and Fuels, Academic Press, (1977) pp 119-141.

39. Harriman A., Private communication.

40. Albery W.J., Bartlett P.N., Bowen W.R., Fisher F.S. and Foulds A.W., J. Electronal. Chem., accepted for publication.

41. Albery W.J., Bowen W.R., Fisher F.S. and Turner A.D., J. Electroanal. Chem., two papers accepted for publication.

42. Perone S.P. and Birk J.R., Anal. Chem., 38, 1589 (1966).

43. Birk J.R. and Perone S.P., Anal. Chem., 40, 496 (1968).

44. Stapelfeldt H.E. and Perone S.P., Anal. Chem., 41, 628 (1969).

45. Kirschner G.L. and Perone S.P., Anal. Chem., 44, 443 (1972).

46. Patterson J.I.H. and Perone S.P., Anal. Chem., 44, 1978 (1972).

47. Fratoni S.S. Jr., and Perone S.P., Anal. Chem., 48, 287 (1976) and 48, 296 (1976).

48. Fratoni S.S. Jr., and Perone S.P., J. Electrochem. Soc., 123, 1672 (1976).

49. Dahnke K.F. and Perone S.P., J. Electrochem. Soc., 123, 1677 (1976).

50. Karman T., Z. angew. Math. Mech., 1, 233 (1921).

51. Cochran W.G., Proc. Camb. Phil. Soc. Math. Phys. Sci., 30, 365 (1934).

52. Riddiford A.C., Advances in Electrochemistry and Electrochemical Engineering (ed. Delahay), Vol. 4, Interscience.

53. Levich V.G., Acta. Phys-Chim., URSS, 17. 257 (1942).

54. Bartlett P.M., Private communication.

55. Abramovitz M. and Stegun I.A. (Eds.), Handbook of Mathematical Functions, Dover, New York (1965).

56. Field N.J.R., D.Phil. Thesis, Oxford (1968).

57. Turner A.D., D.Phil. Thesis, Oxford (1977).

58. Coles B.A., Private communication

59. Egdell R.G., Part II Thesis, Oxford (1974).

60. Jarzebski Z.M. and Marton J.P., J. Electrochem. Soc., 123 345c (1976).

61. De Gryse R., Gomes W.P., Condon F. and Vennik J., J. Electrochem Soc., 122, 711 (1975).

62. Hillman A.R. and Bartlett P.N., Private communication.

63. Heslop N.W., Private communication.

64. Chadwick A.T., D. Phil. Thesis, Oxford (1977).

65. Hatchard C.G. and Parker C.A., Proc. Roy. Soc., A235, 518 (1956).

66. Anderson S. and Seddon K.R., J. Chem. Res., (5) 74 (1979).

67. Dwyer F.P., Humpoletz J.E., and Nyholm R.S., J. Proc. Roy. Soc. New South Wales, 80, 212 (1976).

68. International Critical Tables, McGraw Hill, 5, 10 (1928).

69. Hitchman M.L. and Albery W.J., Electrochimica Acta, 17, 787 (1972).

70. Foulds A.W. and Bartlett P.N., Private communication.

71. Caldin E.F., Crooks J.E. and Queen A., J. Phys. E (Sci Instr.), 6, 930 (1973).

72. Albery W.J., Daul C. and Fisher F.S., J. Electroanal. Chem., Submitted for publication.

73. Foulds, A.W., Private communication.

74. Davies J.P., Private communication.

75. Albery W.J., Bowen R.W. and Archer M.D., J. Photochem., accepted for publication.

76. Hillman A.R., Private communication.

77. Pilling M.J., Private communication.

78. Osif T.L., Lichin N.N. and Joffman M.Z., J. Phys. Chem., 82, 1778 (1978).

79. Leffler J.E. and Grunwald E., Rates and Equilibria of Organic Reactions, Wiley, (1963).

80. Braddock J.N. and Meyer T.J., J.A.C.S., 95, 3158 (1973).

81. Cramer J.L. and Meyer T.J., Inorg. Chem., 13, 1250 (1974).

82. Sutin N., J. Photochem., 10, 19 (1979).

83. Mason B., Principles of Geochemistry, John Wiley and Sons, (1952).

84. Van Houten J. and Watts R.J., J.A.C.S., 98, 4853 (1976).

85. Albery W.J., Bowen W.D., Fisher F.S., Foulds A.W., Hall K.J., Hillman A.R., Egdell R.G. and Orchard A.F., J. Electroanal. Chem., to be published.